Theoretical modelling of formyl halide hydrolysis

Rickard, Gail

Award date:
2001

Awarding institution:
University of Bath

Theoretical Modelling of Formyl Halide Hydrolysis

Submitted by

Gail Rickard

for the degree of PhD of the University of Bath

2000

ProQuest LLC
789 East Eisenhower Parkway
P.O. Box 1346
Ann Arbor, MI 48106-1346

For my family

I hope this explains what I've been doing for the last few years …

Acknowledgements

I would like to thank my supervisor Professor Ian Williams for all the help and encouragement he has given me over the past four years, especially during those times when I thought that nothing would ever work. Thank you to the EPSRC and the University of Bath for funding.

Thank you to all those in the Ian Williams research group without whose help I could not have completed this project. Thanks also to Mick Hand for starting the work on the chloromethanediol conformers, and to Carol Burgess (University College Dublin) for her help with calculating free energies of solvation from classical molecular dynamics. Thanks to Stuart Firth-Clark for making me feel less guilty about eating chocolate by having the sweetest tooth of anybody I've ever met, and to Vicent Moliner for his help and for generally making the lab a nicer place to work. Special thanks to Gus Ruggiero for his help with using CHARMM and GRACE, for making sure we always had music in the lab, and for making sure I always received email of one sort or another.

I would also like to thank all the friends I've made in the organic chemistry section whose various fires and chemically induced ailments reminded me why I gave up the life of a practical chemist. Thanks especially to Gini, Gian (Geezer-Gi), the Matt's Clarke and Leese, the Louise's Tonks and Haughton, for making life a whole lot more entertaining.

A big thank you to Mark for being so lovely to live with, for all the lifts into Uni, for not cooking fish when my washing was drying, for eating my biscuits, for being a great friend and someone I'll miss loads.

Finally thanks to my own ginger Mat. He knows why.

Summary

The hydrolysis reactions of formyl fluoride and chloride are the subject of this thesis. These compounds are significant as they are intermediates in the tropospheric decomposition pathways of several hydrochlorofluorocarbons (HCFCs) and hydrofluorocarbons (HFCs).

The hydrolysis reactions have been studied using a variety of theoretical modelling techniques. *Ab initio* levels of theory have been used to investigate the bimolecular hydrolysis of formyl chloride in the gas phase. One- and two-step mechanisms have been considered, as well as the low energy interconversions of the intermediate conformers for the two-step mechanism. One- and two-step mechanisms have also been studied at the *ab initio* level of theory for the termolecular hydrolysis of formyl chloride and fluoride, in which the reactions are catalysed by a second water molecule. Free energies for the competing processes have been calculated at temperatures and pressures consistent with tropospheric conditions.

The hydrolysis of the formyl halides was then investigated as a process occurring within a water droplet. The system has been studied using a hybrid QM/MM potential with the AM1 Hamiltonian used to describe the QM region, and TIP3P for the explicit solvent molecules in the MM region. Potential energies have been calculated for the species involved in the one- and two-step reaction pathways. Free energies of solvation and free energies in solution have also been calculated for the AM1/TIP3P reaction species using a technique involving molecular dynamics calculations and based on the Born theory of solvation.

Contents

1. AN INTRODUCTION TO MOLECULAR MODELLING METHODS

1.1 Quantum Mechanics

1.1.1 *Ab initio* Molecular Orbital Calculations

1.1.1.1 Introduction to Molecular Orbital Calculations

The theoretical investigations in this project have been carried out using molecular orbital methods.[1-5] These quantum mechanical calculations provide approximate solutions to the non-relativistic time-independent Schrödinger equation:

$$H\Psi = E\Psi \qquad \text{(Equation 1.1)}$$

where H is the Hamiltonian operator that represents the sum of the kinetic and potential energy of the system; Ψ is the wavefunction; and E is the energy of the system. The Hamiltonian operator, H, includes terms for the potential and kinetic energy of both the nuclei and the electrons.

$$H = \sum_{a>b}\frac{Z_a Z_b}{r_{ab}} - \sum_{a,i}\frac{Z_a}{r_{ai}} + \sum_{i>j}\frac{1}{r_{ij}} - \sum_{i} \tfrac{1}{2}\nabla_i^2 - \sum_{a}\frac{1}{2m_a}\nabla_a^2 \qquad \text{(Equation 1.2)}$$

where a and b are nuclei, i and j are electrons, $\frac{Z_a Z_b}{r_{ab}}$ is the repulsion between nuclei (Z_a, Z_b are the nuclear charges, r_{ab} is the distance between them), $-\frac{Z_a}{r_{ai}}$ is the coulombic attraction between nuclei and electrons, $\frac{1}{r_{ij}}$ is the repulsion between electrons i and j, $-\tfrac{1}{2}\nabla_i^2$ is the electronic kinetic energy term and $-\tfrac{1}{2}m_a\nabla_a^2$ the nuclear kinetic energy term (m_a is the mass of nucleus a and $\nabla^2 = \frac{\partial^2}{\partial x^2} + \frac{\partial}{\partial y^2} + \frac{\partial^2}{\partial z^2}$).

The Hamiltonian is simplified by assuming the Born-Oppenheimer approximation. In this situation the motion of the electrons is decoupled from the motion of the nuclei.

This separation of nuclear and electronic motions is possible because the nuclear masses are much greater than those of the electrons, the nuclei therefore move much more slowly. The electron distribution thus depends only on the instantaneous positions of the nuclei and the Schrödinger equation can then be solved for electron motion in a field of fixed nuclei. The total wavefunction for the system is written as:

$$\Psi_{tot}(\text{nuclei,electrons}) = \Psi(\text{electrons})\Psi(\text{nuclei}) \qquad \text{(Equation 1.3)}$$

The total energy equals the sum of the nuclear energy and electronic energy:

$$E_{tot} = E(\text{electrons}) + E(\text{nuclei}) \qquad \text{(Equation 1.4)}$$

The total energy can thus be calculated by adding a constant nuclear repulsion term to the electronic energy (E_e). The equation solved to determine properties of a given system is thus the electronic Schrödinger equation:

$$H_e\Psi_e = E_e\Psi_e \qquad \text{(Equation 1.5)}$$

The subscripts will be omitted from this point on and it will be assumed that H, Ψ, and E refer to the electronic motion only.

The average value of the energy can be calculated by multiplying Equation 1.5 by Ψ^* (the complex conjugate of the wavefunction) and integrating over all space and spin co-ordinates:

$$E = \frac{\int \Psi^* H \Psi d\tau}{\int \Psi^* \Psi d\tau} = \frac{\langle \Psi^* | H | \Psi \rangle}{\langle \Psi^* | \Psi \rangle} \qquad \text{(Equation 1.6)}$$

The electronic wavefunction is the product of the molecular orbitals that include a spin function. The wavefunction must be antisymmetric and the electrons indistinguishable. Arranging the orbitals in a determinant ensures antisymmetry, e.g. for a Li atom:

$$\Psi = \frac{1}{\sqrt{6}} \begin{vmatrix} \psi_{1s}(1) & \overline{\psi}_{1s}(1) & \psi_{2s}(1) \\ \psi_{1s}(2) & \overline{\psi}_{1s}(2) & \psi_{2s}(2) \\ \psi_{1s}(3) & \overline{\psi}_{1s}(3) & \psi_{2s}(3) \end{vmatrix} \qquad \text{(Equation 1.7)}$$

where $1/\sqrt{6}$ is a normalisation constant. A function written without a bar is 'spin-up', whereas an overlined function corresponds to 'spin-down'. This is known as a Slater determinant. It can be written just as the diagonal and left as understood that the product has to be antisymmetrised and normalised:

$$\Psi \equiv \left|\psi_{1s}\overline{\psi}_{1s}\psi_{2s}\right| \qquad \text{(Equation 1.8)}$$

It is usual for the solutions of the Schrödinger equation to be orthogonal and normalised so that the overall probability that the electron exists somewhere in any particular state is 1, i.e.:

$$\int \Psi^{*}\Psi d\tau = S_{ij} \qquad \text{(Equation 1.9)}$$

where S_{ij}, the overlap integral, is 1 when i=j, and 0 when i≠j, when integrated over all space and spin co-ordinates.

The molecular spin orbitals can be written as a linear combination of a finite set of N one-electron basis functions:

$$\psi_i = \sum_{\mu=1}^{N} c_{\mu i}\phi_{\mu} \qquad \text{(Equation 1.10)}$$

where ψ_i is an individual molecular spin orbital, $\phi_1 \cdots \phi_N$ are prescribed basis functions, and $c_{\mu i}$ are the molecular orbital expansion coefficients. The problem of finding the orbitals is thus reduced to finding a finite set of linear coefficients for each orbital ψ_i. The method used to calculate these expansion coefficients is based on Hartree-Fock theory.

1.1.1.2 Hartree-Fock Theory

Hartree-Fock theory is a variational method hence the 'best' wavefunction is obtained when the energy is minimised. As the first derivative of the energy is 0 at a minimum

then the optimum wavefunction for a given basis set can be found by minimising the energy with respect to the coefficients $c_{\mu i}$ (as in Equation 1.11):

$$\frac{\partial E}{\partial c_{\mu i}} = 0 \qquad \text{(Equation 1.11)}$$

In the Hartree-Fock approximation electrons are treated as independent particles that move in an averaged field created by the nuclei and other electrons. A many electron system can then be treated as a series of one-electron problems.

For a closed shell system the Hartree-Fock equations are given as:

$$F\psi_i = \varepsilon_i \psi_i \qquad \text{(Equation 1.12)}$$

where ε_i is the one-electron energy of molecular orbital ψ_i, and F is called the Fock operator. It has the form:

$$F(1) = H^{core}(1) + \sum_{j=1}^{N/2} \{2J_j(1) - K_j(1)\} \qquad \text{(Equation 1.13)}$$

where H^{core} is the average kinetic energy plus the nuclear-electronic attraction energy, J_j is the coulomb operator and K_j is the exchange operator. These operators are related to the $\frac{1}{r_{ij}}$ terms in the molecular Hamiltonian, H, i.e. the electron repulsion terms. The sum of the coulomb and exchange integrals in Equation 1.13 accounts for all the electronic interaction energy.

The Fock operator is itself a function of the molecular orbitals ψ_i, through the coulomb and exchange operators. The Hartree-Fock equations are therefore not linear and must be solved iteratively using the self-consistent field approach (SCF). In this approach a trial set of solutions for the molecular spin orbitals are obtained for the Hartree-Fock equations. These are used to calculate the exchange and Coulomb operators. The Hartree-Fock equations are then solved for a new set of molecular spin orbitals, which

are used in the next iteration. The procedure is repeated until the results for all the electrons no longer change, when they are said to be self-consistent.

1.1.1.3 The Roothaan-Hall Equations

Roothaan[6] and Hall[7] independently recast the Hartree-Fock equations in matrix form for closed-shell systems. The Roothaan-Hall equations are:

$$\sum_{\upsilon=1}^{N}\left(F_{\mu\upsilon}-\varepsilon_i S_{\mu\upsilon}\right)c_{\upsilon i}=0 \qquad \mu=1,2,.....N \qquad \text{(Equation 1.14)}$$

with the normalisation conditions:

$$\sum_{\mu=1}^{N}\sum_{\upsilon=1}^{N}c_{\mu i}^{*}S_{\mu\upsilon}c_{\upsilon i}=1 \qquad \text{(Equation 1.15)}$$

ε_i is the one-electron energy of molecular orbital ψ_i, $S_{\mu\upsilon}$ are the elements of the overlap matrix:

$$S_{\mu\upsilon}=\int\phi_{\mu}^{*}(1)\phi_{\upsilon}(1)d\tau_1 \qquad \text{(Equation 1.16)}$$

and $F_{\mu\upsilon}$ are elements of the Fock matrix:

$$F_{\mu\upsilon}=H_{\mu\upsilon}^{core}+\sum_{\lambda=1}^{N}\sum_{\sigma=1}P_{\lambda\sigma}\left[(\mu\upsilon|\lambda\sigma)-\tfrac{1}{2}(\mu\lambda|\upsilon\sigma)\right] \qquad \text{(Equation 1.17)}$$

where $H_{\mu\upsilon}^{core}$ is a matrix representing the energy of a single electron moving in a field of bare nuclei. $P_{\lambda\sigma}$ are the elements of the one-electron density matrix (summed over occupied molecular orbitals only) which are multiplied by two-electron repulsion integrals $(\mu\upsilon|\lambda\sigma)$.

The electronic energy can then be evaluated by:

$$E=\tfrac{1}{2}\sum_{\mu=1}^{N}\sum_{\upsilon=1}^{N}P_{\mu\upsilon}\left(F_{\mu\upsilon}+H_{\mu\upsilon}^{core}\right) \qquad \text{(Equation 1.18)}$$

The total energy is then calculated by adding a term for the internuclear repulsion to the electronic energy.

The Roothaan-Hall equations are again solved using the SCF approach as the Fock matrix, $F_{\mu\upsilon}$, depends on the molecular orbital coefficients, $c_{\mu i}$, through the density matrix.

1.1.1.4 Basis Sets

Consideration also needs to be given to the type of basis set used for *ab initio* quantum mechanical calculations on molecular systems. As has already been stated molecular orbitals can be expressed as linear combinations of one-electron functions known as basis functions (Equation 1.10). The basis functions are generally centred on the atomic nuclei and resemble atomic orbitals. The exact expansion of Equation 1.10 would require an infinite basis set, which is not practical. Smaller sets of basis functions must therefore be chosen which result in a compromise between accuracy and efficiency.

Two major types of basis function are used in *ab initio* molecular orbital calculations. These are Slater type orbitals (STOs) and gaussian functions. Solutions of the Schrödinger equation for hydrogen-like atoms suggest the use of spherical atomic orbitals of the form:

$$\phi = R_{nl}(r)Y_{lm}(\theta,\phi) \qquad \text{(Equation 1.19)}$$

where R is a radial function and Y is the angular part of the function (a spherical harmonic). STOs are used for the radial function and have the form:

$$R_{nl}(r) = Nr^{n-1}e^{-\zeta r} \qquad \text{(Equation 1.20)}$$

where ζ is the orbital exponent, and r is the position vector (x,y,z). For example the STO for a 1s orbital would be:

$$R_{1s}(r) = 2\zeta^{3/2}e^{-\zeta r} \qquad \text{(Equation 1.21)}$$

The integrals related to the Slater functions are difficult to evaluate especially when the atomic orbitals are centred on different nuclei. STOs are therefore commonly replaced by gaussian functions, which lead to simpler integral equations. Gaussian functions have the form $\exp(-\alpha r^2)$, and *ab initio* calculations use basis functions of the form:

$$g(\alpha,r) = x^a y^b z^c \exp(-\alpha r^2) \qquad \text{(Equation 1.22)}$$

where α is a constant that determines the radial extent of the function, x, y, z are the Cartesian variables, and a, b and c are integral powers of x, y and z. The advantage of using gaussian functions is that it is possible to express the product of two gaussians as a single gaussian. Many-centre two-electron integrals thus reduce to simpler forms.

The disadvantages of gaussian functions are that they do not have a cusp at the origin and they decay to zero more quickly than Slater functions. These deficiencies are important since they mean that a gaussian function does not adequately reproduce the form of real atomic orbitals. These problems are minimised by using a linear combination of gaussians to replace a single STO (Equation 1.23).

$$\phi_\mu = \sum_{i=1}^{L} d_{i\mu} g_i(\alpha_{i\mu}) \qquad \text{(Equation 1.23)}$$

$d_{i\mu}$ is the coefficient of the primitive gaussian function g_i, which has exponent $\alpha_{i\mu}$, and L is the number of functions in the expansion. If the coefficients $d_{i\mu}$ are fixed then the basis functions ϕ_μ are called contracted gaussians and the individual g_i functions primitive gaussians. The basis sets in *ab initio* calculations use contracted gaussians with both the coefficients and exponents predetermined and constant throughout the calculation.

Minimal basis sets usually contain the number of functions required to accommodate the filled orbitals of each atom plus all the atomic orbitals within a shell. Thus for all the elements in the same row of the periodic table the same number of functions are used. Problems with minimal basis sets, such as the fact that the functions cannot expand or contract in size with molecular environment, and that they cannot describe non-spherical electronic distributions, can be overcome if more than one function is used for each orbital. This gives rise to double- and triple-zeta basis sets where the number of functions used to describe orbitals is doubled or tripled. Alternatively split valence basis sets can be used in which the number of functions used to describe the core orbitals is different to that used for the valence orbitals. Thus for the 6-31G basis set six primitive gaussian functions represent each core orbital. The valence orbitals are split with a contracted part described by 3 gaussians and a diffuse part by one gaussian.

Basis sets can be further enhanced by the addition of polarisation and/or diffuse functions. Polarisation functions are denoted by an asterisk and are included to improve the model for molecules where charge distribution is anisotropic. For example the 6-31G* basis set adds a set of six d-type primitive gaussians to the 6-31G basis set description of each heavy atom. For species such as anions where large portions of the electron density exists away from the nuclei highly diffuse functions can be added to the basis set. These are denoted by a '+' sign.

Different basis sets produce different wavefunctions and energies. As the basis set mathematical flexibility is extended so the SCF energy becomes lower. The energy approaches a limiting value as the basis set approaches mathematical completeness. The limiting energy is the lowest that can be achieved for a single determinantal wavefunction. This is termed the Hartree-Fock energy. The Hartree-Fock energy is not

as low as the true energy of the system. To improve on the Hartree-Fock energy post - SCF methods must be used. These are discussed below.

1.1.1.5 Electron Correlation

The electron correlation energy is the contribution arising from electrons interacting with one another instantaneously. Hartree-Fock theory does not adequately represent electron correlation. It includes exchange correlation, the correlation effect arising from pairs of electrons with the same spin, but does not account for the correlation of the motion of electrons of opposite spin. This is because the self-consistent field method assumes that the electrons move in an average potential of the other electrons, resulting in the instantaneous position of an electron being unaffected by the presence of a neighbouring electron. In reality the motions of electrons are correlated and they tend to avoid each other more than suggested by Hartree-Fock theory giving rise to a lower energy. The correlation energy is therefore defined as the difference between the limiting Hartree-Fock energy and the true total energy of the system.

$$E_{correlation} = E_{true} - E_{H\text{-}F} \qquad \text{(Equation 1.24)}$$

Popular approaches to incorporating the correlation energy into *ab initio* molecular orbital calculations include configuration interaction and Møller-Plesset perturbation theory.

1.1.1.5.1 *Configuration Interaction*

The basic premise of configuration interaction (CI) is that excited configurations are included in the description of an electronic state. In Hartree-Fock calculations, if there are K basis functions, then 2K spin orbitals are produced. If the 2K spin orbitals are

filled with N electrons then there are 2K-N unoccupied, virtual orbitals. However, the wavefunction is expressed only in terms of the occupied orbitals. In CI calculations occupied spin orbitals are replaced by virtual orbitals to generate possible excited configurations and the overall wavefunction is described as a linear combination of the ground and excited configuration wavefunctions. The general CI wavefunction can be written:

$$\Psi = c_0\Psi_0 + c_1\Psi_1 + c_2\Psi_2 + \cdots \qquad \text{(Equation 1.25)}$$

where Ψ_0 is the Hartree-Fock single determinant wavefunction, and Ψ_1, Ψ_2, etc are wavefunctions that represent configurations obtained from replacing one or more occupied spin orbitals with a virtual spin orbital and are expressed as determinants. The coefficients c_0, c_1, are mixing coefficients whose values are chosen to minimise the energy of the system.

Full configuration interaction, where all possible configurations are considered, is not usually undertaken due to the large number of integrals that must be calculated. It is therefore more common to limit the excited configurations considered. For example, in configuration interaction singles (CIS) only wavefunctions that differ from Ψ_0 by a single spin orbital are included.

1.1.1.5.2 *Møller-Plesset Many Body Perturbation Theory*

An alternative way to include electron correlation is that proposed by Møller and Plesset based upon perturbation theory. In perturbation theory the molecular Hamiltonian is divided into two parts:

$$H = H_o + \lambda V \qquad \text{(Equation 1.26)}$$

where the 'true' Hamiltonian operator H is expressed as the sum of a Hamiltonian H_o which is exactly soluble, and a perturbation λV applied to H_o (with λ a parameter that can vary between 0 and 1). It is assumed that V is a small perturbation to H_o with the result that the perturbed wavefunction (Ψ) and energy (E) can be expressed as a power series in V in terms of the parameter λ.

$$\Psi = \Psi^{(0)} + \lambda\Psi^{(1)} + \lambda^2\Psi^{(2)} + \lambda^3\Psi^{(3)} + \ldots\ldots = \sum \lambda^n\Psi^{(n)} \qquad \text{(Equation 1.27)}$$

$$E = E^{(0)} + \lambda E^{(1)} + \lambda^2 E^{(2)} + \lambda^3 E^{(3)} + \ldots\ldots \quad = \sum \lambda^n E^{(n)} \qquad \text{(Equation 1.28)}$$

When λ=0 then H=H_o, $\Psi=\Psi^{(0)}$, and E= $E^{(0)}$, but when λ=1 then H equals its true value.

The perturbed wavefunction and energy are substituted back into the Schrödinger equation:

$$(H_o + \lambda V)(\Psi^{(0)} + \lambda\Psi^{(1)} + \ldots) = (E^{(0)} + \lambda E^{(1)} + \ldots)(\Psi^{(0)} + \lambda\Psi^{(1)} + \ldots) \qquad \text{(Equation 1.29)}$$

The variable is λ in Equation 1.29. Each power of λ is linearly independent of all other powers of λ. This means that Equation 1.29 can be solved for all values of λ only if it is satisfied for each power of λ separately. E.g. collecting terms having the zeroth power of λ gives:

$$H_o\Psi^{(0)} = E^{(0)}\Psi^{(0)} \qquad \text{(Equation 1.30)}$$

Therefore after expanding the products, it is possible to equate the co-efficients on each side of the equation for each power of λ. This leads to a series of relations representing successively higher orders of perturbations, the first three of which are shown below:

$$(H_o - E^{(0)})\Psi^{(0)} = 0 \qquad \text{(Equation 1.31a)}$$

$$(H_o - E^{(0)})\Psi^{(1)} = (E^{(1)} - V)\Psi^{(0)} \qquad \text{(Equation 1.31b)}$$

$$(H_o - E^{(0)})\Psi^{(2)} = (E^{(1)} - V)\Psi^{(1)} + E^{(2)}\Psi^{(0)} \qquad \text{(Equation 1.31c)}$$

These are general results for perturbation theory. In Møller-Plesset[8] perturbation theory H_0 is defined as the sum of the one-electron Fock operators for the N electrons:

$$H_0 = \sum_{i=1}^{N} F_i \qquad \text{(Equation 1.32)}$$

The Hartree-Fock determinant and all of the excited determinants are eigenfunctions of H_0, and these are the solutions to the part of the divided Hamiltonian which has already been solved.

Since the wavefunctions are orthonormal, and H_0 is the sum of the Fock operators, then $E^{(0)}$ is the sum of the orbital energies:

$$E^{(0)} = \left\langle \Psi^{(0)} \middle| H_0 \middle| \Psi^{(0)} \right\rangle = \sum_i \varepsilon_i \qquad \text{(Equation 1.33)}$$

The same type of product can be determined for $E^{(1)}$ using linear algebra on Equation 1.31b:

$$E^{(1)} = \left\langle \Psi^{(0)} \middle| V \middle| \Psi^{(0)} \right\rangle \qquad \text{(Equation 1.34)}$$

As $H=H_0+V$ adding $E^{(0)}$ and $E^{(1)}$ gives the Hartree-Fock energy:

$$\begin{aligned} E^{(0)} + E^{(1)} &= \left\langle \Psi^{(0)} \middle| H_0 \middle| \Psi^{(0)} \right\rangle + \left\langle \Psi^{(0)} \middle| V \middle| \Psi^{(0)} \right\rangle \\ &= \left\langle \Psi^{(0)} \middle| (H_0 + V) \middle| \Psi^{(0)} \right\rangle \\ &= \left\langle \Psi^{(0)} \middle| H \middle| \Psi^{(0)} \right\rangle \\ &= E^{HF} \end{aligned} \qquad \text{(Equation 1.35)}$$

Therefore in order to improve on the Hartree-Fock energy Møller-Plesset perturbation theory to at least second-order is required (MP2). The expression for $E^{(2)}$ is:

$$E^{(2)} = -\sum \frac{\left| \left\langle \Psi^{(0)} \middle| V \middle| \Psi_t \right\rangle \right|^2}{E_t - E^{(0)}} \qquad \text{(Equation 1.36)}$$

where Ψ_t is an arbitrary excited wavefunction and E_t the energy resulting from that wavefunction. This expression will only be non-zero for double excitations according to Brillouin's theorem. Higher excitations also result in a zero value because the Hamiltonian contains only one and two electron terms (i.e. all interactions between electrons occur pairwise).

The $\left|\left\langle \Psi^{(0)} \middle| V \middle| \Psi_t \right\rangle\right|^2$ and $(E_t\text{-}E^{(0)})$ terms are always positive. For $(E_t\text{-}E^{(0)})$ this is because $E^{(0)}$ is the lowest energy eigenvalue of the unperturbed system, and the expression is just the difference in orbital energies of the excited and ground state. This means that the value of $E^{(2)}$ is always negative. This can cause problems, however, because although lowering the energy is what the exact correction should do, Møller-Plesset perturbation theory is not variational and can sometimes give energies lower than the 'true' energy.

The expressions for the third and fourth order energy corrections can also be derived (MP3 and MP4), and these can have positive or negative values. MP4 is more commonly used than MP3 but it is computationally expensive and is often restricted to determining single point energies for a geometry obtained using a lower level of theory, often MP2.

1.1.2 Semi-Empirical Molecular Orbital Calculations

Ab initio calculations quickly become prohibitively expensive as the size of the molecule being studied increases. This is because the number of integrals required increases as the fourth power of the number of basis functions in the molecule. Semi-empirical molecular orbital methods have therefore been developed which make approximations to reduce the number of integrals to be evaluated and hence the cost of these calculations for larger molecules.

The commonly used methods only explicitly consider the valence electrons of the system. The core electrons are neglected, as they play little part in chemical bonding, and are defined as part of the nuclear core. Semi-empirical calculations generally use

basis sets made up of Slater-type orbitals, which allow further approximations because of the orthogonality of these orbitals.

The common feature of most semi-empirical methods is that they employ techniques to simplify the matrices used to calculate orbital overlap. Such methods include the zero-differential overlap approximation (ZDO), the complete neglect of differential overlap approach (CNDO),[9] the intermediate neglect of differential overlap (INDO)[10] for monatomic one-centre integrals, and the neglect of diatomic differential overlap (NDDO).[11]

These early semi-empirical methods have been superseded as computational resources have improved. The first widely used method was MINDO/3[12] (modified INDO) in which some of the parameterisation was based on experimental data rather than *ab initio* calculations. The modified neglect of diatomic overlap (MNDO)[13] was introduced to overcome the limitations of MINDO/3 caused by the INDO approximation such as its inability to cope with systems containing lone pairs. However this model was not without its own limitations, like being unable to accurately model intermolecular hydrogen bonds because of a tendency to over estimate the repulsion between atoms at a separation distance approximately equal to their Van der Waals radii.

The Austin Model 1 (AM1)[14] was developed to eliminate the above problem with MNDO by modifying the monatomic parameterised core-core repulsion term using gaussian functions. Attractive and repulsive gaussians were used with the attractive gaussians designed to overcome the repulsion directly and centred in the region where the repulsions were too large. The repulsive gaussians were centred at smaller internuclear separation distances.

1.2 Potential Energy Surfaces

A potential energy surface (PES) specifies the way the energy of a molecular system varies with small changes in its structure. It is a mathematical relationship linking molecular structure and the resultant energy. If a system contains N atoms then the energy is a function of 3N-6 internal co-ordinates. As it is impossible to visualise the entire energy surface except where the energy is a function of one or two co-ordinates, potential energy surfaces are commonly represented as two-dimensional plots like those shown in Figure 1.1. The x-axis corresponds to the reaction co-ordinate, which symbolises the nuclear reorganisation that occurs during a reaction. The y-axis shows the energy changes that result when the reactants transform into products. The energy plotted can be any thermodynamic energy, i.e. internal energy (U), enthalpy (H), or free energy (G).

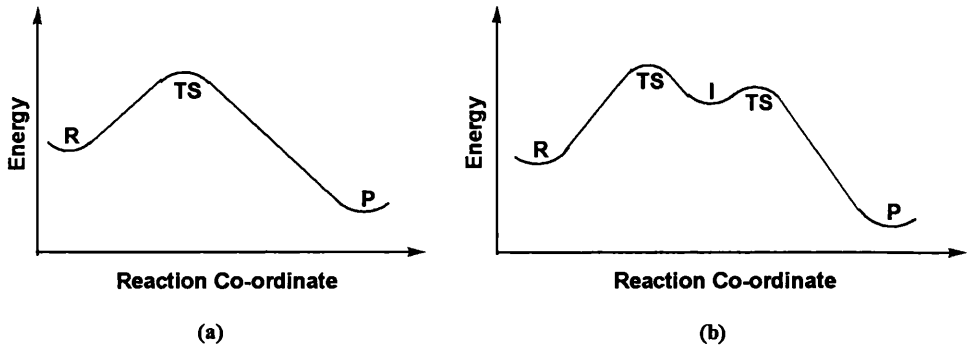

Figure 1.1 Energy profiles for (a) a single step reaction transforming reactants, R, to products, P, via the transition state, TS. (b) a two step reaction proceeding from reactants to a high energy intermediate, I, then on to products.

The parts of the PES of most interest when studying chemical reactions are the stationary points. These occur where the first derivative of the energy with respect to the nuclear co-ordinates is zero. Minimum energy points, such as the reactants and products in Figure 1.1, correspond to stable structures. There may be large numbers of these local minima on the energy surface with the lowest energy arrangement known as the global energy minimum.

Transition states are also stationary points but are saddle points rather than minima on the energy surface and provide the lowest energy path between two minima. The second derivative matrix of the energy with respect to the nuclear co-ordinates contains all positive eigenvalues for a minimum energy species. In the case of a transition structure this matrix contains a single negative eigenvalue with the remaining values positive. This is a consequence of the fact that a transition structure is a maximum in one direction (the reaction vector) and a minimum in all other dimensions.

1.2.1 Characterisation of Stationary Points on a PES

In the investigation of chemical reaction pathways it is vital to characterise the stationary points on the PES. The routine characterisation method involves calculating the vibrational frequencies of minimum energy and transition structures. Transition structures can be further characterised by calculating the intrinsic reaction co-ordinate.

1.2.1.1 Vibrational Frequencies

Vibrational frequencies may be used in several ways to characterise the stationary points on a potential energy surface. The first is as a means of distinguishing between local minima, which have all real frequencies, and first order saddle points, which have a single imaginary frequency. Another major use of calculated normal mode vibrational frequencies is to provide thermodynamic properties of molecules via statistical mechanics. This is discussed in more detail in Chapter 5.

The normal mode vibrational frequencies of a molecule are calculated using the approximation that at equilibrium the molecule can be treated as a harmonic oscillator.

The total energy, E, of a molecule containing N atoms close to its equilibrium structure can then be expressed:

$$E = \tfrac{1}{2}\sum_{i=1}^{3N} \dot{q}_i^2 + V_{eq} + \tfrac{1}{2}\sum_{i=1}^{3N}\sum_{j=1}^{3N} k_{ij} q_i q_j \qquad \text{(Equation 1.37)}$$

where V_{eq} is the potential energy at the equilibrium nuclear configuration, q_i and q_j are the mass weighted Cartesian displacements (defined in terms of the locations, x_i, of the nuclei relative to their equilibrium positions, $x_{i,eq}$, and their masses, M_i, (Equation 1.38)), and k_{ij} are quadratic force constants.

$$q_i = M_i^{1/2}\left(x_i - x_{i,eq}\right) \qquad \text{(Equation 1.38)}$$

The summations in Equation 1.37 are over 3N displacements of the N atoms. The displacements corresponding to translation and rotation of the molecule as a whole result in zero force constants. The remaining 3N-6 (non-linear molecule) or 3N-5 (linear molecule) displacements are the vibrational modes. The force constants are the second derivatives of the potential energy with respect to the mass-weighted Cartesian displacements evaluated at the equilibrium nuclear configuration, i.e.:

$$k_{ij} = \left(\frac{\partial^2 V}{\partial q_i \partial q_j}\right)_{eq} \qquad \text{(Equation 1.39)}$$

The force constants may be evaluated by numerical or analytical differentiation methods, with the choice of procedure dependent on the quantum mechanical model used. Once the force constants have been calculated the harmonic vibrational frequencies, υ_i, can be obtained from the relationship:

$$\upsilon_i = \frac{\sqrt{k_i}}{2\pi} \qquad \text{(Equation 1.40)}$$

where k_i is the force constant for the mode. The zero point vibrational energy can then be obtained from the expression:

$$ZPVE = \sum_{i=1}^{3N-6} \tfrac{1}{2} h\upsilon_i \qquad \text{(Equation 1.41)}$$

where h is Planck's constant and υ_i is the frequency of mode i.

Systematic errors occur in the values of the frequencies computed in this manner. Frequencies calculated at the Hartree-Fock level of theory are approximately 10% higher than experimental values. One reason for this is that Hartree-Fock calculations use a harmonic description for molecular vibrations, but even in the region at the bottom of the energy well anharmonicity of the potential function does occur. Other contributions to the errors at the Hartree-Fock level include basis set truncation and neglect of correlation. It is therefore common practice to scale the calculated frequencies, or the zero-point vibrational energies derived from them, to eliminate these errors. The scale factors applied are specific to the level of theory and the basis set used. In this thesis frequencies are reported that have been computed at the HF/6-31G* and MP2(full)/6-31G* levels of theory. The scale factor used for the HF/6-31G* model was 0.8929[15,16] for both frequencies and zero-point vibrational energies. For the frequencies calculated at the MP2(full)/6-31G* level of theory scale factors of 0.9427 and 0.9661 were used for the frequencies and zero-point energies respectively.[17]

1.2.1.2 Intrinsic Reaction Co-ordinate (IRC)

Once a transition structure has been located on a PES it is necessary to characterise it. Vibrational frequencies can determine that the species located is definitely a transition structure. However, it can be difficult to ascertain whether this transition structure connects the reactant and products of interest just from inspection of the normal mode

corresponding to the imaginary frequency. IRC[18] calculations can be used to verify the nature of the transition structure.

An IRC calculation starts at the first order saddle point and moves downhill to the two minima associated with it. It is the path that would be followed by a particle moving along the steepest descent paths with an infinitely small step down to each minimum when the system is described by mass-weighted co-ordinates. The eigenvector corresponding to the imaginary frequency of the transition structure is used to obtain the initial directions towards the minima. The minima can then be located efficiently using a simple steepest descents algorithm with a reasonable step size that yields a path that oscillates about the true minimum energy path. A better approximation to the reaction pathway can be achieved by including correction terms to the path taken by the steepest descents algorithm. An IRC calculation can therefore definitively connect two minima on a PES by a path that proceeds via the transition structure between them.

1.3 Transition State Theory[19]

In the preceding sections the concept of the transition state has been introduced, and as previously stated it is the crucial structure at the highest energy point along a reaction co-ordinate. This section is concerned with briefly illustrating how chemically useful information can be obtained from the transition state. The basis for this is transition state theory. The underlying premise of transition state theory is that a reaction occurs between A and B proceeding through the transition state, TS, which then undergoes unimolecular decay into products P with a rate constant $k^{\ddagger}$. It is assumed that the transition state is in equilibrium with the reactants, i.e.:

$$A + B \rightleftharpoons [TS] \longrightarrow P \qquad \text{(Equation 1.42)}$$

The rate of decay of the transition state to products can be written:

$$\text{Rate} = k^{\ddagger}[TS] \qquad \text{(Equation 1.43)}$$

The equilibrium constant for the formation of the transition state, $K^{\ddagger}$, is then given by:

$$K^{\ddagger} = \frac{[TS]}{[A][B]} \qquad \text{(Equation 1.44)}$$

Since it is also known that:

$$\text{Rate} = k[A][B] \qquad \text{(Equation 1.45)}$$

k, $k^{\ddagger}$, and $K^{\ddagger}$ can be related by the expression:

$$k = k^{\ddagger}K^{\ddagger} \qquad \text{(Equation 1.46)}$$

From statistical thermodynamics it can also be shown that:

$$k^{\ddagger} = k_B T/h \qquad \text{(Equation 1.47)}$$

where k_B is Boltzmann's constant, h is Planck's constant, and T is the temperature. Substitution into Equation 1.46 gives an expression in which the rate constant, k, for the reaction is related to the equilibrium constant for transition state formation, $K^{\ddagger}$:

$$k = k_B T K^{\ddagger}/h \qquad \text{(Equation 1.48)}$$

$K^{\ddagger}$ has one less degree of freedom (3N-7 instead of 3N-6) than an equilibrium constant relating reactants and products. This is because one vibrational mode of the transition state corresponds to motion along the reaction pathway. Thermodynamic properties such as the Gibbs free energy of activation can be determined from $K^{\ddagger}$ *via* the expression:

$$\Delta G^{\ddagger} = -RT\ln K^{\ddagger} \qquad \text{(Equation 1.49)}$$

1.4 Molecular Mechanics

Molecular mechanics methods are used in situations where the system under investigation is too large to be studied using even semi-empirical quantum mechanical

methods. Quantum mechanics is concerned with the electrons in a system whereas in molecular mechanics electronic motions are ignored and only the nuclear positions are considered. The consequences of using this type of technique are that properties cannot be calculated that are dependent upon the electronic distribution of a molecule, and that investigation of reactions is not possible because modelling is restricted to molecular ground states.

MM models (also known as force fields) represent a molecule as a collection of spheres joined by springs. Classical physics can then describe the motions of these atoms via simple potential energy functions and thus large chemical systems can be studied. There are various contributions to a molecular mechanics model of interactions within a system. These include bond stretches, the opening and closing of bond angles, and rotations about single bonds. The most useful force fields are those for which the parameters developed to describe these contributions for a small set of molecules can be applied to a wider range of problems.

In MM calculations the energy of the molecule is the sum of the steric and non-bonded interactions present, i.e.:

$$E_{total} = E_{bond} + E_{angle} + E_{torsion} + E_{non\text{-}bonded} \qquad \text{(Equation 1.50)}$$

where E_{bond}, E_{angle}, $E_{torsion}$, and $E_{non\text{-}bonded}$ are the total bond length, bond angle, torsion angle, and non-bonded energies respectively. A simple functional form for the force field is:

$$E_{total}(r^N) = \sum_{bond} \frac{k_l}{2}(l_i - l_0)^2 + \sum_{angle} \frac{k_\theta}{2}(\theta_i - \theta_0)^2 + \sum_{torsion} \frac{V_n}{2}(1 + \cos(n\omega - \gamma)) + \sum_{i=1}^{N} \sum_{j=i+1}^{N} \left(4\varepsilon_{ij} \left[\left(\frac{\sigma_{ij}}{r_{ij}} \right)^{12} - \left(\frac{\sigma_{ij}}{r_{ij}} \right)^{6} \right] + \frac{q_i q_j}{4\pi\varepsilon_0 r_{ij}} \right) \qquad \text{(Equation 1.51)}$$

$E_{total}(r^N)$ is the total energy as a function of the positions, r, of N particles. The first term in Equation 1.51 is a harmonic potential with force constant k_l which models how the energy changes as the bond length l_i deviates from the reference value l_0. The next term relates to the bond angles and is again a harmonic function where k_θ is the force constant, θ_i is the bond angle and θ_0 is the reference bond angle. The third term is a torsional potential that models how the energy changes as a bond rotates, V_n is the rotational barrier height, n the periodicity of rotation, ω the torsion angle, and γ (the phase factor) determines where the torsion angle passes through its minimum value. The fourth term in Equation 1.51 is the sum of the non-bonded interactions. This term can be broken down into van der Waals and electrostatic interactions. The van der Waals part is modelled by a Lennard-Jones potential where σ_{ij} is the collision diameter (the separation distance of atoms i and j for which the energy is zero), r_{ij} is the distance between i and j, and ε_{ij} is the well depth. The electrostatic interactions are calculated using a Coulomb potential where q_i and q_j are partial charges on atom centres i and j, and ε_0 is the permittivity of free space.

This functional form of the force field is not unique. Other terms may be added to improve the performance of the force field but the four components of Equation 1.51 are invariably present. As the parameters (the various constants k_l, V_n, and σ_{ij} etc) must also be specified it is possible to obtain different results from force fields with the same functional form but which use different parameter values. A further idea common to most force fields is that of an atom type. The atom type contains information about the hybridisation state of an atom as well as its atomic number.

1.5 Solvation

1.5.1 Continuum Models

Many reactions occur in solution rather than in the gas phase as has been considered so far. It is therefore necessary to be able to model solvation to understand such processes more completely. A popular way of incorporating solvation is to use continuum models. One collection of models of this type is known as Self-Consistent Reaction Field (SCRF) methods. These methods all model the solvent as a continuum of uniform dielectric constant, ε (known as the reaction field). The solute is then placed into a cavity within the solvent. The models differ in the way they define the cavity and the reaction field.

The simplest SCRF model is that of Onsager[20] in which the solute occupies a fixed spherical cavity of radius a_0 within the solvent field (Figure 1.2(a)). Net stabilisation occurs because a dipole in the solute induces a dipole in the medium, and the electric field applied by the solvent dipole in turn interacts with the molecular dipole. A more realistic approach is taken in the polarisable continuum method (PCM)[21,22] in which the cavity shape is obtained from the van der Waals radii of the atoms of the solute (Figure 1.2(b)). In this method the effect of polarisation of the solvent continuum is computed by numerical integration. The calculation proceeds as follows. The cavity surface is determined, then the fraction of each atom's van der Waals sphere that contributes to the cavity is divided into a number of small surface elements of calculable surface area. A point charge is associated with each surface element, which represents the polarisation of the solvent. The total electrostatic potential at each surface element, $\phi(r)$, equals the sum of the potentials due to the solute, $\phi_\rho(r)$, and the other surface charges, $\phi_\sigma(r)$:

$$\phi(r) = \phi_\rho(r) + \phi_\sigma(r) \qquad \text{(Equation 1.52)}$$

The contribution $\phi_\sigma(r)$ is calculated using Coulomb's law. Initial values for the point charges of the surface elements are calculated from the electric field gradient due to the solute alone:

$$q_i = -\left[\frac{\varepsilon - 1}{4\pi\varepsilon}\right] E_i \Delta S \qquad \text{(Equation 1.53)}$$

ε is the dielectric constant of the medium, E_i is the electric field gradient, and ΔS is the surface element area. The charges are modified iteratively until they are self-consistent. SCF calculations are then initiated where new values of the surface charges are calculated from the current wavefunction with the calculations continuing until the solute wavefunction and the surface charges are self-consistent.

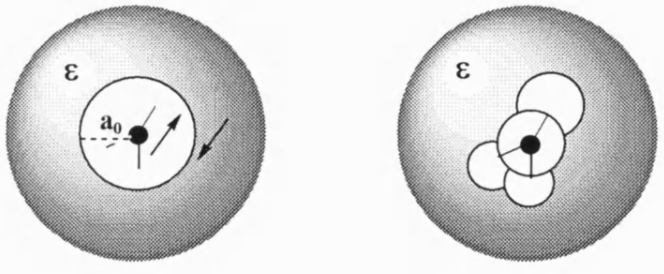

(a) (b)

Figure 1.2 Illustrations of (a) Onsager's and (b) the PCM continuum models.

In this thesis two more recent continuum models have been used to represent solvation effects. These are discussed below.

1.5.1.1 COSMO

The implementation of the COSMO[23] continuum model in Gaussian 98[24] is one of the methods used in the investigation of solvent effects in this thesis. COSMO is based on

the screening in conductors and is an acronym for Conductor-like Screening Model. In this method the cavity surface, the interface between the cavity and the dielectric, is called the 'solvent accessible surface' (SAS). The first step of the COSMO approach is the same as the PCM model, i.e. the cavity is constructed and the SAS is segmented. A suitable SAS is constructed in COSMO using the assumption that the geometry of the solvent molecules can be described by an effective radius R^{solv}. The centres of the solvent molecules are excluded from a sphere radius $R_\alpha = R_\alpha^{vdw} + R^{solv}$ where R_α^{vdw} is the van der Waals radius of the solute atom α (Figure 1.3).

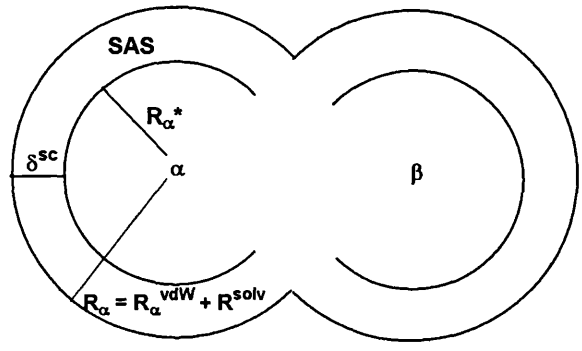

Figure 1.3 Schematic of the construction of the SAS. The outer circles indicate the surface accessible area to the centres of the solvent molecules. The inner circles indicate the surface accessible to the solvent charges.

The effective charges responsible for the dielectric screening are not located at the centres of the solvent molecules. Instead they are assumed to be at a distance of δ^{sc} outside the centre. Their minimum distance to a solute atom α is thus: $R_\alpha^* = R_\alpha - \delta^{sc}$. The value of δ^{sc} for each solvent has to be found empirically. The segmentation of the SAS is done atomwise to ensure that each segment is connected to a single solute atom. This enables efficient calculation of the gradients with respect to the atomic positions. This means that in COSMO the effect of polarisation of the solvent continuum is computed analytically.

1.5.1.2 SM5.4

The second continuum method used in this thesis is Cramer and Truhlar's Solvation Model 5.4 (SM5.4)[25] implemented in the AMSOL[26] program. The solvation models in AMSOL are based on NDDO semi-empirical molecular orbital methods with the terms required to calculate the free energy of solvation included in the solute Hamiltonian.

The free energy of solvation is based on two terms. The first term accounts for electric polarisation of the continuum-dielectric solvent and is a generalised Born approximation (GBA) contribution. The second term is a solvent-accessible-surface-area (SASA) term that accounts for the free energy of cavity formation, dispersion interactions, and first solvation shell effects.

The partial charges used in the first term are obtained either from an NDDO Mulliken population analysis or a Charge Model 1 (CM1) method.[27] The CM1 methods begin with partial charges calculated by an NDDO Mulliken population analysis and map these charges to new sets of partial charges that reproduce experimental dipole moments more accurately. The mappings are achieved through a set of scale factors and offsets that depend on the atomic number with some parameters also dependent on bond orders. The result is that the charges are shifted locally within the molecule so that individual bond dipoles are changed but the overall charge on the molecule stays constant.

The particular solvation method used in this thesis is SM5.4A. This is actually a class of models in which the atomic charges are obtained using the CM1 method. The SM5.4A methods can be used to model a variety of solvents however in this case it was restricted to modelling aqueous solution in conjunction with the AM1 Hamiltonian.

This class of models uses functional forms for the microscopic surface tensions that are dependent on solute atomic numbers and geometries.

1.5.2 Quantum Mechanics / Molecular Mechanics

An alternative approach to modelling solvation is to represent the solvent molecules explicitly. This would be prohibitively costly in terms of computational resources if all the molecules were treated quantum mechanically. Hybrid quantum mechanical/ molecular mechanical (QM/MM) methods have therefore been developed in which the strengths of both types of treatment are combined. QM/MM methods possess a QM core that contains the atoms most influenced by the electronic reorganisation that can occur during a reaction. This core is surrounded by a MM forcefield representing the solvent molecules, and the two parts are joined by several interaction terms. Hybrid QM/MM methods are described in more detail in Chapter 6.

1.6 Algorithms for Exploring Potential Energy Surfaces

1.6.1 Minimisation Algorithms

Minimisation algorithms are used to locate minima on potential energy surfaces from a starting geometry. They are used to locate the nearest local minima rather than the global minimum on the energy surface. The most popular minimisation methods make use of the information provided by derivatives of the energy with respect to the Cartesian or internal co-ordinates of the system. The first derivative of the energy (the gradient) indicates where the minimum lies and its magnitude shows the steepness of the slope. Second derivatives indicate the curvature of the function, which can be used to predict where the function will pass through a stationary point. For derivative

methods using Cartesian co-ordinates the function can be written as a Taylor series expansion about the point x_k:

$$V(x) = V(x_k) + (x-x_k)V'(x_k) + \tfrac{1}{2}(x-x_k)^2V''(x_k) + \ldots \quad \text{(Equation 1.54)}$$

where V(x) is the potential energy, $V'(x_k)$ and $V''(x_k)$ are the first and second derivatives of the function, and x_k corresponds to the current configuration of the system. For a multidimensional function the vector **x** replaces the variable x and matrices are used for the derivatives.

The minimisation methods are classified by the highest order derivative they use. First order methods use only the gradients, whereas second order methods use both first and second derivatives.

1.6.1.1 First Order Minimisation Algorithms

The commonly used first order minimisation methods are the steepest descents and conjugate gradients methods. The starting point for each method is the user provided initial configuration of the system. The algorithms then gradually change the co-ordinates of the atoms as they move the system closer to the minimum point, with the molecular configuration of each step obtained from the previous one.

1.6.1.1.1 Steepest Descents Method

In the steepest descents method each step is taken in the direction parallel to the net force (i.e. in the opposite direction to the gradient). This direction is represented by the 3N-dimensional vector, $\mathbf{s_k}$:

$$\mathbf{s_k} = -g_k \quad \text{(Equation 1.55)}$$

when there are 3N Cartesian co-ordinates, and g_k is the gradient. An arbitrary initial step size is taken along the vector $\mathbf{s_k}$ and if the energy decreases then the step size is increased by a standard factor (e.g. 1.2). This process continues as long as the energy is reduced with each iteration. If a step results in an increase in energy the step size is reduced (e.g. by 0.5) as it is assumed that the algorithm has passed over the minimum. This method is generally robust even when the starting point is far from a minimum but the path taken oscillates and may not be the best route to the minimum.

1.6.1.1.2 Conjugate Gradients Method

The conjugate gradients method[28] produces a path that does not oscillate as the steepest descents path does. In conjugate gradients methods the first step is the same as the steepest descents (namely moving in the opposite direction of the gradient) but after the first step moves in a direction $\mathbf{v_k}$ from point $\mathbf{x_k}$. $\mathbf{v_k}$ is calculated from the gradient at that point and the previous direction vector $\mathbf{v_{k-1}}$:

$$\mathbf{v_k} = -g_k + \gamma_k \mathbf{v_{k-1}} \qquad \text{(Equation 1.56)}$$

γ_k is a scalar constant computed from the gradients at that point and the previous point. In quadratic regions of the surface with M variables then the minimum will be reached in M steps. If the starting configuration is not too far from the minimum then the conjugate gradients method converges more efficiently than the steepest descent method.

1.6.1.2 Second Order Minimisation Algorithms

Second order minimisation methods use both the first and second derivatives of the energy. This means that for a system with 3N Cartesian co-ordinates the vector of 3N

first derivatives and the 3N x 3N second derivative matrix (the force constant matrix) must be computed.

1.6.1.2.1 The Newton-Raphson Method

The simplest second order minimisation method is the Newton-Raphson method. It is based on the multidimensional function:

$$\mathbf{x}_{k+1} = \mathbf{x}_k - V'(\mathbf{x}_k)V''^{-1}(\mathbf{x}_k) \qquad \text{(Equation 1.57)}$$

where $\mathbf{x}_{k+1}$ is the next position vector, $V'(\mathbf{x}_k)$ is the first derivative matrix at $\mathbf{x}_k$, and $V''^{-1}(\mathbf{x}_k)$ is the inverse matrix of the second derivatives. The need to compute this last matrix for each step can be computationally expensive so the Newton-Raphson method is usually restricted to small systems. It is most useful minimising structures that are relatively close to the minimum.

1.6.1.2.2 Adopted Basis Newton Raphson (ABNR)[29]

The ABNR algorithm is a method suitable for application to large systems. Unlike the Newton-Raphson method ABNR does not use the full set of vectors, but instead uses a smaller basis that is limited to the subspace in which the system has made the greatest progress in the previous moves. The second derivative matrix for this subspace is constructed by finite differences from the displacement and first derivative vectors. Newton-Raphson minimisation is then applied in the subspace of the co-ordinates spanned by these displacements.

1.6.2 Transition State Location

Transition state location on a PES is more challenging than finding minimum energy structures because they are more sensitive to the type of step taken by an algorithm. Transition states are first order saddle points that have one negative eigenvalue in the force constant matrix (the hessian). The hessian only has this property in the quadratic region of the PES surrounding the transition state. Some algorithms can only locate a transition state if the initial structure provided is good enough to be within this portion of the energy surface. Other more robust methods have therefore been developed which enable the location of transition structures from starting points further away from the transition state.[30] Several of these methods are briefly described below.

1.6.2.1 Eigenvector Following Algorithm (EF)

The eigenvector following method[31] is composed of the following steps. An initial guess is provided for the position of the transition state. The gradient vector and the hessian matrix are calculated at this point. The hessian is then diagonalised and the number of negative eigenvalues determined. If only one negative eigenvalue is present then this mode is followed, if not an alternative mode can be chosen and followed. The chosen mode is maximised and all others minimised. Steps are taken and the hessian updated after each step until convergence criteria are met. Baker[32] incorporated this algorithm into the Gaussian program, and it is the standard transition state searching method in this program.

1.6.2.2 Conjugate Peak Refinement

The conjugate peak refinement algorithm[33] was proposed as a reliable method for locating transition states for systems with large numbers of atoms on complex energy surfaces. The method needs a continuous energy function and its first derivative, but it does not use the second derivatives. The input consists of the reactant and product structures. A line search is then carried out between these two minima and a maximum located along this line. Lines are then drawn from this point to the two initial minima and the process repeated. In this way further maxima can be located between the reactants and products. Simultaneous minimisation along the conjugate vector for each maximum gives the refined saddle points. CPR is therefore a method that can locate multiple saddle points along a reaction path.

A potential problem with CPR arises if the potential energy surface is not quadratic. In this case the directions of the line minimisations may not be conjugate to the maximisation direction and consequently the algorithm may converge to a minimum rather than a saddle point. To overcome this problem it is necessary to maximise along one conjugate direction and minimise along all others simultaneously. This ensures that the minimisations are all conjugate to the maximisation. This is the approach taken in the P-RFO method.

1.6.2.3 Partial Rational Function Operator (P-RFO)

The P-RFO algorithm constructs a step representing maximisation of one eigenvector of the hessian and minimisation in all other directions. This approach is repeated and leads to a saddle point, i.e. a point where the maximised direction is a stationary maximum and all other directions are stationary minima.

Since only one initial point is defined in the P-RFO method it is not possible to use the approach taken in the CPR method to determine the direction in which to maximise. Instead an eigenvector of the initial hessian is chosen. As the order of the eigenvectors that emerges from matrix diagonalisation routines is dependent only on the magnitude of the eigenvalues it is necessary after each hessian update to confirm that the correct mode is still being followed. This is usually achieved by choosing the mode of the latest step that has the greatest overlap with the mode followed in the previous step. As maximisation in the direction of a mode should reduce the value of the eigenvalue associated with it, then even if the mode is not the lowest one to start with, it will be by the end of the saddle point search.

2. THE ATMOSPHERIC CHEMISTRY OF FORMYL HALIDES

2.1 Introduction

The aim of this chapter is to show the atmospheric relevance of the formyl halides, how they are produced, their atmospheric lifetimes, and the importance of their hydrolysis as a possible degradation mechanism. In order to do this a brief introduction to some features of the atmosphere and the species present within it is necessary.[34]

The earth's atmosphere is separated into regions that have very different properties. The troposphere is the region closest to the earth's surface. It extends for roughly the first 10 –17 km of the atmosphere, with temperatures in the range of 290 – 210 K. In the troposphere the temperature falls with increasing altitude, with the result that cold air lies above warm air. Thus convection currents are established that drive the patterns of wind and weather and lead to the uptake of materials from the surface. At a particular altitude the temperature starts to rise again as a result of absorption of solar radiation. The altitude at which this occurs varies with the season and latitude. This region of the atmosphere is known as the stratosphere, and it extends to an altitude of ~50 km. In the stratosphere warm air lies above cold air, and there are no convection currents to cause mixing.

There is a diffuse boundary between the troposphere and stratosphere called the tropopause. It is within this boundary that the temperature gradient reverses. Trace compounds introduced from the earth's surface may be rapidly transported both vertically and horizontally throughout the troposphere. However, transport of these species across the tropopause and within the stratosphere is much slower. As the

chemical reactions discussed in this thesis only occur in the troposphere and stratosphere, the higher regions of the atmosphere including the mesosphere and the thermosphere will not be considered here.

Organic compounds released into the atmosphere may be removed by several mechanisms. These include physical removal by precipitation ('rain-out'), chemical reaction in the troposphere, transport into the stratosphere, and chemical reaction in the stratosphere. The conditions in the different atmospheric regions generally control the type of mechanism that occurs.[35,36]

In the atmosphere solar radiation of wavelength <190 nm is absorbed before it reaches the stratosphere. The stratosphere itself absorbs ultraviolet light in the wavelength range ~190 – 330 nm. It is ozone that almost completely absorbs the UV radiation between 240 – 290 nm. Consequently, essentially no UV radiation of wavelength <290 nm, which is harmful to life, reaches the earth's surface.

The discovery of the Antarctic ozone hole in 1985[37] confirmed the danger to the atmosphere detected in 1975 by Molina and Rowland,[38] that emissions of man-made chlorofluorocarbon compounds (CFCs) could lead to significant depletion of the ozone layer. The problems with CFCs are caused by their stability and because they are chemically inert. This results in these compounds having exceedingly long atmospheric lifetimes. They can therefore provide a route for the transport of chlorine to the stratosphere. At altitudes higher than the ozone layer CFCs are photolysed, releasing chlorine atoms that catalytically destroy ozone molecules:

$$Cl + O_3 \rightarrow ClO + O_2 \qquad (2.1)$$

$$ClO + O \rightarrow Cl + O_2 \qquad (2.2)$$

The impact of ozone depletion, such as a higher incidence of skin cancer, eventually led the major CFC manufacturers to agree to the phase-out of CFC production. This agreement accelerated the effort to find replacement compounds.

2.2 Sources of Formyl Halides in the Atmosphere

Hydrochlorofluorocarbons (HCFCs) and hydrofluorocarbons (HFCs) were proposed as suitable replacements for CFCs in applications such as refrigeration and air conditioning. These compounds have the appropriate physical and chemical properties for these applications, and were considered viable alternatives to CFCs because they contain at least one hydrogen atom. The presence of hydrogen makes these compounds susceptible to tropospheric degradation initiated by OH radicals present in the troposphere (reaction 2.3), and consequently should make them ineffective vehicles for chlorine transport to the stratosphere.[39,40]

$$CX_3CHYZ + OH \rightarrow CX_3CYZ + H_2O \qquad (2.3)$$

The reaction of HCFCs and HFCs with OH radicals provides the major degradation pathway for these compounds in the troposphere. The reaction has been studied extensively for a large range of HCFC and HFC compounds, and rate constants calculated.[41-52] The typical value of the rate constant for OH radical attack is in the order of $1x\ 10^{-14}$ cm^3 $molecule^{-1}$ s^{-1}.

The hydrogen-atom abstraction (reaction 2.3) yields a haloalkyl radical, which may then add to molecular oxygen to give a haloalkylperoxy radical, e.g. CX_3CYZO_2 (reaction 2.4).

$$CX_3CYZ + O_2 \xrightarrow{M} CX_3CYZO_2 \qquad (2.4)$$

The haloalkylperoxy radical, CX_3CYZO_2, is stabilised by a collision partner M. The reaction is rapid, although the rate constants vary depending on the nature of the substituents.[53-58]

The haloalkylperoxy radicals may react with NO, NO_2 and HO_2 radicals under tropospheric conditions (reactions 2.5 – 2.7)[59-64]

$$CX_3CYZO_2 + NO \rightarrow CX_3CYZO + NO_2 \quad (2.5)$$

$$CX_3CYZO_2 + NO_2 \xrightarrow{M} CX_3CYZO_2NO_2 \quad (2.6)$$

$$CX_3CYZO_2 + HO_2 \rightarrow CX_3CYZOOH + O_2 \quad (2.7)$$

The relative rate constants for the reactions of these species with the CX_3CYZO_2 radicals, and their atmospheric concentrations, make the dominant loss process for the haloalkylperoxy radicals the reaction with NO to form haloalkoxy radicals (reaction 2.5).

The chemistry of the haloalkoxy radical is dependent on the degree of substitution by, and the nature of, the halogen substituents. The potential reaction pathways are given by reactions 2.8 to 2.10.

$$CX_3CYClO \rightarrow CX_3C(O)Y + Cl \quad (2.8)$$

$$CX_3CYZO \rightarrow CX_3 + C(O)YZ \quad (2.9)$$

$$CX_3CHYO + O_2 \rightarrow CX_3C(O)Y + HO_2 \quad (2.10)$$

Experimental studies have provided data on which process is favoured.[65-71] Radicals of the type CX_2ClO (X=H, F, or Cl) eliminate a Cl atom, but when the radical species is CH_2ClO then reaction 2.10 is preferred. CX_3CYZO (X=F, Cl) radicals decompose *via* Cl atom elimination rather than C-C bond fission. CX_3CH_2O (X=H, F, Cl) radicals react either with O_2 to form an aldehyde and a HO_2 radical, or undergo C-C bond

cleavage. CX_3CF_2O radicals undergo C-C bond fission. For CX_3CHYO (Y=Cl, F) radicals the relative importance of the C-C bond fission process and reaction with O_2 is a function of the nature of the substituents.

Carbonyl halides are thus tropospheric degradation products of HCFCs and HFCs. Two classes of carbonyl halide are produced, those that contain a hydrogen atom (CXHO) (hereafter known as formyl halides), and those that do not (CX_2O). The two classes of compound decompose in the troposphere *via* different mechanisms, the decomposition of CXHO molecules is initiated through a chemical reaction whereas degradation of CX_2O species is initiated by photodissociation. This thesis is concerned with the degradation mechanisms of the CXHO class of molecules, and therefore subsequent sections will only describe reactions applicable to these species.

2.3 Degradation Processes for Formyl Halides

The degradation of formyl halides could be initiated by photodissociation, by reaction with hydroxyl radicals, by homogeneous hydrolysis, or by heterogeneous reaction. The photodissociation of CXHO (X=F, Cl) molecules is unlikely to occur in the troposphere. The CClHO[72] and CFHO[73] UV absorption spectra are similar to that of CH_2O,[74] but shifted to shorter wavelengths, with the absorption maximum at 260 nm and 218 nm respectively for CClHO and CFHO. As stated earlier UV radiation of wavelength <290 nm is almost completely absorbed in the stratosphere, and consequently photolytic decay of formyl chloride and fluoride is unlikely to be a major tropospheric degradation process. Photolysis may become a viable process in the lower stratosphere,[75-78] if the tropospheric lifetimes of the formyl halides were long enough for transport to the stratosphere to occur.

The second possible degradation pathway is *via* reaction with OH radicals (reaction 2.11). Libuda *et al.*[72] reported an upper limit to the rate constant of reaction 2.11 for formyl chloride of $<3.2 \times 10^{-13}$ cm^3 $molecule^{-1}$ s^{-1} at 298 K.

$$CXHO + OH \rightarrow XCO + H_2O \qquad (2.11)$$

This led to an estimate of the tropospheric lifetime of >45 days for CClHO with respect to reaction with OH radicals, when atmospheric concentrations of OH were taken into account. CFHO is expected to have a longer lifetime with respect to OH radical reaction, as fluorine strengthens the C-H bond.

The hydrolysis of formyl halides, *via* a homogeneous or heterogeneous process, is the remaining possible tropospheric degradation pathway. Theoretical and experimental studies have been reported for the gas phase hydrolysis of formyl fluoride and chloride. Libuda *et al.*[72] derived an upper limit to the rate constant for reaction 2.12 for formyl chloride of $<5 \times 10^{-22}$ cm^3 $molecule^{-1}$ s^{-1}. Thus the reaction is slower than reaction with OH radicals, but due to the much larger concentration of water in the troposphere they estimate a tropospheric lifetime of <2 hours for CClHO with respect to the reaction with water vapour.

$$CXHO + H_2O \rightarrow HX + HCO_2H \qquad (2.12)$$

It has not been possible to locate analogous data for formyl fluoride hydrolysis, but it should exhibit similar behaviour to CClHO. Hydrolysis should therefore provide an efficient degradation process for formyl halides.

The mechanism of reaction 2.12 is not fully understood, but a possible mechanism is written as equations 2.13 and 2.14.

$$CXHO + H_2O \rightarrow CXH(OH)_2 \qquad (2.13)$$

$$CXH(OH)_2 \rightarrow HX + HCO_2H \qquad (2.14)$$

The activation barrier for the initial addition of a single water molecule is ~43 kcal mol^{-1} in the gas phase, with only minor halogen substituent effects.[79] A different theoretical study examined the same addition process for formaldehyde and found that it was catalysed by the participation of a second water molecule.[80] It was therefore postulated that formyl halide hydrolysis may occur rapidly in contact with a water droplet.

Investigating the gas phase hydrolysis reaction experimentally has proven difficult due to competing processes, such as reaction of the formyl halide with water on the reaction chamber walls. The aim of this thesis is therefore to attempt to elucidate the reaction mechanism for formyl halide hydrolysis using theoretical methods. The reaction has been studied in the gas phase as a bimolecular and termolecular process, and as a condensed phase process occurring within a water droplet.

3. GAS PHASE BIMOLECULAR HYDROLYSIS OF FORMYL CHLORIDE

3.1 Introduction

The atmospheric relevance of the formyl halides CXHO (where X=F,Cl) and the importance of their hydrolysis as a degradation pathway have been discussed in Chapter 2. The simplest way to view the hydrolysis reaction is as a bimolecular process occurring in the gas phase, i.e. one CXHO molecule reacting with one water molecule to yield products. This was the approach taken in a previous theoretical study where reactions **3-a** to **3-g** (Figure 3.1) were examined by *ab initio* molecular orbital theory with electron correlation for the X=H, F and Cl cases.[79]

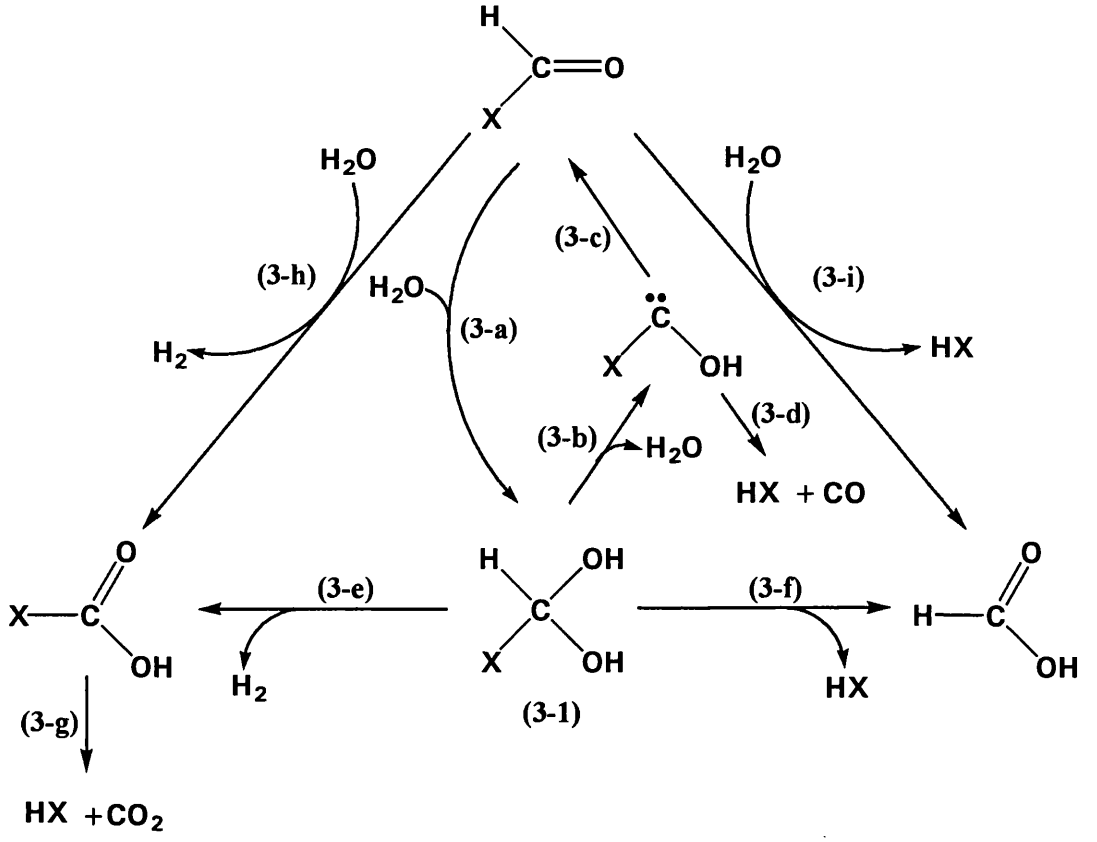

Figure 3.1

In the earlier investigation Francisco and Williams assumed that the conformation of the $CXH(OH)_2$ tetrahedral intermediate **3-1** produced by the addition of H_2O to CXHO was

independent of the nature of the substituent X for those substituents they considered. The $CXH(OH)_2$ species reported was based on the conformer obtained from the initial addition of water to formaldehyde. It appears that the intermediate for the X=F and Cl cases was then presumed to have this same conformation. It was also assumed that the decomposition of the diol adduct could proceed without any conformational changes in its geometry.

In this chapter the bimolecular hydrolysis of formyl chloride is described more fully using *ab initio* molecular orbital calculations. The geometries of stable conformers of the $CClH(OH)_2$ intermediate, their relative energies and the barriers to their interconversions are reported. Reactions **3-a**, **3-e**, and **3-f** (Figure 3.1) have been re-examined, transition structures have been located and intrinsic reaction co-ordinate (IRC) calculations performed upon them. These calculations have made it possible to determine whether the $CClH(OH)_2$ conformer reported as the intermediate for the hydrolysis by Francisco and Williams was correct, and also if a conformational change would be required before the decomposition could proceed.

In the previous study of the hydrolysis it was also assumed that the reaction had to proceed through the $CXH(OH)_2$ tetrahedral intermediate, and that the one step direct eliminations **3-h** and **3-i** (Figure 3.1) would not occur. Investigations of the direct elimination of H_2 and HCl have therefore been included in this chapter. Transition structures have been located for both reactions and are presented along with a comparison of the energetics between the one and two step processes. The penultimate section of this chapter is an overview of the bimolecular hydrolysis of formyl chloride and is followed by a conclusion.

3.2 Methods

The mechanism of the gas phase bimolecular hydrolysis of formyl chloride has been examined using *ab initio* molecular orbital calculations available in the Gaussian 92[81] suite of programs. All species were optimised at the Hartree-Fock level of theory with the 6-31G* basis set (denoted HF/6-31G*). The minima and transition states were characterised by determination of their harmonic vibrational frequencies. Intrinsic reaction co-ordinate (IRC) calculations were performed to determine the nature of the reactant and product species. Single point energy calculations using second order Møller-Plesset perturbation theory with the core orbitals frozen and the 6-311+G(d,p) basis set were carried out on the HF/6-31G* optimised geometries (denoted MP2(fc)/6-311+G**//HF/6-31G*).

3.3 Results and Discussion

3.3.1 The Conformers of the $CClH(OH)_2$ Intermediate

The $CClH(OH)_2$ adduct (**3-1**) formed as the product of reaction **3-a** (Figure 3.1) is a molecule that can exist as a number of stable conformers which are simple rotamers of one another. The nature of the functional groups present in this molecule result in the relative stabilities and geometries of its conformers being influenced by the anomeric effect, therefore a brief description of this effect is given below.

3.3.1.1 The Anomeric Effect

The anomeric effect is usually defined as the preference of electronegative substituents for the axial configuration at the anomeric centre of a pyranose ring,[82] as shown in Figure 3.2.

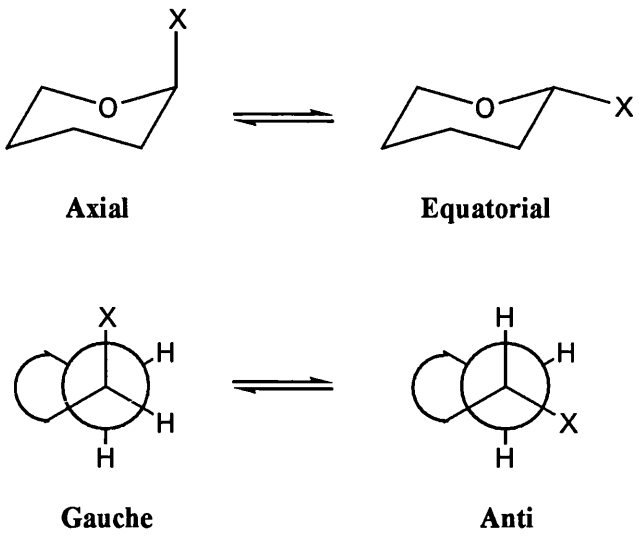

Figure 3.2

This type of effect can also be observed in acyclic compounds. Lemieux[83] and Eliel[84] termed the general preference for the gauche conformation about a carbon-hetero atom bond in R-X-C-Y systems as the generalised anomeric effect but it can also include systems where the central atom is something other than carbon.[85,86]

Many varieties of systems have been studied using both experimental and computational methods.[87-89] It has been determined that the anomeric effect does not only influence the relative stabilities of the conformers of a compound but also significantly affects their geometries. Several trends in the differences from standard bond lengths and angles have been observed. However for the purposes of this thesis discussion is restricted to those trends directly applicable to the compounds in this chapter.

It has been shown that for $X\text{-}CH_2\text{-}Y$ molecules where X and Y are identical, *e.g.* methanediol, there is a shortening in both the C-X and C-Y bond lengths relative to the C-X bond length in $X\text{-}CH_3$. There is also a marked conformational dependence on the

variation in these bond lengths and the X-C-Y bond angle. The expected stabilisation of the gauche versus anti conformers has been observed.[90-94]

Compounds of the type R-O-CH_2-X show a slightly different pattern. When X is a halogen atom the C-O bonds are shorter and the C-X bonds longer than standard values. This lengthening of the C-X bond only occurs when the halogen is in an axial position for a cyclic molecule or there is a gauche conformation about the RO-CX bond for acyclic species.[95-98]

In much of the literature fluorine has been chosen as the X atom and doubts remained about whether second row elements, including chlorine, would show similar behaviour. However a theoretical investigation by Schleyer *et al.*[99] where molecules containing second row elements were studied showed that for $HOCH_2X$ where X=Cl there was an appreciable stabilisation energy for the gauche conformer. This molecule is a model for α-chlorinated ethers where experimental data revealed the preference for gauche conformations.[100]

3.3.1.2 The Stereoelectronic Basis for the Anomeric Effect

Explanations for the basis of the anomeric effect have evolved over the past four decades as the range of compounds exhibiting the stabilisation of gauche conformations and geometrical distortions due to this type of stereoelectronic effect has expanded.[101,102] The explanation for the origin of the effect which best accounts for the bond length changes and conformational preferences observed is negative hyperconjugation.[103,104]

The simplest example to illustrate this principle is FCH_2F. Representations of the molecular orbitals of relevance in this molecule are shown in Figure 3.3. The three p-orbitals of the carbon atom are divided as follows. Two are principally involved in σ-bonds with the two fluorine atoms resulting in two $\sigma_{C\text{-}F}$ bonding and two $\sigma^*_{C\text{-}F}$ antibonding orbitals (one of each is shown). The third orbital, denoted p_z, is involved in bonding the two hydrogen atoms of the CH_2 group (as in π_1 and π_3) but also has the correct symmetry to undergo π-type overlap with the p_z lone pairs on the fluorine atoms. This results in a significant π-contribution to bonding in the CF_2 group (referred to as n-π* overlap), and leads to shorter and stronger C-F bonds than in monosubstituted alkyl fluorides.

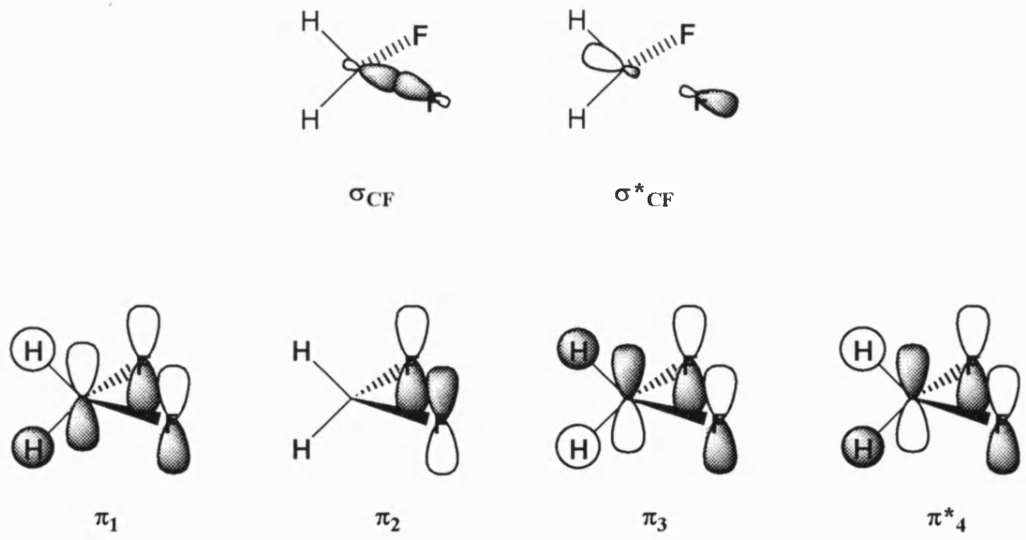

Figure 3.3

In addition to the above π-type overlap the p-type lone pairs of the fluorine atoms lying in the FCF plane have the correct symmetry for overlap with the σ-orbitals of the other C-F bond (Figure 3.4).

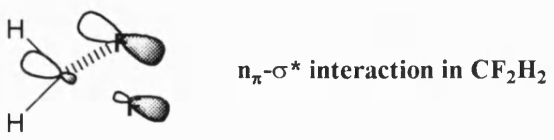

Figure 3.4

This interaction with the $\sigma^*_{C\text{-}F}$ orbital (n-σ^* overlap) is also stabilising. Calculations by Wolfe *et al.* suggest that the n-σ^* stabilisation is larger due to the relative energies of the σ^* and π^* orbitals.[105]

It is relatively simple to extend this principle to $ROCH_2X$ systems. The major difference being that oxygen has only one non-bonding pair of p-type electrons compared to two in fluorine. This lone pair is significantly higher in energy than those of fluorine and can therefore be expected to be a more effective π-donor with adjacent orbitals of the correct symmetry. The antibonding $\sigma^*_{C\text{-}O}$ orbital is also higher in energy than $\sigma^*_{C\text{-}F}$ and is thus a poorer acceptor. These properties mean that oxygen acts predominantly as a π-donor with the carbon-halogen system as the acceptor. However the conformation around the RO-CX bond determines the efficiency and mechanism of the donor-acceptor process (Figure 3.5).

n_π-π^* interaction in $ROCH_2X$ **n_π-σ^* interaction in $ROCH_2X$**

(3-2) **(3-3)**

Figure 3.5

The R-O-C-X system needs to be planar for n-π^* overlap and the staggered conformer **3-2** with a 180° ROCX dihedral angle is likely to be preferred. If n-σ^* donation is to occur a rotation of 90° about the C-O bond resulting in conformer **3-3** is required. Since this n-σ^* interaction is dominant in CH_2F_2, and oxygen is a better donor and poorer $\sigma^*_{C\text{-}O}$ acceptor than F, then the expected most important lone pair interaction in $ROCH_2X$ is n-$\sigma^*_{C\text{-}X}$. This would then result in a preference for conformer **3-3** over **3-2**.

The extent of π-donation interactions to bonding in $CH_2(OR)_2$ species is similarly dependent on the conformation about the two C-O bonds. Different conformers result in n-π* or n-σ* interactions dominating the bonding (Figure 3.6). In conformation **3-4** the n-π* overlap is optimal but n-σ* interactions are not possible. In conformer **3-5** n-σ* overlap is now possible across one C-O bond but the extended π-system of **3-4** has disappeared and as a consequence the other C-O bond has minimal π-character. The final conformation **3-6** has a dihedral angle of 90° about both C-O bonds and therefore n-σ* overlap is possible across both C-O bonds, however n-π* is prevented.

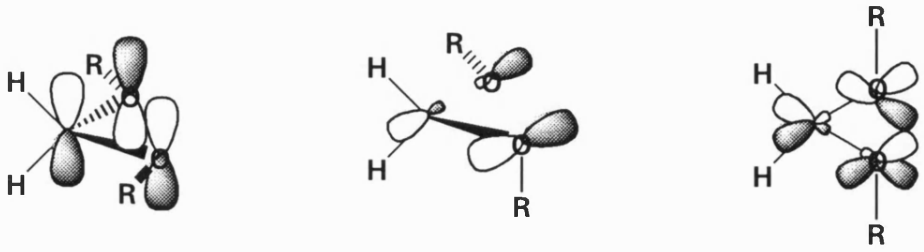

(3-4) **(3-5)** **(3-6)**

Figure 3.6

The compounds discussed in this section have been selected to provide insight into the trends in the relative stabilities and geometric distortions that have been observed in the current study of the conformers of $CClH(OH)_2$, the tetrahedral intermediate of the hydrolysis reaction of formyl chloride.

3.3.2 Relative Energies of the $CClH(OH)_2$ Conformers

The naming convention for the $CClH(OH)_2$ conformers is presented in Figure 3.7. They have been named according to the approximate values of their two HOCCl dihedral angles. This convention will be used throughout the remainder of this thesis.

Define dihedrals:

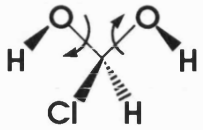

Left: HOCCl=0°
Right: HOCCl=0°

Therefore name of diol = $(\theta_{Left},\theta_{Right})$ = (0,0)

Figure 3.7

The four minimum energy species located for $CClH(OH)_2$ at the HF/6-31G* level of theory are shown in Figure 3.8. Their total and relative energies are reported in Table 3.1, and the most important features of their geometries in Table 3.2.

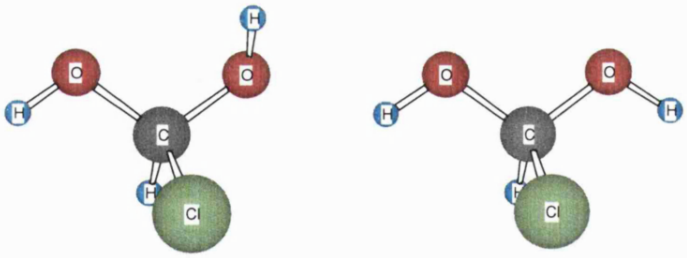

(-60,-60) **(-60,+60)**

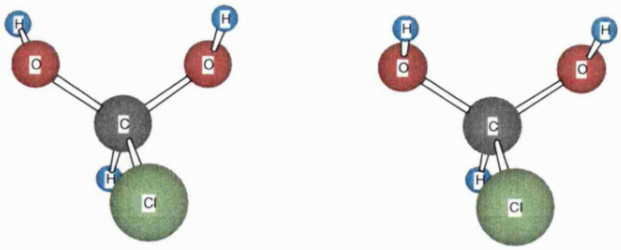

(180,-60) **(+60,-60)**

Figure 3.8

Table 3.1 - Total and Relative Energies of $CClH(OH)_2$ Conformers

Species	HF/6-31G*			MP2(fc)/6-311+G**//HF/6-31G*		
	Total (Hartrees)	Relative (kJ mol^{-1})	ZPVE (kJ mol^{-1})	Total (Hartrees)	Relative (kJ mol^{-1})	Relative + ΔZPVE (kJ mol^{-1})
(-60,-60)	-648.80764	0	137	-649.59708	0	0
(-60,+60)	-648.80172	16	136	-649.59154	15	14
(180,-60)	-648.80533	6	137	-649.59552	4	4
(+60,-60)	-648.80542	6	136	-649.59463	6	5

The lowest energy conformer is the (-60,-60) species. The (180,-60) and (+60,-60) conformers have similar energies and are 4 and 5 kJ mol^{-1} higher in energy respectively than the (-60,-60) species. The (-60,+60) conformer has the highest relative energy at 14 kJ mol^{-1}.

The $CClH(OH)_2$ molecule has three electronegative atoms connected through a single carbon atom. It is very similar to the CH_2X_2, $ROCH_2X$, and $CH_2(OR)_2$ cases described in section 3.3.1.2 and as such the energy differences between the four conformers should be the result of the anomeric effect. The three electronegative substituents are in competition with one another and as a consequence the relative energies of the conformers may be different to those cases described in the previous section.

Table 3.2 - HF/6-31G* Optimised Geometries of the $CClH(OH)_2$ Conformers[a]

Co-ordinate	(-60,-60)	(-60,+60)	(180,-60)	(+60,-60)
CCl	1.842	1.851	1.792	1.827
CO^L	1.361	1.348	1.371	1.357
CO^R	1.342	1.347	1.360	1.357
O^LCCl	108.9	110.5	106.1	109.4
O^RCCl	111.1	110.5	111.5	109.4
H^LO^LCCl	-50.7	-58.3	-178.7	53.8
H^RO^RCCl	-72.8	58.8	-61.0	-53.8

[a] Bond lengths in Angstroms, angles in degrees.
[L] Atom on 'left hand side' of molecule as defined in Figure 3.7.
[R] Atom on 'right hand side' of molecule as defined in Figure 3.7.

The (-60,-60) conformer has two gauche interactions about the HO-CCl bonds and one gauche interaction about a HO-CO bond. This arrangement allows the possibility of n-σ* overlap across both HO-CCl bonds and across one HO-CO bond. As oxygen has only one non-bonding pair of electrons the n-σ* interactions that dominate will therefore be dependent on the relative π-donor and acceptor abilities of oxygen and chlorine. Oxygen is a good π-donor and chlorine a good π- acceptor so the geometry of the (-60,-60) conformer would be expected to show lengthening of the C-Cl bond. It is also expected that the C-O bonds would both be shorter than standard values but that the HO-CO bond with the gauche interaction would be slightly shorter again. The bond lengths in Table 3.2 show that this is indeed the case.

The (-60,+60) conformer again has two gauche interactions about the HO-CCl bonds but has no gauche interactions about the HO-CO bonds. This conformer is symmetrical and therefore it is expected that its geometry should have both C-O bonds the same length but shorter than standard values, as well as a longer C-Cl bond than usual. These trends are again clearly visible in the geometry of the (-60,+60) shown in Table 3.2.

The (180,-60) species has only one gauche interaction about a HO-CCl bond but has two gauche interactions about the HO-CO bonds. The consequence of this arrangement is the possibility of n-σ^* overlap across both HO-CO bonds and across one HO-CCl bond. The result being short C-O bonds with the bond gauche to the C-Cl bond slightly shorter than the other, and a small increase in C-Cl bond length that is less than for the (-60,-60) and (180,-60) conformers.

The (+60,-60) conformer has gauche interactions about both HO-CCl bonds and about both HO-CO bonds. It may be expected that the stabilisation resulting from the four potential n-σ^*overlaps would make this the lowest energy conformer. However this arrangement introduces destabilising 1,3-diaxial type interactions between the two hydroxyl groups which cancel out some of the energy gains. The C-O bond lengths show the predicted shortening and are equivalent due to the symmetry of this conformer. The C-Cl bond also shows the anticipated lengthening compared to standard values.

The relative energies of these four conformers indicate that gauche interactions about the HO-CCl bonds provide greater stabilisation to the molecule than the same type of interactions about HO-CO bonds. This is probably due to the greater effectiveness of the $\sigma^*_{C\text{-}Cl}$ orbital as a π-acceptor compared with the $\sigma^*_{C\text{-}O}$ orbital. However as the (-60,+60) conformer has the highest relative energy and yet still has two gauche interactions about the HO-CCl bonds it would appear that gauche interactions about the HO-CO bonds still provide significant stabilisation.

A further potentially conformationally dependent factor that could affect the relative energies of these conformers is that of intramolecular hydrogen bonding. This would be

feasible within the (-60,-60), (180,-60), and (+60,-60) conformers with one, two and two intramolecular hydrogen bonds respectively between the hydroxyl groups. The formation of the same type of hydrogen bonds is prevented in the (-60,+60) conformer due to the relative positions of the protons of the hydroxyl groups. This provides a further possible explanation for the much higher energy of the (-60,+60) species compared to the small differences amongst the other conformers.

3.3.3 Interconversions of the $CClH(OH)_2$ Conformers

An extra aspect to this investigation has been the study of the interconversion pathways that link the minimum energy conformers. Although $CClH(OH)_2$ is not a chiral molecule many of its individual conformers do have distinct non-superimposable mirror images. This study has therefore concentrated on the interconversions between one set of $CClH(OH)_2$ conformers and the pathway which links the (-60,-60) conformer and its mirror image (+60,+60).

Six transition state conformers of $CClH(OH)_2$ have been located that link the minimum energy rotamers discussed in the previous section and are shown in Figure 3.9. These transition states are predominantly species in which one hydroxyl group eclipses either the C-Cl or C-H bond. The exception to this is the [180,180] species where the hydroxyl groups eclipse each other.

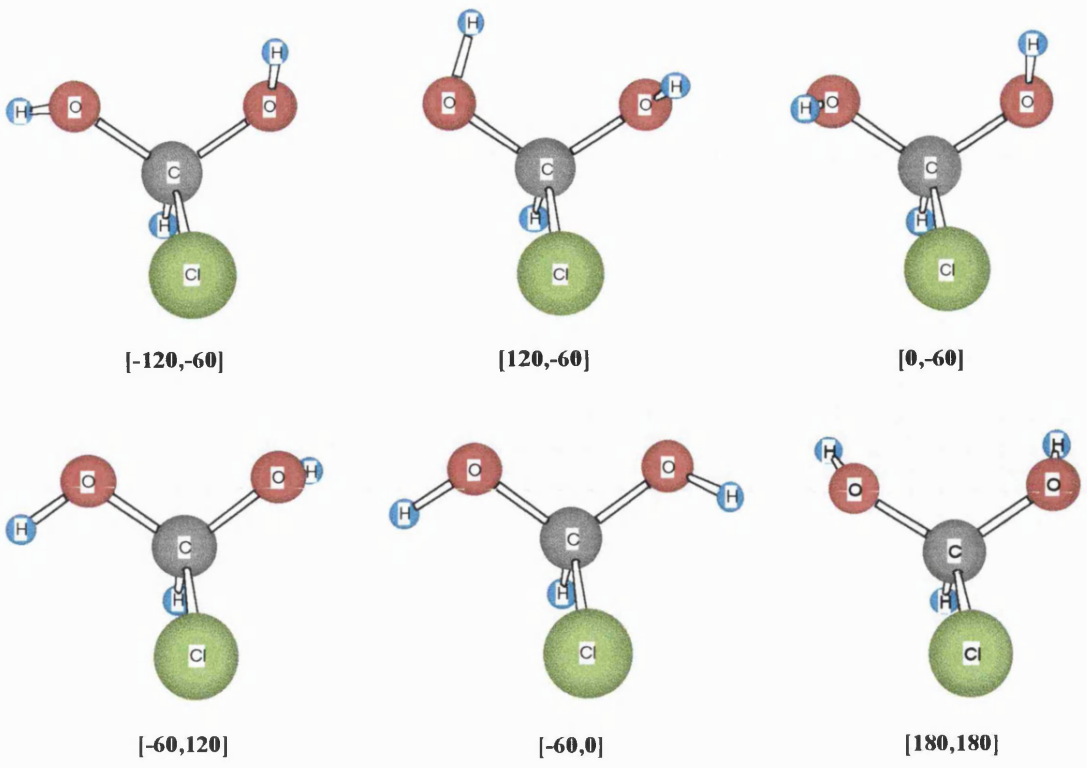

Figure 3.9

The total and relative energies of the transition states are given in Table 3.3, and the most significant features of their geometries in Table 3.4.

Table 3.3 - Total and Relative Energies of the Transition States for the Interconversions of the $CClH(OH)_2$ Conformers

Species	HF/6-31G*			MP2(fc)/6-311+G**//HF/6-31G*		
	Total (Hartrees)	Relative[b] (kJ mol^{-1})	ZPVE (kJ mol^{-1})	Total (Hartrees)	Relative[b] (kJ mol^{-1})	Relative[b] + ΔZPVE (kJ mol^{-1})
[-60,120]	-648.79823	25	135	-649.58914	21	19
[-60,0]	-648.80028	19	135	-649.59048	17	15
[-120,-60]	-648.80325	12	135	-649.59335	10	8
[120,-60]	-648.80293	12	135	-649.59213	13	11
[0,-60]	-648.80495	7	135	-649.59434	7	5
[180,180]	-648.79322	38	134	-649.58499	32	29

[b] Energies relative to the (-60,-60) conformer of $CClH(OH)_2$.

Table 3.4 - HF/6-31G* Optimised Geometries of the Interconversion Transition State $CClH(OH)_2$ Conformers[c]

Co-ordinate	[-60,120]	[-60,0]	[180,180]
CCl	1.816	1.840	1.769
CO^L	1.360	1.350	1.372
CO^R	1.354	1.355	1.372
O^LCCl	110.0	110.6	107.2
O^RCCl	109.0	110.2	107.2
H^LO^LCCl	-50.7	-69.7	196.1
H^RO^RCCl	130.6	10.2	-196.9

Co-ordinate	[-120,-60]	[120,-60]	[0,-60]
CCl	1.813	1.811	1.830
CO^L	1.367	1.365	1.367
CO^R	1.353	1.364	1.350
O^LCCl	107.8	108.7	108.9
O^RCCl	110.4	110.2	110.6
H^LO^LCCl	-123.9	124.4	14.6
H^RO^RCCl	-70.0	-39.6	-74.2

[c] Bond lengths in Angstroms, angles in degrees; L and R superscripts represent left and right respectively.

These conformers exhibit the same conformationally dependent trends in bond lengths and angles as the minimum energy rotamers. The [180,180] conformer has the highest relative energy and this is likely to be because it has no gauche interactions about the HO-CCl bonds and the two stabilising HO-CO gauche interactions are offset by the 1,3-diaxial interactions of the hydroxyl groups.

Figure 3.10 shows the interconversion pathways of the conformers, with the reaction and activation energies for these interconversions reported in Table 3.5. The reaction pathways are then discussed.

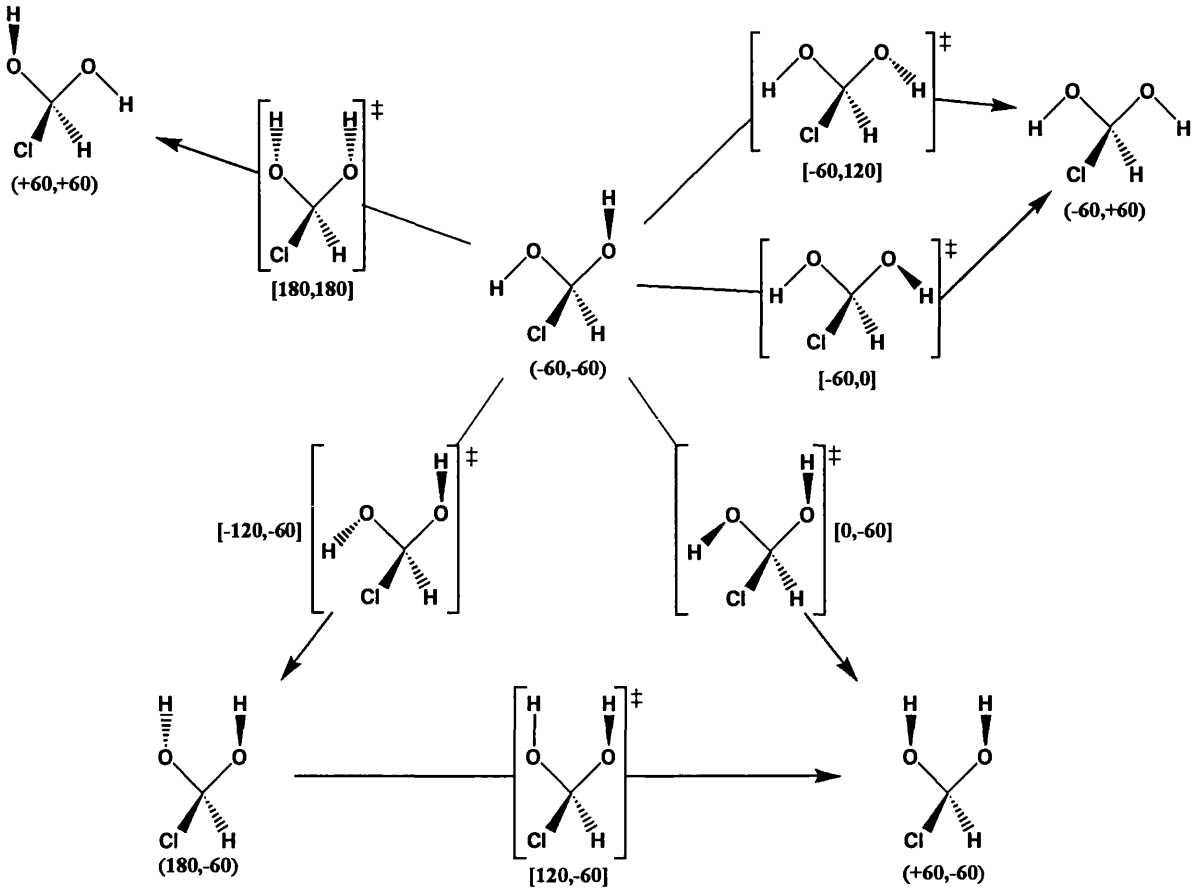

Figure 3.10

The conversion from the (-60,-60) to the (-60,+60) conformer can occur *via* the [-60,120] or [-60,0] transition states. The activation energies for these processes are 19 and 15 kJ mol^{-1} respectively, and the enthalpy of reaction at 0 K is 14 kJ mol^{-1}. The two routes are possible due to the symmetry of the (-60,+60) rotamer.

The (-60,-60), (180,-60), and (+60,-60) conformers are similar in energy with small energy barriers between them. They are connected by the [-120,-60], [120,-60], and [0,-60] transition states respectively. The (+60,-60) conformer is symmetrical and is common to both sets of mirror image rotamers. A low energy route between the sets of conformers therefore exists as a result of these interconversions.

The conversion of the lowest energy conformer, (-60,-60), to its mirror image, (+60,+60), occurs *via* the [180,180] transition state with an activation energy of 29 kJ mol^{-1} at 0 K. This is the largest energy barrier of any of the interconversions between the diol conformers. The likely explanation for this higher barrier is that rotation has to occur about both O-H bonds to effect the transformation from (-60,-60) to its mirror image (+60,+60) whereas for the other interconversion processes rotation need only occur about a single O-H bond. The transition state is symmetrical and this process also creates a pathway between the two sets of mirror image conformers.

Table 3.5 - Reaction and Activation Energies (kJ mol^{-1}) for the Interconversion Pathways of the $CClH(OH)_2$ Conformers

Reaction Process	HF/6-31G*	MP2(fc)/6-311+G** //HF/6-31G*	ΔZPVE	MP2(fc)/6-311+G** //HF/6-31G*+ ΔZPVE
(-60,-60) → (-60,+60)	16	15	-1	14
(-60,-60) → [-60,120]	25	21	-2	19
(-60,-60) → [-60,0]	19	17	-2	15
(-60,-60) → (180,-60)	6	4	0	4
(-60,-60) → [-120,-60]	12	10	-2	8
(180,-60) → (+60,-60)	0	2	-1	1
(180,-60) → [120,-60]	6	9	-2	7
(-60,-60) → (+60,-60)	6	6	-1	5
(-60,-60) → [0,-60]	7	7	-2	5
(-60,-60) → (+60,+60)	0	0	0	0
(-60,-60) → [180,180]	38	32	-3	29

Figure 3.11 is a two-dimensional representation of the potential energy surface for $CClH(OH)_2$ and shows the relative energies and interconverions of the rotamers. All the energies given have been calculated at the MP2(fc)/6-311+G** level of theory and include the zero point vibrational energy. The values in parentheses represent the

relative energies of the minima and those in square brackets the relative energies of the transition states. The '*' symbol indicates that the conformer is a mirror image of another species present on the map.

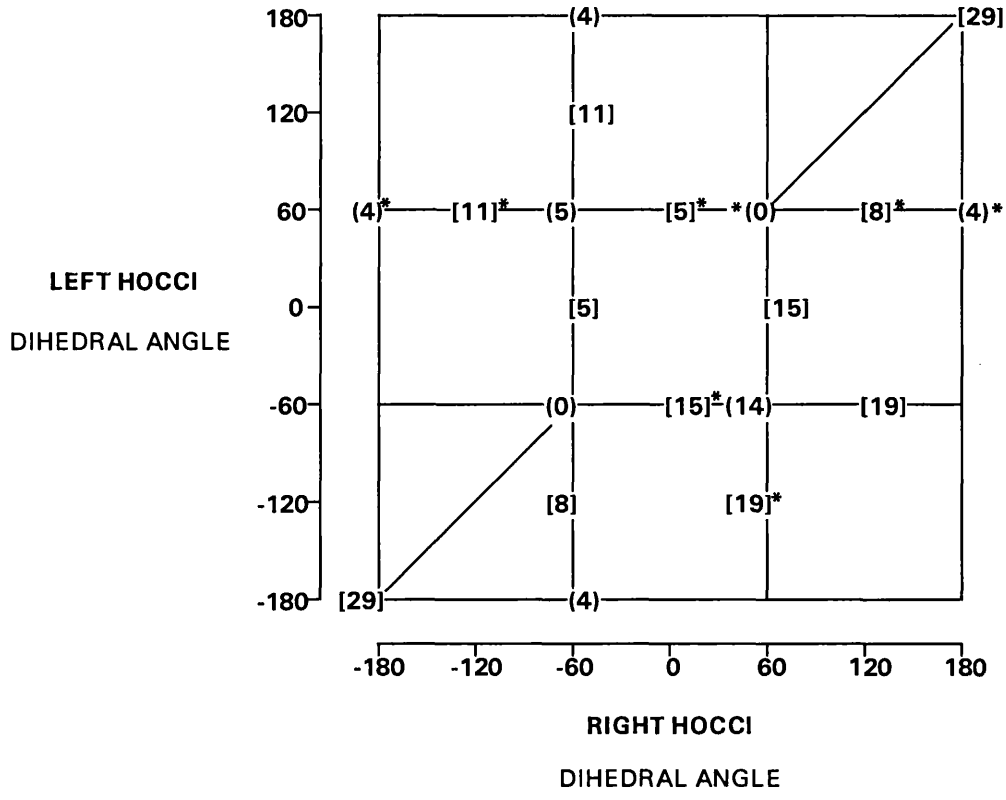

Figure 3.11

It is interesting to note that the (-60,180) conformer of $CClH(OH)_2$ does not exist on the HF/6-31G* potential energy surface. As it was not clear why this should be the case an attempt was made to locate this species at a higher level of theory to see if electron correlation would affect this result. The MP2(full)/6-311+G** level of theory was used but the (-60,180) conformer could not be located as a fully optimised structure.

The maximum energy species of $CClH(OH)_2$ was the (0,0) conformer (not shown). This conformer was a second order maximum on the potential energy surface and so was not fully optimised as it did not provide a low energy path between the conformers.

The $CClH(OH)_2$ conformers have been studied in order to provide insight into the hydrolysis reaction of CClHO. The following sections will therefore relate these conformers and their interconversions to the overall reaction scheme.

3.3.4 $CClHO + H_2O \rightarrow CClH(OH)_2$: Intermediate Formation

In the original study by Francisco and Williams a single transition structure was reported for the addition of a water molecule to CClHO to form the $CClH(OH)_2$ tetrahedral intermediate. This reaction has been re-examined and an additional transition state located at the HF/6-31G* level of theory. Three-dimensional representations of both structures are shown in Figure 3.12. The atom distances are given in Ångstroms.

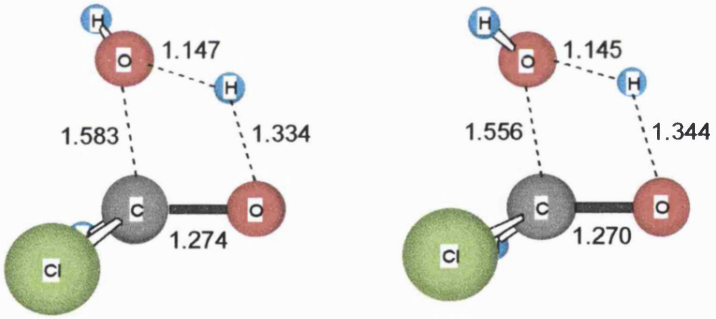

[TS 3-1] [TS 3-2]

Figure 3.12

[TS 3-2] is the transition state located by Francisco and Williams, whilst [TS 3-1] is the additional structure found during the current investigation. The significant parts of their optimised geometries are shown in Table 3.6, and their total and relative energies are reported in Table 3.7.

Table 3.6- HF/6-31G* Optimised Geometries of the Transition States for the Addition of H_2O to CClHO[d]

Co-ordinate	[TS 3-1]	[TS 3-2]
CO	1.582	1.556
CO'	1.274	1.270
O'H'	1.334	1.344
CCl	1.781	1.817
O'CO	94.7	95.5
H'O'C	77.4	77.0
HOC	113.9	114.5
H'O'CO	0.2	3.1
HOCO'	108.7	-115.0

[d] Bond lengths in Angstroms, angles in degrees.

[TS 3-1] and [TS 3-2] each contain a nearly coplanar four-membered ring and have very similar structures. The major difference in their geometries arises from the relative position of the non-transferred hydrogen atom of the water molecule. This hydrogen is 'trans' in [TS 3-1] and 'cis' in [TS 3-2] with respect to the chlorine atom. The hydrogen bonding interaction possible between this proton and the chlorine in [TS 3-2] stabilises this species by 9 kJ mol^{-1} at 0 K compared to [TS 3-1].

IRC calculations have been performed from each of these transition structures to determine whether they led to the same conformer of the intermediate. This indeed proved to be the case because both pathways led to the lowest energy (-60,-60) conformer of $CClH(OH)_2$. This finding contradicted the earlier results of Francisco and Williams. In their study, at the same level of theory, the geometry reported for the tetrahedral intermediate for X=Cl was the (180,-60) conformer. The explanation for this discrepancy may simply be that the earlier study investigated the hydrolysis of CXHO where X=H, F and Cl. The IRC calculations may only have been carried out on the

formaldehyde species for which the equivalent of the (180,-60) conformer had the lowest energy of the possible intermediate structures. The problem may then have resulted because the formyl halides would not necessarily exhibit the same behaviour as formaldehyde.

Table 3.7 - Total and Relative Energies for Species Involved in the CClHO + H_2O $\rightarrow$ $CClH(OH)_2$ Reaction

	HF/6-31G*			MP2(fc)/6-311+G**//HF/6-31G*		
Species	Total (Hartrees)	Relative (kJ mol^{-1})	ZPVE (kJ mol^{-1})	Total (Hartrees)	Relative (kJ mol^{-1})	Relative + ΔZPVE (kJ mol^{-1})
CClHO + H_2O	-648.79236	0	115	-649.59046	0	0
[TS 3-1]	-648.70466	230	120	-649.52079	184	187
[TS 3-2]	-648.70934	218	121	-649.52462	173	178
(-60,-60)	-648.80764	-40	137	-649.59708	-17	2

The enthalpy of reaction at 0 K for this addition is close to thermoneutral at 2 kJ mol^{-1}. The activation energies are large at 187 and 178 kJ mol^{-1} at 0 K respectively for [TS 3-1] and [TS 3-2]. The imaginary frequencies corresponding to the reaction co-ordinate vibrational mode are very similar at 2068i cm^{-1} for [TS 3-1] and 2055i cm^{-1} for [TS 3-2].

The reverse reaction, elimination of H_2O, occurs preferentially *via* the breakage of the O^R-H^R and C-O^L bonds of the (-60,-60) conformer. The transfer of this proton between the two oxygen atoms is facilitated by the hydrogen bond interaction present between the H^R and O^L atoms.

3.3.5 Decomposition of the $CClH(OH)_2$ Intermediate

The decomposition of the $CClH(OH)_2$ diol *via* elimination of HCl and H_2 has also been re-examined. It has been found that decomposition can occur from either the (-60,-60) or the symmetrical (-60,+60) conformer (see Figure 3.8). The possible decomposition mechanisms for each of these conformers are discussed below.

3.3.5.1 Decomposition of the (-60,-60) Conformer of $CClH(OH)_2$

The unimolecular decomposition of the (-60,-60) conformer can occur *via* elimination of HCl or H_2. The elimination of HCl is the lower energy path by a considerable margin. The transition states for these elimination processes are shown in Figure 3.13, their geometries in Table 3.8, and their total and relative energies are reported in Table 3.9. The atom distances are given in Angstroms.

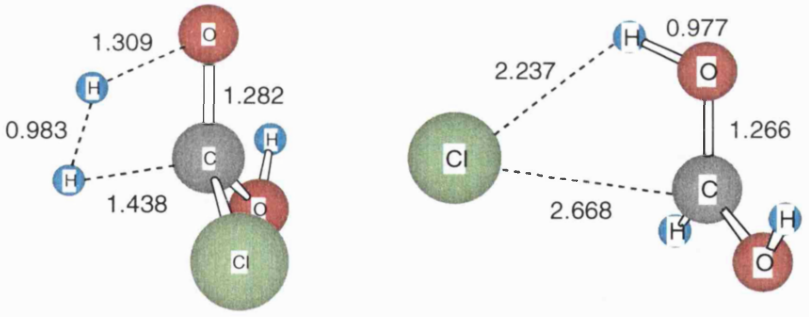

[TS 3-3] [TS 3-4]

Figure 3.13

Table 3.8 - HF/6-31G* Optimised Geometries of the Transition States for 1,2-Elimination Reactions from the (-60,-60) Conformer of $CClH(OH)_2$[e]

Co-ordinate	[TS 3-3]	Co-ordinate	[TS 3-4]
CO	1.282	CCl	2.668
CO'	1.316	CO	1.266
OH	1.309	OH	0.977
CH"	1.438	CO'	1.265
HOC	64.7	OCCl	84.3
H"CO	99.3	HOC	107.2
HOCO'	113.3	HOCCl	-22.2
H'O'CO	-12.7	O'COCl	-129.0
H"COH	1.0	H'O'CO	12.4

[e] Bond lengths in Angstroms, angles in degrees.

The decomposition route through [TS 3-3] yields H_2 and chloroformic acid (ClC(O)OH) in its most stable conformation where HOCO=0°. Examination of the bond lengths in the transition state shows that the 1,2-elimination of H_2 is a concerted process with both the O-H bond and C-H" largely broken and the formation of the H-H" bond advanced at the HF/6-31G* level of theory.

The 1,2-elimination of HCl *via* [TS 3-4] results in the formation of formic acid (HC(O)OH), again in its more stable conformer with HOCO=0°. [TS 3-4] shows marked variations in geometry to [TS 3-3]. In this process the O-H bond stays basically intact but the C-Cl bond is largely broken in the transition state. These differences are caused by chlorine being a much better leaving group than a hydrogen atom, hence the breakage of the C-Cl bond in [TS 3-4] before the abstraction of the proton to eliminate HCl.

Both decomposition routes feature four-centre transition states. However due to the nature of the eliminated products the values of imaginary frequencies associated with the reaction co-ordinates are markedly dissimilar. Elimination of H_2 has an imaginary frequency of 2728i cm^{-1} and elimination of HCl an imaginary frequency of 180i cm^{-1} corresponding to the reaction co-ordinate.

Table 3.9 - Total and Relative Energies for Species Involved in the Decomposition of the (-60,-60) Conformer of $CClH(OH)_2$

	HF/6-31G*			MP2(fc)/6-311+G**//HF/6-31G*		
Species	Total (Hartrees)	Relative (kJ mol^{-1})	ZPVE (kJ mol^{-1})	Total (Hartrees)	Relative (kJ mol^{-1})	Relative + ΔZPVE (kJ mol^{-1})
(-60,-60)	-648.80764	0	137	-649.59708	0	0
[TS 3-3]	-648.63584	451	109	-649.45910	362	337
[TS 3-4]	-648.77811	78	134	-649.55107	121	118
$H_2 + ClCO_2H$	-648.79028	46	100	-649.58110	42	9
$HCl + HCO_2H$	-648.82229	-38	116	-649.60474	-20	-39

The elimination of H_2 has an enthalpy of reaction of 9 kJ mol^{-1} at 0 K. The energy barrier to this reaction is 337 kJ mol^{-1} which is prohibitively large. It is therefore unlikely that $CClH(OH)_2$ would decompose through this pathway. Elimination of HCl is a much lower energy decomposition route. It has an energy barrier of 118 kJ mol^{-1} at 0 K, and is exothermic with an enthalpy of reaction of –39 kJ mol^{-1}. This pathway is therefore likely to be preferred.

3.3.5.2 Decomposition of the (-60,+60) Conformer of $CClH(OH)_2$

The (-60,+60) conformer of $CClH(OH)_2$ could also decompose *via* the 1,2-elimination of HCl or H_2. The transition states and their geometries for these processes are shown

in Figure 3.14 (the atom distances are given in Angstroms) and Table 3.10 respectively, and their total and relative energies reported in Table 3.11.

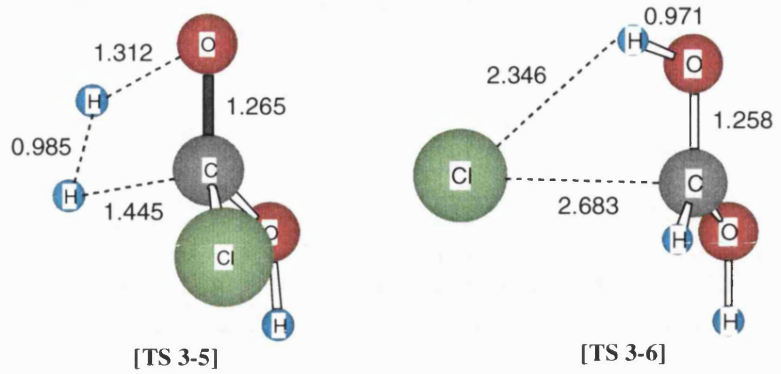

Figure 3.14

Table 3.10- HF/6-31G* Optimised Geometries of the Transition States for 1,2-Elimination Reactions from the (-60,+60) Conformer of $CClH(OH)_2$[f]

Co-ordinate	[TS 3-5]	Co-ordinate	[TS 3-6]
CO	1.265	CCl	2.683
CO'	1.315	CO	1.258
OH	1.312	OH	0.971
CH"	1.445	CO'	1.268
HOC	64.7	OCCl	87.2
H"CO	100.0	HOC	107.5
HOCO'	111.3	HOCCl	23.6
H'O'CO	170.2	O'COCl	131.5
H"COH	-0.7	H'O'CO	179.0

[f] Bond lengths in Angstroms, angles in degrees.

The geometries of [TS 3-5] and [TS 3-6] are very similar to [TS 3-3] and [TS 3-4] respectively. The major difference lies in the position of the hydroxyl hydrogen atom not transferred during either process. Decomposition of the (-60,-60) conformer has HOCO dihedral angles for this proton of –12.7° and 12.4°. However the decomposition of the (-60,+60) conformer has HOCO dihedral angles for this proton of 170.2° and

179.0°. This results in the formation of the higher energy conformers of the chloro/formic acids (HOCO=180°) when 1,2-elimination occurs from the (-60,+60) conformer compared to the lower energy conformers of these acids (HOCO=0°) yielded from the (-60,-60) conformer.

The geometries of [TS 3-5] and [TS 3-6] again showed that the elimination of H_2 is a much more concerted type of process than the elimination of HCl due to the superiority of chlorine as a leaving group. The symmetry of the (-60,+60) conformer means that the elimination reactions can occur *via* the breakage of either O-H bond. The imaginary frequencies corresponding to the reaction co-ordinates are 2754i cm^{-1} for [TS 3-5] and 174i cm^{-1} for [TS 3-6]. These are very close to the values for the reaction *via* [TS 3-3] and [TS 3-4] respectively.

Table 3.11 - Total and Relative Energies for Species Involved in the Decomposition of the (-60,+60) Conformer of $CClH(OH)_2$

	HF/6-31G*			MP2(fc)/6-311+G**//HF/6-31G*		
Species	Total (Hartrees)	Relative (kJ mol^{-1})	ZPVE (kJ mol^{-1})	Total (Hartrees)	Relative (kJ mol^{-1})	Relative + ΔZPVE (kJ mol^{-1})
(-60,+60)	-648.80172	0	136	-649.59154	0	0
[TS 3-5]	-648.63206	445	109	-649.45593	356	332
[TS 3-6]	-648.77398	73	135	-649.54704	117	116
$H_2 + ClCO_2H$	-648.78518	43	100	-649.57790	36	4
$HCl + HCO_2H$	-648.81252	-28	115	-649.59731	-15	-34

The energetics for the 1,2-elimination of H_2 and HCl from the (-60,+60) conformer are also comparable with those for the (-60,-60) conformer. The variation occurs because both the reactant and product species are higher in energy for the (-60,+60) processes than the (-60,-60) reaction species.

The degradation of the $CClH(OH)_2$ intermediate has been shown to occur *via* either the (-60,-60) or the (-60,+60) conformers. As was stated in section 3.3.3 these conformers are linked by the [-60,120] and [-60,0] transition states with low energy barriers. The product of the initial addition of water to CClHO is the (-60,-60) conformer of $CClH(OH)_2$, therefore decomposition can either proceed directly from this species or after transformation to the (-60,+60) rotamer. In the gas phase the other conformers of the diol do not lead to decomposition pathways for elimination of H_2 or HCl. The calculated barriers for the reactions indicate that the H_2 elimination pathway is not energetically viable and hence that the decomposition is likely to proceed *via* the alternate route of HCl elimination.

3.3.6 $CClHO + H_2O \rightarrow HCl + HCO_2H$

The preceding sections focussed on the hydrolysis of CClHO *via* pathways that involved the $CClH(OH)_2$ diol. The investigation has been extended to examine the hydrolysis as a one step process where the tetrahedral intermediate is not formed and the reaction proceeds directly to elimination products.

In this section the one step elimination of HCl is examined. Two transition states have been located for this process and are shown in Figure 3.15. The atom distances are given in Angstroms. Important parameters of their optimised geometries are reported in Table 3.12.

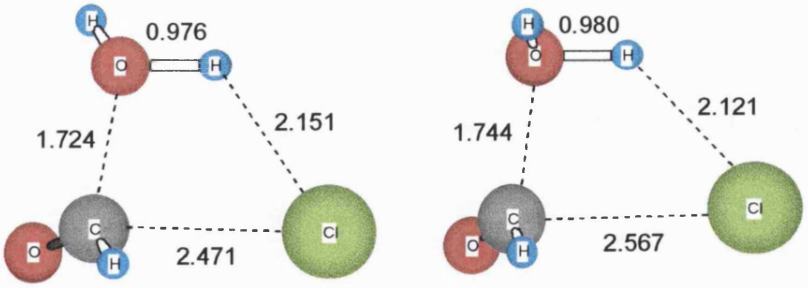

[TS 3-7] [TS 3-8]

Figure 3.15

Transition structures [TS 3-7] and [TS 3-8] exhibit similar geometrical properties to the transition states for the elimination of HCl from $CClH(OH)_2$. The elimination follows the trend of [TS 3-4] and [TS 3-6] and proceeds with the C-Cl bond breaking followed by the abstraction of a proton.

Table 3.12 - HF/6-31G* Optimised Geometries of the Transition States for the Direct Elimination of HCl from CClHO[g]

Co-ordinate	[TS 3-7]	[TS 3-8]
CO'	1.135	1.127
CCl	2.471	2.567
CO	1.724	1.744
HO	0.976	0.980
H'OC	108.7	114.6
HOC	99.6	97.0
OCO'Cl	93.4	88.9
H'OCO'	-8.3	149.8
HOCO'	-120.8	-99.2

[g] Bond lengths in Angstroms, angles in degrees.

[TS 3-7] and [TS 3-8] both contain the expected four-centre transition structure. Their geometries are largely the same with the C-Cl bond broken and the H'-O bond intact in each case. The similarity of these transition states is apparent in the values of the

imaginary frequencies associated with the reaction co-ordinate. These are 353i cm^{-1} and 334i cm^{-1} respectively for [TS 3-7] and [TS 3-8].

The variations in the geometries of [TS 3-7] and [TS 3-8] are caused by the relative position of the non-transferred hydrogen atom of the water molecule. In [TS 3-7] this proton is 'cis' to the C=O bond whereas in [TS 3-8] it is 'cis' to the C-H bond. This hydrogen can therefore form a hydrogen bond interaction in [TS 3-7] that is not possible for [TS 3-8]. The geometries of [TS 3-7] and [TS 3-8] also show that in [TS 3-8] the C-Cl distance is 0.096Å longer, the H'-O bond 0.004Å longer, and the H'-Cl distance 0.030Å shorter compared to [TS 3-7]. Contrary to this trend the C-O distance is 0.020Å greater in [TS 3-8] than [TS 3-7]. Although in most respects the elimination of HCl is more advanced in [TS 3-8] the formation of the C-O single bond of the formic acid is actually less so for this transition state.

The differences in the transition states lead to the formation of different conformers of formic acid. [TS 3-7] yields the lower energy conformer of formic acid where HOCO=0° and [TS 3-8] the higher energy conformer (HOCO=180°).

The total and relative energies of [TS 3-7] and [TS 3-8] are shown in Table 3.13.

Table 3.13 - Total and Relative Energies for Species Involved in the CClHO + H_2O → HCl + HCO_2H Reaction

	HF/6-31G*			MP2(fc)/6-311+G** //HF/6-31G*		
Species	Total (Hartrees)	Relative (kJ mol^{-1})	ZPVE (kJ mol^{-1})	Total (Hartrees)	Relative (kJ mol^{-1})	Relative + ΔZPVE (kJ mol^{-1})
H_2O + CClHO	-648.79236	0	115	-649.59046	0	0
[TS 3-7]	-648.74467	125	126	-649.54426	121	131
[TS 3-8]	-648.73769	144	125	-649.53785	138	147
HCl + HCO_2H(cis)	-648.82229	-79	116	-649.60474	-37	-37
HCl + HCO_2H(trans)	-648.81252	-53	115	-649.59731	-18	-18

The one step elimination of HCl from CClHO is exothermic irrespective of the path taken. However the exothermicity is reduced by 18 kJ mol^{-1} at 0 K when the products include the higher energy conformer of formic acid. The energy barrier for HCl elimination *via* [TS 3-7] is 16 kJ mol^{-1} lower than that for [TS 3-8]. This difference is likely to be due in part to the stabilising hydrogen bonding interaction present in [TS 3-7] that is not possible in [TS 3-8]. The energy barriers are decreased slightly by the inclusion of electron correlation but are increased by a larger amount when the zero point vibrational energy is also included. The pattern is different for the reaction energies where including electron correlation increases the reaction energy by 35 or 42 kJ mol^{-1} but the zero point vibrational energy makes a negligible contribution to the energy difference.

3.3.7 $CClHO + H_2O \rightarrow H_2 + ClCO_2H$

Direct elimination of H_2 can also occur from the reaction of CClHO and a water molecule. Two transition states have been located for this elimination at the HF/6-31G* level of theory. Three-dimensional representations of these structures are shown in Figure 3.16. Significant features of their optimised geometries are reported in Table 3.14, and their total and relative energies are shown in Table 3.15.

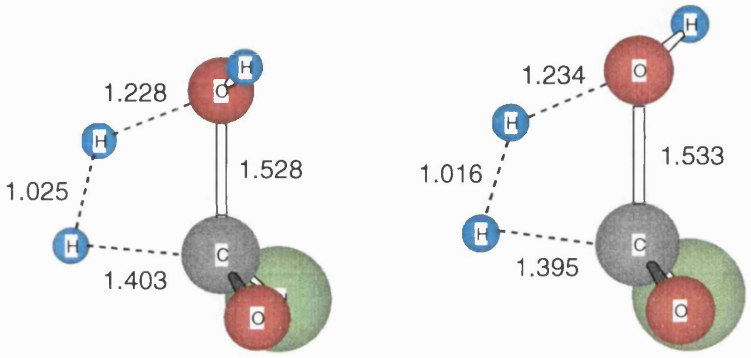

[TS 3-9] [TS 3-10]

Figure 3.18

Table 3.14 - HF/6-31G* Optimised Geometries of the Transition States for the Direct Elimination of H_2 from CClHO[h]

Co-ordinate	[TS 3-9]	[TS 3-10]
CH"	1.403	1.395
CO	1.528	1.533
HO	1.228	1.234
H"CO'	115.1	115.7
H'OC	105.8	113.4
HOC	67.3	67.5
H'OCO'	-5.2	128.0
HOCO'	-114.2	-119.3

[h] Bond lengths in Angstroms, angles in degrees.

The geometries of [TS 3-9] and [TS 3-10] show that the direct elimination of H_2 is a concerted process. This follows the trend observed for the elimination of H_2 from $CClH(OH)_2$ where both protons leave in a synchronous manner. [TS 3-9] and [TS 3-10] each contain the anticipated four-centre transition structure. Their geometries are similar with the both C-H" and H-O bonds largely broken in each case. The structural closeness of these transition states is apparent in the values of the imaginary frequencies corresponding to the reaction co-ordinate. These are 2587i cm^{-1} and 2585i cm^{-1} respectively for [TS 3-9] and [TS 3-10].

The variations in the geometries of [TS 3-9] and [TS 3-10] are due to the recurring difference in the relative position of the non-transferred hydrogen atom of the water molecule. In [TS 3-9] this proton is 'cis' to the C=O bond whereas in [TS 3-10] it is 'cis' to the C-Cl bond. This hydrogen can therefore form a hydrogen bond interaction in both [TS 3-9] and [TS 3-10] providing stabilisation for both transition states. The structural variations in the transition states result in the formation of different conformers of chloroformic acid. [TS 3-9] yields the lower energy conformer where HOCO=0° and [TS 3-10] the higher energy conformer of the acid (HOCO=180°).

Table 3.15 - Total and Relative Energies for Species Involved in the CClHO + H_2O $\rightarrow$ H_2 + $ClCO_2H$ Reaction

	HF/6-31G*			MP2(fc)/6-311+G** //HF/6-31G*		
Species	Total (Hartrees)	Relative (kJ mol^{-1})	ZPVE (kJ mol^{-1})	Total (Hartrees)	Relative (kJ mol^{-1})	Relative + ΔZPVE (kJ mol^{-1})
H_2O + CClHO	-648.79236	0	115	-649.59046	0	0
[TS 3-9]	-648.62901	429	109	-649.46722	324	318
[TS 3-10]	-648.62360	443	108	-649.46502	329	323
H_2 + $ClCO_2H$(cis)	-648.79028	5	100	-649.58110	25	11
H_2 + $ClCO_2H$(trans)	-648.78518	19	100	-649.57790	33	20

The one step elimination of H_2 is endothermic independent of the decomposition route. The reaction energy for the [TS 3-10] process is higher as the products include the less stable chloroformic acid conformer. The inclusion of electron correlation increases the reaction energies but a large part of this increase is offset when the zero point vibrational energy is taken into account.

The energy barriers for H_2 elimination are very close in value for [TS 3-9] and [TS 3-10]. As stated above this is probably due to the possibility of intramolecular hydrogen bonding in both transition states. However the actual energy barriers are still too large for these to be viable decomposition pathways for CClHO hydrolysis.

3.3.8 Overview of the Gas-Phase Bimolecular Hydrolysis of CClHO

The bimolecular hydrolysis of formyl chloride can occur *via* either a one- or two-step mechanism. All the transition states for the reactions examined contain a four-centre

ring. The strain inherent in the formation of these four-membered rings is likely to provide a major contribution to the energy barriers for these reaction processes.

The two step reaction involves the initial addition of the water molecule to CClHO form the lowest energy (-60,-60) conformer of the $CClH(OH)_2$ adduct *via* [TS 3-1] or [TS 3-2] (Figure 3.19). The reaction is essentially thermoneutral at 0 K with high energy barriers for both paths.

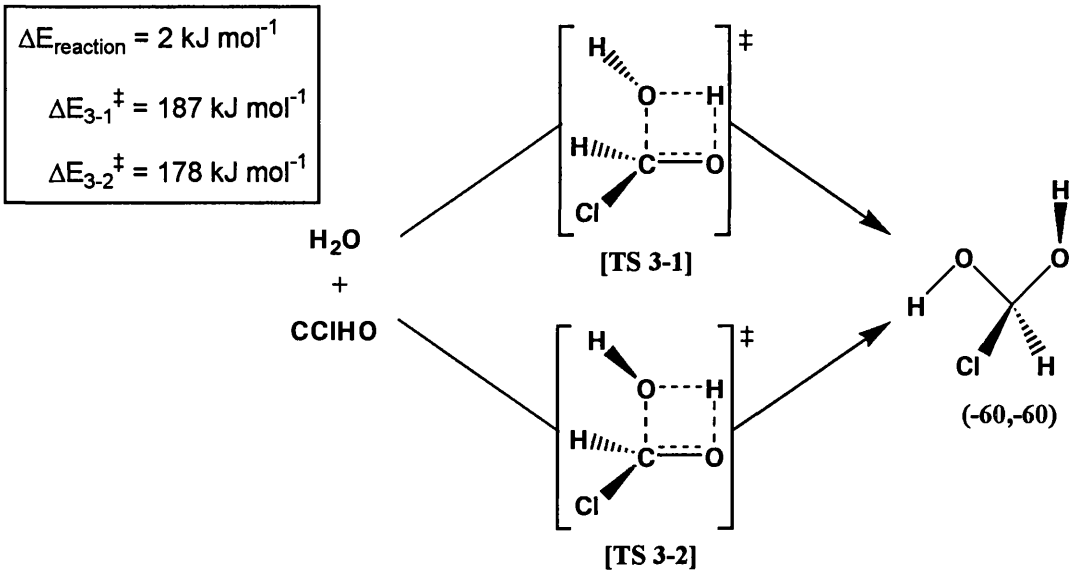

Figure 3.19

This conformer of the diol can then decompose through the [TS 3-3] or [TS 3-4] reaction paths to yield either chloroformic or formic acid in their most stable conformation (Figure 3.20). The $CClH(OH)_2$ conformer initially formed does not therefore need to undergo a conformational change before decomposition can occur. The elimination of H_2 is endothermic and elimination of HCl strongly exothermic. The difference in the energy barriers is 219 kJ mol^{-1} at 0 K with elimination of HCl the energetically favoured process.

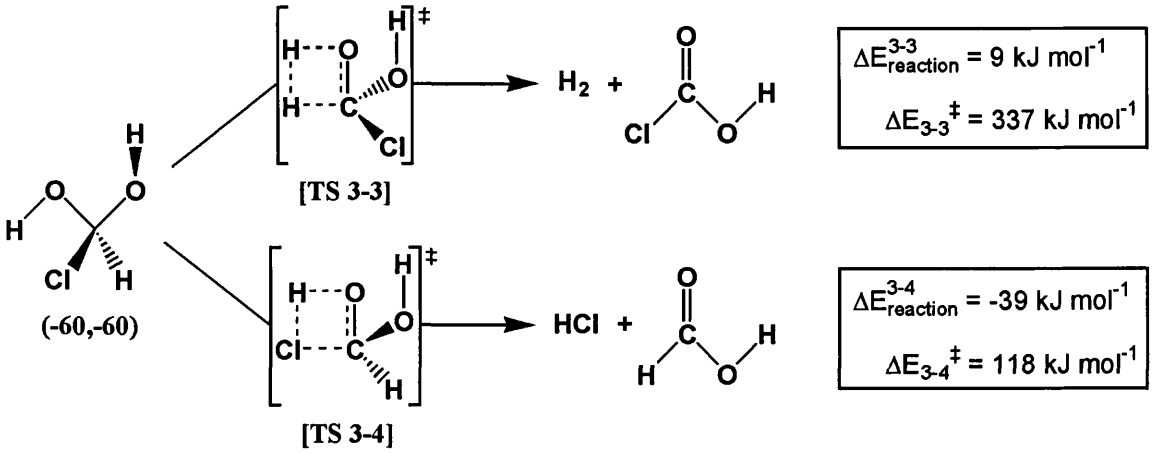

Figure 3.20

Alternatively the (-60,-60) conformer can undergo a low energy transformation to the (-60,+60) rotamer *via* either the [-60,0] or [-60,120] transition state (see section 3.3.3). This conformer can then also decompose through 1,2-elimination of either H_2 or HCl to give chloro/formic acid. In this case the conformer of the acid produced is the higher energy species where HOCO=180° (Figure 3.21). The remaining $CClH(OH)_2$ conformers do not lead to decomposition pathways for the reaction routes considered in this study. The reaction energies and energy barriers are similar to those for the elimination of H_2 and HCl from the (-60,-60) conformer.

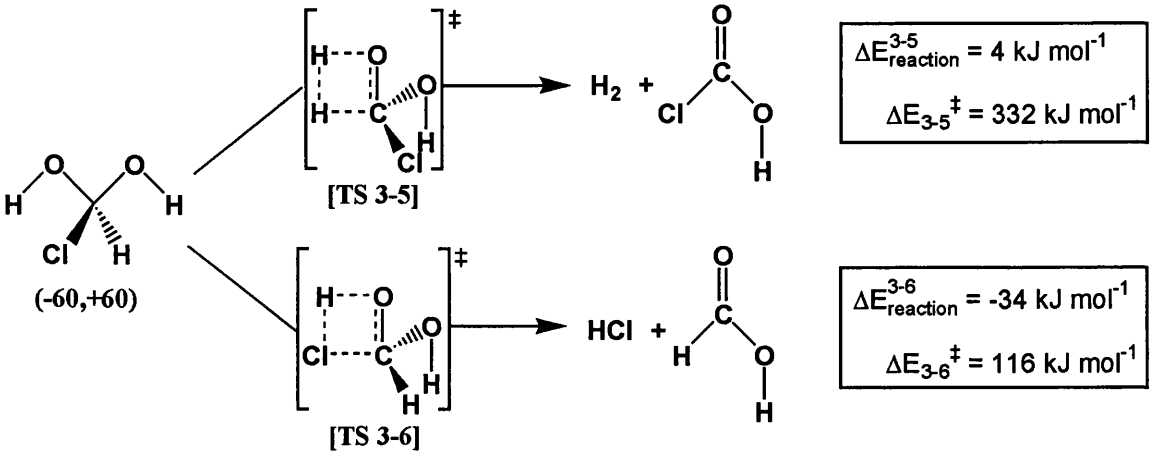

Figure 3.21

The one step reactions involve the direct elimination of HCl or H_2 from CClHO + H_2O. Elimination of HCl proceeds *via* either [TS 3-7] or [TS 3-8] to yield formic acid. The

difference lies in the conformer of the acid formed (Figure 3.22). The reaction energy is decreased and the energy barrier increased when the product is the higher energy conformer of formic acid.

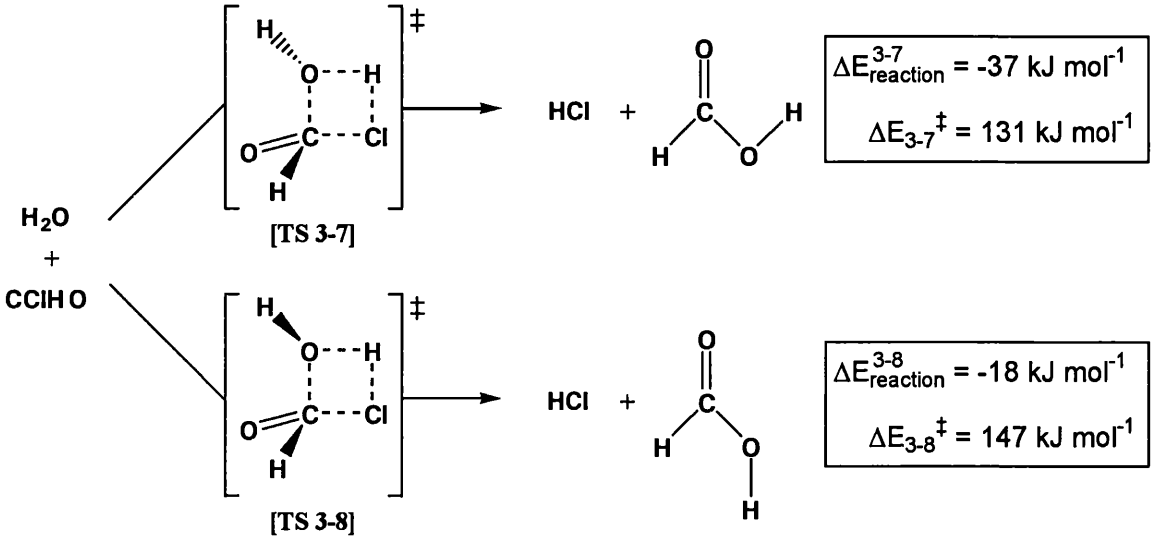

Figure 3.22

The direct elimination of H_2 can also occur *via* two distinct transition states, [TS 3-9] and [TS 3-10] (Figure 3.23). The difference between the two paths again lies in the conformer of the chloroformic acid formed. The reaction energy and the barrier height are increased when the less stable acid conformer is the product.

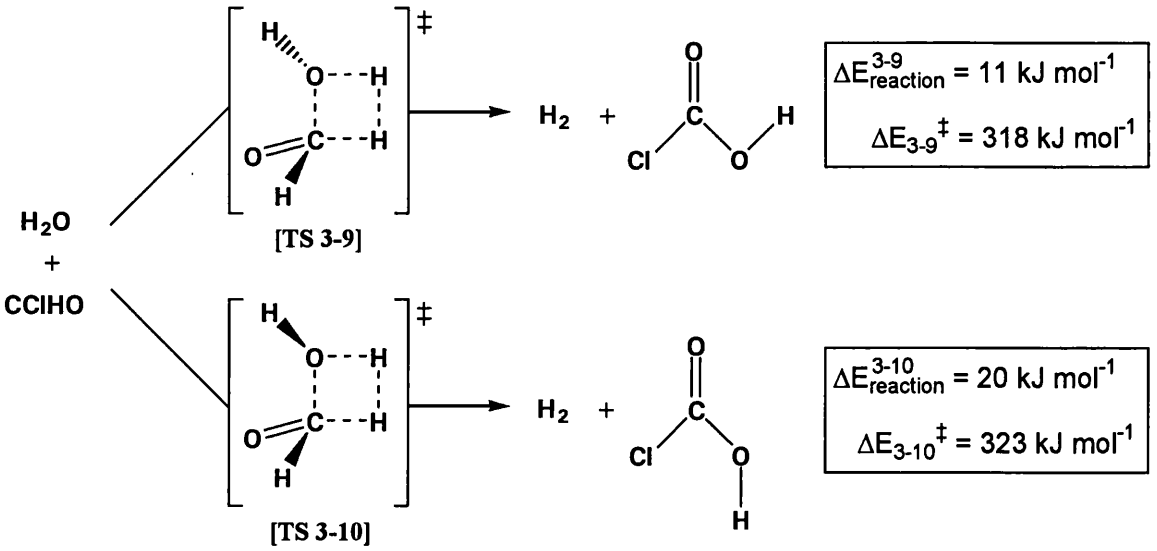

Figure 3.23

The overall reaction energies for bimolecular formyl chloride hydrolysis show that H_2 elimination is endothermic and HCl elimination exothermic at 0 K irrespective of the decomposition route. The degree of endo/exothemicity is determined by the conformation of the chloro/formic acid product.

The energy barriers for the two-step mechanism show that the initial addition of water to formyl chloride is the rate limiting step when followed by HCl elimination from $CClH(OH)_2$. If H_2 is eliminated from the intermediate then the second step becomes rate limiting. In addition the barrier for elimination of H_2 is prohibitively large hence the hydrolysis is not likely to proceed *via* this route.

The direct elimination of HCl has energy barriers between 29 – 56 kJ mol^{-1} lower than the rate limiting step of the two-step mechanism. The bimolecular hydrolysis of formyl chloride is thus more likely to occur *via* the direct decomposition routes than through the two-step process.

The two paths for direct elimination of H_2 have slightly lower energy barriers than the two-step process. However as these activation energies are still huge the decomposition of CClHO to H_2 and chloroformic acid by whichever route will not be important to the hydrolysis mechanism.

3.4 Conclusions

The present investigation has confirmed that the reaction process important for the gas phase bimolecular hydrolysis of formyl chloride is decomposition to HCl and formic acid. There are two possible mechanisms for the reaction. The first is a two-step

process where addition of a water molecule to CClHO to form the $CClH(OH)_2$ tetrahedral intermediate is followed by the 1,2-elimination of HCl. The second mechanism involves the direct elimination of HCl from formyl chloride water to yield formic acid. The one-step elimination is the lower energy route. The lowest energy path is *via* [TS 3-7] with an activation enthalpy of 131 kJ mol^{-1} and an enthalpy of reaction of –37 kJ mol^{-1} at 0 K.

Experimental data about this gas phase reaction is scarce therefore comparison of the calculated energy barrier with an experimentally determined value has proven problematic. The closest reaction for which an experimental activation energy has been available is the gas phase hydrolysis of $Cl_2C=O$. Libuda *et al.* reported an activation energy of 59 kJ mol^{-1} for the gas phase hydrolysis of Cl_2CO.[72] They were unable to determine a value for the analogous CClHO reaction because the formyl chloride reacted with moisture present on the walls of their apparatus. However they could say that the formyl chloride hydrolysis reaction was faster than that of Cl_2CO and hence should have a lower activation barrier.

The calculated energy barrier is clearly much higher than that predicted by experiment. A major contribution to this barrier is likely to be the formation of the four-membered ring present in the transition state. It has been hypothesised that this barrier could be reduced by a second water molecule catalysing the reaction. This would involve the formation of a less strained six-membered ring arrangement in the transition state. An investigation of the proposed mechanism involving catalysis by a second water molecule is reported in Chapter 4.

4. GAS PHASE TERMOLECULAR HYDROLYSIS OF FORMYL HALIDES

4.1 Introduction

In Chapter 3 the hydrolysis of formyl chloride was examined in the gas phase as a bimolecular process. The lowest energy path (Figure 4.1) for this reaction had a calculated energy barrier of 131 kJ mol^{-1} at 0 K which was much higher than the approximate value for the experimental activation energy of <59 kJ mol^{-1}. As stated in Chapter 3 a large element of the calculated barrier is likely to be due to the energy required to form the strained four-centre transition state. A mechanism whereby the transition state does not contain this strained arrangement should therefore decrease the energy barrier.

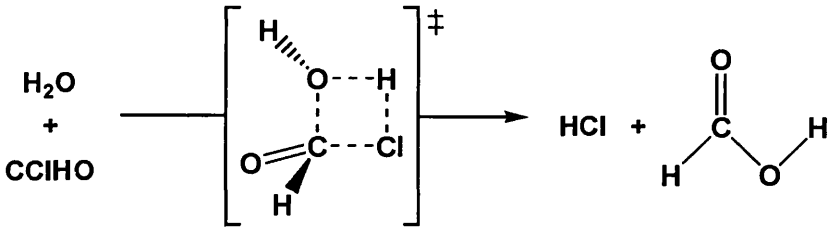

Figure 4.1

Previous theoretical studies have provided evidence that hydration of the carbonyl group can be catalysed by additional water molecules. Williams *et al.* proposed a gas phase termolecular reaction for the hydration of formaldehyde with a second water molecule acting as a bifunctional catalyst.[106,107] They reported a reduction of 27 kcal mol^{-1} in the Gibbs free energy of activation at 25°C for methanediol formation.

A later study examined the addition of ammonia catalysed by one or two water molecules.[108] This investigation found a decrease in the Gibbs free energy of activation of 39 kJ mol^{-1} with one water molecule catalysing the reaction. In each study

the transition state for the catalysed reaction contained a six-membered ring structure with the water acting as a bifunctional catalyst as shown in Figure 4.2.

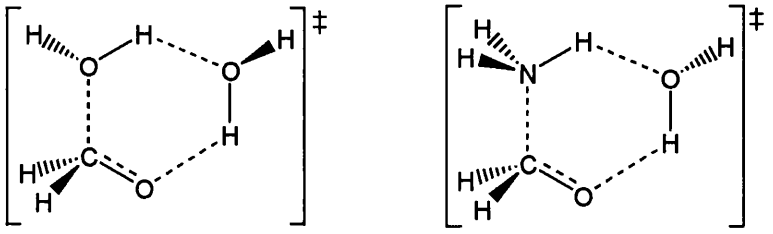

Figure 4.2

The addition of water to formaldehyde continued to be of interest as a model for hydration of the carbonyl group in water solvent. Wolfe *et al.* examined the neutral hydration of formaldehyde by a single water and by clusters of up to four water molecules.[109] They predicted that the major channel for this hydration was *via* a cyclic co-operative mechanism in which two additional water molecules provided the catalysis in water solvent. Thus the transition state for this channel contained an eight-membered ring. In a later study they updated the way they calculated basis set superposition error (BSSE) and low frequency corrections and concluded that in fact the major hydration channel involved four non-spectator water molecules.[110]

These studies of formaldehyde hydration promote the idea that the inclusion of extra water molecules may prove vital to successfully modelling the hydrolysis of the formyl halides. As major reductions in activation energies have been noted when even a single extra water molecule is included in the model, the gas phase formyl halide hydrolysis has been investigated as a termolecular reaction where a second water molecule catalyses the reaction. The results of *ab initio* molecular orbital calculations used to study the reaction are reported in this chapter.

The gas phase termolecular hydrolysis of both formyl fluoride and chloride have been examined in order to determine whether the nature of the substituent affects the preferred reaction mechanism. The reaction paths studied have been limited to those that have already been adjudged important to the hydrolysis, namely the one- and two-step elimination of HX to yield formic acid. Transition states have been located and characterised for both mechanisms, and the energies of the processes compared for the two halogen substituents. The energies have also been compared to those for the analogous CXHO + $1H_2O$ reaction processes to determine whether any energetic advantage is gained by the presence of the second water molecule.

4.2 Methods

The gas phase termolecular hydrolysis of the formyl halides has been investigated using *ab initio* molecular orbital calculations in the Gaussian 92[81] and Gaussian 94[111] suites of programs. It proved necessary to optimise the reaction species for the water catalysed formyl halide hydrolysis with the inclusion of electron correlation. Several of the chlorinated species could not be located on the Hartree-Fock potential energy surfaces studied, even when the size and flexibility of the basis set was increased.

Transition states have been located for the one- and two-step reaction mechanisms for both formyl fluoride and chloride. All species were optimised at the MP2 level of theory with all orbitals active and the 6-31G* basis set (denoted MP2(fu)/6-31G*). IRC calculations were performed to locate reactant and product complexes. The minima and transition states were characterised by determination of their harmonic vibrational frequencies again at the MP2(fu)/6-31G* level of theory.

4.3 Results and Discussion

The atoms of all the species reported in this chapter have been numbered according to the following scheme to avoid confusion when discussing specific proton transfers etc.

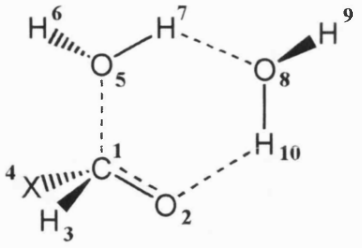

Figure 4.3

4.3.1 $CXHO + 2H_2O \rightarrow CXH(OH)_2 + H_2O$

Two sets of transition states have been located for the formation of the $CXH(OH)_2$ tetrahedral intermediate where X=F and Cl. Three-dimensional representations of their structures and those of the associated reactant and product complexes are shown in Figures 4.4 and 4.5.

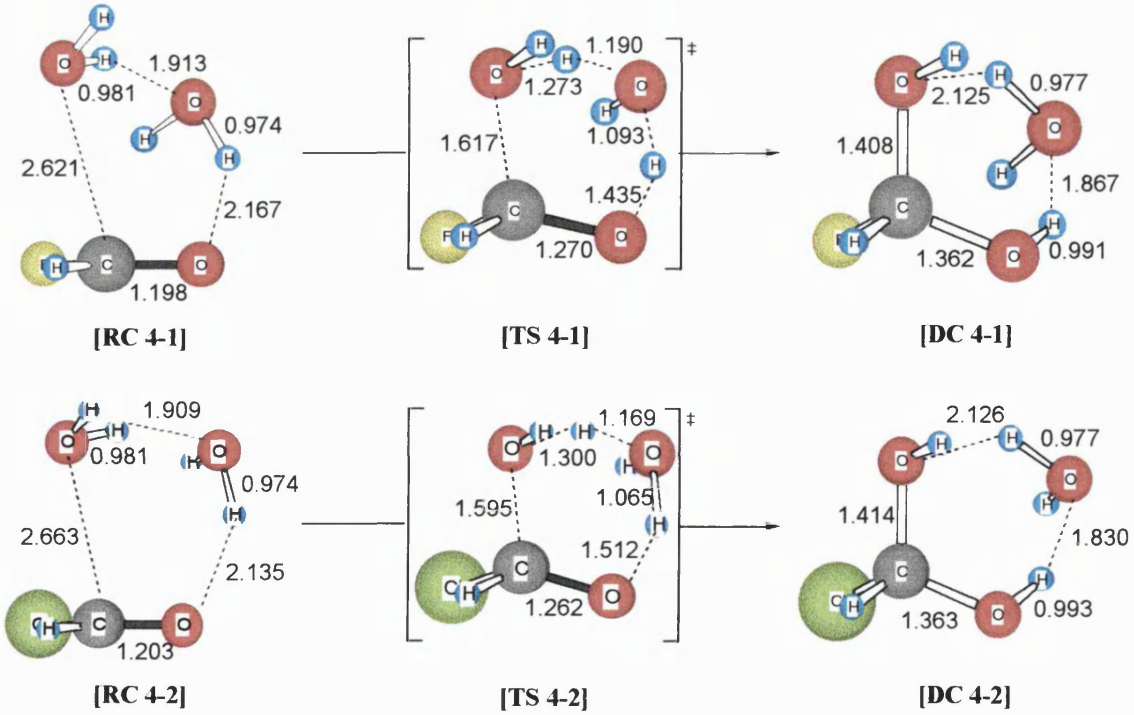

Figure 4.4

The transition states [TS 4-1] and [TS 4-2] have similar geometries with each containing the anticipated six-membered ring. Although the processes are similar the unscaled imaginary frequencies corresponding to the reaction co-ordinate vibrational modes of 1227 and 998i cm^{-1} for X=F and Cl respectively differ by 229 cm^{-1}. This indicates that the [TS 4-2] transition state is 'looser' than the analogous fluorinated species [TS 4-1].

Table 4.1 - MP2(fu)/6-31G* Optimised Geometries for Transition States for the $CXHO + 2H_2O \rightarrow CXH(OH)_2$ (+60,180)+ H_2O Reaction[a]

Co-ordinate	X=F	X=Cl
CX	1.397	1.886
O^8O^5	2.406	2.412
H^7O^5C	94.1	95.1
O^8O^5C	82.9	84.0
$H^{10}O^8O^5$	75.9	77.3
$H^6O^5CO^2$	-61.2	-62.5
$H^7O^5CO^2$	45.5	44.4
$O^8O^5CO^2$	41.5	40.8
$H^9O^8O^5C$	79.7	79.9
$H^{10}O^8O^5C$	-22.5	-22.5

[a] Bond lengths in Ångstroms, angles in degrees.

Significant features of the transition state geometries not shown in Figure 4.4 are reported in Table 4.1. The non-transferred hydrogen atoms (H^6 and H^9) of the two water molecules are 'trans' to one another. The H^6-O^5 bond is 'trans' to the C-X bond for both substituents. The lack of zwitterionic intermediates and the direct formation of the diol-water complexes [DC 4-1] and [DC 4-2] as products show that the process is concerted for both X=F and Cl. However the atom distances within the six-membered ring system of [TS 4-1] and [TS 4-2] indicate that the proton transfers are asynchronous.

Evaluation of the Pauling bond orders* gives values of 0.65 (X=F) and 0.62 (X=Cl) for the H^7-O^5 bond and 0.84 (X=F) and 0.87 (X=Cl) for the H^{10}-O^8 bond. The transfer of H^7 between O^5 and O^8 is thus much further advanced than the transfer of H^{10} between O^8 and O^2. The significant variations in the transition state geometries [TS 4-1] and [TS 4-2] occur in the atom distances within the six-membered ring. The transfer of H^7 from O^5 to O^8 and the C-O^5 σ-bond formation are more advanced in [TS 4-2] than [TS 4-1]. However the transfer of H^{10} from O^8 to O^2 and C=O^2 π-bond breakage are less advanced when X=Cl compared to X=F.

Optimisation of the reactant-like species from IRC calculations have shown that the atoms of the formyl halide lie in a plane perpendicular to that containing the O^5, H^7, O^8, H^{10} along with the C and O^2 atoms of the CXHO molecule. The IRC calculations also show that the products of this reaction process for both halogen substituents are the (+60,180) conformer of the $CXH(OH)_2$ diol hydrogen bonded to the second water molecule. It has been assumed that this complex could then easily dissociate into the isolated component species. The total and relative energies of all the reacting species are reported in Table 4.2.

* Pauling bond order formula [112]: $n=\exp[(r_1-r_n)/c]$, where r_1 and r_n are lengths for bond order 1 and n respectively. c=0.67 for a single bond and 0.3 for a double bond [113].

Table 4.2 – Total and Relative Energies for Species Involved in the $CXHO + 2H_2O \rightarrow CXH(OH)_2$ (+60,180) + H_2O

Species	MP2(fu)/6-31G*			
	Total (Hartrees)	Relative (kJ mol^{-1})	ZPVE (kJ mol^{-1})	Relative + ΔZPVE (kJ mol^{-1})
$CFHO + 2H_2O$	-365.62774	0	168	0
[RC 4-1]	-365.65640	-75	188	-56
[TS 4-1]	-365.61563	32	186	49
[DC 4-1]	-365.66056	-86	201	-54
F-(+60,180) + H_2O	-365.63821	-27	188	-8
$CClHO + 2H_2O$	-725.63194	0	163	0
[RC 4-2]	-725.65909	-71	183	-52
[TS 4-2]	-725.62204	26	183	45
[DC 4-2]	-725.66472	-86	196	-54
Cl-(+60,180) + H_2O	-725.64219	27	184	-7

The relative enthalpies show that the formation of the reactant complexes is highly exothermic for both X=F and Cl. The energy barriers are 105 and 97 kJ mol^{-1} respectively for X=F and Cl relative to the reactant complexes. The product complexes have similar energies to the reactant complexes, and there is then an endothermic process to produce the isolated (+60,180) conformer of $CXH(OH)_2$ plus a water molecule from the hydrogen bonded diol-water species [DC 4-1] and [DC 4-2]. The overall reaction enthalpies for the isolated species are exothermic for X=F and Cl by –8 and –7 kJ mol^{-1} respectively.

The alternative transition states for this addition reaction are shown in Figure 4.5. They resemble those in Figure 4.4 but the differences in their geometries compared to the earlier transition states result in different reactant and product complexes.

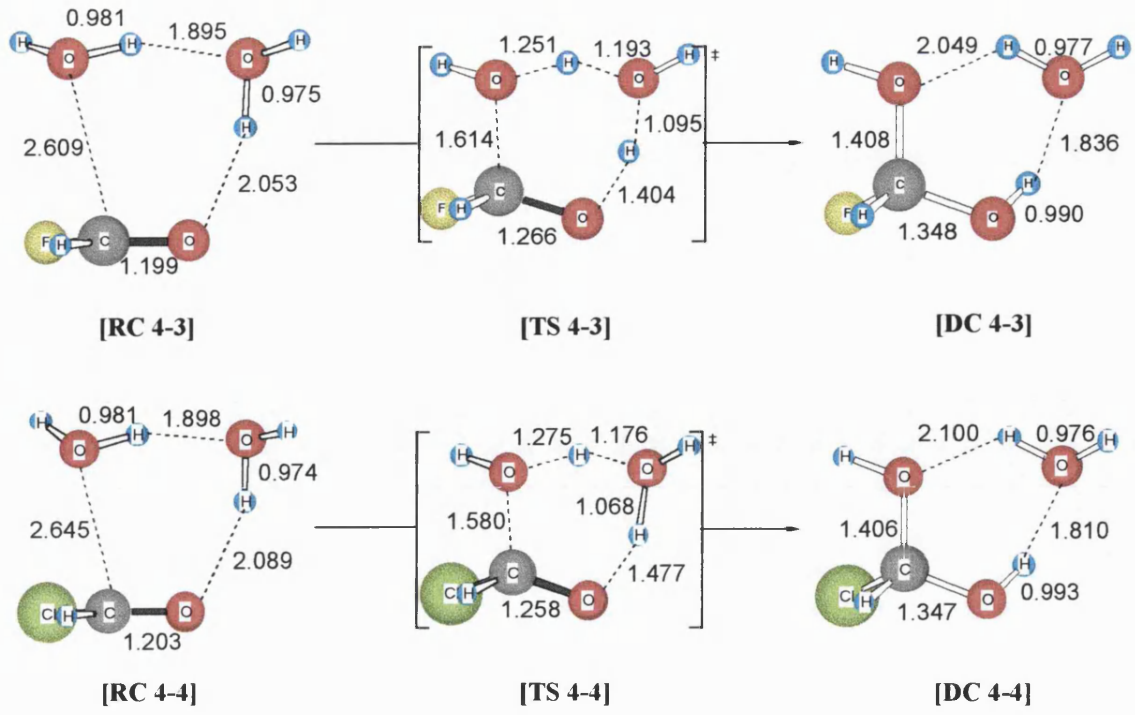

Figure 4.5

These transition states are structurally similar to [TS 4-1] and [TS 4-2] with the prominent feature, the six-membered ring, clearly observable. The major difference is that in [TS 4-3] and [TS 4-4] the H^6-O^5 bond is 'cis' instead of 'trans' to the C-X bond. This makes hydrogen bond interactions feasible for [TS 4-3] and [TS 4-4] that are not possible in [TS 4-1] and [TS 4-2]. The non-transferred hydrogen atoms (H^6 and H^9) of the water molecules remain 'trans' to each other. There are again only minor differences between the X=F and Cl transition state geometries as demonstrated in Figure 4.5 and Table 4.3. The same trends in atom distances within the six-membered rings of [TS 4-1] and [TS 4-2] are evident in [TS 4-3] and [TS 4-4].

Table 4.3 - MP2(fu)/6-31G* Optimised Geometries for Transition States for the $CXHO + 2H_2O \rightarrow CXH(OH)_2$ (+60,+60)+ H_2O Reaction[b]

Co-ordinate	X=F	X=Cl
CX	1.408	1.929
O^8O^5	2.392	2.396
H^7O^5C	99.7	100.2
O^8O^5C	88.3	88.8
$H^{10}O^8O^5$	75.1	76.4
$H^6O^5CO^2$	140.0	145.1
$H^7O^5CO^2$	26.1	29.1
$O^8O^5CO^2$	24.3	26.6
$H^9O^8O^5C$	-111.7	-113.2
$H^{10}O^8O^5C$	-9.8	-10.7

[b] Bond lengths in Ångstroms, angles in degrees.

The unscaled imaginary frequencies corresponding to the reaction co-ordinate vibrational modes have values of 1253 and 1055i cm^{-1} respectively for [TS 4-3] and [TS 4-4]. These values are slightly higher than for [TS 4-1] and [TS 4-2] but do show the same distinct difference between the fluorine and chlorine substituted species.

If the reaction proceeds *via* [TS 4-3] or [TS 4-4] then the product is the (+60,+60) conformer of the $CXH(OH)_2$ intermediate hydrogen bonded to the second water molecule irrespective of the substituent. The transition states show the expected trends in atomic distances in the six-membered rings with the proton transfers concerted but asynchronous. The total and relative energies of the reaction species are reported in Table 4.4.

Table 4.4 – Total and Relative Energies for Species Involved in the $CXHO + 2H_2O \rightarrow CXH(OH)_2$ (+60,+60) + H_2O

	MP2(fu)/6-31G*			
Species	Total (Hartrees)	Relative (kJ mol^{-1})	ZPVE (kJ mol^{-1})	Relative + ΔZPVE (kJ mol^{-1})
$CFHO + 2H_2O$	-365.62774	0	168	0
[RC 4-3]	-365.65638	-75	188	-56
[TS 4-3]	-365.61682	29	185	45
[DC 4-3]	-365.65990	-84	200	-54
F-(+60,+60) + H_2O	-365.64057	-34	188	-14
$CClHO + 2H_2O$	-725.63194	0	163	0
[RC 4-4]	-725.65933	-72	183	-53
[TS 4-4]	-725.62204	26	181	43
[DC 4-4]	-725.66355	-83	195	-52
Cl-(+60,+60) + H_2O	-725.64400	-32	184	-11

The energy barriers are 101 and 96 kJ mol^{-1} respectively for X=F and Cl relative to the reactant complexes. These are smaller than the activation energies for [TS 4-1] and [TS 4-2]. The probable cause of the reduced barriers is the hydrogen bond interaction that is possible in [TS 4-3] and [TS 4-4] and their respective reactant complexes. The product complexes have virtually identical energies to the reactant complexes with both much lower in energy than the isolated reactant species.

The isolated (+60,+60) conformer of $CXH(OH)_2$ and a water molecule are produced when the hydrogen bonded diol-water species disassociates. The overall reaction enthalpies for the isolated species are exothermic for X=F and Cl by –14 and –11 kJ mol^{-1} respectively. The greater exothermicity than when the products include the

(+60,180) conformer is due to the (+60,+60) species being the more stable conformer of the $CXH(OH)_2$ intermediate.

The reaction paths for water catalysed $CXH(OH)_2$ formation shown in Figures 4.4 and 4.5 yield different conformers of the diol depending upon how the reactants come together to form the initial encounter complex. If the two water molecules come together such that the non-transferred proton, H^6, bonded to O^5 is 'trans' to the C-X bond then the product is the (+60,180) conformer of the diol. However if the reactants form an encounter complex where this same proton is 'cis' to the C-X bond then the reaction occurs *via* [TS 4-3] or [TS 4-4] and the (+60,+60) conformer is produced.

The property common to all the transition states is that the additional water molecule acts as a bifunctional catalyst playing a full part in the reaction. Protons are transferred to and from this water molecule in an asynchronous manner such that transfer of a hydrogen atom to the water is further advanced than transfer of a proton from the water. The O-H atom distances in all four transition states and the asynchronicity of the proton transfers result in [TS 4-1] to [TS 4-4] resembling a $CXHO(OH)^-$ species hydrogen bonded to a hydroxonium ion, H_3O^+.

4.3.2 $\underline{CXH(OH)_2 + H_2O \rightarrow HX + HCO_2H + H_2O}$

In section 4.3.1 it was shown that gas phase $CXH(OH)_2$ formation could occur *via* transition states containing a six-centred ring due to the presence of a second water molecule. The initial product was a hydrogen bonded complex of the diol and a water molecule. It seemed likely that elimination of HX could proceed from this type of species, and hence that the decomposition of $CXH(OH)_2$ could also be catalysed by a

water molecule. This reaction has therefore been re-examined with a water molecule included in the model and transition states have been located for both X=F and Cl species.

A single transition state has been located for the water catalysed decomposition of the $CXH(OH)_2$ diol for X=F and Cl. The paths lead from the (+60,+60) conformer of the intermediate to HX and HCO_2H hydrogen bonded to the additional water molecule. This complex can then dissociate to the isolated species. Attempts were made to find transition states linking the (+60,180) conformer to the elimination products to provide other complete reaction channels but these were unsuccessful. Three-dimensional representations of the transition states and their corresponding reactant and product complexes are shown in Figure 4.6 and additional significant features of their geometries reported in Table 4.5.

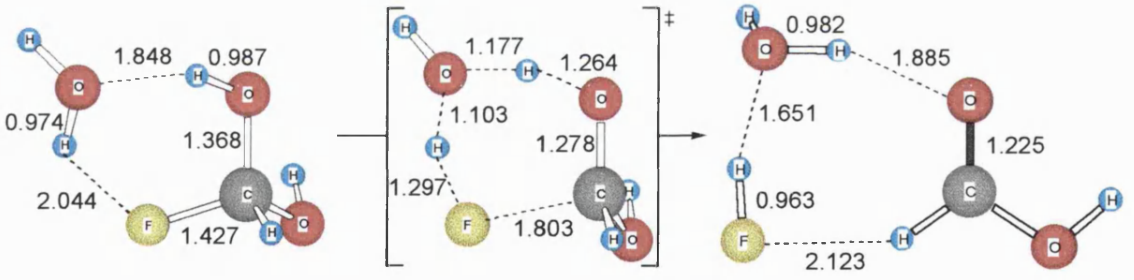

[DC 4-5] **[TS 4-5]** **[PC 4-5]**

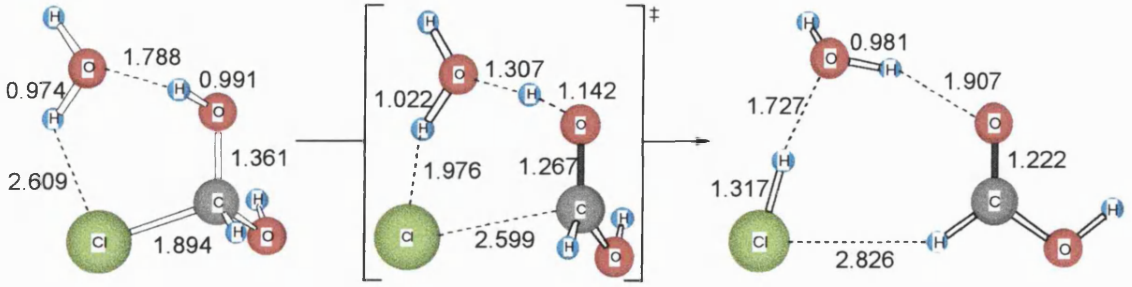

[DC 4-6] **[TS 4-6]** **[PC 4-6]**

Figure 4.6

Table 4.5 - MP2(fu)/6-31G* Optimised Geometries for Transition States for the $CXH(OH)_2 + H_2O \rightarrow HX + HCO_2H + H_2O$ Reaction[c]

Co-ordinate[d]	X=F	X=Cl
CO^2	1.334	1.305
O^8O^5	2.388	2.430
XCO^2	103.7	106.9
O^8O^5C	98.2	105.8
$H^9O^8O^5$	75.8	88.1
XCO^2O^5	113.9	111.1
$H^6O^5CO^2$	148.4	162.6
$O^8O^5CO^2$	141.5	156.8
$H^9O^8O^5C$	335.2	322.1

[c] Bond lengths in Ångstroms, angles in degrees.
[d] Atom numbering system identical to Figure 4.3.

The transition states [TS 4-5] and [TS 4-6] both contain the expected dominant feature of a six-membered ring. However there are clear differences between the structures of [TS 4-5] and [TS 4-6]. This is a result of the difference in the efficiencies of fluorine and chlorine as leaving groups. In the fluorine case the proton transfers between the oxygen atoms and from oxygen to fluorine are concerted although transfer of H^6 is further advanced than that of H^9 as can be seen from the Pauling bond orders for the breaking H-O bonds of 0.66 and 0.82 respectively. The C-F bond is largely broken with a Pauling bond order of 0.57. The formation of the C=O π-bond is also underway with a bond order of 1.35.

The process is still concerted for chlorine but more asynchronous as it is a better leaving group than fluorine. In this case the bond orders for the breaking H-O bonds are 0.80 and 0.93 respectively, *i.e.* the hydrogen atoms transfer is less advanced than for fluorine. However the bond order for the C-Cl bond is 0.35 so this bond is essentially broken

before proton transfer occurs. The C=O π-bond formation occurs to approximately the same degree as for the fluorine case with a bond order of 1.37.

The second water molecule exhibits identical behaviour for this process as for the initial addition of water to CXHO. It acts as a bifunctional catalyst with proton acceptance further advanced than proton donation. In [TS 4-5] the structure again resembles a H_3O^+ species hydrogen bonded to the remaining atoms. The structure of [TS 4-6] is different and appears to be much more like the [DC 4-6] species with the C-Cl bond broken.

In both cases it is the hydrogen atom (H^6) bonded to the 'right-hand' oxygen atom (O^5) of the $CXH(OH)_2$ intermediate that is transferred to the water molecule (see Chapter 3 section 3.3.2 for definition of left and right hand side of $CXH(OH)_2$). The remaining diol proton (H^{19}) is not transferred and becomes part of the formic acid that is produced in its lowest energy conformer where HOCO=0°.

The structural variations in the transition states caused by the differing efficacy of the halogens as leaving groups resulted in significant differences in the energy barriers for this process as shown in Table 4.6.

Table 4.6 – Total and Relative Energies for Species Involved in the $CXH(OH)_2$ (+60,+60) + $H_2O \rightarrow HX + HCO_2H + H_2O$ Reaction

	MP2(fu)/6-31G*			
Species	Total (Hartrees)	Relative (kJ mol^{-1})	ZPVE (kJ mol^{-1})	Relative + ΔZPVE (kJ mol^{-1})
F-(+60,+60) + H_2O	-365.64057	0	188	0
[DC 4-5]	-365.66037	-52	199	-41
[TS 4-5]	-365.62496	41	185	38
[PC 4-5]	-365.67464	-89	192	-86
HF + HCO_2H + H_2O	-365.63527	14	170	-3
Cl-(+60,+60) + H_2O	-725.64400	0	184	0
[DC 4-6]	-725.66390	-52	194	-43
[TS 4-6]	-725.64749	-9	185	-8
[PC 4-6]	-725.68126	-98	182	-100
HCl + HCO_2H + H_2O	-725.65326	-24	164	-44

The hydrogen bonded species comprising the (+60,+60) conformer of $CXH(OH)_2$ and a water molecule is much lower in energy than the isolated compounds at 0 K. There is no significant difference in the relative energies of the fluorine and chlorine species. Conversely the energy barrier to the reaction is 44 kJ mol^{-1} higher for the fluorine compound compared to chlorine when the barrier is calculated relative to the diol-water complex. The activation enthalpies are 79 and 35 kJ mol^{-1} respectively for X=F and Cl. The relative energy of [TS 4-6] is so low that it is actually a lower energy species than the isolated reactant molecules.

There is also a large discrepancy in the reaction enthalpy for X=F or Cl. The differences in the relative energies of the product complexes are not large at 14 kJ mol^{-1} and so if the reaction enthalpies are calculated between the reactant and product

complexes they are –45 and –57 kJ mol^{-1} respectively for X=F and Cl. However if the reaction enthalpies are calculated between the isolated reactant and product molecules then the reaction energy is 41 kJ mol^{-1} more exothermic for the chlorinated versus fluorinated species. It is also notable that if the enthalpy of reaction is calculated in this way then it is almost thermoneutral when X=F but considerably exothermic for the analogous X=Cl reaction.

4.3.3 $CXHO + 2H_2O \rightarrow HX + HCO_2H + H_2O$

The alternative reaction path for water catalysed formyl halide hydrolysis is the one-step mechanism with direct elimination of HX to yield formic acid. Transition states have been located for this reaction for both X=F and Cl. These are depicted in Figure 4.6 along with the corresponding reactant and product species. Other significant features of their geometries are reported in Table 4.7.

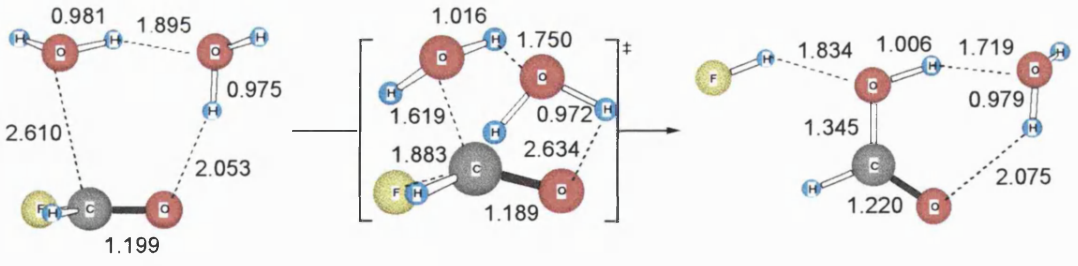

[RC 4-7] **[TS 4-7]** **[PC 4-7]**

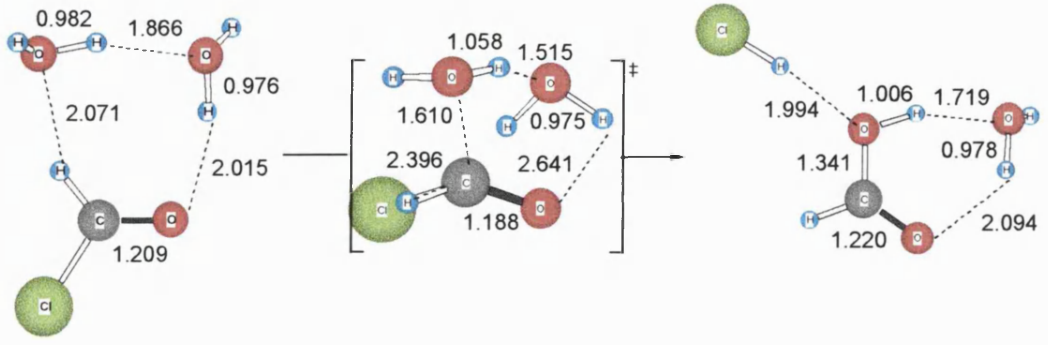

[RC 4-8] **[TS 4-8]** **[PC 4-8]**

Figure 4.7

Table 4.7 - MP2(fu)/6-31G* Optimised Geometries for Transition States for the $CXHO + 2H_2O \rightarrow HX + HCO_2H + H_2O$ Reaction[e]

Co-ordinate	X=F	X=Cl
H^3O^2	1.054	0.993
O^3O^2	2.625	2.538
H^3O^2C	84.2	101.4
O^3O^2C	87.9	92.6
XCO^1O^2	91.0	98.0
$H^3O^2CO^1$	125.3	145.5
$H^2O^2CO^1$	28.3	40.6
$O^3O^2CO^1$	49.0	48.6
$H^5O^3O^2C$	56.2	61.0
$H^4O^3O^2C$	-43.0	-43.0

[e] Bond lengths in Ångstroms, angles in degrees.

Figure 4.7 illustrates the differences between this reaction and those discussed in the previous sections. In the processes described in sections 4.3.1 and 4.3.2 the second water molecule acted as a bifunctional catalyst with hydrogen atoms transferred to and from it. In this case the additional water molecule does not take part in any proton transfers but stabilises the transition state by remaining hydrogen bonded to the first water molecule and the carbonyl oxygen atom. [TS 4-7] and [TS 4-8] are actually more like the direct elimination transition states for the $CXHO + 1H_2O$ reaction discussed in Chapter 3. Structurally they resemble [TS 3-7] or [TS 3-8] with a water molecule hydrogen bonded to the non-transferred proton of the participating water molecule and the carbonyl oxygen atom.

The C-X bond is largely broken in the transition state with a bond order of 0.45 for X=F and 0.39 for X=Cl. In agreement with chemical intuition the C-Cl bond breakage is slightly further advanced than that of the C-F bond. The greater ease of breaking the

C-Cl over the C-F bond is also indicated by the imaginary frequencies corresponding to the reaction co-ordinate vibrational modes of 225i cm^{-1} and 611i cm^{-1} respectively for X=Cl and F.

It is the hydrogen atom (H^6) of the water molecule which is 'cis' to the halogen that is eliminated during the reaction but the H^6-O^5 bond that needs to break for this to occur basically remains intact in the transition state. The H^7-O^5 bond of this water molecule is slightly elongated for both X=F and Cl as it acts as a hydrogen bond donor to the oxygen (O^8) of the second water. The second water also acts as a double hydrogen bond donor to the carbonyl oxygen atom in the transition state. This is in contrast to its behaviour in the reactant and product complexes where it donates a single hydrogen bond. However these bifurcated hydrogen bonds are much longer than the linear hydrogen bonds present in the reactant and product complexes.

An additional difference between the X=F and Cl cases lies in the relative geometries of the formyl halide in the reactant complexes. The [RC 4-7] reactant complex is identical to [RC 4-3] and has the carbon and oxygen atoms of the CFHO molecule lying in a plane with the O^5, O^8, H^7, and H^{10} atoms. The C-F and C-H^3 bonds are perpendicular to this plane. When X=Cl the CClHO molecule twists so that the four atoms all lie in the same plane as the O^5, O^8, H^7, and H^{10} atoms, namely the atoms of the water molecules taking part in hydrogen bonds. The chlorine atom is twists away from the waters and the H^3 atom of CClHO makes a hydrogen bond with the O^5 atom.

The product complexes for X=F and Cl are alike with the extra water molecule hydrogen bonded to the formic acid. All the atoms lie in the same plane except the H^9

atom which does not participate in hydrogen bonding. The proton of the HX forms a hydrogen bond with the hydroxyl oxygen (O^5) of the formic acid.

The differences in the behaviour of the halogens and the structural variations that result from this lead to the large discrepancies observable in the reaction and activation energies reported in Table 4.8.

Table 4.8 – Total and Relative Energies for Species Involved in the CXHO + $2H_2O$ → HX + HCO_2H + H_2O Reaction

	MP2(fu)/6-31G*			
Species	Total (Hartrees)	Relative (kJ mol^{-1})	ZPVE (kJ mol^{-1})	Relative + ΔZPVE (kJ mol^{-1})
CFHO + $2H_2O$	-365.62774	0	168	0
[RC 4-7]	-365.65638	-75	188	-56
[TS 4-7]	-365.60772	53	190	74
[PC 4-7]	-365.67152	-115	191	-93
HF + HCO_2H + H_2O	-365.63527	-20	170	-18
CClHO + $2H_2O$	-725.63194	0	163	0
[RC 4-8]	-725.66246	-80	184	-60
[TS 4-8]	-725.63161	1	187	24
[PC 4-8]	-725.68404	-137	181	-119
HCl + HCO_2H + H_2O	-725.65326	-56	164	-55

The formation of the reactant complex is slightly more exothermic when the substituent is chlorine rather than fluorine. The chlorinated reactant complex for this one-step process is also the lowest energy of the three reactant complexes located for the termolecular hydrolysis reaction. The additional hydrogen bond present in the [RC 4-8] species between the H^3 and O^5 atoms is the likely cause of the extra stability of this configuration of the reactant molecules.

The energy barriers for the X=F or Cl reactions differ by considerable amounts. The activation enthalpies are 130 and 84 kJ mol^{-1} for the fluorine and chlorine cases respectively when calculated relative to the reactant complexes. The barrier for the fluorine reaction is therefore 46 kJ mol^{-1} higher than when the substituent is chlorine. This value is comparable to the difference calculated in the energy barriers for the $CXH(OH)_2 + H_2O \rightarrow HX + HCO_2H + H_2O$ reaction described in section 4.3.2. The energy barriers are significantly lower if calculated relative to the isolated reactant molecules with values of 74 and 24 kJ mol^{-1} respectively for X=F and Cl.

The enthalpies of reaction are also markedly substituent dependent. The reaction is exothermic for both fluorine and chlorine processes but is much more exothermic when the halogen present is chlorine. When calculated between isolated reactant and product molecules the chlorine reaction is 37 kJ mol^{-1} more exothermic than the equivalent fluorine process. If the reaction enthalpy is calculated between the reactant and product hydrogen bonded complexes then the chlorine reaction is still more exothermic than the fluorine process but only by 22 kJ mol^{-1}.

4.3.4 Overview of the Gas Phase Termolecular Hydrolysis of the Formyl Halides

This section provides an overview of the termolecular hydrolysis of the formyl halides. A comparison of the activation and reaction enthalpies of the termolecular and bimolecular processes is also included. In order to make direct comparisons possible the reaction species for the CClHO bimolecular reaction have been re-optimised at the MP2(fu)/6-31G* level of theory and their relative energies recalculated at this level. Only the species along the lowest energy paths for the one- and two-step mechanisms of the bimolecular hydrolysis are reported.

4.3.4.1 The Gas Phase Bimolecular Hydrolysis of Formyl Fluoride

The inclusion of the hydrolysis of CFHO necessitated locating transition states for its bimolecular hydrolysis in order to determine whether this reaction is catalysed by a second water molecule. The reaction species for both X=F and Cl optimised at the MP2(fu)/6-31G* level of theory for the two-step bimolecular hydrolysis mechanism are shown in Figure 4.8. Figure 4.9 shows the species for the one-step mechanism optimised at the same level of theory.

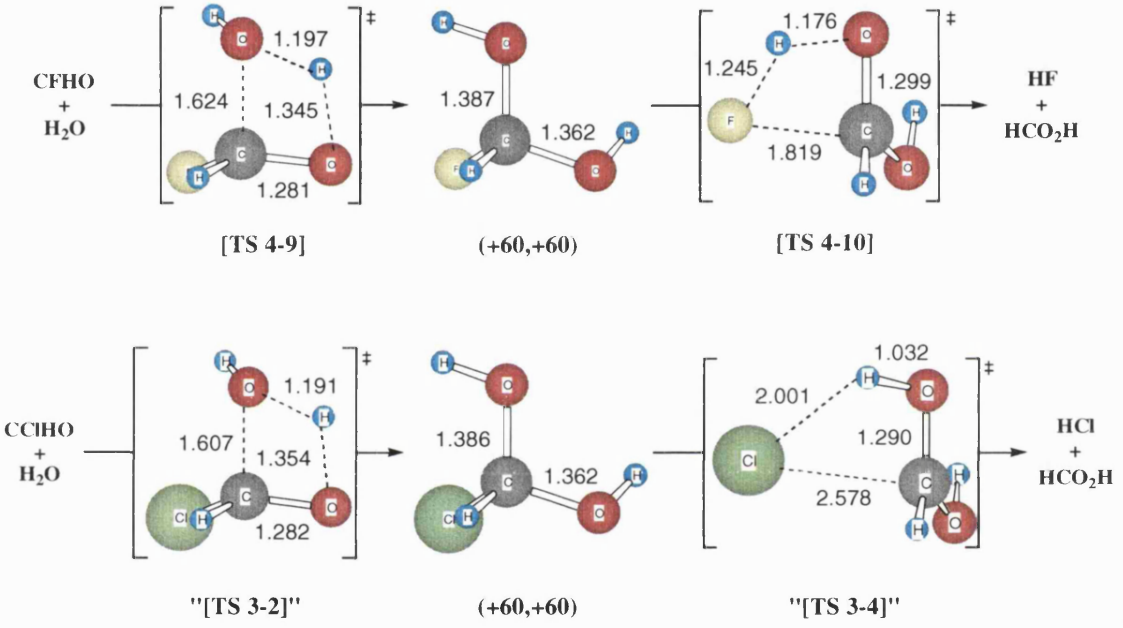

Figure 4.8

IRC calculations showed that the two-step bimolecular hydrolysis of CFHO occurs *via* the formation of the same conformer of the $CXH(OH)_2$ diol as the CClHO reaction. The transition state for this initial addition reaction is structurally comparable to the chlorine species. However the transition state which provides a route for decomposition of the $CFH(OH)_2$ diol has important structural differences to the analogous chlorine transition state. The atom distances in the transition states indicate that elimination of HF occurs in a more concerted manner than that of HCl with the breaking H-O bond

longer for fluorine than chlorine and the C-X bond breakage further advanced for chlorine over fluorine.

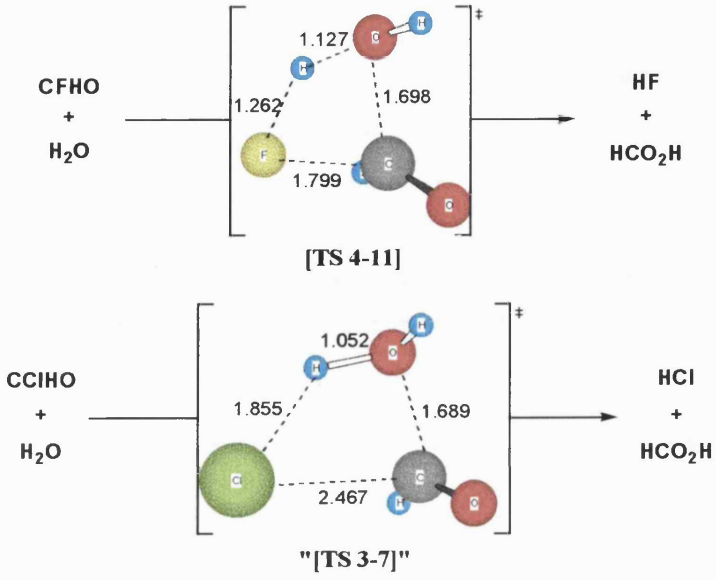

Figure 4.9

This trend is also evident in the transition state geometries for the one-step mechanism where the H-O bond of the hydrogen that is eliminated as part of the HX molecule is 0.075Å longer for the fluorine case. The bond orders of the C-X bonds in the transition states for the direct elimination of HX also verify the difference between the behaviour of the halogens with values of 0.51 and 0.35 respectively for X=F and Cl.

The energies of these reaction paths have also been evaluated at the MP2(fu)/6-31G* level of theory. In general they follow the patterns for the CClHO bimolecular hydrolysis with the initial addition of water to the formyl fluoride the rate determining step of the two-step mechanism. The decomposition step of this mechanism has a lower energy barrier but when X=F the difference between the barrier heights is not as great as in the chlorine case.

In common with CClHO the CFHO one-step process also has a lower energy barrier than that of the first step of the two-step mechanism. Thus for CFHO bimolecular hydrolysis the one-step process is energetically favoured despite the more concerted nature of the direct elimination compared to CClHO hydrolysis. The relative enthalpies of the reaction species calculated at the MP2(fu)/6-31G* level of theory are depicted in the graphs that follow.

4.3.4.2 The Two-Step Mechanism of the Gas Phase Termolecular Hydrolysis of the Formyl Halides

The two-step mechanism for the hydrolysis of formyl fluoride and chloride in the presence of a second water molecule results in the initial formation of a $CXH(OH)_2$ diol hydrogen bonded to the additional water molecule. This can occur *via* transition states [TS 4-1] to [TS 4-4] and it is possible to form either the (+60,+60) or the (+60,180) conformer of the diol intermediate. The energies are alike for the formation of either diol and for both X=F and Cl as can clearly be seen by the overlapping lines in Figure 4.10.

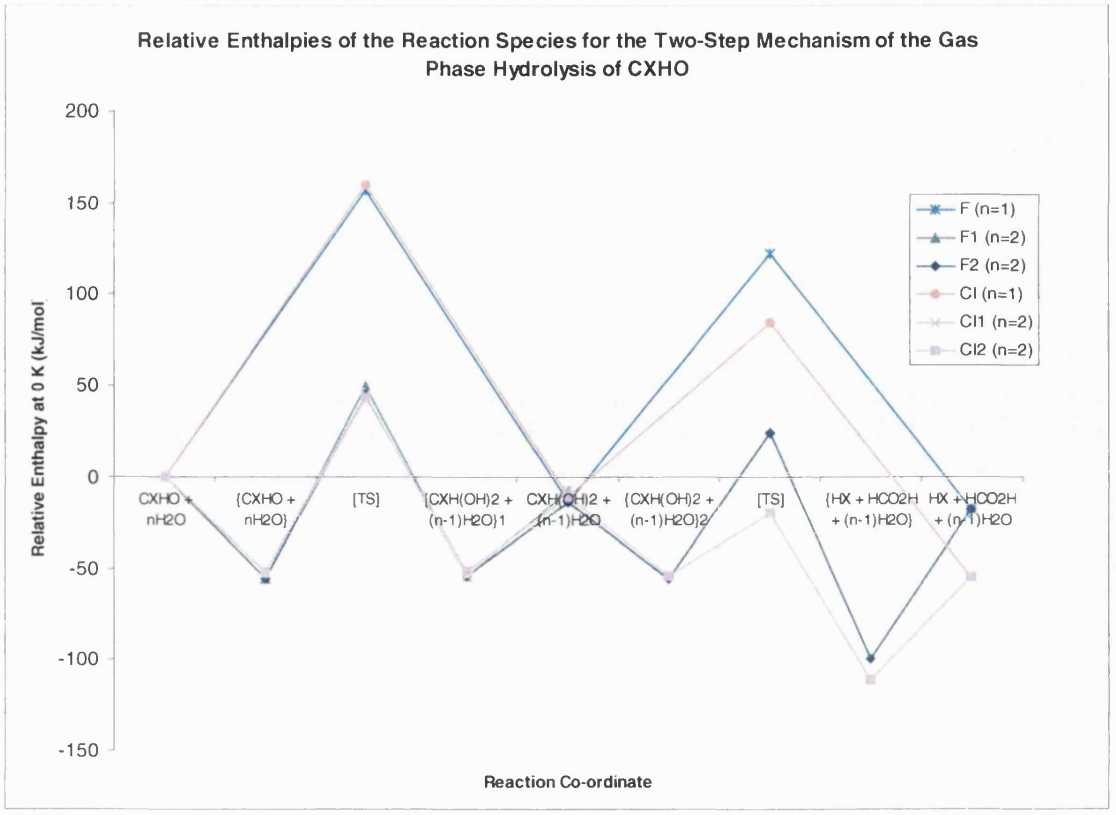

Figure 4.10

The relative energies of the reactant complexes, transition states, diol-water complexes, and the isolated diol plus water species are virtually identical for both diol forming paths and both halogens. There is an initial decrease in energy of –52 to -56 kJ mol^{-1} with the formation of the reactant encounter complex. Depending on the relative structure of the encounter complex the reaction proceeds *via* transition states [TS 4-1] to [TS 4-4] to either the (+60,180) or (+60,+60) conformer of the $CXH(OH)_2$ diol hydrogen bonded to the second water molecule. There is then an energy cost for dissociation of this complex to the isolated molecules.

There are significant differences between the transition states for the decomposition of the $CXH(OH)_2$ diol to HX and formic acid. The structural differences are most likely caused by the fact that chlorine is a better leaving group than fluorine. In the chlorine case the elimination tends to proceed with the initial departure of Cl^- followed by

abstraction of H^+ from oxygen. The reaction is much more concerted when X=F rather than Cl.

Transition states for the decomposition of $CXH(OH)_2$ could only be located which linked the (+60,+60) conformer to the products. The results indicate that the (+60,180) conformer of the diol would need to undergo transformation to the (+60,+60) conformer before decomposition could proceed. However this transformation could take place through a low energy path as described in Chapter 3.

The (+60,+60)-water complexes [DC 4-5] and [DC 4-6] are the complexes from which diol decomposition proceeds. They do not have the same structure as the (+60,+60)-water complexes [DC 4-3] and [DC 4-4] which are produced from the initial addition of water to the formyl halide. The difference lies in the way the water molecule is hydrogen bonded to the diol. In [DC 4-3] and [DC 4-4] the H^{10} atom of the 'left hand' hydroxyl group acts as a hydrogen bond donor to the O^8 atom of the water molecule, and the water acts as hydrogen bond donor to the O^5 atom of the diol. In [DC 4-5] and [DC 4-6] it is the H^6 atom of the 'right hand' hydroxyl group that acts as a hydrogen bond donor to the water molecule, and the water acts as a hydrogen bond donor to the halogen instead of the 'left hand' oxygen of the diol. [DC 4-5] and [DC 4-6] are marginally more stable arrangements for both halogens.

There are marked variations in the energy barriers for the diol decomposition reaction that are dependent upon whether the halogen substituent is fluorine or chlorine. The fluorine barrier is 46 kJ mol^{-1} larger than the chlorine barrier when calculated relative to the diol-water complex. In the chlorine case the transition state [TS 4-6] is lower in energy than the isolated reactant molecules and the isolated diol and water species. For

fluorine the transition state [TS 4-5] is higher in energy than the isolated reactant molecules but only by 24 kJ mol^{-1}.

It is clear from Figure 4.10 that the addition of a second water molecule to the model for the gas phase hydrolysis of the formyl halides does reduce the activation energy for the reaction. This water molecule acts as a bifunctional catalyst with proton transfers to and from it for both parts of the two-step mechanism. It appears to catalyse the addition of water to the formyl chloride marginally more than for formyl fluoride. This is suggested by the fact that the barrier when X=Cl becomes slightly smaller than for X=F compared to the bimolecular case where this situation is reversed. The difference in the barrier heights also occurs for the decomposition step indicating that this process is also better catalysed when X=Cl rather than F.

The activation enthalpy for the bimolecular hydrolysis at 0 K is 157 kJ mol^{-1} for X=F and 160 kJ mol^{-1} for X=Cl. If the activation enthalpies at 0 K are compared with those for the bimolecular process (calculated relative to isolated reactant molecules) then the decrease from the addition of a second water is 110 kJ mol^{-1} when X=F and 115 kJ mol^{-1} when X=Cl. If the energy barriers for the termolecular process are calculated relative to the reactant encounter complexes then the inclusion of the second water molecule results in reductions of 56 and 64 kJ mol^{-1} respectively for the X=F and Cl cases. The second water molecule is thus an effective catalyst for the two-step mechanism of this gas phase reaction.

4.3.4.3 The One-Step Mechanism of the Gas Phase Termolecular Hydrolysis of the Formyl Halides

The one-step mechanism for the termolecular hydrolysis of formyl fluoride and chloride occurs through direct elimination of HX to yield product complexes where HX and formic acid are hydrogen bonded to the second water molecule. The product complexes can then dissociate to the isolated product molecules. This decomposition route occurs *via* transition states [TS 4-7] and [TS 4-8]. Figure 4.11 displays graphically the relative energies for the species along the reaction path for both the bimolecular and termolecular reactions. The relative energies of the reactant complexes are similar for X=F and Cl, however as stated in section 4.3.3 their structures are quite different due to the relative position of the CXHO molecule.

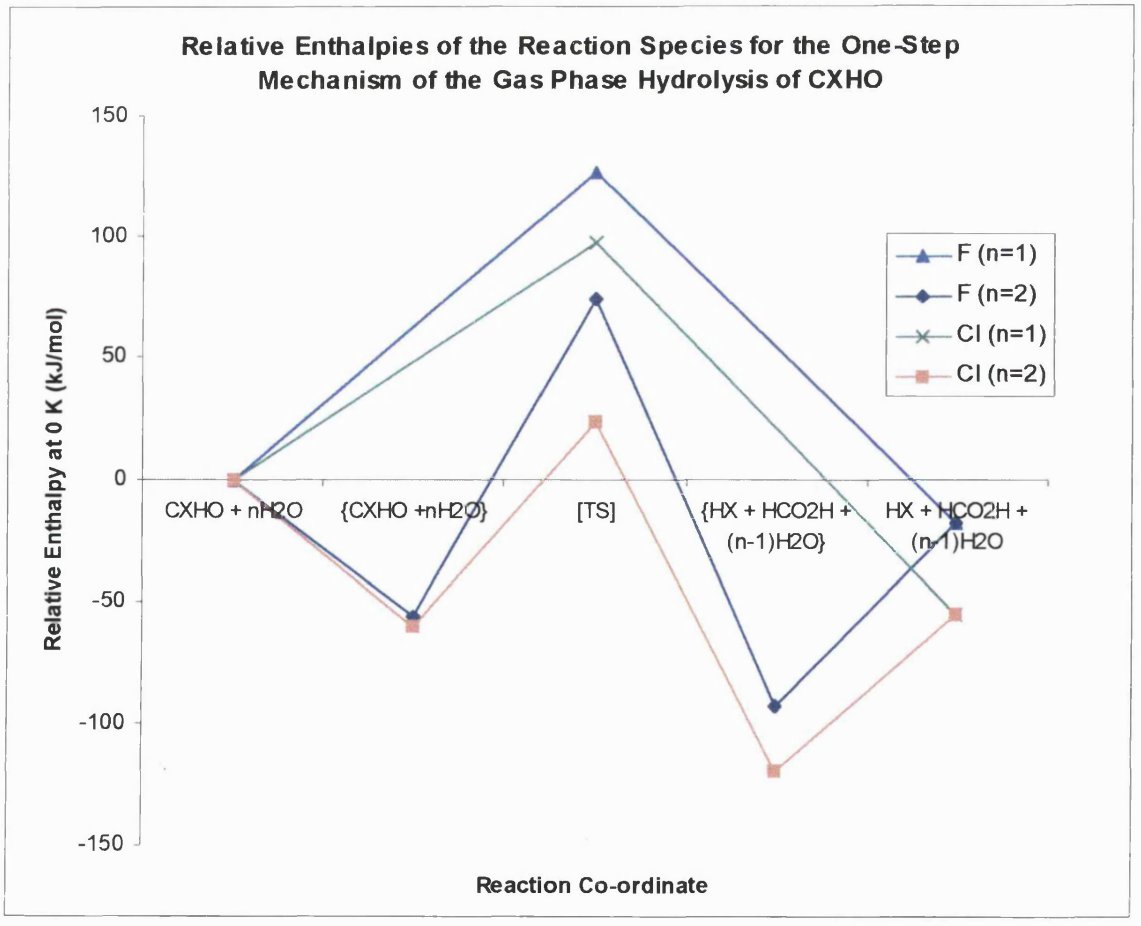

Figure 4.11

There are significant variations between the fluorine and chlorine transition state geometries. These differences are comparable to those observed for the decomposition of the $CXH(OH)_2$ intermediate in the two-step mechanism and as such are likely to be caused by the same property, namely the greater efficiency of chlorine as a leaving group than fluorine. When X=Cl the elimination tends to proceed through the initial departure of Cl^- followed by abstraction of H^+. In the case of fluorine the reaction progresses in a more synchronous fashion.

The transition states are essentially the same as the bimolecular direct elimination structures with the additional water molecule hydrogen bonded to them. This extra water molecule does not take part in any proton transfers rather it reduces the energy of the transition states by stabilising the charge build up through hydrogen bonding. This is in contrast to the two-step mechanism where the additional water molecule acts as a bifunctional catalyst for both the adduct formation and decomposition steps.

The elimination products are lower in energy for chlorine over fluorine both when part of a hydrogen bonded complex and as separate molecules. As the water molecule and formic acid molecules are common products for both reactions then the difference arises due to the relative energies of the HX species produced *i.e.* HCl has a lower relative energy than HF.

The product complex for this reaction, [PC 4-8], is lower in energy than [PC 4-6], the species produced as a result of the decomposition of the $CClH(OH)_2$ intermediate. However, when X=F the product complex for the diol decomposition reaction is lower in energy. In [PC 4-5] the HF molecule acts both as a hydrogen bond donor and acceptor whereas in [PC 4-7] the HF acts purely as a hydrogen bond donor. In [PC 4-6]

the chlorine atom does not form a strong hydrogen bond with the formic acid and the more stable arrangement of the molecules is the [PC 4-8] species. The more stable arrangement of the molecules in the product complex is thus dependent on the nature of the halogen involved.

It is evident from Figure 4.11 that the energy barrier for the direct elimination of HX is dependent on the halogen involved. The barrier for the termolecular process is 46 kJ mol^{-1} higher when X=F rather than X=Cl when calculated relative to the reactant complexes, with both [TS 4-7] and [TS 4-8] higher in energy than the isolated reactant species.

The one-step bimolecular hydrolysis has an activation enthalpy at 0 K of 127 kJ mol^{-1} when X=F and 98 kJ mol^{-1} when X=Cl. If the termolecular activation enthalpy is calculated relative to the isolated reactant molecules then the energy barrier decreases by 53 kJ mol^{-1} for X=F and 74 kJ mol^{-1} for X=Cl in the presence of the second water molecule. If calculated relative to the reactant complexes then the energy barrier actually increases by 3 kJ mol^{-1} when X=F, and only decreases by 14 kJ mol^{-1} if X=Cl when compared to the bimolecular processes. The effect of the additional water molecule is therefore less clear for the one-step mechanism. This is because the water molecule does not act as a bifunctional catalyst in [TS 4-7] and [TS 4-8] but instead stabilises the transition states through hydrogen bonding. This does not result in a reduction in the energy barrier when X=F but does if the substituent is chlorine.

The termolecular hydrolysis of the formyl halides accentuates the differences in behaviour of fluorine and chlorine. The deviations in the energy barriers for the one- and two-step mechanisms of this process highlight these differences. When X=Cl the

barrier for direct elimination to HCl and formic acid is 12 kJ mol^{-1} lower than the activation enthalpy for the two-step reaction. However if X=F then the energy barrier for the one-step mechanism is 29 kJ mol^{-1} higher than that for the two-step mechanism. These results suggest that the termolecular hydrolysis of formyl fluoride would occur *via* the formation of the $CFH(OH)_2$ intermediate followed by decomposition of the diol to elimination products, whereas for formyl chloride the one-step direct elimination mechanism would be the preferred reaction route.

4.4 Conclusions

The investigation of the hydrolysis of the formyl halides as a termolecular process has shown that the preferred mechanism is dependent upon the nature of the halogen. The termolecular hydrolysis of formyl fluoride would be predicted to occur *via* the two-step mechanism, while the analogous formyl chloride reaction would be expected to proceed *via* the one-step direct elimination mechanism. This confirms the conclusions predicted by the study of the bimolecular process for formyl chloride. However the preferred mechanism for the hydrolysis of formyl fluoride changes from the one- to the two-step process when an extra water molecule is added to the reaction model.

As stated in Chapter 3 the closest available experimental data to the hydrolysis of formyl chloride relates to the analogous, slower, reaction of Cl_2CO which has an activation energy of 59 kJ mol^{-1} at room temperature. The lowest calculated energy barrier for the termolecular hydrolysis of formyl chloride is 24 kJ mol^{-1} (relative to the isolated reactant molecules) or 84 kJ mol^{-1} (relative to the reactant complex) at 0 K. These values are in much better agreement with the experimental data than those calculated for the bimolecular hydrolysis reaction. It therefore appears that the

inclusion of a second water molecule to the model for the hydrolysis of formyl chloride improves the description of the reaction.

It has not been possible to uncover any experimental data relating to the hydrolysis of formyl fluoride. This lack of data with which to compare the calculated energy barriers has proven irritating but as with the paucity of data relating to formyl chloride, is probably caused by difficulties in handling the molecules involved. The consequence of having no experimental data is that it has been impossible to quantify the quality of the termolecular model of the reaction. However, the results for the fluorine substituent are similar to those for chlorine and it has therefore been assumed that the inclusion of a second water molecule in the model also improves the description of the formyl fluoride hydrolysis reaction.

The energy barriers reported in both Chapters 3 and 4 have been calculated at 0 K and as such are activation enthalpies for the gas phase hydrolysis of formyl fluoride and chloride. Although the values are in relatively good agreement with experiment the fact that they have been calculated at 0 K means that by definition entropy effects are not included. The formation of the reactant encounter complexes for the termolecular reaction would be an entropically disfavoured process and as such may decrease the catalytic effect of the additional water molecule. The hydrolysis of the formyl halides occurs in the troposphere at temperatures significantly higher than 0 K where entropy effects may be important. A further study of this gas phase reaction has therefore been carried out to determine the extent of entropy effects on the reaction by calculating the Gibbs free energies of activation and reaction for these processes. The results of this investigation are reported in Chapter 5.

5. GIBBS FREE ENERGIES FOR THE GAS PHASE HYDROLYSIS OF FORMYL HALIDES

5.1 Introduction

The gas phase hydrolysis of the formyl halides has thus far only been examined at 0 K. The calculated activation energies reported in Chapter 4 include the zero point vibrational energies but do not take account of the possible entropy effects that may arise from bringing together the individual molecules for the reaction to occur. As these reactions occur in the troposphere, in conditions very different to those at 0 K, it seemed advisable to try to determine the entropy effects on the activation and reaction energies by modelling the processes at temperatures and pressures more representative of the troposphere.

The physical conditions in the troposphere are dependent upon the altitude. In general the temperature and pressure both decrease with increasing altitude, but the absolute values are dependent upon a variety of factors including the season. One aim of this investigation has been to gain an understanding of how the energetics of the gas phase hydrolysis of the formyl halides might alter with different atmospheric conditions.

In order to take entropy effects into account it has been necessary to calculate free energies as these contain both enthalpy and entropy terms. The Gibbs free energies of the reaction species have therefore been calculated for temperatures and pressures ranging from 298 – 215 K and 1.0 – 0.1 atm respectively. This range of conditions was chosen as being representative of tropospheric conditions during the summer in the Northern Hemisphere at a latitude of 40° N.[114,115]

The decreases in temperature and pressure will have opposing effects on the entropy. As the temperature decreases the entropy should decrease and as the pressure decreases the entropy should increase. If these opposing forces cancel each other out then there should be negligible changes in the free energies of reaction and activation for the hydrolysis for the range of temperature and pressure values examined.

A further aspect of this study has been to determine whether entropy effects counteract the catalytic effect of the additional water molecule in the termolecular hydrolysis reaction. Gibbs free energies have therefore been calculated for the reaction species involved in both the gas phase bimolecular and termolecular hydrolysis processes and the reaction and activation free energies compared with the enthalpies calculated at 0 K.

5.2 Methods

Gibbs free energies of the reaction species for the gas phase hydrolysis of the formyl halides have been calculated using Gaussian 94.[111] It is only the species along the lowest energy paths for the one-and two-step mechanisms for the bi- and termolecular reactions that have been included. The calculations have been carried out on the fully optimised reactant, transition state, and product structures described in Chapters 3 and 4. The structures included were [TS 4-9], [TS 4-10], "[TS 3-2]", "[TS 3-4]", [TS 4-11], "[TS 3-7]" for the bimolecular processes. The [TS 4-3], [TS 4-4], [TS 4-5], [TS 4-6], [TS 4-7], [TS 4-8] transition structures, along with their associated reactant and product hydrogen bonded complexes, were included for the termolecular reactions. These structures were all optimised at the MP2(fu)/6-31G* level of theory. The Gibbs free energies have been calculated at this same level of theory for the following temperatures and pressures:

298.15 K	1 atm	(0 km)
290 K	0.9 atm	(1 km)
260 K	0.5 atm	(5-6 km)
235 K	0.3 atm	(9 km)
220 K	0.2 atm	(12 km)
215 K	0.1 atm	(16 km)

The numbers in brackets give the approximate altitude in kilometres that correspond to the individual temperature and pressure combinations.

In order to evaluate the free energy the harmonic vibrational frequencies of a molecule must first be calculated. The frequencies of the species studied were all calculated at the MP2(fu)/6-31G* level of theory. A brief description of how the free energy can be related to the harmonic frequencies through statistical thermodynamics is given below.

5.2.1 Calculation of Free Energies[116-118]

The relationship that relates the free energy of a system to other thermodynamic properties is:

$$\Delta G = \Delta H - T\Delta S \qquad \text{(Equation 5.1)}$$

where ΔG, ΔH, and ΔS are the changes in free energy, enthalpy, and entropy respectively associated with 1 mole of reaction at constant temperature and pressure. The enthalpy can be evaluated at 0 K by adding the zero-point vibrational energy to the total potential energy obtained from an *ab initio* molecular orbital calculation. Thermal energy corrections can then be made to determine the enthalpy term for a particular temperature and pressure. Therefore the unknown term in the equation that needs to be calculated so that the free energy can be determined is the entropy of the system.

The molar entropy for a material with a singlet electronic ground state can be partitioned as in Equation 5.2.

$$S = S(vib) + S(rot) + S(trans) = 0 \quad \text{at 0 K} \qquad \text{(Equation 5.2)}$$

The task is then to calculate these vibrational, rotational, and translational contributions to the entropy. In order to do this the molecular partition function, Q, must first be determined.

Q is defined as the ratio between the total number of molecules in a system, N, and the number of molecules in the zero energy level, n_0:

$$Q = \frac{N}{n_0} = \sum e^{-(\varepsilon_i - \varepsilon_0)/k_B T} \qquad \text{(Equation 5.3)}$$

ε_i is the energy of molecular energy level i, ε_0 is the energy of the zero energy level, k_B is the Boltzmann constant, and T is the absolute temperature. If all the molecules are in the ground state then $n_0 = N$ and consequently $Q = 1$.

The molecular partition function can be related to the entropy for one mole of non-localised molecules, such as a gas, through Equation 5.4:

$$S = k_B N_A \ln Q + k_B N_A T \frac{\partial(\ln Q)}{\partial T} - k_B \ln(N_A!) \qquad \text{(Equation 5.4)}$$

where N_A is the Avogadro constant and the remaining terms are the same as those defined for Equation 5.3. Q therefore provides a way of linking the properties of the molecular energy levels, ε_i, with that of the entropy of the molecules. As Q increases then so does the molar entropy.

The molecular energy levels, ε_i, can correspond to electronic, vibrational, translational or rotational energy levels. The majority of stable covalent compounds are in their

electronic ground states at typical temperatures. The electronic molecular partition function *Q(elec)* for singlet states would therefore be 1, and there would be no electronic contribution to the molar entropy for these molecules. The following sections describe how the remaining contributions to the entropy may be calculated.

5.2.1.1 Translational Entropy

The molecular kinetic energy of an ideal gas leads to Equation 5.5 for the translational molecular partition function, *Q(trans)*:

$$Q(trans) = \left(\frac{2\pi m k_B T}{h^2}\right)^{3/2} .V \qquad \text{(Equation 5.5)}$$

where m = molecular mass, T = absolute temperature, V = volume, k_B = the Boltzmann constant, and h = Planck's constant. This in turn leads to the expression for the translational entropy of n moles of an ideal gas:

$$S(trans) = nR.\ln\left\{\frac{e^{5/2}.V}{N_A}\left(\frac{2\pi m k_B T}{h^2}\right)^{3/2}\right\} \qquad \text{(Equation 5.6)}$$

where all the symbols are the same as in Equation 5.5, N_A is the Avogadro constant and e is the base of natural logarithms.

5.2.1.2 Vibrational Entropy

The total vibrational molecular partition function, *Q(vib)*, is the product of the vibrational molecular partition functions for each individual vibrational mode of a molecule:

$$Q(vib) = Q(vib.1).Q(vib.2).....Q(vib.i) \qquad \text{(Equation 5.7)}$$

$$= \prod Q(vib.i)$$

where *Q(vib.i)* is the value for a single harmonic mode i of frequency υ_i and is given by:

$$Q(vib.i) = \frac{1}{1 - e^{-h\upsilon_i / k_B T}} \qquad \text{(Equation 5.8)}$$

Thus the vibrational contribution to the molar entropy is dependent upon the values of the individual harmonic modes as well as the overall number of them.

5.2.1.3 Rotational Entropy

The number of rotational degrees of freedom of a molecule is 2 (linear molecule) or 3 (non-linear molecule). The molecular energy levels of a rotational mode are closer together than those for a vibrational mode. The higher energy levels of a rotational mode are therefore more likely to be populated and the rotational entropy of a compound is higher than the vibrational entropy.

The rotational molecular partition function for non-linear polyatomic molecules is given as:

$$Q(rot) = \frac{8\pi^2}{\sigma h^3} (I_1 . I_2 . I_3)^{1/2} (2\pi k_B T)^{3/2} \qquad \text{(Equation 5.9)}$$

where I_1, I_2, I_3 are the principal moments of inertia of the molecule, σ is the symmetry factor (the number of indistinguishable configurations of the molecule that can be generated by rotation of the whole molecule), and the remaining symbols are as defined for Equation 5.5.

Once the components of the partition function have been determined at a particular temperature and pressure then the total entropy can be calculated, and hence the free energy. In Gaussian 94 the entropy and free energy are automatically evaluated at 298.15 K and 1 atm after a frequency calculation. Evaluation of these properties at

different temperatures and pressures is easily achieved by specifying the values in the input script.

A further factor that needs to be specified in the input is a scaling factor used by Gaussian 94 during the calculation of the thermal energy corrections. This factor is used to eliminate known systematic errors in calculated frequencies. A scaling factor of 0.9661[119] is used for the computation of thermal energy corrections at the MP2(fu)/6-31G* level of theory. All the free energies reported in this chapter include this scaling factor for the thermal energy corrections.

5.3 Results and Discussion

The calculated relative free energies are presented in graph format so that the overall effects of the pressure and temperature changes can be observed more easily. The relative enthalpy changes are also plotted so that the free energy results can be compared with those at 0 K, and hence an estimate of the effect entropy has on the water catalysed reaction can be obtained.

5.3.1 Free Energies for the Gas Phase Two-Step Hydrolysis of the Formyl Halides

The relative Gibbs free energies of the reaction species for the two-step hydrolysis of CFHO are shown in Figure 5.1. Figure 5.2 shows the data for the analogous CClHO reaction.

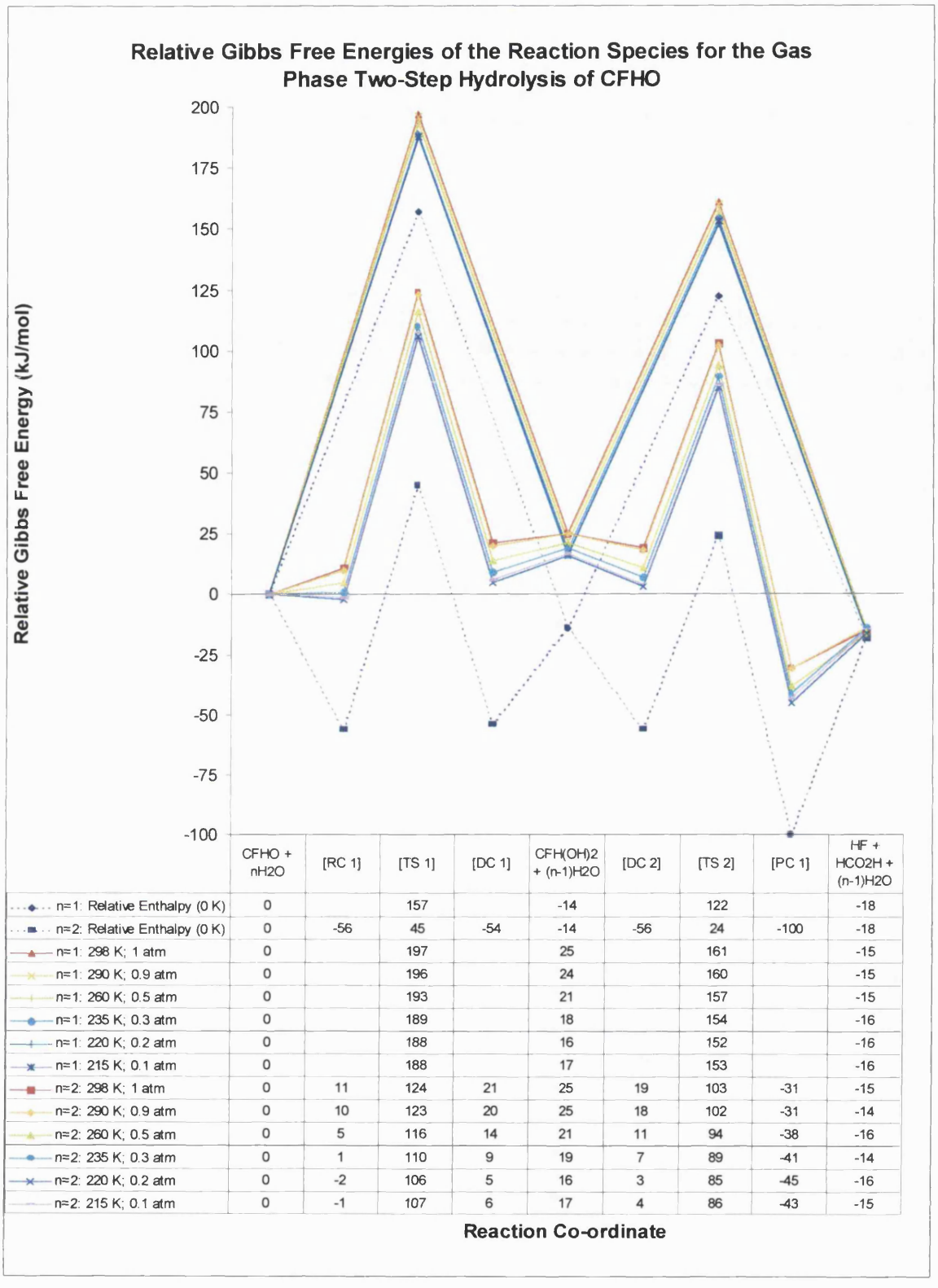

	CFHO + nH2O	[RC 1]	[TS 1]	[DC 1]	CFH(OH)2 + (n-1)H2O	[DC 2]	[TS 2]	[PC 1]	HF + HCO2H + (n-1)H2O
n=1: Relative Enthalpy (0 K)	0		157		-14		122		-18
n=2: Relative Enthalpy (0 K)	0	-56	45	-54	-14	-56	24	-100	-18
n=1: 298 K; 1 atm	0		197		25		161		-15
n=1: 290 K; 0.9 atm	0		196		24		160		-15
n=1: 260 K; 0.5 atm	0		193		21		157		-15
n=1: 235 K; 0.3 atm	0		189		18		154		-16
n=1: 220 K; 0.2 atm	0		188		16		152		-16
n=1: 215 K; 0.1 atm	0		188		17		153		-16
n=2: 298 K; 1 atm	0	11	124	21	25	19	103	-31	-15
n=2: 290 K; 0.9 atm	0	10	123	20	25	18	102	-31	-14
n=2: 260 K; 0.5 atm	0	5	116	14	21	11	94	-38	-16
n=2: 235 K; 0.3 atm	0	1	110	9	19	7	89	-41	-14
n=2: 220 K; 0.2 atm	0	-2	106	5	16	3	85	-45	-16
n=2: 215 K; 0.1 atm	0	-1	107	6	17	4	86	-43	-15

Figure 5.1

The first major observable effect of the inclusion of entropy is that for both the fluorine and chlorine cases the general pattern of relative energies of the various species along

the reaction co-ordinate is the same as at 0 K. However, the actual energies of these species changes considerably for both the one and two water instances.

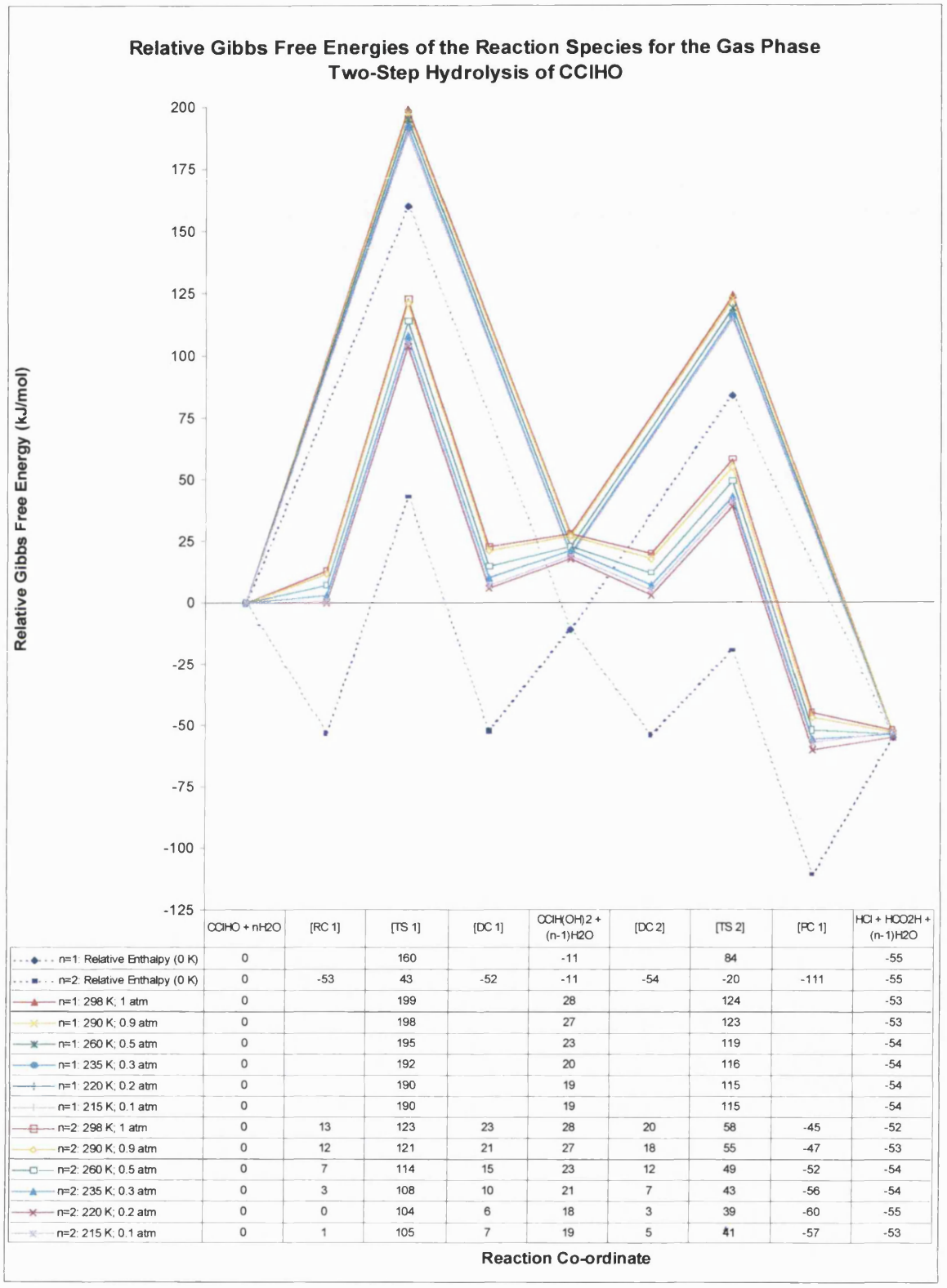

	CClHO + nH2O	[RC 1]	[TS 1]	[DC 1]	CClH(OH)2 + (n-1)H2O	[DC 2]	[TS 2]	[PC 1]	HCl + HCO2H + (n-1)H2O
n=1: Relative Enthalpy (0 K)	0		160		-11		84		-55
n=2: Relative Enthalpy (0 K)	0	-53	43	-52	-11	-54	-20	-111	-55
n=1: 298 K; 1 atm	0		199		28		124		-53
n=1: 290 K; 0.9 atm	0		198		27		123		-53
n=1: 260 K; 0.5 atm	0		195		23		119		-54
n=1: 235 K; 0.3 atm	0		192		20		116		-54
n=1: 220 K; 0.2 atm	0		190		19		115		-54
n=1: 215 K; 0.1 atm	0		190		19		115		-54
n=2: 298 K; 1 atm	0	13	123	23	28	20	58	-45	-52
n=2: 290 K; 0.9 atm	0	12	121	21	27	18	55	-47	-53
n=2: 260 K; 0.5 atm	0	7	114	15	23	12	49	-52	-54
n=2: 235 K; 0.3 atm	0	3	108	10	21	7	43	-56	-54
n=2: 220 K; 0.2 atm	0	0	104	6	18	3	39	-60	-55
n=2: 215 K; 0.1 atm	0	1	105	7	19	5	41	-57	-53

Figure 5.2

The energy barrier for the rate-determining first step of the bimolecular reaction is increased by 31 – 40 kJ mol^{-1} and 30 - 39 kJ mol^{-1} respectively for formyl fluoride and chloride when entropy effects were included. However the energy barrier for the unimolecular decomposition of the $CXH(OH)_2$ intermediate is essentially unaffected by the inclusion of entropy. It is therefore apparent that it is only the first step for which entropy effects are important. The free energy barriers for this step range from 188 – 197 kJ mol^{-1} and 190 - 199 kJ mol^{-1} for CFHO and CClHO respectively, with the lowest values occurring at the lower limit of the temperature and pressure ranges studied. The energy barriers for this reaction decrease as both the temperature and pressure are lowered. This indicates that for the temperature and pressure combinations examined the temperature has the greater effect.

The overall reaction energies exhibit only minor differences between the enthalpy value at 0 K and the free energies. The reaction remains exoergonic, to approximately the same extent irrespective of the conditions, for the range of temperatures and pressures considered here. As previously noted, the overall exoergonicity of the hydrolysis of formyl chloride is considerably greater than for the analogous formyl fluoride reaction.

There are significant variations in the reaction energy for the formation of the (+60,+60) conformer of the $CXH(OH)_2$ intermediate. The most important feature to note is that the diol becomes a higher energy species than the isolated reactant molecules. The first step of the two-step hydrolysis mechanism therefore becomes endoergonic at temperatures and pressures typical of the troposphere. The process is endoergonic by 17 - 25 kJ mol^{-1} when X=F and by 19 - 28 kJ mol^{-1} when X=Cl. The greatest energy penalty is again incurred for the 298 K, 1 atm temperature, pressure combination.

The formation of the $CXH(OH)_2$ intermediate is endoergonic because it is an entropically disfavoured process as two reactant molecules are brought together to form a single diol molecule. If the transition from an exothermic to an endoergonic process is to occur then the entropy component of the free energy must be greater than the enthalpy contribution. Thus this is what happens in this case, the entropy term outweighs the enthalpy term for the conditions considered, and the reaction becomes endoergonic.

The free energy of reaction for the unimolecular decomposition of the $CXH(OH)_2$ molecule is significantly more exoergonic than the same reaction at 0 K. This is a consequence of the fact that the relative free energy of the diol species is raised but that of the products is not. There will also be a positive entropy change on going from the intermediate species to the products. The free energy and enthalpy barriers to unimolecular decomposition of $CClH(OH)_2$ are both 96 kJ mol^{-1} compared to 136 kJ mol^{-1} for $CFH(OH)_2$. The 40 kJ mol^{-1} difference is a clear indication that chlorine is a better leaving group than fluorine.

The barrier height for the termolecular formation of the $CXH(OH)_2$ intermediate also increases when entropy effects are included. If calculated relative to the reactant complex the energy barriers increase by 7 – 12 kJ mol^{-1} and 8 – 14 kJ mol^{-1} respectively for formyl fluoride and chloride. The smaller increases in barrier height for the termolecular versus bimolecular reactions are the result of the different ways the reactants are defined. If the free energy barriers for the termolecular processes are calculated relative to the isolated reactant molecules, as they are for the bimolecular processes, then they are 62 - 72 kJ mol^{-1} and 61 – 80 kJ mol^{-1} higher respectively when X=F and Cl than the barriers at 0 K. In agreement with intuition the termolecular

processes are therefore affected to a greater extent by entropy contributions to the free energy than the bimolecular processes. The free energy barriers decrease as the temperature and pressure are lowered to the 220 K, 0.2 atm temperature, pressure combination and then remain constant. This suggests that the temperature has the greater effect on the entropy at the higher temperatures examined but that as the temperature and pressure decrease the pressure becomes more important until the two factors balance each other.

The energy barrier for the bimolecular decomposition of the $CXH(OH)_2$ intermediate, when evaluated relative to the diol-water complex, is marginally increased by the inclusion of entropy, the largest increase being only 4 kJ mol^{-1} for both halogen substituents. This follows the pattern exhibited for the unimolecular decomposition of the $CXH(OH)_2$ intermediate.

The relative energies of all the species along the reaction co-ordinate are raised for both the bimolecular and termolecular reactions. The general features of the profiles are the same for the bimolecular reaction irrespective of the temperature and pressure conditions. The termolecular hydrolysis of formyl fluoride also follows this trend but that of formyl chloride does not. It is the second step of the mechanism for which this reaction profile changes. At 0 K the transition state for the bimolecular decomposition of the $CClH(OH)_2$ molecule is lower in energy than the isolated diol and water species. The free energy profiles are different; the decomposition transition state has a higher energy than the diol and water molecules. A further variation occurs in the relative energies of the product complexes. At 0 K the dissociation of the product complexes to the separate product molecules is highly endothermic, however at the lower ranges of

the temperatures and pressures considered the energies are raised to the extent that the process becomes exoergonic.

The increases in the relative energies of the termolecular reaction species are large for both the formyl fluoride and chloride cases. The stabilisation imparted by the creation of intermolecular hydrogen bonds results in the formation of the reactant complexes being exothermic by 56 or 53 kJ mol^{-1} when X=F or Cl respectively at 0 K. At the typical tropospheric conditions considered, the formation of the reactant complex becomes either thermoneutral or endoergonic. The higher the temperature and pressure, the more endoergonic the process becomes. The stabilisation provided by the hydrogen bonds is thus negated by the decrease in the entropy associated with bringing together the reactant molecules to form the complexes in these conditions.

The free energy change for the transformation of the reactants to the diol-water complex is positive by 7 – 10 kJ mol^{-1} and 6 – 10 kJ mol^{-1} for X=F and Cl respectively. At 0 K this process is essentially thermoneutral, which suggests that the entropy contribution to the free energy is greater for the diol-water complexes than for the reactant complexes. The decrease in entropy is likely to be due to the change of three reactant molecules into two intermediate species as intermolecular hydrogen bonds exist in both complexes.

The difference in the free energies and enthalpies between the two diol-water species is very small but it is the complex that decomposes to products that is the more stable species. It is therefore evident that the intermolecular hydrogen bonding arrangement present in the second diol-water complex provides slightly greater stabilisation.

The difference in energy between the isolated diol and water molecules and the diol-water complexes is considerably reduced by the inclusion of entropy. At 0 K the separate diol and water molecules are 30 - 33 kJ mol^{-1} higher in energy than the first and second diol-water complexes. Entropy contributions to the free energies decrease these differences to 4 – 15 kJ mol^{-1} in tropospheric conditions. The smallest energy differences occur for the highest temperature and pressure combinations, again indicating that the entropy effects are most important at the highest temperatures and pressures considered.

The overall effect of the inclusion of entropy on the two-step mechanism is to raise the relative energies of all species along the reaction co-ordinate relative to the isolated reactant and product molecules. The result for the termolecular processes is that all the reaction species have higher energies than the separate reactant molecules for conditions typical of the troposphere. This is in contrast to the results at 0 K where for formyl chloride hydrolysis only the transition state for adduct formation is higher in energy than the reactants, and for formyl fluoride hydrolysis where just the transition states have higher relative energies than the reactants.

The rate-determining step for the two-step mechanism remains the formation of the $CXH(OH)_2$ intermediate for the bimolecular and termolecular processes and for both halogen substituents. It is noticeable that the termolecular processes are more susceptible to the effect entropy has on the relative energies of the reaction species. The termolecular processes are also more sensitive to variations in the temperature and pressure conditions than the bimolecular processes. However, it is clear that even with the inclusion of entropy effects, and the differences caused by the variations in

temperature and pressure conditions, the termolecular processes are still energetically preferred to the bimolecular processes for both formyl fluoride and chloride.

5.3.2 Free Energies for the Gas Phase One-Step Hydrolysis of the Formyl Halides

The relative free energies of the reaction species for the one-step hydrolysis of CFHO are plotted in Figure 5.3. The same data for the hydrolysis of formyl chloride is presented in Figure 5.4.

The reaction profiles for the bi- and termolecular one-step hydrolysis processes exhibit similar features to the two-step processes on the inclusion of entropy effects. The energies of all reaction species are raised relative to the reactant and product molecules at the temperatures and pressures examined.

The reactant complex for the one-step termolecular hydrolysis of formyl fluoride is identical to that for the two-step mechanism and consequently has the same energy. This is not the case for the formyl chloride reactant complex, which has a different structure and a slightly lower energy than that for the two-step mechanism. The free energies of the reactant complexes for both formyl fluoride and chloride again illustrate the effect of the entropy contribution to the free energy. The formation of these complexes is energetically unfavourable at the higher end of the range of temperatures and pressures considered, indicating that the entropy term outweighs the stabilisation imparted by the formation of hydrogen bonds in these complexes.

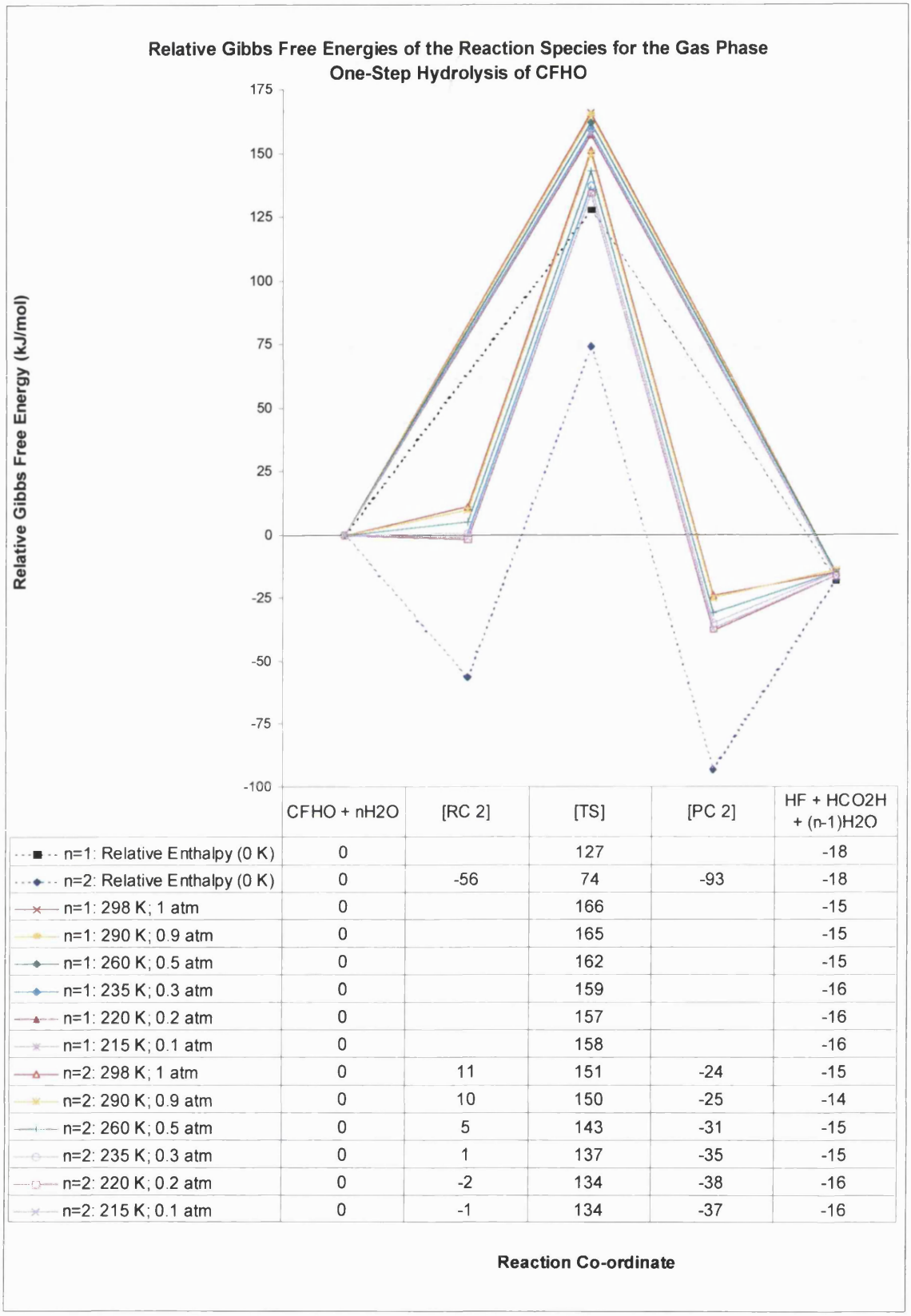

	CFHO + nH2O	[RC 2]	[TS]	[PC 2]	HF + HCO2H + (n-1)H2O
n=1: Relative Enthalpy (0 K)	0		127		-18
n=2: Relative Enthalpy (0 K)	0	-56	74	-93	-18
n=1: 298 K; 1 atm	0		166		-15
n=1: 290 K; 0.9 atm	0		165		-15
n=1: 260 K; 0.5 atm	0		162		-15
n=1: 235 K; 0.3 atm	0		159		-16
n=1: 220 K; 0.2 atm	0		157		-16
n=1: 215 K; 0.1 atm	0		158		-16
n=2: 298 K; 1 atm	0	11	151	-24	-15
n=2: 290 K; 0.9 atm	0	10	150	-25	-14
n=2: 260 K; 0.5 atm	0	5	143	-31	-15
n=2: 235 K; 0.3 atm	0	1	137	-35	-15
n=2: 220 K; 0.2 atm	0	-2	134	-38	-16
n=2: 215 K; 0.1 atm	0	-1	134	-37	-16

Figure 5.3

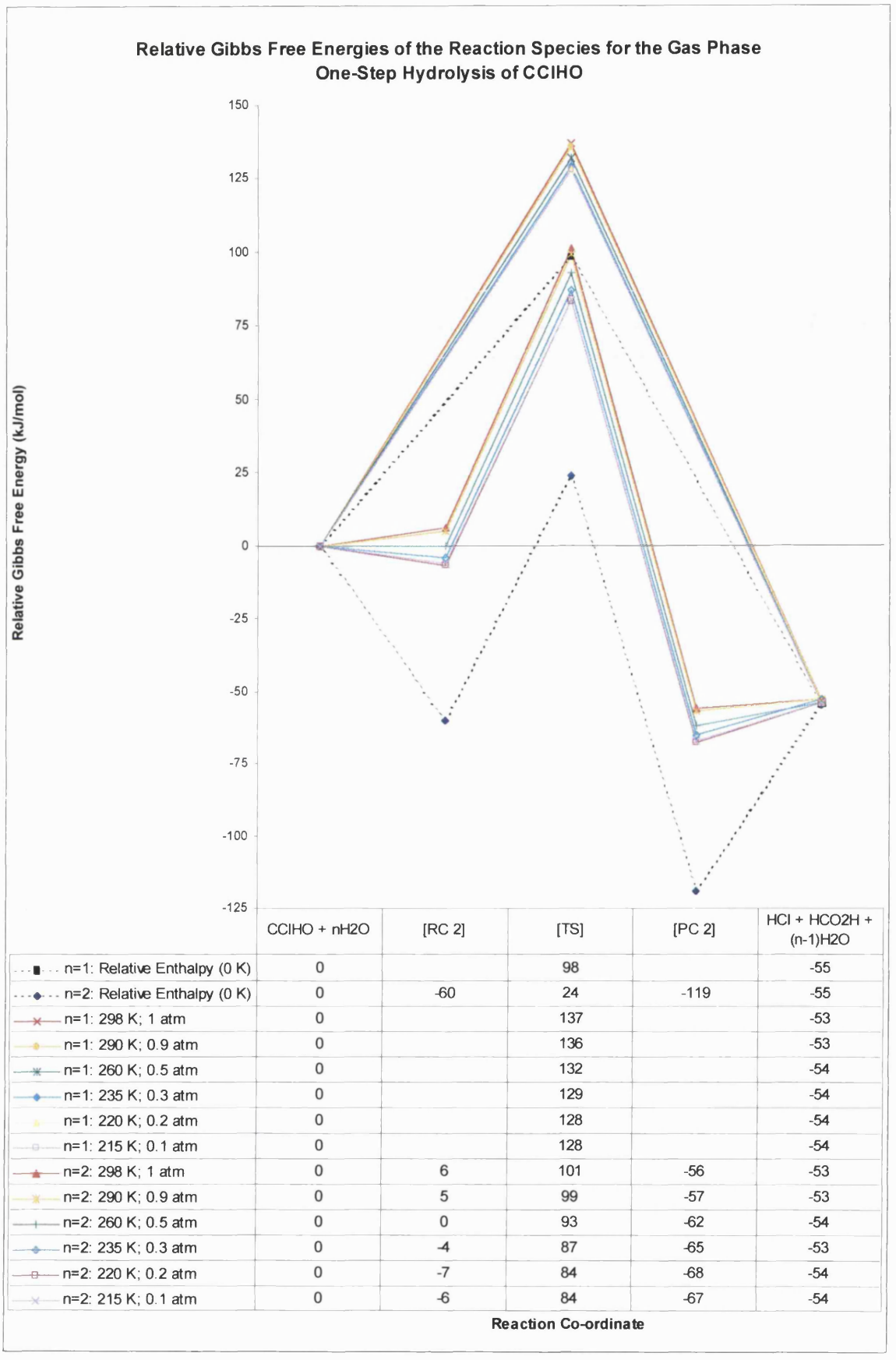

	CClHO + nH2O	[RC 2]	[TS]	[PC 2]	HCl + HCO2H + (n-1)H2O
n=1: Relative Enthalpy (0 K)	0		98		-55
n=2: Relative Enthalpy (0 K)	0	-60	24	-119	-55
n=1: 298 K; 1 atm	0		137		-53
n=1: 290 K; 0.9 atm	0		136		-53
n=1: 260 K; 0.5 atm	0		132		-54
n=1: 235 K; 0.3 atm	0		129		-54
n=1: 220 K; 0.2 atm	0		128		-54
n=1: 215 K; 0.1 atm	0		128		-54
n=2: 298 K; 1 atm	0	6	101	-56	-53
n=2: 290 K; 0.9 atm	0	5	99	-57	-53
n=2: 260 K; 0.5 atm	0	0	93	-62	-54
n=2: 235 K; 0.3 atm	0	-4	87	-65	-53
n=2: 220 K; 0.2 atm	0	-7	84	-68	-54
n=2: 215 K; 0.1 atm	0	-6	84	-67	-54

Figure 5.4

The increases in the energy barriers for the one-step bimolecular processes are comparable with those evaluated for the rate-determining first step of the two-step mechanism. They range from 31 – 39 kJ mol^{-1} for formyl fluoride and 30 – 39 kJ mol^{-1} for formyl chloride. The increases for the termolecular processes of 5 – 10 kJ mol^{-1} and 6 – 11 kJ mol^{-1} respectively for X=F and Cl are also consistent with the increases observed for the two-step mechanism when evaluated relative to the reactant complexes. The increases of 60 – 77 kJ mol^{-1} and 59 – 76 kJ mol^{-1} for the same barriers, calculated relative to the reactant molecules, are also comparable to those for the two-step mechanism.

The relative energies of the transition states are increased to the extent that for formyl fluoride hydrolysis all the free energies of the termolecular species are higher in energy than the enthalpy of the bimolecular species. This also occurs for the hydrolysis of formyl chloride but only at the highest temperature and pressure combinations. This does not occur for the profiles of the two-step hydrolysis mechanism.

The energies of the product complexes are raised relative to the reactants in tropospheric conditions. The product complex for the one-step hydrolysis mechanism of formyl fluoride is less stable than that for the two-step mechanism. The dissociation of this complex to product molecules is therefore less endothermic for the one-step mechanism. The reverse is the case for formyl chloride hydrolysis where the product complex that is produced from the one-step mechanism is the more stable species. The relative energies of the product complexes are the same as at 0 K, but the differences in the free energies between the complexes and the separate product molecules are significantly smaller than the enthalpy at 0 K.

The effect of examining the one-step hydrolysis mechanism at typical tropospheric temperatures and pressures is that, in agreement with the results for the two-step mechanism, the energies of all the species along the reaction co-ordinate are raised relative to the reactants and products, and the energy barriers increase for both the bi- and termolecular processes.

The termolecular processes are more sensitive to the variations in temperature and pressure than the bimolecular processes. The termolecular processes are also more susceptible to entropy effects on the relative energies of the reaction species. The level of catalysis that results from the introduction of an extra water molecule is less than that for the two-step mechanism. This is true for the reaction occurring at 0 K as well as at tropospheric temperatures and pressures. However despite this reduction in catalytic efficacy the termolecular processes are still energetically preferred to the bimolecular processes for both formyl fluoride and chloride.

5.4 Conclusions

Gibbs free energies have been determined at a range of temperatures and pressures for the reaction species along the lowest energy reaction paths of the one- and two-step mechanisms for the bimolecular and termolecular hydrolysis of the formyl halides. The dominant feature for each process is that the energies of all the reaction species are raised relative to the isolated reactant molecules when entropy effects are included. This trend occurs irrespective of the temperature and pressure, the mechanism, the halogen substituent, and whether the reaction is a bimolecular or termolecular process.

The mechanisms proposed for the bimolecular and termolecular processes remain the same as those predicted in Chapters 3 and 4 for the temperature and pressure ranges considered here. Thus for the bimolecular hydrolysis the one-step mechanism is preferred for both formyl fluoride and chloride. The most energetically favourable mechanisms for the termolecular hydrolysis are the two-step process for formyl fluoride and the one-step process for formyl chloride.

The activation free energies for the energetically favoured mechanisms are 158 – 166 kJ mol^{-1} and 128 – 137 kJ mol^{-1} for the bimolecular hydrolysis of formyl fluoride and chloride respectively. The free energies of activation of the preferred mechanisms for the termolecular hydrolysis are 108 – 113 kJ mol^{-1} for formyl fluoride and 90 – 95 kJ mol^{-1} for formyl chloride (calculated relative to the reactant complexes). These free energy barriers are 107 – 124 kJ mol^{-1} and 84 – 101 kJ mol^{-1} respectively when X=F and Cl and when evaluated relative to the separate reactant molecules. The catalytic effect of a second water molecule is therefore retained in tropospheric conditions, but the quantitative effect on the energy barriers is less than for the reaction at 0 K. The reduction in the catalytic effect is 30 – 39 kJ mol^{-1} for both formyl fluoride and chloride if the termolecular barriers are calculated relative to the isolated reactant molecules.

The altitude at which the hydrolysis of the formyl halides occurs will affect the activation energies of the processes. At low altitudes the temperature has the greater effect on the entropy contribution to the free energy. At higher altitudes in the troposphere the pressure becomes an equally important factor, balancing the opposing effect of the temperature, and consequently the activation energies decrease. The results presented in this chapter therefore suggest that the hydrolysis of the formyl halides is more likely to occur at higher altitudes in the troposphere.

The calculated free energies of activation of the bimolecular and termolecular hydrolysis processes remain high at tropospheric temperatures and pressures. A possible way to reduce the calculated energy barriers would be to again increase the number of water molecules in the system to see if extra catalysis would occur. However the work of Wolfe *et al.*[120,121] on formaldehyde shows that although the lowest energy path for hydration occurs with four water molecules present the catalytic effect of the third and fourth water molecules are much less than that of the second. Similar behaviour is likely for the fluoro and chloro substituted versions of this reaction. The work involved in locating the necessary transition states, reactant and product complexes with third and fourth water molecules present did not seem justified for the minor energetic gain expected. A different approach to the reaction has therefore been taken and is discussed in chapters 6 and 7 of this thesis.

6. QM/MM MODELLING OF FORMYL HALIDE HYDROLYSIS

6.1 Introduction

In recent years the focus of atmospheric chemistry research, both experimental and theoretical, has shifted away from the study of gas phase reactions. This change has occurred due to the realisation that heterogeneous and multiphase processes[122,123] play an important role in many areas of atmospheric chemistry. In particular heterogeneous reactions taking place on polar stratospheric cloud (PSC) particles[124-132] and sulfuric acid aerosols[133-141] have been identified as being important in explaining ozone depletion in the stratosphere.

In recognition of the possibility that heterogeneous and multiphase processes may also be important to the chemistry of the troposphere it was decided to investigate the hydrolysis of the formyl halides as a reaction occurring within a water droplet. The main impetus for considering this hydrolysis as a condensed phase rather than a gas phase reaction came from experimental data. The work by Libuda *et al.*[72] indicated that the hydrolysis of formyl chloride was much faster with water molecules condensed on the walls of the reaction chamber than the gas phase molecules. In addition, as can be seen from chapters 4 and 5 the hydrolysis can be catalysed by an additional water molecule. However the catalytic effect is reduced at tropospheric temperatures and pressures due to unfavourable entropy contributions to the free energy. If the reacting water molecules were already part of a larger system (as in Figure 6.1), then bringing them together in an appropriate configuration for the reaction to take place should not incur such heavy entropic penalties.

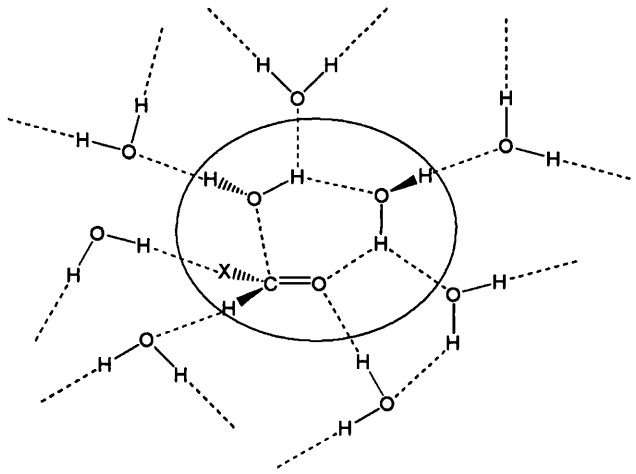

Figure 6.1

The gas phase hydrolysis of the formyl halides was studied using *ab initio* quantum mechanical (QM) methods due to the small number of atoms involved. QM calculations quickly become prohibitively computationally expensive as the system studied increases in size. It was therefore not possible to use pure QM calculations to investigate the condensed phase hydrolysis of formyl halides due to the inclusion of the large number of water molecules that make up the water droplet. Molecular mechanics (MM) methods are usually used for studying larger systems. However, as it is not generally possible to model bond making and breaking processes using MM techniques, studying reactions with MM methods is not feasible. Consequently combined quantum mechanical molecular mechanical (QM/MM) methods have been developed. These techniques treat the atoms that take an active part in the reaction quantum mechanically, and the remainder of the system using a molecular mechanics force field. A hybrid QM/MM method was therefore chosen as a practical and affordable approach to modelling formyl halide hydrolysis within a water droplet. Consideration of computing costs has also meant that QM/MM calculations using *ab initio* molecular orbital methods for the QM part have not been possible and semi-empirical calculations have been used instead.

6.2 Methods

The specific hybrid QM/MM method chosen to investigate the heterogeneous hydrolysis of the formyl halides has utilised the GRACE[142] and CHARMM24b2[29,143] programs. Brief descriptions of the general principles of QM/MM modelling, and of the GRACE program are given below.

6.2.1 GRACE

GRACE was developed to bring together the different codes necessary for carrying out QM/MM modelling. Its internal algorithms and structures allow control over external quantum mechanical, molecular mechanical, and visualisation codes to enable novel approaches to modelling. GRACE provides a more sophisticated control system than is available in the codes it calls as well as access to its own optimisers and analytical tools. Its novel features include a range of optimisers for minima, saddle points and IRC paths. GRACE provides for visualisation of eigenvectors during saddle point location *via* interfaces with external visualisation programs such as RasMol[144] and XMol.[145] GRACE writes pdb files that can be read and animated in XMol or RasMol. This process enables the user to make sure that the correct mode is followed. The most advanced built-in interface in GRACE is with CHARMM24b2. It is this interface that has been exploited to investigate condensed phase formyl halide hydrolysis. The AM1 based QM/MM method in CHARMM has been used with GRACE providing the ability to locate refined transition structures and IRC paths from these structures.

6.2.2 QM/MM

The approach used in this thesis to model the hydrolysis of the formyl halides occurring within a water droplet is a combined quantum mechanical (QM) and molecular mechanical (MM) method. The water droplet is divided into two regions, the first contains the reacting atoms of interest and is treated quantum mechanically so that the bond making and breaking processes can be investigated. The second region contains the atoms surrounding the reacting core, in this case solvent molecules, which are described using a molecular mechanics force field (Figure 6.2).

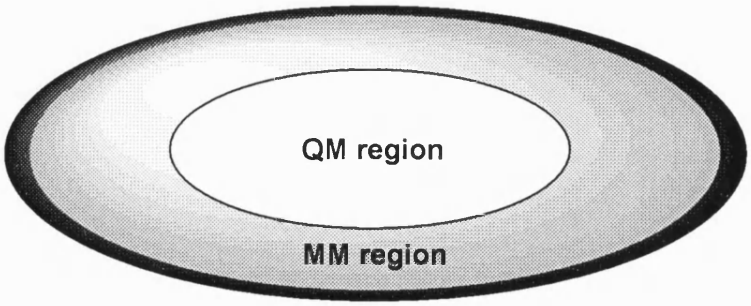

Figure 6.2

The total energy (E_{TOTAL}) for the system can then be written:

$$E_{TOTAL} = E_{QM} + E_{MM} + E_{QM/MM} \qquad \text{(Equation 6.1)}$$

where E_{QM} is the energy of the parts of the system treated exclusively by quantum mechanics, and E_{MM} is the energy arising from the parts described purely by molecular mechanics. $E_{QM/MM}$ is the interaction energy between the QM and MM parts of the system.

The total energy of the system at a particular configuration (E_{TOTAL}) is obtained by solving the time-independent Schrödinger equation:

$$H_{eff}\Psi(r_i,R_a,R_M) = E_{TOTAL}(R_a,R_M)\Psi(r_i,R_a,R_M) \qquad \text{(Equation 6.2)}$$

where H_{eff} is an effective Hamiltonian for the entire system, and Ψ is the wavefunction for the complete system. r_i and R_a represent the co-ordinates of the electrons and nuclei respectively in the QM region, and R_M the co-ordinates of the atoms in the MM region. The effective Hamiltonian, H_{eff}, can also be broken down into contributions from the various parts of the system:

$$H_{eff} = H_{QM} + H_{MM} + H_{QM/MM} \qquad \text{(Equation 6.3)}$$

where H_{QM} is a standard Hamiltonian specific to the method chosen for the QM part. H_{MM} is the standard energy for the MM part, E_{MM} (see section 1.4 for a more detailed description of E_{MM}). $H_{QM/MM}$ is a Hamiltonian describing the interaction between the QM and MM regions.

In CHARMM the AM1[14] and MNDO[13] semi-empirical methods are used to describe the QM atoms. These semi-empirical methods only explicitly consider the valence electrons, the core electrons are included in the nuclear core. In this thesis the reacting atoms are treated quantum mechanically using the AM1[14] Hamiltonian, and the solvent molecules are treated with molecular mechanics. Thus there are no atoms on the border of the QM and MM regions and the energy term for the interaction between the QM and MM atoms of the system is due only to the non-bonded interactions. The Hamiltonian $H_{QM/MM}$ can then be written as:

$$H_{QM/MM} = -\sum_i \sum_M \frac{q_M}{r_{i,M}} + \sum_a \sum_M \frac{Z_a q_M}{R_{a,M}} + \sum_a \sum_M \left(\frac{A_{a,M}}{R_{a,M}^{12}} - \frac{C_{a,M}}{R_{a,M}^{6}} \right) \qquad \text{(Equation 6.4)}$$

The subscripts i, a, and M refer to a quantum mechanical electron, a quantum mechanical nucleus, and a molecular mechanical nucleus respectively. q_M is the partial charge of nucleus M and Z_a is the charge on the QM nucleus a. $r_{i,M}$ is the distance between the electron i and the MM nucleus M. $R_{a,M}$ is the distance between QM and MM nuclei. The first two terms of Equation 6.4 account for the electrostatic

interactions between QM electrons and MM nuclei, and QM and MM nuclei respectively. The third term represents the van der Waals interactions between the QM and MM nuclei. The second and third terms do not involve electronic co-ordinates and are therefore constant for a given nuclear configuration.

6.2.3 AM1/CHARMM and GRACE QM/MM Modelling

In this thesis QM/MM calculations using the AM1[14] Hamiltonian for the QM part of the system have been performed. The search for saddle points is achieved using a two-zone optimiser[146] as shown in Figure 6.3. The fast cycling zone provides an 'environment' surrounding a slow-cycling 'core'. In the context of the current investigation the 'core' represents the reacting atoms, namely the formyl halide plus one or two water molecules.

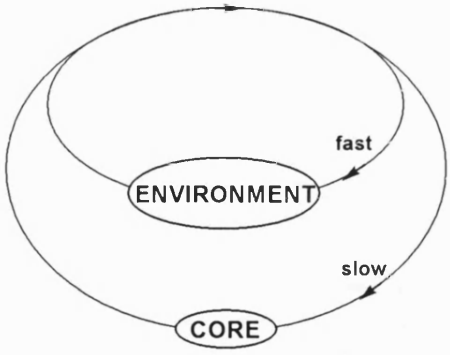

Figure 6.3

The algorithm attempts to maintain the gradient of the environment at zero and the potential energy at a minimum. It then searches for a saddle point in the degrees of freedom for the core. Before each energy and gradient evaluation for the core, the environment is optimised to a minimum. Thus the number of cycles of the optimiser acting on the environment is much greater than for the core.

The ABNR[29] optimiser is used to minimise the environment and stores only a diagonal hessian and a small number of previous steps and gradient vectors. It has been chosen because it is an internal CHARMM routine and is more efficient than the available external routine in GRACE due to faster inter-process communications. A full hessian matrix is only stored and maintained for the core.

After the transition structure has been refined then the hessian for the core atoms can be used to start an intrinsic reaction co-ordinate (IRC) calculation in both directions to locate reactant and product species.

6.2.4 Computational Procedure

The following method has been used to locate transition states for the hydrolysis of the formyl halides occurring within a water droplet. In this study only the actual reacting parts of the process have been examined. The initial diffusion of the formyl halide molecule into the water droplet, the ordering of the solvent into a configuration from which a reaction can occur, and the post reaction processes such as diffusion away of the product molecules were beyond the scope of this investigation.

In order to set up the system the solute ($CXHO + nH_2O$ where X=F,Cl and n=1,2) was embedded in a pre-formed 15 Å radius TIP3P[147] water sphere. The TIP3P MM forcefield models water using a rigid water monomer represented by three electrostatic sites. A partial negative charge centred on the oxygen atom (-0.834) is balanced by partial positive charges on the hydrogen atoms (0.417). The van der Waals interaction between the water monomers is represented by a single Lennard-Jones term between the oxygen atoms.

Once the solute was embedded in the water sphere a MM minimisation of the solvent around the solute was performed using CHARMM. The resulting system was a sphere containing the solute surrounded by approximately 500 water molecules. This system was divided into QM and MM regions and a transition state search initiated using the two-zone optimiser in GRACE.

Initial guesses for saddle point calculations were obtained by solvating the optimised gas phase transition structures described in Chapters 3 and 4. Transition structures for both the gas phase bimolecular and termolecular hydrolysis processes were solvated. There were therefore either seven or ten atoms in the QM core depending on whether one or two water molecules were to be treated quantum mechanically. The environment (*i.e.* solvent) was continually optimised to a minimum root mean square (r.m.s.) gradient of 0.001 kcal mol^{-1} $Å^{-1}$. The core was optimised to a first order saddle point until no element of the gradient vector of the entire system was greater than 0.03 kcal mol^{-1} $Å^{-1}$. IRC calculations were performed in both directions from the saddle point to determine the nature of the reactant and product species. The reactant- and product-like structures from the IRC calculations were optimised to energy minima using the QM/MM AM1/TIP3P method resident in CHARMM.

6.3 Results and Discussion

6.3.1 QM/MM Modelling of the Bimolecular Hydrolysis of Formyl Halides

6.3.1.1 $CXHO + 1H_2O \rightarrow CXH(OH)_2$

The AM1/TIP3P optimised transition states for the formation of the $CXH(OH)_2$ where the solute contains the formyl halide and one water molecule are shown in Figure 6.5. The solute plus all solvent water molecules within 2.8 Å of the solute are displayed. The atom distances are given in Angstroms. The TIP3P waters are shown in blue and grey, and the quantum water in red and white. The quantum atoms are numbered according to the scheme presented in Figure 6.4. All of the structures shown in this chapter are displayed in the same way. [TS 6-1] and [TS 6-2] contain fluorine and [TS 6-3] and [TS 6-4] contain a chlorine substituent.

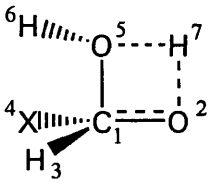

Figure 6.4

Each of the transition states pictured had only one negative eigenvalue in the hessian of the core showing that they are all first-order saddle points. In [TS 6-1] and [TS 6-3] the H^6-O^5 bond eclipses the C-X bond whereas in [TS 6-2] and [TS 6-4] the H^6-O^5 bond eclipses the C-H^3 bond instead. The proton transfer is advanced in all four cases as evidenced by the elongated H^7-O^5 bond [TS 6-1] to [TS 6-4].

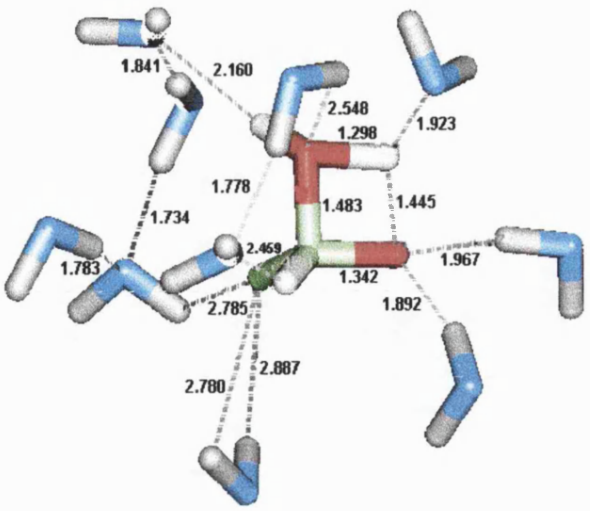

[TS 6-1]

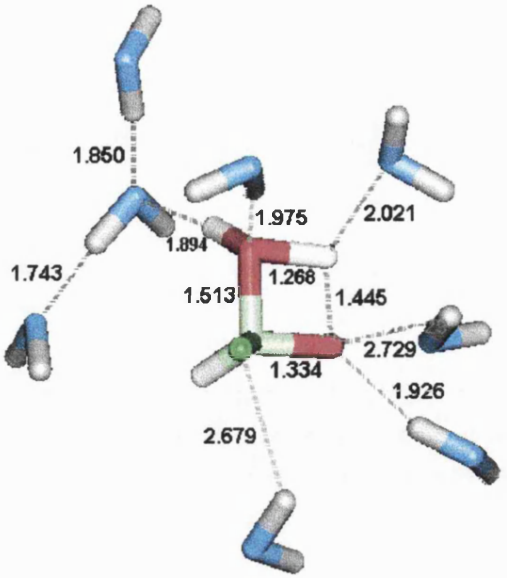

[TS 6-2]

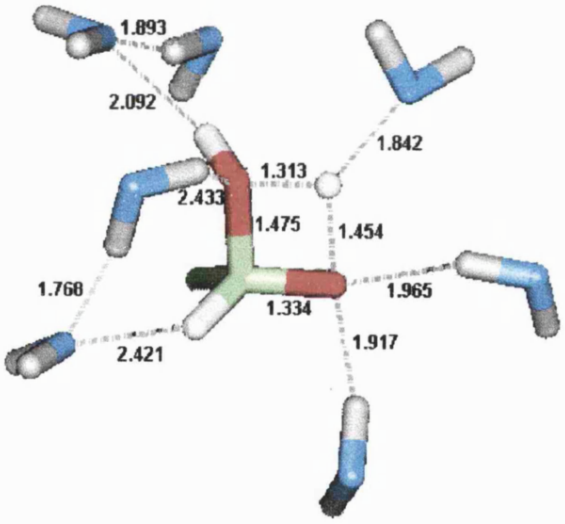

[TS 6-3]

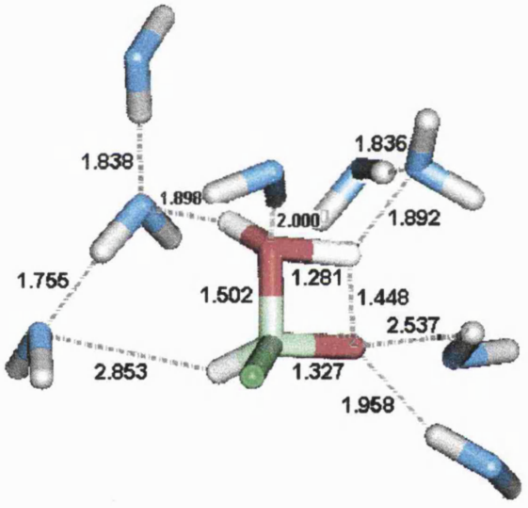

[TS 6-4]

Figure 6.5

Overall the geometries of the quantum atoms of these transition states are similar to those of the gas phase structures. It is therefore the arrangement of the solvent molecules around the quantum atoms that is of greater interest. One of the advantages of QM/MM over continuum methods is that specific solute-solvent interactions are

involved. These can provide insight into the structural stabilisation that solvation offers. It should be noted that although distinct solvation structures are displayed for the transition states shown above (and the structures shown in the remainder of this chapter) these pictures are only snapshots of stationary points. They are not unique but may be regarded as members of a large group of similar stationary points. Any reorganisation of the solvent may perturb the system enough to produce a new transition structure. This structure can be similar or dissimilar in energy and structure to the original transition state. However, allowing for the fact that the snapshots pictured in Figure 6.5 are not unique there are still features of the solvent structures common to the four transition states.

The first noticeable feature is that a solvent water molecule forms a strong hydrogen bond interaction with the proton (H^7) transferred during the reaction. This hydrogen bond is also observable in the reactant structures (see Figure 6.6) but is not as strong in these species as evidenced by the longer hydrogen bond lengths. This hydrogen bond may provide a greater stabilising effect in the transition state than in the reactant species and thus assist the proton transfer in a way not possible in the gas phase. The non-transferred proton (H^6) of the quantum water molecule also acts a hydrogen bond donor to a solvent water in each transition state. Another feature clearly visible in the solvent structures is that the halogen atom, whether fluorine or chlorine, is not well solvated. It forms at best only very weak hydrogen bond interactions with the TIP3P waters. This feature is also observable in the reactant and product species.

The reactant structures that result from optimising the 'reactant'-like species from the IRC calculations give similar structures for both halogen substituents. Example reactant

structures are shown in Figure 6.6, and are numbered according to the transition states from which they are derived.

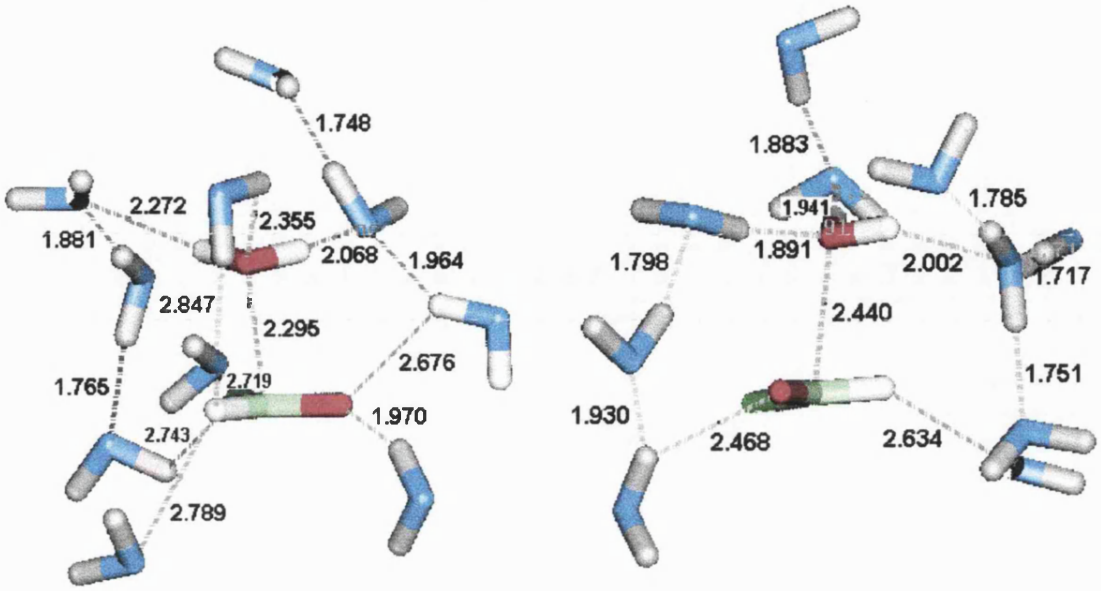

[R 6-1] **[R 6-4]**

Figure 6.6

The reactant structures are all similar with the quantum water acting as expected as a hydrogen bond donor and acceptor. An interesting feature of the solvent arrangement is that in each case the carbonyl oxygen atom of the formyl halide accepts one strong hydrogen bond and one much weaker interaction. This pattern is retained in [TS 6-2] and [TS 6-4] but in [TS 6-1] and [TS 6-3] the orientation of the solvent molecule changes and consequently this oxygen atom (O^2) forms two strong hydrogen bonds.

Transition states [TS 6-1] to [TS 6-4] lead to the formation of different conformers of the $CXH(OH)_2$ intermediate. [TS 6-1] and [TS 6-3] yield the (+60,-60) conformer and [TS 6-2] and [TS 6-4] the (180,-60) conformer (for definition of naming system of $CXH(OH)_2$ conformers refer to Figure 3.7). [D 6-1] and [D 6-4] are examples of each conformer of the solvated diol species and are shown in Figure 6.7.

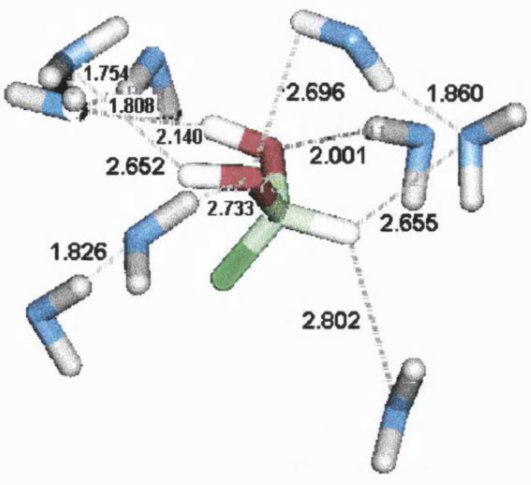

[D 6-1]

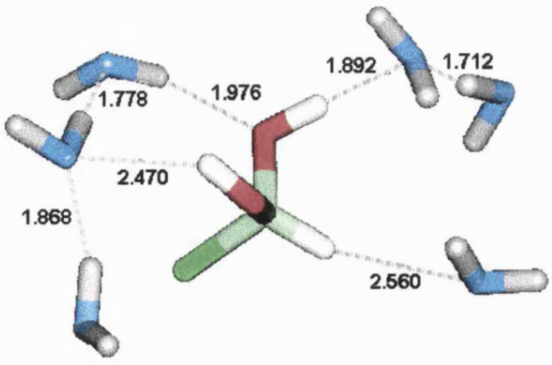

[D 6-4]

Figure 6.7

The nature of the halogen substituent does not affect the conformer of the intermediate produced. It is the relative position of the H^6-O^5 bond in the transition states that determines which conformer is formed. The formation of different conformers of the diol intermediate is not consistent with the *ab initio* results reported in chapter 3. The gas phase results predict that the (-60,-60) conformer is produced from both the possible reaction paths. In order to investigate the reason for this difference, gas phase transition states for these processes were located at the AM1 level of theory, IRC calculations performed and the reactant and product structures determined. These *in vacuo* AM1 calculations gave the same results as the AM1/TIP3P calculations, namely that different conformers of the $CXH(OH)_2$ diol are formed from the two reaction paths. These results show that it is the level of theory used in the QM/MM calculations rather than the effect of solvation that is responsible for the difference between the gas phase and solvated reactions.

In the solvated diol structures pictured the halogens remain poor hydrogen bond acceptors. The hydroxyl (H^6O^5) group of the diols with the ~180° or ~60° HOCX

dihedral angle forms strong hydrogen bond interactions with the TIP3P waters. In contrast the other hydroxyl group (H^7O^2) where HOCX ~ -60° forms only weak interactions with the solvent molecules.

The total and relative energies of all of the AM1/TIP3P species discussed so far are reported in Table 6.1.

Table 6.1 – Total and Relative Energies of the AM1/TIP3P CXHO + $1H_2O \rightarrow$ $CXH(OH)_2$ Reaction Species

	AM1 (qm)		AM1/TIP3P	
Species	Total (kcal/mol)	Relative (kJ/mol)	Total (kcal/mol)	Relative (kJ/mol)
[R 6-1]	-155.8	0	-6377.0	0
[TS 6-1]	-115.3	170	-6329.9	197
[D 6-1]	-174.1	-77	-6387.7	-45
[R 6-2]	-155.1	0	-6396.0	0
[TS 6-2]	-112.5	178	-6354.3	175
[D 6-2]	-172.8	-74	-6413.8	-74
[R 6-3]	-104.1	0	-6314.6	0
[TS 6-3]	-60.5	182	-6267.8	196
[D 6-3]	-117.1	-54	-6341.5	-112
[R 6-4]	-102.8	0	-6345.6	0
[TS 6-4]	-58.0	187	-6297.6	201
[D 6-4]	-115.6	-54	-6356.5	-45

In order to gain an insight into the energetic effects of solvation on the reaction it is necessary to compare the AM1/TIP3P energy barriers and reaction energies with gas phase results for the same processes. The analogous gas phase results reported in Chapter 3 were calculated at the MP2(fc)/6-311+G**//HF/6-31G* level of theory, and

as previously stated result in different conformers of the intermediate being formed than observed here. Therefore to compare those energies with the AM1/TIP3P results would not be comparing 'like with like'. The 'gas phase' results reported in Table 6.1 have therefore been calculated with this in mind. The energies in Table 6.1 were produced by running single point energy calculations on the bare solute atoms of the AM1/TIP3P optimised structures using the AM1 Hamiltonian. This essentially gives gas phase AM1 energies of the solute geometries. Any differences in the energy barriers and reaction energies in Table 6.1 should therefore be the result of solvation effects.

The AM1/TIP3P and AM1 (qm) barrier heights for the addition of water to the formyl halides exhibit only small differences due to substituent effects. The intramolecular hydrogen bonding which produces a lowering of the energy barrier for the gas phase equivalents of [TS 6-1] or [TS 6-3] is still observable for the AM1/TIP3P chlorinated species. However, as the intermolecular interactions between the solute and solvent are much greater than the single intramolecular interaction possible in the solute, it is probable that the fact that the lower energy barrier occurs for [TS 6-3] is purely coincidental. The relative barriers for the AM1/TIP3P chlorinated transition states may well be altered by different solvation structures. This is what is observed in the case of formyl fluoride, where the relative energies of the AM1/TIP3P transition states are opposite to that expected from the gas phase results.

The more significant variations in the AM1/TIP3P results lie in the values calculated for the reaction energies. As the energy barriers for the four processes are relatively similar, the differences in the reaction energies must arise due to differences in the solvation structures for the $CXH(OH)_2$ intermediates. The conformers of this diol are simple rotamers of each other as discussed in Chapter 3. In the gas phase their relative

energy differences are exceedingly small, in the order of 1 kJ mol^{-1} at the MP2(fc)/6-311+G**//HF/6-31G* level of theory. When solvated, however, their AM1/TIP3P relative energies can differ by as much as 29 kJ mol^{-1} or 67 kJ mol^{-1} for X=F or Cl respectively. These large variations in energies for simple rotamers of the same solute serve as a reminder that the structures pictured here, from which the energies are evaluated, are simple snapshots of non-unique solvation structures.

The unexpected outcome of calculating the energies of the bare solute atoms has been that the AM1 (qm) energy barriers are actually lower than the AM1/TIP3P barriers for these reactions. This suggests that the reactant species are better solvated than the transition states for these essentially bimolecular processes. The AM1 (qm) reaction energies are basically the same for both pathways but show marked substituent effects. The formation of the $CFH(OH)_2$ intermediate is ~20 kJ mol^{-1} more exothermic than that of $CClH(OH)_2$ in the gas phase. This is in contrast to the solvated systems where the solvation effects result in significant variations for the different reaction paths and the substituents.

6.3.1.2 $CXH(OH)_2 \rightarrow HX + HCO_2H$

The AM1/TIP3P transition states for the decomposition of the $CXH(OH)_2$ are shown in Figure 6.8. The atom distances are given in Angstroms. Each of the hessians computed for the quantum atoms of the transition states contained a single negative eigenvalue. Two transition states have been located for the unimolecular decomposition of $CFH(OH)_2$ ([TS 6-5] and [TS 6-6]) whilst only one has been located for $CClH(OH)_2$ ([TS 6-7]).

[TS 6-5] and [TS 6-6] were obtained from the same initial guess structure for the quantum atoms. The different transition structures were obtained because the pre-formed 15 Å water sphere in which the quantum atoms were embedded was rotated by 60 degrees prior to the saddle point search that resulted in the location of [TS 6-6]. The variations in the geometries of [TS 6-5] and [TS 6-6] are therefore purely due to the effect of having a different solvent structure around the solute. [TS 6-7] was also obtained from a saddle point search started from the solute embedded in the rotated water sphere.

A saddle point search was attempted for the solute embedded in the standard non-rotated water sphere for the chlorinated species. It was unsuccessful because the only mode with a negative eigenvalue corresponded to the chlorine atom abstracting the hydrogen atom of the C-H^3 bond. Although it is possible to follow other modes using GRACE none of the remaining modes resembled the one associated with diol decomposition.

Inspection of the solvent structure around the solute showed a possible cause for this unlikely outcome. In the gas phase the transition states for this process showed marked differences in the geometries of the fluorine and chlorine species. When X=Cl the C-Cl bond is effectively already dissociated in the transition state and the chlorine acts as a chloride ion. If this behaviour persists in solution then this chloride would be expected to form strong hydrogen bond interactions with solvent molecules. However the initial solvent structure from which the saddle point search was initiated did not show these interactions. There were therefore no significant chloride-solvent interactions that could stabilise the charge of the chloride and it abstracted the hydrogen from the C-H^3 bond.

It was anticipated that if the chloride could be better solvated in the transition state then this reaction would be less likely to occur because the C-H[3] bond would be 'screened' by a solvent molecule. This proved to be the case when the solute was embedded in the rotated water sphere. The chlorine atom formed good interactions with the solvent and the saddle point search located the transition state [TS 6-7].

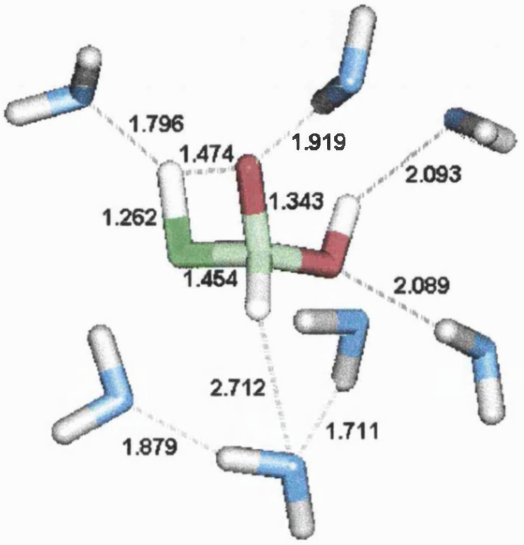

[TS 6-5]

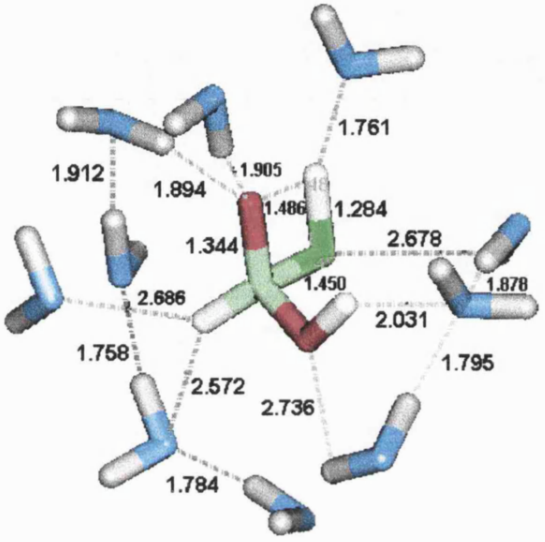

[TS 6-6]

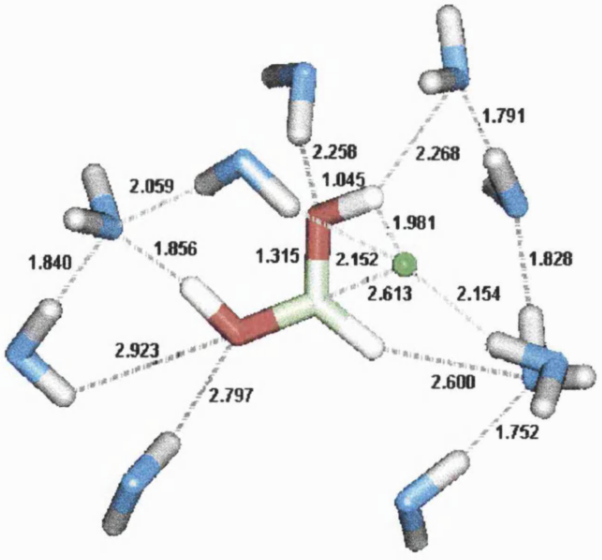

[TS 6-7]

Figure 6.8

The QM atom geometries of these transition structures resemble those seen in the gas phase for this process. When X=F the reaction is clearly more of a concerted process than when X=Cl. In both [TS 6-5] and [TS 6-6] the proton transfer is advanced and the C-F bond only partially broken. In [TS 6-7], where X=Cl, the C-Cl bond is essentially fully broken, but the proton transfer is just beginning.

Examination of the solvent structures for these species shows that the fluorine atom does not act as a hydrogen bond acceptor with solvent water molecules. In contrast the chlorine atom forms hydrogen bonds with both the quantum proton to be transferred and two TIP3P water molecules. This is due to the differences in the partial charges of the fluorine and chlorine in these transition states. Fluorine has a Mulliken charge of –0.20 whereas chlorine has a partial charge of –0.80. The chlorine thus acts more like a chloride ion whilst the fluorine behaviour stays the same as it is in the $CFH(OH)_2$ molecule.

The solvent structures in general show the same type of hydrogen bond interactions with the solvent as observed for the transition states for the formation of the $CXH(OH)_2$ intermediate. The specific interactions for [TS 6-5] to [TS 6-7] have a more profound effect on the reaction process than for the earlier transition states considered. In [TS 6-1] to [TS 6-4] it is the position of the H^6-O^5 bond relative to the C-X bond that appears to determine the nature of the conformer of the diol intermediate formed. In [TS 6-5] to [TS 6-7] it is the solvent arrangement that has the greater effect on which conformer of the $CXH(OH)_2$ intermediate decomposes to give products. Figure 6.9 shows the conformers of the diol which are the result of optimising the structures obtained from IRC calculations.

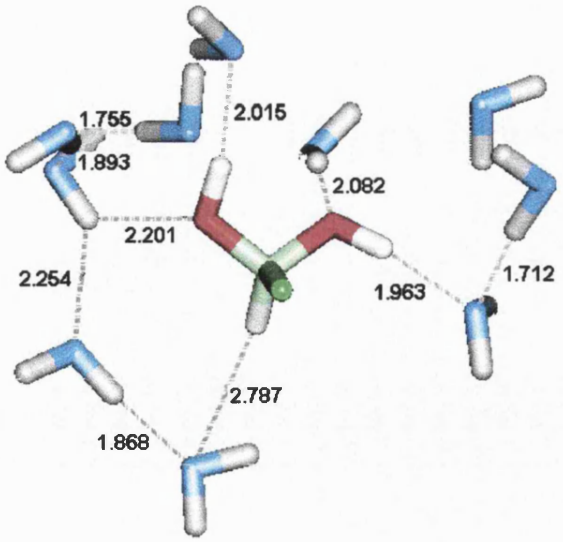

[D 6-5]

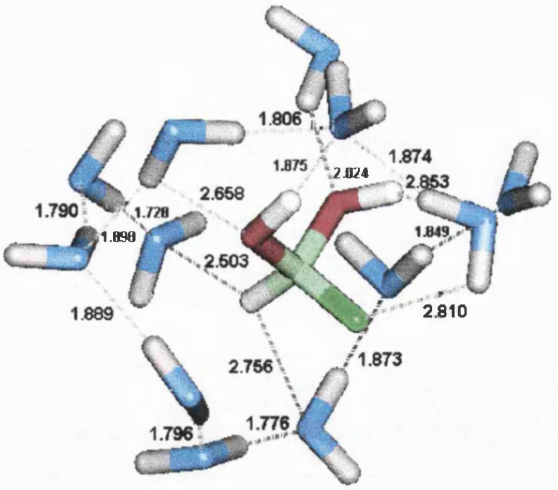

[D 6-6]

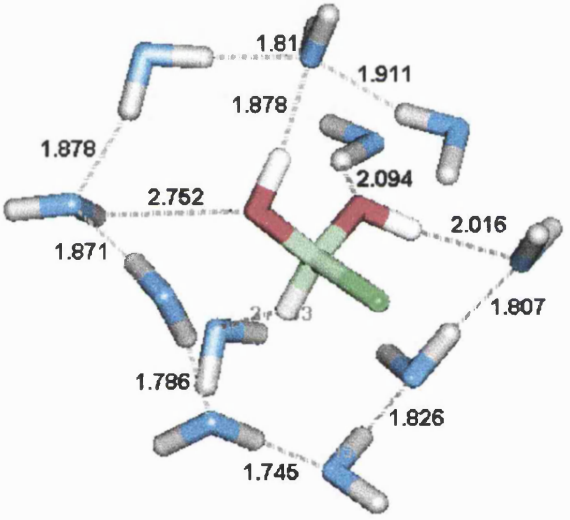

[D 6-7]

Figure 6.9

Different conformers of $CFH(OH)_2$ are observed depending upon which pre-formed 15 Å TIP3P water sphere the solute atoms of the transition state guesses were embedded. [TS 6-5] was the result of embedding the solute into the standard water sphere available within CHARMM. The diol conformer that decomposes through this transition structure is the (+60,+60) species ([D 6-5]). [TS 6-6] resulted from a saddle

point search on solute atoms embedded into the rotated pre-formed water sphere. The diol conformer decomposing through this route is the (+60,-60) species.

A single path has been located for the decomposition of the $CClH(OH)_2$ intermediate. This was obtained from a saddle point search where the solute was embedded in the rotated water sphere. The (+60,+60) conformer of the diol ([D 6-7]) decomposes through [TS 6-7] to yield products. The (+60,+60) conformer of $CClH(OH)_2$ is not one of the species produced by either of the diol forming reaction paths. Therefore the two-steps of the hydrolysis process are not directly connected. However, the $CXH(OH)_2$ is significantly affected by the solvent arrangement of the pre-formed water sphere into which the gas phase transition state is embedded. It is likely that if calculations were performed with further rotations of the pre-formed water sphere before initiating a transition state search, then one of the resulting transition structures would lead from the (+60,-60) or (180,-60) conformers to the products. Alternatively a low energy interconversion between the (+60,-60) or (180,-60) and (+60,+60) conformers could occur to allow decomposition to proceed.

The solvent arrangements around the diols are basically as expected. The hydroxyl groups act as hydrogen bond donors and acceptors with the solvent molecules and the halogens do not.

The product structures shown in Figure 6.10 also exhibit distinct differences between the fluorine and chlorine substituted species.

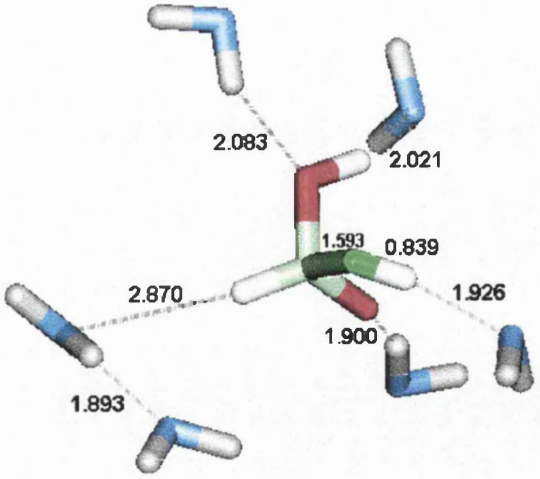

[P 6-5]

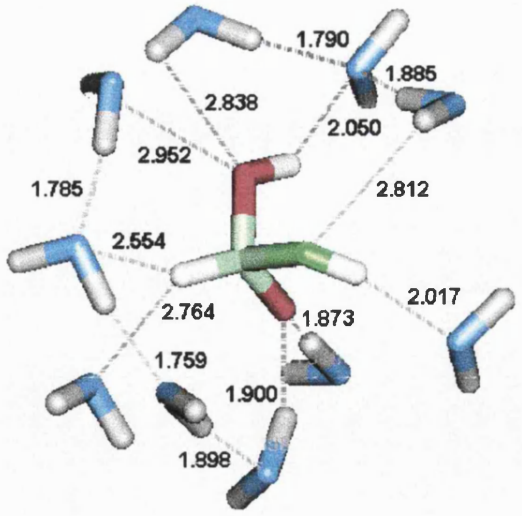

[P 6-6]

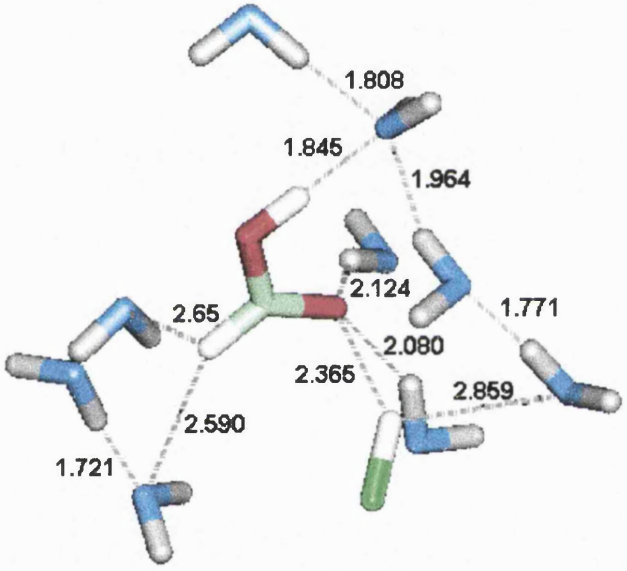

[P 6-7]

Figure 6.10

The products of the decomposition of $CClH(OH)_2$ are the anticipated HCl and HCO_2H molecules. The formic acid is produced in its most stable 'cis' conformer where HOCO = 0° and HCl is produced as a covalent species. The HCl molecule does not form strong interactions with the solvent. The proton retains a hydrogen bond with the carbonyl oxygen of the formic acid, but the chlorine atom does not take part in any

hydrogen bond interactions. The nature of the HCl species produced will be discussed in more detail later.

The formic acid of the product complex [P 6-7] forms the expected hydrogen bond interactions with the solvent except the hydroxyl oxygen atom, which for this particular solvent arrangement, does not act as a hydrogen bond acceptor. However, as has been stated previously, these structures are not unique and are in fact members of a family. It is therefore likely that other, similar solvent arrangements exist in which this oxygen atom does form hydrogen bond interactions with the solvent.

The nature of the products of the decomposition of the $CFH(OH)_2$ intermediate is less straightforward. Optimisation of the product-like structures from IRC calculations on [TS 6-5] and [TS 6-6] resulted in the location of the product structures [P 6-5] and [P 6-6]. It is apparent that in the [P 6-5] and [P 6-6] structures the C-F bond is only partially dissociated. These structures appear to be made up of the lowest energy conformer of formic acid with HF still bonded to the carbon atom.

The solvent structure does not seem to affect the nature of the products, as evidenced by the minor differences in the geometries of the quantum atoms in [P 6-5] and [P 6-6]. The structures of the product species had repercussions for the energetics of these processes. The energies of the [P 6-5] and [P 6-6] species were much higher than those expected for HF and formic acid molecules.

[P 6-5] and [P 6-6] were clearly not the expected product species. However, it was not apparent whether these species would decompose to the separate product molecules *via* a further transition state, or if they were artefacts of the QM/MM method used. In order

to investigate this possibility, line searches were performed on [P 6-5] and [P 6-6] in which the C-F bond distance was elongated in 0.1 Å increments. AM1/TIP3P energies were calculated for each C-F bond distance to see if a maximum energy structure occurred along this path from which a saddle point search could be initiated.

Maximum energy species were found along each path with C-F bond lengths of ~1.8 Å, and the structures obtained were used as initial geometries for the saddle point searches. These resulted in the location of the transition structures [TS 6-5(a)] and [TS 6-6(a)] pictured in Figure 6.11.

IRC calculations were then run from [TS 6-5(a)] and [TS 6-6(a)] from which the product-like species were optimised to the minimum energy structures [P 6-5(a)] and [P 6-6(a)]. The reactant species for these processes were confirmed as [P 6-5] and [P 6-6].

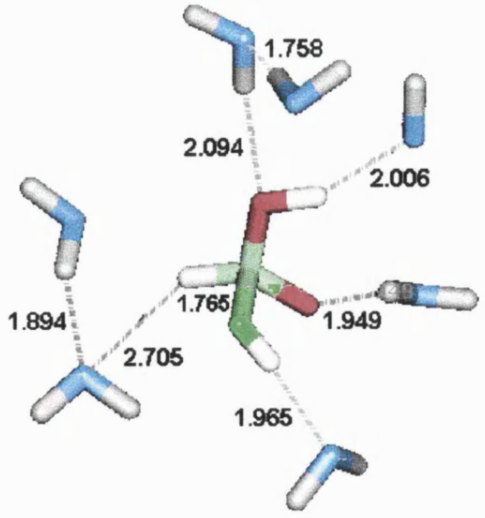

[TS 6-5(a)]

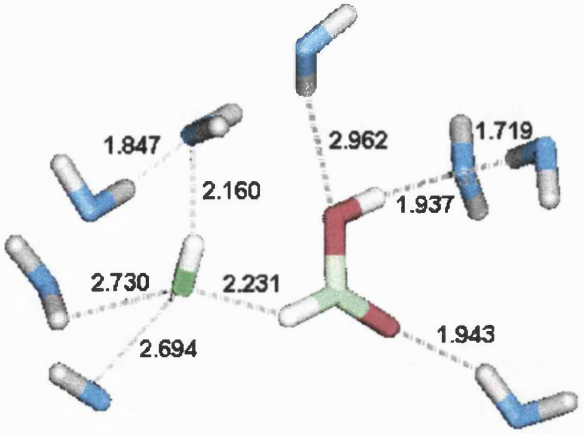

[P 6-5(a)]

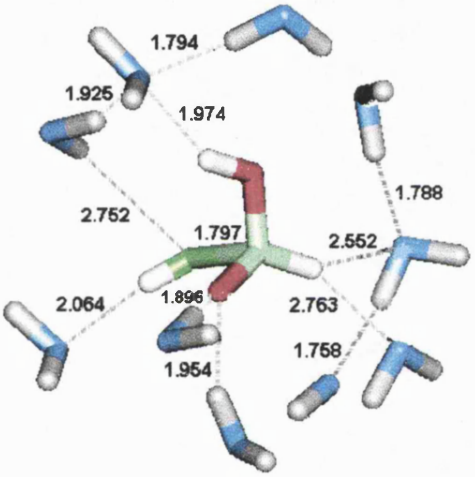

[TS 6-6(a)]

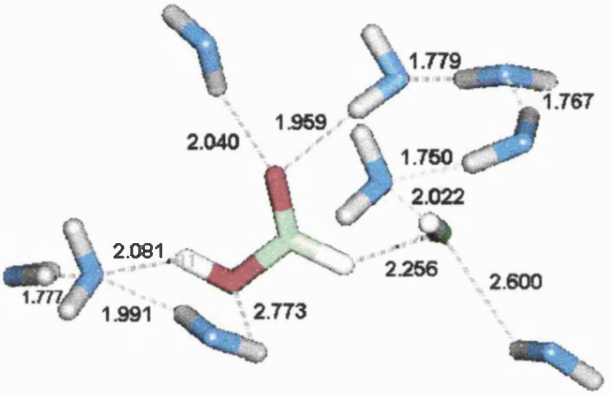

[P 6-6(a)]

Figure 6.11

The geometries of the quantum atoms of [TS 6-5(a)] and [TS 6-6(a)] are essentially identical to those for [P 6-5] and [P 6-6], but with a stretched C-F bond. The [P 6-5(a)] and [P 6-6(a)] product structures contain the expected separated HF and formic acid molecules. In agreement with the [P 6-7] structure for the analogous chlorine substituted process the HF is produced as a covalent species.

The unimolecular decomposition of $CFH(OH)_2$ is therefore a two stage process in which proton transfer occurs first and is then followed by C-F bond cleavage. This is in contrast to $CClH(OH)_2$ decomposition which occurs as an asynchronous yet concerted process with C-Cl bond cleavage followed by proton transfer. The reason for the two-step decomposition of $CFH(OH)_2$ remains unclear and could be caused by one of several factors.

The first possibility is that it is the AM1 description of the fluorine atom that causes the problem. If the AM1 description overestimates the strength of the C-F bond then this could provide an explanation for the lack of C-F bond dissociation in [P 6-5] and [P 6-6]. AM1 calculations were carried out *in vacuo* to model the same decomposition process to see if the same type of problem arose in the gas phase. In fact no such *pseudo* product species as [P 6-5] or [P 6-6] were found and the decomposition of $CFH(OH)_2$ was concerted. Therefore, even if the AM1 description does overestimate the C-F bond strength, it is not this factor alone that causes the stabilisation of the [P 6-5] and [P 6-6] species.

A second possible explanation for the two-steps necessary for C-F bond dissociation involves solute-solvent interactions. It is hypothesised that if the interactions between the solvent and the HF molecule could be made stronger then the C-F bond would dissociate as a concerted process, as hydrogen bonding could stabilise the charge separation during the reaction. This hypothesis has been investigated and the results are discussed in section 6.3.3.

The total and relative energies of the diol, transition state, and product species described in this section are reported in Table 6.2.

Table 6.2 – Total and Relative Energies of the AM1/TIP3P $CXH(OH)_2 \rightarrow HX + HCO_2H$ Reaction Species

	AM1 (qm)		AM1/TIP3P	
Species	Total (kcal/mol)	Relative (kJ/mol)	Total (kcal/mol)	Relative (kJ/mol)
[D 6-5]	-172.9	0	-6379.2	0
[TS 6-5]	-110.3	262	-6318.1	258
[P 6-5]	-155.7	72	-6367.8	48
[TS 6-5(a)]	-157.5	64	-6367.0	51
[P 6-5(a)]	-173.3	-2	-6382.0	-12
[D 6-6]	-174.0	0	-6367.4	0
[TS 6-6]	-109.8	268	-6303.4	268
[P 6-6]	-155.0	79	-6351.3	67
[TS 6-6(a)]	-157.8	68	-6349.5	75
[P 6-6(a)]	-173.0	4	-6363.4	17
[D 6-7]	-117.1	0	-6310.7	0
[TS 6-7]	-76.3	171	-6278.1	136
[P 6-7]	-123.7	-27	-6320.1	-39

The first major noticeable feature of both the AM1 (qm) and AM1/TIP3P energies for the decomposition of $CFH(OH)_2$ is that the energy barriers for the paths *via* [TS 6-5] and [TS 6-6] are much higher than those for $CFH(OH)_2$ formation reported in the previous section. These energy barriers are also significantly larger than those calculated *in vacuo* at the MP2(fu)/6-31G* level of theory. It suggests that the AM1 description may indeed overestimate the C-F bond strength, and that this is the reason for the large energy barriers associated with these decomposition processes.

The gas phase AM1 calculations mentioned above for the decomposition of $CFH(OH)_2$ have also been used to determine whether the large AM1/TIP3P energy barriers are due

to the AM1 description of the reaction or are partially the result of Hammond postulate considerations due to the high relative energies of the [P 6-5] and [P 6-6] species. IRC calculations were performed on the transition state, and the reactant- and product like structures optimised to minimum energy species. The gas phase AM1 energy barrier for this process was 265 kJ mol^{-1} and the reaction was basically thermoneutral. The similarity between this value and the AM1/TIP3P barriers confirms that it is the AM1 description of the reaction that leads to the large energy barriers.

The energy barriers for the decomposition of the $CFH(OH)_2$ intermediates are large enough to make this the rate-determining step of the two-step mechanism. This is a further difference that arises from the use of semi-empirical AM1 method rather than the *ab initio* molecular orbital calculations used in chapters 3 and 4.

The effect of solvation on the energy barriers for the decomposition of $CFH(OH)_2$ is negligible. The differences in the relative energies of the [P 6-5], [TS 6-5], [P 6-6], and [TS 6-6(a)] species upon solvation are small but significant. The AM1 (qm) results on the bare solute atoms show that in the gas phase the [TS 6-5(a)] and [TS 6-6(a)] structures have lower energies than the [P 6-5] and [P 6-6] species respectively. The AM1/TIP3P results show that this situation is reversed within a water droplet. This provides evidence that the solute-solvent interactions are the reason for the stabilisation of the [P 6-5] and [P 6-6] geometries that makes the extra step for complete dissociation of the C-F bond necessary. The energy barriers for the dissociation of the C-F bond are small at 3 and 8 kJ mol^{-1} respectively for the reaction paths through [TS 6-5(a)] and [TS 6-6(a)].

The reaction energy for the decomposition of the (+60,-60) conformer of $CFH(OH)_2$ is exothermic but that for the decomposition of the (+60,+60) conformer is endothermic. However, since the formation of the $CFH(OH)_2$ intermediate is largely exothermic, the overall reaction energy remains exothermic whichever conformer decomposes to products.

The large variation in the relative energies of the solvated $CFH(OH)_2$ conformers may also affect the reaction energies for the decomposition of these species. If the specific solvent arrangement around the $CFH(OH)_2$ molecule is a low energy configuration compared to the many others possible, then as a consequence the first step of the reaction will be more exothermic and the second step less exothermic.

The relative energies of the chlorine substituted species are very different to those for the fluorine species. The AM1/TIP3P energy barrier is much smaller at 136 kJ mol^{-1} and the reaction energy of –39 kJ mol^{-1} shows that the process is more exothermic than the equivalent fluorine substituted reaction. The energy barrier to the process is lower than that for the $CClH(OH)_2$ formation, which remains the rate-determining step of the process. This is consistent with the gas phase results reported in Chapters 3 and 4.

The effect of solvation on the energy barriers for decomposition of the $CClH(OH)_2$ intermediate is more striking. The energy barrier decreases by 37 kJ mol^{-1} when the reaction occurs in the water droplet indicating that the transition state is solvated more effectively than the diol intermediate. The reaction also becomes more exothermic in solution suggesting that the products are also better solvated than the $CClH(OH)_2$ molecule. This is consistent with chemical intuition as having the chloride leaving

group stabilised by hydrogen bonding with the solvent should decrease the energy of the transition state.

6.3.1.3 $CXHO + 1H_2O \rightarrow HX + HCO_2H$

This section concerns the one-step hydrolysis of the formyl halides occurring as a bimolecular process within a water droplet. The AM1/TIP3P transition states located for this process are shown in Figure 6.12. [TS 6-8] and [TS 6-9] represent the fluorine substituted transition states and [TS 6-10] and [TS 6-11] the chlorine substituted species.

The transition structures show the anticipated variations in geometry as a result of the different leaving group abilities of fluorine and chlorine. When the substituent is chlorine the reaction is concerted but the proton transfer and C-Cl bond cleavage are asynchronous. In agreement with the *ab initio* gas phase results the C-Cl bond dissociation occurs first and is followed by the proton transfer. The reverse is the case for the fluorinated species where the proton transfer precedes the C-F bond dissociation.

In [TS 6-8] and [TS 6-10] the H^6-O^5 bond eclipses the C=O bond and in [TS 6-9] and [TS 6-11] eclipses the C-H^3 bond. The geometries of the quantum atoms of these transition states resemble those from the gas phase calculations. The solvent structures are therefore again of more interest.

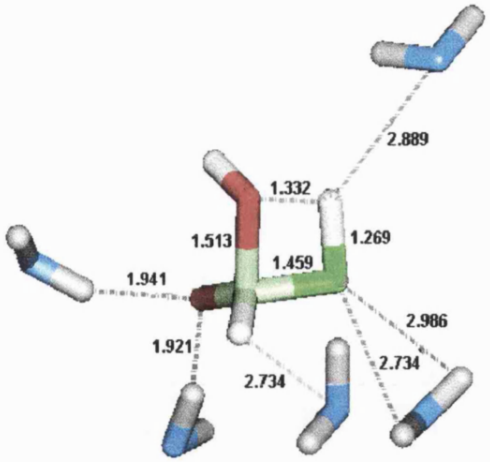

[TS 6-8]

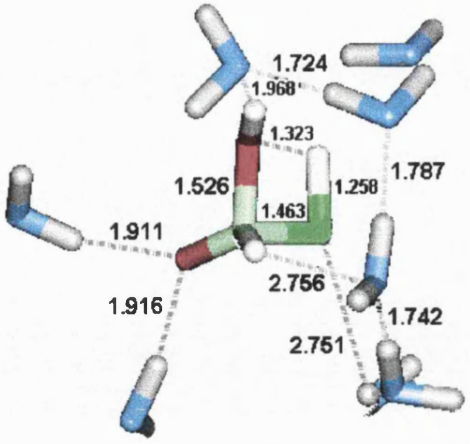

[TS 6-9]

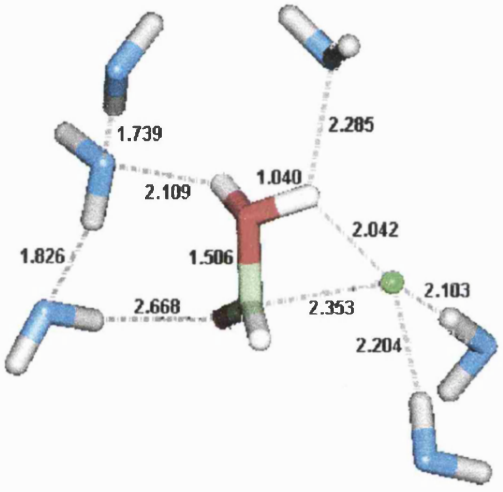

[TS 6-10]

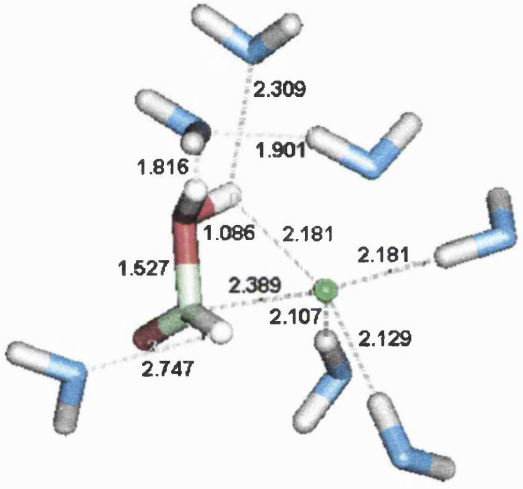

[TS 6-11]

Figure 6.12

The solvent structures surrounding the quantum atoms exhibit many of the same features as those shown in [TS 6-5] to [TS 6-7]. It is these features, along with the obvious variations in the geometries of the quantum atoms, that lead to the differences in the energetics between the two halogen substituents. The chlorine atom forms strong hydrogen bond interactions with the solvent but the fluorine does not. The partial charges of these atoms in the transition states are similar to those for the decomposition

of $CXH(OH)_2$. The chlorine has partial charges of –0.69 and –0.72 respectively in [TS 6-10] and [TS 6-11] whereas fluorine has partial charges of –0.22 in both [TS 6-8] and [TS 6-9]. The result is that the chlorine atom acts as a more effective hydrogen bond acceptor than the fluorine.

A further variation in the solvent structures involves the transferring proton (H^7) acting as a hydrogen bond donor to a solvent water molecule in each of the transition states except [TS 6-9]. This feature is analogous to that observed in the transition structures for the formation of $CXH(OH)_2$. Finally it is evident in all four transition states that the oxygen atom (O^5), originally part of the quantum water molecule, does not act as a hydrogen bond acceptor.

The reactant species located from optimisations of IRC reactant-like structures are similar in structure for X=F and Cl, so only one example of each is shown in Figure 6.13. The reactant structures associated with [TS 6-9] and [TS 6-10] are shown. In [R 6-9] the O^5-H^6 bond is 'trans' and in [R 6-10] it is 'cis' to the C=O^2 bond. An intramolecular hydrogen bond is therefore possible in [R-6-10] (and [R 6-8]) but not in [R 6-9] (or [R 6-11]). These intramolecular interactions are carried through to, and are clearly observable in, the transition structures. In the gas phase these interactions accounted for a 16 kJ mol^{-1} difference in the energy barrier at the MP2(fc)/6-311+G**//HF/6-31G* level of theory when X=Cl.

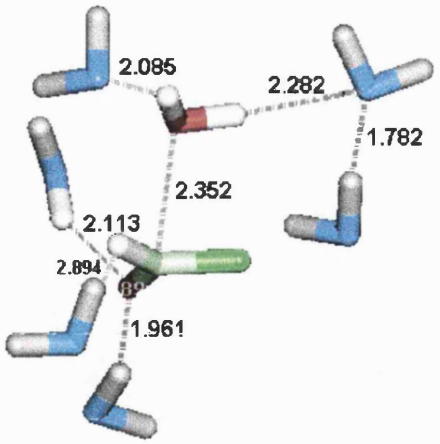

[R 6-9]

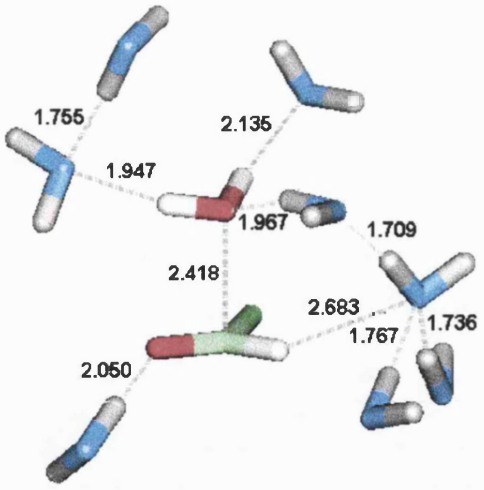

[R 6-10]

Figure 6.13

The product structures located from optimising the product-like species from IRC calculations differ considerably, and are dependent on whether the halogen substituent is fluorine or chlorine. Examples of these structures are shown in Figure 6.14. The two reaction paths yield different conformers of formic acid. The reaction routes through [TS 6-8] and [TS 6-10] result in the formation of the lower energy conformer of formic acid where HOCO = 0°. The paths through [TS 6-9] and [TS 6-11] lead to the formation of the higher energy conformer of formic acid where HOCO = 180°.

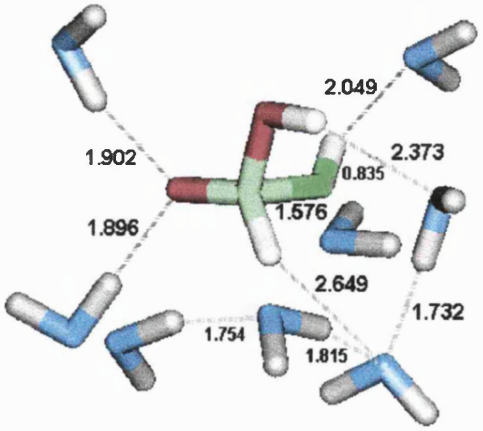

[P 6-9]

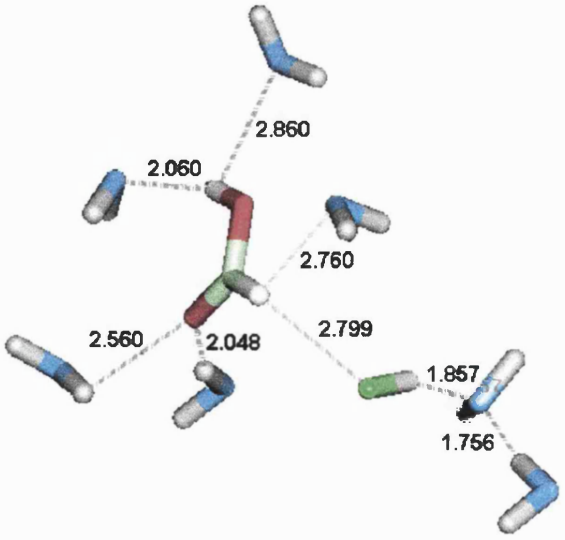

[P 6-10]

Figure 6.14

The same type of product structures are observed for the one-step mechanism as the decomposition of $CXH(OH)_2$. In the [P 6-10] and [P 6-11] structures the product molecules of HCl and formic acid are separated, and form strong hydrogen bonds with solvent molecules. The [P 6-8] and [P 6-9] species exhibit the by now familiar feature of a partially dissociated C-F bond.

An identical approach to that of section 6.3.1.2 was taken for locating fully dissociated product species when X=F. This resulted in the location of the [TS 6-8(a)], [P 6-8(a)], [TS 6-9(a)], and [P 6-9(a)] species shown in Figure 6.15. The geometries of the QM atoms of the transition states again resembled those of the [P 6-8] and [P 6-9] species that they link to the [P 6-8(a)] and [P 6-9(a)] structures. The reaction path involves the simple dissociation of the C-F bond, followed by reorientation of the HF molecule to form hydrogen bonds with both the formic acid and solvent.

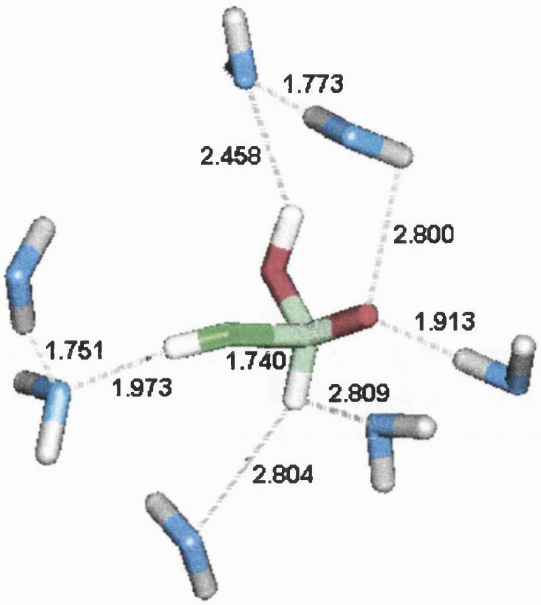

[TS 6-8(a)]

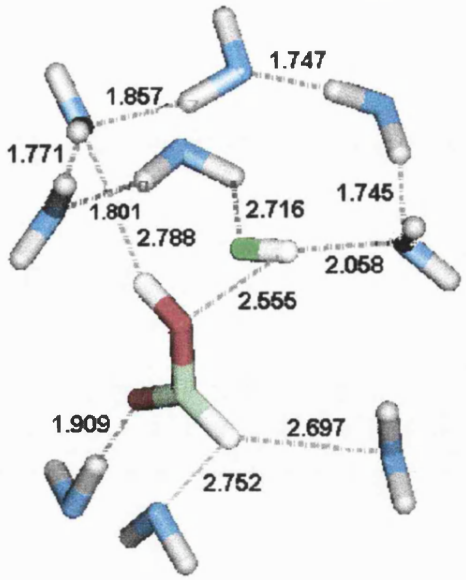

[P 6-8(a)]

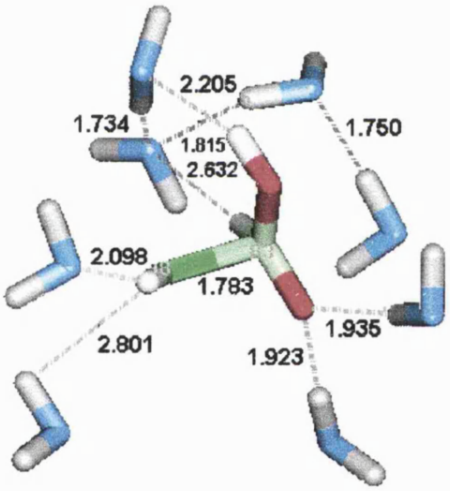

[TS 6-9(a)]

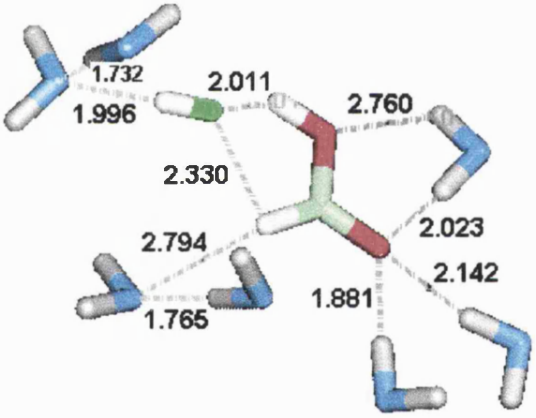

[P 6-9(a)]

Figure 6.15

The stabilisation of the [P 6-8] and [P 6-9] species by solvation necessitates a further step in the process for direct elimination of HF from formyl fluoride and water. The reaction is therefore no longer strictly a one-step process once explicit solvation effects are taken into account.

The total and relative energies of the solvated species discussed in this section are reported in Table 6.3.

Table 6.3 – Total and Relative Energies of the AM1/TIP3P CXHO + $1H_2O \rightarrow$ HX + HCO_2H Reaction Species

	AM1 (qm)		AM1/TIP3P	
Species	Total (kcal/mol)	Relative (kJ/mol)	Total (kcal/mol)	Relative (kJ/mol)
[R 6-8]	-154.5	0	-6361.3	0
[TS 6-8]	-97.5	239	-6307.6	225
[P 6-8]	-152.1	10	-6367.6	-26
[TS 6-8(a)]	-153.7	3	-6367.3	-25
[P 6-8(a)]	-172.3	-74	-6380.2	-79
[R 6-9]	-153.5	0	-6361.8	0
[TS 6-9]	-89.3	269	-6300.2	258
[P 6-9]	-147.1	27	-6362.7	-4
[TS 6-9(a)]	-150.1	14	-6361.4	2
[P 6-9(a)]	-167.3	-58	-6378.6	-70
[R 6-10]	-105.6	0	-6267.8	0
[TS 6-10]	-69.3	152	-6237.8	126
[P 6-10]	-121.6	-67	-6286.5	-78
[R 6-11]	-104.8	0	-6269.8	0
[TS 6-11]	-60.8	184	-6232.9	154
[P 6-11]	-114.6	-41	-6287.2	-73

The AM1 (qm) and AM1/TIP3P relative energies both show that the direct elimination of HX is extremely dependent on the halogen substituent. The AM1/TIP3P energy barriers are approximately 100 kJ mol^{-1} higher when the substituent is fluorine rather than chlorine. There is also a ~30 kJ mol^{-1} variation in the energy barriers between the

'cis' and 'trans' transition state routes. This variation is due to the quantum atoms as evidenced by the values of the AM1 (qm) relative energies in Table 6.3.

The AM1/TIP3P reaction energies for the direct elimination of HCl show that the process is largely exothermic, and are similar with only a 5 kJ mol^{-1} difference between the two reaction paths. In contrast the AM1 (qm) reaction energies have a 26 kJ mol^{-1} variation between the product species. Solvation of the products therefore reduces the energy difference between the two sets of products and suggests that the [P 6-9(a)] species is more effectively solvated than [P 6-8(a)].

The overall AM1/TIP3P reaction energies for the elimination of HF are exothermic to essentially the same extent as the elimination of HCl. The AM1 (qm) results again have a larger variation in the reaction energies than the AM1/TIP3P energies, and the reduction of the difference upon solvation is also clearly observable. However, the effect of solvation is considerably reduced for the fluorine substituted species compared to the analogous chlorine reactions.

The relative energies of [P 6-8], [TS 6-8(a)], [P 6-9], and [TS 6-9(a)] show the same trends as those species involved in the decomposition of $CFH(OH)_2$. If just the quantum atoms are considered then the initially formed product species are higher in energy than the transition states corresponding to C-F bond dissociation. The effect of solvation is to stabilise the [P 6-8] and [P 6-9] structures to the extent that they become minimum energy species, and must pass through [TS 6-8(a)] and [TS 6-9(a)] for full C-F bond dissociation to occur.

The effect of solvation on the energy barriers for the direct elimination of HX is also substituent dependent. If X=F then solvation results in 14 and 11 kJ mol^{-1} reductions in the energy barriers respectively for [TS 6-8] and [TS 6-9]. However, if X=Cl then the decreases in the energy barriers are 26 and 30 kJ mol^{-1} respectively for [TS 6-10] and [TS 6-11] when solvation is included. The transition states containing chlorine clearly form stronger interactions with the solvent than those containing fluorine, particularly the halogen substituent itself.

Overall the AM1/TIP3P results show that the preferred reaction paths are those *via* the 'cis' transition states [TS 6-8] and [TS 6-10]. Thus, although solvation reduces the energy barriers for these processes, the favoured mechanism is not altered from that of the gas phase.

6.3.1.4 One-Step Versus Two-Step Bimolecular Hydrolysis of Formyl Halides

QM/MM modelling of the bimolecular hydrolysis of formyl chloride occurring within a water droplet has shown that the preferred reaction mechanism remains the same as that for the gas phase process. It is still the one-step, direct elimination of HCl that is energetically favoured. The lowest AM1/TIP3P energy barrier for this process is 126 kJ mol^{-1} compared to 196 kJ mol^{-1} for the rate-determining first step of the two-step mechanism.

The preferred mechanism for the bimolecular hydrolysis of formyl fluoride within a water droplet is less straightforward. The rate-determining step of the two-step mechanism changes to being the decomposition of the $CFH(OH)_2$ intermediate rather than the formation of that intermediate. This is a result of using the AM1 Hamiltonian

to describe the QM part of the system. The lowest energy barrier for the one-step mechanism is 225 kJ mol^{-1} compared to 258 kJ mol^{-1} for the decomposition of $CFH(OH)_2$ of the two-step mechanism. At first glance the one-step mechanism is the more energetically favourable process and should be the preferred mechanism. However, as the first step of the two-step process is significantly exothermic this may provide the impetus for overcoming the second, rate-determining energy barrier. This hydrolysis could therefore feasibly proceed *via* either mechanism.

6.3.2 QM/MM Modelling of the Termolecular Hydrolysis of Formyl Halides

6.3.2.1 $CXHO + 2H_2O \rightarrow CXH(OH)_2 + H_2O$

The AM1/TIP3P transition structures for the formation of the $CXH(OH)_2$ intermediate, in which two water molecules are treated quantum mechanically, are shown in Figure 6.17. The atom distances are given in Angstroms. [TS 6-12] and [TS 6-13] have fluorine as the halogen substituent and in [TS 6-14] the substituent is chlorine. The QM atoms are numbered according to the scheme in Figure 6.16.

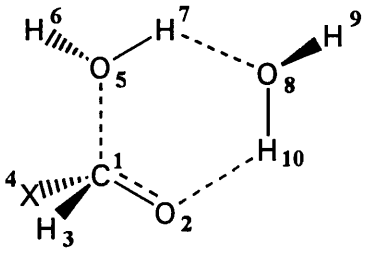

Figure 6.16

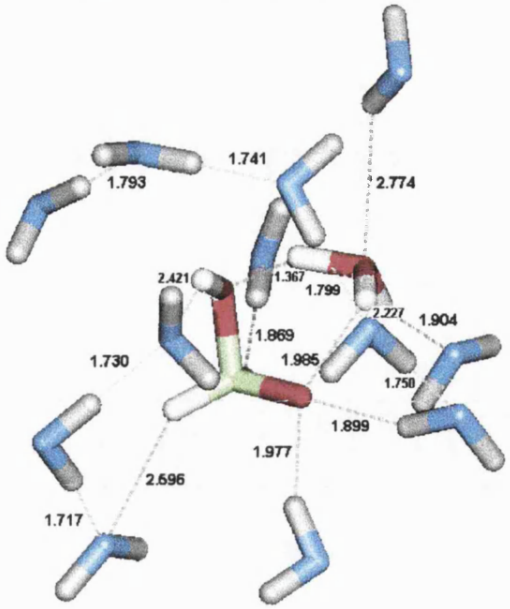

[TS 6-12]

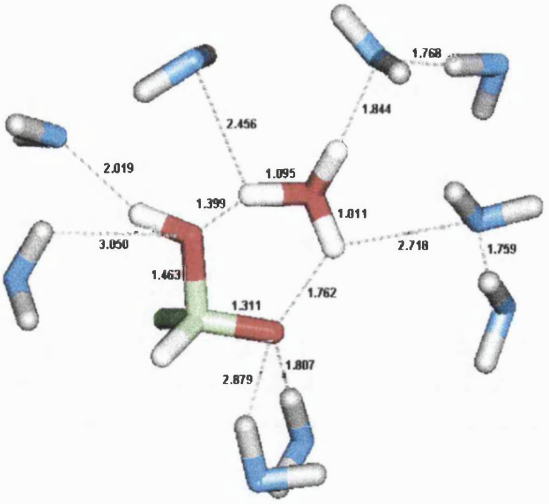

[TS 6-13]

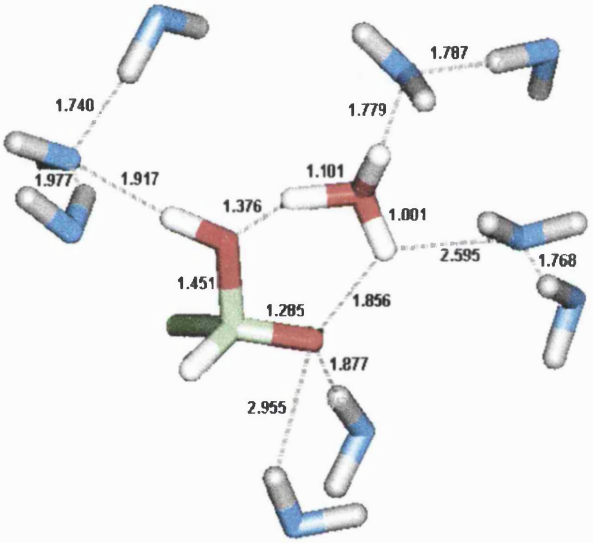

[TS 6-14]

Figure 6.17

The QM atoms of the two fluorine transition states [TS 6-12] and [TS 6-13] differ due to the relative position of the non-transferred proton (H^6) of the water molecule ($H^6O^5H^7$). This in turn affects the orientation of the second water molecule that forms the H_3O^+ species in the transition states. In [TS 6-12] the orientation of the H_3O^+ species is such that H^9 and H^{10} both act as hydrogen bond donors to the O^2 oxygen

atom, and H^7 acts as a hydrogen bond donor to the O^5 atom. In [TS 6-13] and [TS 6-14] it is only H^{10} that acts as a hydrogen bond donor to the O^2 atom. H^9 forms a strong hydrogen bond interaction with a solvent molecule.

The proton transfers that occur in these processes are concerted but asynchronous, and the transition structures are similar to those located in the gas phase. The proton transfer from one quantum mechanical water molecule to the other occurs before proton transfer from a water molecule to the carbonyl oxygen atom of the formyl halide.

The solvent arrangements around the solutes are comparable for [TS 6-13] and [TS 6-14]. The H_3O^+ acts as a good hydrogen bond donor but not as a hydrogen bond acceptor due to the build up of positive charge in this species. This is also observable in the [TS 6-12] structure but other features of the solvent arrangement are very different to [TS 6-13] and [TS 6-14]. There is a greater number of solvent water molecules within 2.8 Å of the solute in [TS 6-12] and by simple inspection of the structures [TS 6-12] does appear better solvated than in [TS 6-13] and [TS 6-14].

The reactant structures for the three reaction paths are shown in Figure 6.18. The reactants are numbered according to the transition state from which they were derived. The structures of the fluorine reactant species differ due to the orientations of the quantum water molecules. The reactant species derived from [TS 6-14] is unusual in that a structure much closer to that of [R 6-13] would be expected due to the similarity of the transition structures [TS 6-13] and [TS 6-14]. However the structure of [R 6-14] is actually much more like that of [R 6-12].

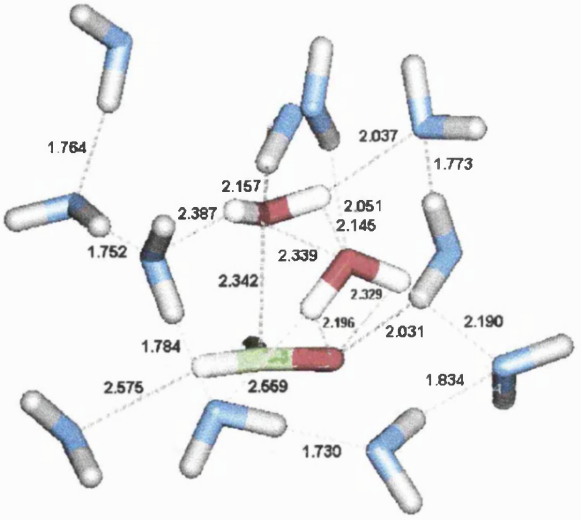

[R 6-12]

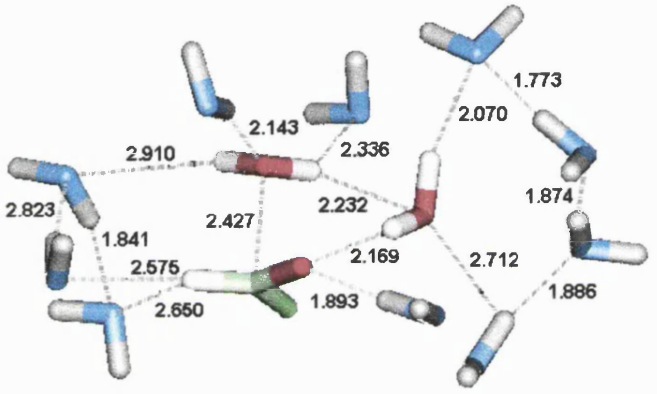

[R 6-13]

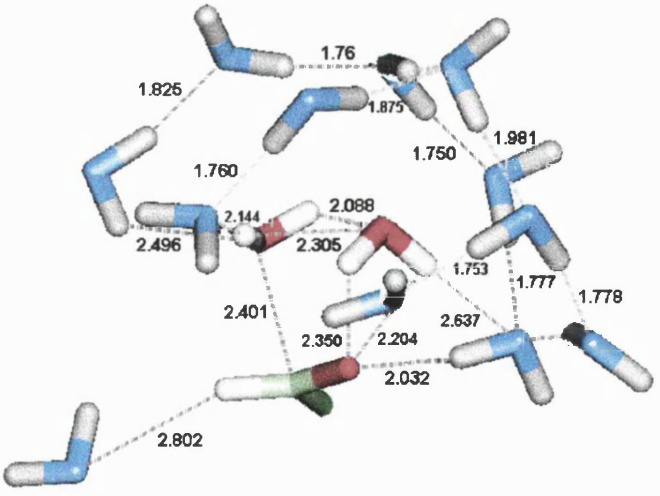

[R 6-14]

Figure 6.18

The orientations of the quantum water molecules in the reactant species [R 6-13] are such that there is a single hydrogen bond interaction between them. [R 6-12] and [R 6-14] have a different pattern in the interactions between the AM1 water molecules. In these species the quantum waters form a bifurcated system in which two hydrogen bonds are donated from each water to a single oxygen atom. This bifurcation feature is different to the hydrogen bond patterns normally associated with water molecules and is a known artefact of the AM1 description of water molecules, *e.g.* reference [148].

The $CXH(OH)_2$ intermediate structures formed from these three reaction processes are shown in Figure 6.19. Two separate conformers of the diol are formed when X=F, the (+60,180) and (+60,+60) conformers respectively for the reaction routes *via* [TS 6-12] and [TS 6-13]. The single reaction process for X=Cl results in the formation of the (+60,+60) conformer of the diol. These results are consistent with the conformers formed *in vacuo* at the MP2(fu)/6-31G* level of theory.

The orientation of the quantum water molecule in the diol-water complexes [D 6-12] to [D 6-14] is dependent on the conformer of the diol produced. If the (+60,180) conformer of the diol is produced then the AM1 water acts as a hydrogen bond donor to the oxygen atom that forms part of the hydroxyl group antiperiplanar to the fluorine atom. The QM water molecule also forms a hydrogen bond with the proton of the other hydroxyl group of the diol. If the (+60,+60) conformer of the diol is produced then the QM water molecule forms slightly different hydrogen bond interactions with the diol. It again accepts a hydrogen bond from the hydroxyl group forming a 60-degree angle with the C-X bond. One proton from the QM water donates a hydrogen bond to the halogen, and the other acts as a hydrogen bond donor to a solvent molecule.

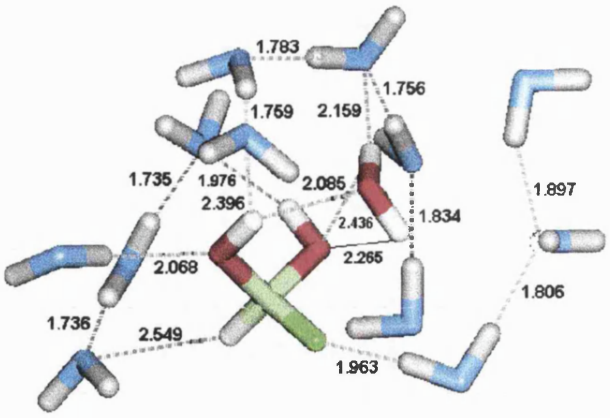

[D 6-12]

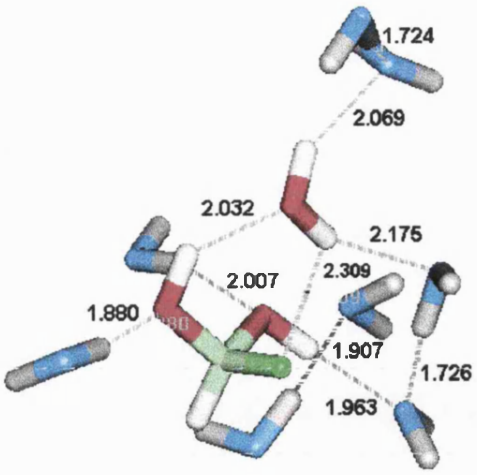

[D 6-13]

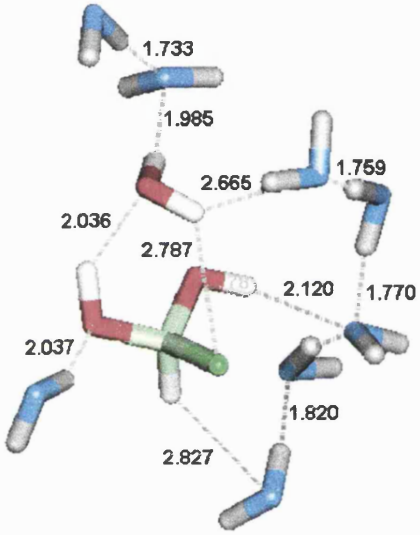

[D 6-14]

Figure 6.19

The total and relative energies of the AM1/TIP3P optimised species are reported in Table 6.4.

Table 6.4 – Total and Relative Energies of the AM1/TIP3P $CXHO + 2H_2O \rightarrow CXH(OH)_2 + H_2O$ Reaction Species

	AM1 (qm)		AM1/TIP3P	
Species	Total (kcal/mol)	Relative (kJ/mol)	Total (kcal/mol)	Relative (kJ/mol)
[R 6-12]	-222.1	0	-6412.7	0
[TS 6-12]	-186.0	151	-6383.9	120
[D 6-12]	-239.0	-71	-6427.2	-61
[R 6-13]	-218.6	0	-6425.8	0
[TS 6-13]	-180.0	162	-6390.2	148
[D 6-13]	-235.9	-72	-6438.0	-51
[R 6-14]	-172.9	0	-6373.3	0
[TS 6-14]	-128.9	184	-6342.5	129
[D 6-14]	-181.2	-35	-6385.0	-49

The AM1/TIP3P energy barriers for the termolecular formation of $CXH(OH)_2$ are comparable for the two halogen substituents. The formation of the (+60,180) conformer of the $CFH(OH)_2$ intermediate is a lower energy process than the formation of the (+60,+60) conformer. The analogous process for the formation of the (+60,+60) conformer of the $CClH(OH)_2$ has a lower energy barrier by 19 kJ mol^{-1}. This is the same trend as observed for the gas phase processes.

The AM1 (qm) compared to the AM1/TIP3P relative energies show that the energy barriers for these processes are decreased in the presence of solvent. If X=F then the reduction is 31 or 14 kJ mol^{-1} for the reaction paths through [TS 6-12] and [TS 6-13] respectively. The effect of solvation if X=Cl is considerably larger with a decrease in the energy barrier of 55 kJ mol^{-1}. It is not clear why the effect of solvation is greater for

the chlorine substituted species as both the quantum geometries and the solvent structures for [TS 6-13] and [TS 6-14] look very similar.

The AM1/TIP3P reaction energies are also comparable for the three processes. Each process is significantly exothermic, the most exothermic being the termolecular formation of the (+60,180) conformer of $CFH(OH)_2$. The AM1 (qm) results show a different pattern in the reaction energies. The effect of solvation on the fluorine reaction paths is to reduce the degree of exothermicity of the reactions. The opposite is the case for the chlorine pathway, which becomes more exothermic when solvation is included.

The AM1 (qm) energies also show that when the AM1 Hamiltonian is used to describe the QM atoms there is a large discrepancy between the reaction energies for the halogen substituents. These gas phase energies predict the formation of $CFH(OH)_2$ to be 36 – 37 kJ mol^{-1} more exothermic than the formation of $CClH(OH)_2$. This significant variation is not evident in the MP2(fu)/6-31G* gas phase results, and again highlights the differences between the *ab initio* and semi-empirical molecular orbital methods.

6.3.2.2 $CXH(OH)_2 + H_2O \rightarrow HX + HCO_2H + H_2O$

The AM1/TIP3P transition state structures for the decomposition of the $CXH(OH)_2$ intermediate, in which an additional water molecule has been treated quantum mechanically, are shown in Figure 6.20. In [TS 6-15] the halogen substituent is fluorine and in [TS 6-16] the substituent is chlorine.

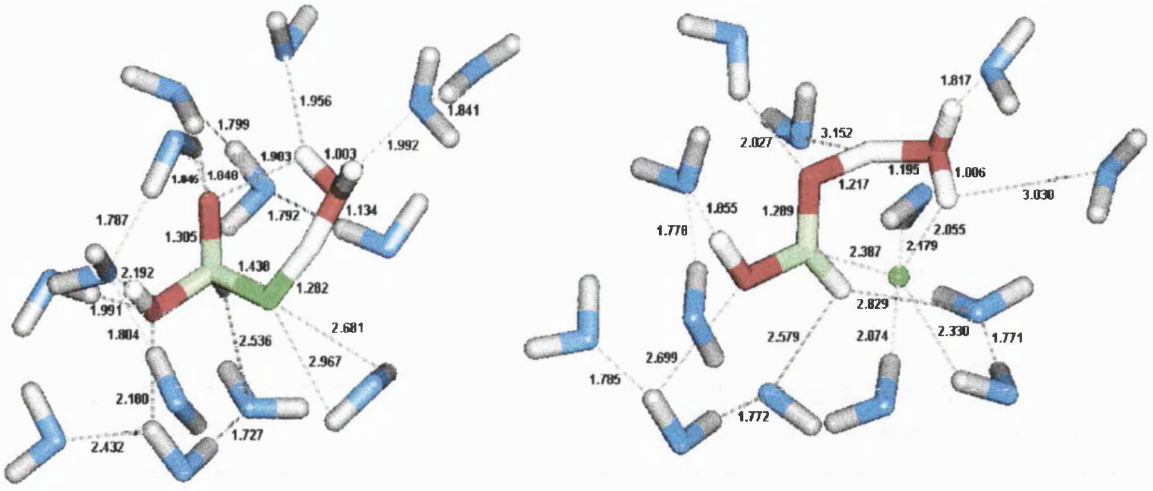

[TS 6-15] **[TS 6-16]**

Figure 6.20

The transition structures show the anticipated variations in the geometries of the quantum atoms. The fluorine atom does not act as an effective hydrogen bond acceptor in [TS 6-15] unlike the chlorine atom in [TS 6-16] which forms strong hydrogen bonds with both quantum and TIP3P hydrogen atoms. This again illustrates how substituent effects may perturb reaction processes.

The proton transfers are more advanced in [TS 6-15] than [TS 6-16]. The transfer of a hydroxyl proton to the QM water molecule is essentially complete in [TS 6-15], and the transfer of a proton to the fluorine atom is underway. In contrast the proton transfer from the hydroxyl group of the diol to the QM water is only partially complete in [TS 6-16], and the proton transfer to the chlorine is only just beginning.

The solvent-solute interactions around [TS 6-15] and [TS 6-16] are also substituent dependent. The same types of interaction occur between the QM oxygen and hydrogen atoms and the solvent molecules in both transition structures. The differences arise as a result of the behaviour of the halogen substituents. As in earlier sections, where

fluorine and chlorine are the leaving groups, the C-Cl bond is effectively dissociated in [TS 6-16] and results in a partial charge on the chlorine of –0.74 whereas the charge of the fluorine in [TS 6-15] is –0.26. This difference leads to the better solvation of the chlorine over fluorine in the transition structures.

Optimisation of the reactant- and product-like structures from IRC calculations have shown that it is the (+60,+60) conformer of the $CXH(OH)_2$ intermediate which decomposes through [TS 6-15] and [TS 6-16]. Figure 6.21 shows the diol structures for both halogen substituents. They have been named according to the transition state from which they were derived.

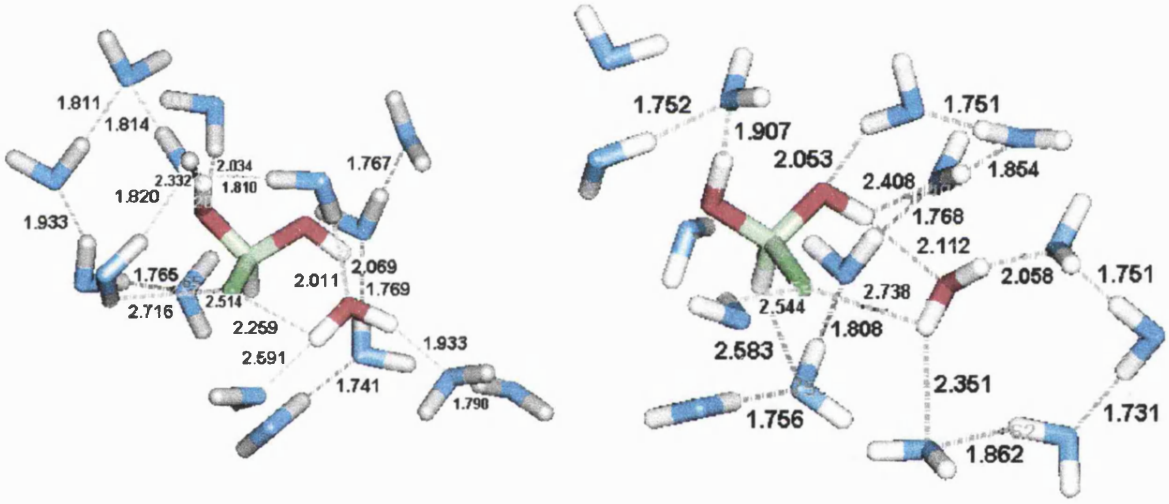

[D 6-15] **[D 6-16]**

Figure 6.21

[D 6-15] and [D 6-16] both contain the (+60,+60) conformer of the $CXH(OH)_2$ diol along with a water molecule in the quantum region. These diol structures differ from the [D 6-13] and [D 6-14] species in the orientation of the QM water molecule. In [D 6-13] and [D 6-14] the quantum water molecule accepts a hydrogen bond from the hydroxyl group making a 60-degree angle with the C-X bond, but in [D 6-15] and [D 6-16] this water molecule instead accepts a hydrogen bond from the other hydroxyl

group. In both sets of diol species the AM1 water also acts as a hydrogen bond donor to the halogen atom. Therefore in order for the two-step reaction to proceed to products the orientation of the QM water molecule needs to change from that observed in [D 6-13] and [D 6-14] to that in [D 6-15] and [D 6-16].

The optimised product-like structures from IRC calculations for these processes are shown in Figure 6.22. The product species also exhibit structural features consistent with those previously located in this chapter. The C-F bond is not fully dissociated in [P 6-15], increasing the energy of the products relative to the reactants. In [P 6-16] the HCl exists as a separate species hydrogen bonded to the formic acid. In both [P 6-15] and [P 6-16] the formic acid product formed is the lowest energy conformer where HOCO = 0°. Inspection of the bond length and partial charges indicates that the HCl is eliminated as a covalent species during these processes. However the nature of the hydrogen chloride will be examined in greater detail in subsequent sections.

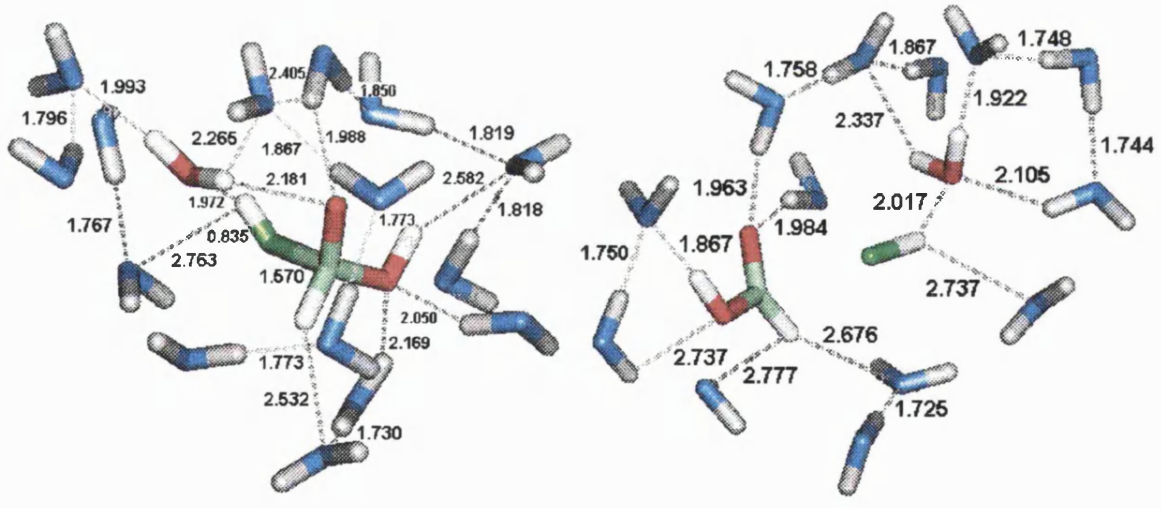

[P 6-15] [P 6-16]

Figure 6.22

A transition state, [TS 6-15(a)], has been located for the dissociation of the [P 6-15] species to separated product molecules. [TS 6-15(a)] was located using the same

protocol as similar structures in previous sections. IRC calculations were then run and the reactants confirmed as [P 6-15]. [TS 6-15(a)] and the optimised product structure [P 6-15(a)] are shown in Figure 6.23. The covalent HF molecule forms hydrogen bond interactions with both QM and solvent atoms. The bimolecular decomposition of the $CFH(OH)_2$ intermediate therefore becomes a two-step process when occurring within a water droplet, as opposed to a concerted one-step process *in vacuo*.

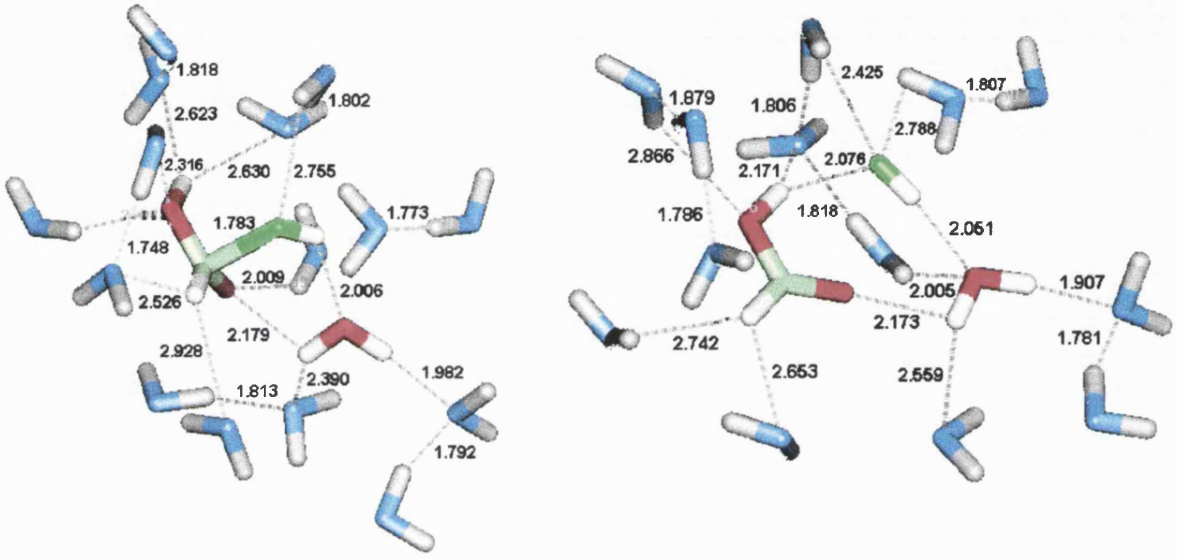

[TS 6-15(a)] **[P 6-15(a)]**

Figure 6.23

The total and relative energies of the AM1/TIP3P optimised species are reported in Table 6.5. The energy barriers for the decomposition of the $CXH(OH)_2$ intermediate catalysed by an extra water molecule are extremely susceptible to substituent effects. As chlorine is the better leaving group it is not surprising to find that the AM1/TIP3P energy barrier for elimination of HCl from [D 6-16] is 49 kJ mol^{-1} lower than the analogous process involving elimination of HF.

Table 6.5 – Total and Relative Energies of the AM1/TIP3P $CXH(OH)_2 + H_2O \rightarrow HX + HCO_2H + H_2O$ Reaction Species

	AM1 (qm)		AM1/TIP3P	
Species	Total (kcal/mol)	Relative (kJ/mol)	Total (kcal/mol)	Relative (kJ/mol)
[D 6-15]	-234.4	0	-6429.0	0
[TS 6-15]	-180.8	224	-6384.9	185
[P 6-15]	-223.5	46	-6416.8	51
[TS 6-15(a)]	-224.0	44	-6415.3	57
[P 6-15(a)]	-238.9	-19	-6429.9	-4
[D 6-16]	-180.9	0	-6353.7	0
[TS 6-16]	-144.5	152	-6321.1	136
[P 6-16]	-184.4	-15	-6365.7	-50

The AM1/TIP3P energy barriers are also higher than those for the water catalysed formation of $CXH(OH)_2$. This was not unexpected for the fluorine process as this trend was evident in both the AM1/TIP3P and AM1 gas phase energies for the two-step bimolecular hydrolysis of CFHO. The difference between the bimolecular and termolecular two-step processes for CFHO is that the energy barrier for the second step of the termolecular reaction is not high enough for this step to become rate-determining. In agreement with the *ab initio* gas phase results the diol formation remains the rate-determining step for the termolecular process.

In the chlorine case a larger energy barrier for the second step was not consistent with the bimolecular hydrolysis results. However as the barrier is only 7 kJ mol^{-1} higher than for the formation of $CClH(OH)_2$ this does not make a large impact on the process as a whole, and the formation of the diol intermediate remains the rate-determining step.

The effect of solvation on the energy barriers for the water catalysed decomposition of the $CXH(OH)_2$ intermediate is to decrease the barrier heights. Unexpectedly, solvation reduces the energy barrier for $CFH(OH)_2$ decomposition by more than for $CClH(OH)_2$ decomposition. This is inconsistent with previous results, as the strong Cl-solvent interactions would be anticipated to stabilise the [TS 6-16] structure relative to the diol species more than the weak F-solvent interactions in [TS 6-15].

The reaction energies are also substituent dependent, the decomposition of $CClH(OH)_2$ is strongly exothermic with an AM1/TIP3P reaction energy of -50 kJ mol^{-1}. In contrast decomposition of $CFH(OH)_2$ is almost thermoneutral. Solvation affects the fluorine and chlorine substituted species differently. Solvation actually reduces the exothermicity of the process when X=F but the reverse is the case when X=Cl. The relative energies of the [P 6-15] and [TS 6-15(a)] show the expected reversal of order when solvation effects are included.

6.3.2.3 $CXHO + 2H_2O \rightarrow HX + HCO_2H + H_2O$

The AM1/TIP3P transition structures located for the one-step hydrolysis of CXHO, in which two water molecules are treated quantum mechanically, are shown in Figure 6.24. In [TS 6-17] the halogen substituent is fluorine and in [TS 6-18] and [TS 6-19] the substituent is chlorine.

[TS 6-19] was located from a saddle point search on the [TS 4-2] geometry embedded in a water sphere. It was anticipated that [TS 6-19], being close in structure to [TS 6-12], would result in the formation of the $CClH(OH)_2$ intermediate. However,

instead an elimination process occurred and provided a direct route to the final products of the hydrolysis.

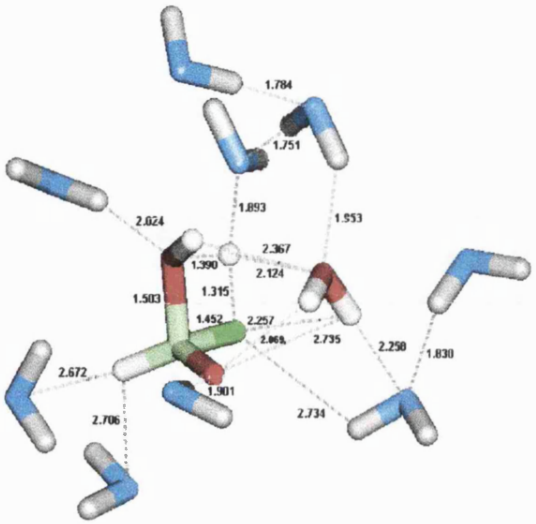

[TS 6-17]

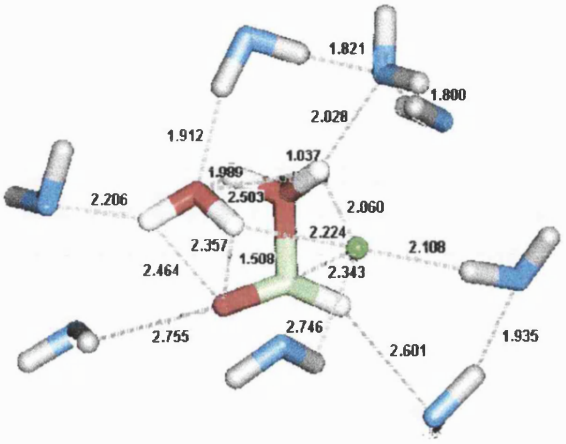

[TS 6-18]

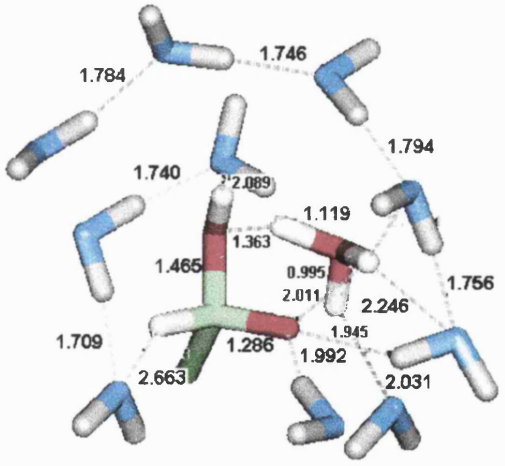

[TS 6-19]

Figure 6.24

[TS 6-17] and [TS 6-18] are based on the [TS 4-7] and [TS 4-8] transition state geometries respectively. The reacting atoms resemble the bimolecular direct elimination transition states with the second water molecule in the quantum region hydrogen bonded to them. They follow the trend of the proton transfer being more

advanced for the fluorine process, and the C-X bond more dissociated for the chlorine process.

The solvent structures in [TS 6-17] and [TS 6-18] are different due to the variations in the charge distributions of the quantum atoms. The chlorine atom has a large partial charge compared to the fluorine and thus forms stronger interactions with the solvent. The extra quantum water molecule acts as a hydrogen bond donor and acceptor to quantum and MM atoms in both [TS 6-17] and [TS 6-18].

[TS 6-19] has a very different structure. A proton transfer between the two quantum water molecules results in the formation of a H_3O^+ species in the transition structure. A second proton transfer was expected to occur between the H_3O^+ and the oxygen atom originating from the formyl chloride. Instead the C-Cl bond dissociated and the chloride abstracted a proton from the H_3O^+ causing elimination of HCl. Formic acid was also formed during the process in the lowest energy conformer. The second water molecule remained hydrogen bonded to the formic acid in the product structure.

Although this result was unexpected due to the structure of [TS 6-19] it does have a precedent involving the solvolysis of ^{t}butyl chloride. Ruggiero[149] attempted to locate an initial guess of the AM1/TIP3P S_N2 transition state for the nucleophilic attack of a water molecule on ^{t}butyl chloride *via* the calculation of a reaction profile. However after a C-Cl bond separation of 2.9 Å was reached the chloride would abstract a proton from the cationic ^{t}butyl fragment to give HCl and ^{iso}butylene. Ruggiero suspected that this elimination reaction might have been an artefact of the limited size of the QM region in the hybrid calculations.

In the case of the reaction path *via* [TS 6-19] it is more likely that the elimination reaction proceeds due to a lack of hydrogen bond interactions between the chlorine and solvent molecules. It is the proton of the H_3O^+ that points in the same direction as the chlorine atom in the transition structure that is abstracted and becomes part of the HCl molecule. If solvent molecules formed hydrogen bonds with the chlorine then this proton may be 'screened' from the chlorine atom and the elimination may be prevented. This thus appears to be a situation similar to that described earlier for the unimolecular decomposition of $CClH(OH)_2$ and may be a consequence of the particular solvent arrangement here. If the saddle point search was initiated from a different solvent structure then the formation of the $CClH(OH)_2$ intermediate may have occurred.

The reactant structures for these processes are very similar to those shown in Figure 6.18 and so pictures of them have been omitted in this section. This is interesting in itself as the equivalent gas phase structure of [R 6-18], [RC 4-8], has the formyl chloride molecule twisted 90 degrees so that the chlorine atom points away from the water molecules. This is not the case for [R 6-18] where the formyl chloride has the same orientation as in all the other reactant structures. This may be a consequence of solvation or the AM1 description of the QM atoms.

The product structures optimised from IRC calculations for the reaction paths *via* [TS 6-17] to [TS 6-19] are shown in Figure 6.25.

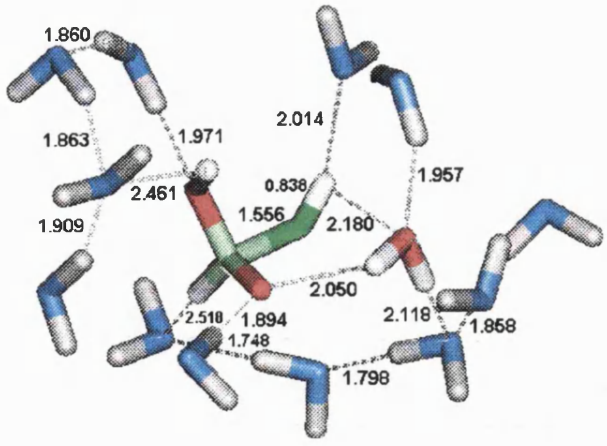

[P 6-17]

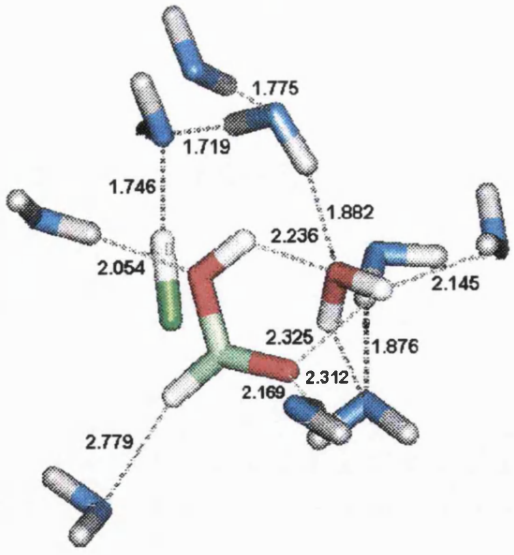

[P 6-18]

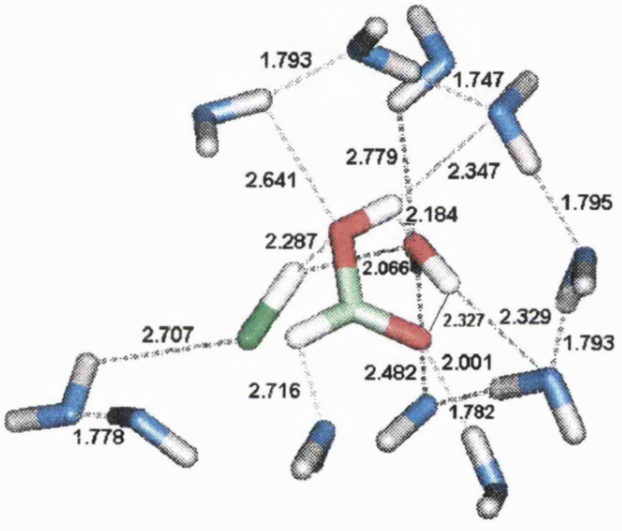

[P 6-19]

Figure 6.25

The products derived from [TS 6-17], [P 6-17], exhibit the same structural properties as those from earlier calculations. The C-F bond is not fully dissociated and the HF and formic acid products remain joined through these atoms. The quantum water molecule donates hydrogen bonds to the carbonyl oxygen of the formic acid and a MM water molecule. It also acts as a hydrogen bond acceptor to a solvent water molecule.

The reaction paths through [TS 6-18] and [TS 6-19] both result in the formation of HCl and formic acid in its more stable conformation. The differences between them lie in the hydrogen bond interactions between the QM atoms and the solvent arrangements. In [P 6-18] the hydrogen atom of the HCl molecule interacts with a solvent molecule whereas in [P 6-19] this proton interacts with QM oxygen atoms.

The transition state for the dissociation of the C-F bond in [P 6-17] to form the separate product molecules was located using the same method as in previous sections, and is shown in Figure 6.26. The familiar geometry of the QM atoms is observable, with a C-F bond length of 1.771 Å in [TS 6-17(a)]. The separate product molecules in [P 6-17(a)] exhibit typical hydrogen bond interactions with both QM and solvent atoms.

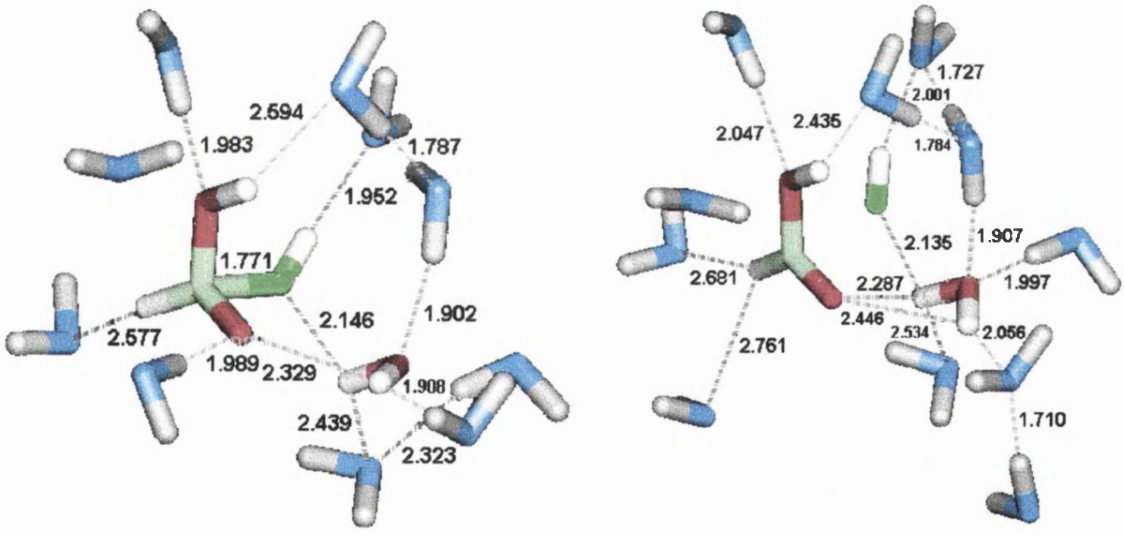

[TS 6-17(a)] **[P 6-17(a)]**

Figure 6.26

The total and relative energies of the AM1/TIP3P optimised species for these direct elimination reactions are reported in Table 6.6.

Table 6.6 – Total and Relative Energies of the AM1/TIP3P CXHO + $2H_2O \rightarrow HX + HCO_2H + H_2O$ Reaction Species

	AM1 (qm)		AM1/TIP3P	
Species	Total (kcal/mol)	Relative (kJ/mol)	Total (kcal/mol)	Relative (kJ/mol)
[R 6-17]	-223.9	0	-6424.3	0
[TS 6-17]	-168.5	232	-6373.1	214
[P 6-17]	-223.1	3	-6428.6	-18
[TS 6-17(a)	-221.5	10	-6427.3	-13
[P 6-17(a)]	-236.0	-51	-6442.0	-74
[R 6-18]	-171.2	0	-6369.9	0
[TS 6-18]	-141.0	126	-6344.6	106
[P 6-18]	-186.2	-63	-6387.7	-74
[R 6-19]	-172.1	0	-6359.2	0
[TS 6-19]	-132.3	166	-6328.1	130
[P 6-19]	-188.6	-69	-6371.6	-52

The energy barriers for these processes show the expected variations due to substituent effects. The barrier height when X=F is much higher than for either of the chlorine reaction paths due to the differences in efficiencies of the halogens as leaving groups.

The AM1/TIP3P energy barrier for the [TS 6-19] process is 24 kJ mol^{-1} higher than that of the [TS 6-18] process. The likely cause of this variation is the difference in the geometries of the QM atoms of [TS 6-18] and [TS 6-19] structures and consequently in their solvent structures. The barrier for the [TS 6-19] process is much closer to that for the [TS 6-14] process, which produces the $CClH(OH)_2$ intermediate.

The energy barriers are reduced when solvent effects are included but the decrease is slightly greater for the chlorine species. There is also a variation in the effect of solvation between the two chlorine reaction paths. Solvation provides greater stabilisation of the [TS 6-19] transition structure than [TS 6-18], and results in a larger reduction of the barrier height for this process.

All the processes are exothermic both *in vacuo* and when solvation effects are included. The [TS 6-17] and [TS 6-18] reactions become more exothermic in the presence of solvent, but the reaction *via* [TS 6-19] becomes less exothermic. This indicates that for the [TS 6-17] and [TS 6-18] processes the products are better solvated than the reactants, but that for the path *via* [TS 6-19] the reverse is true.

6.3.2.4 One-Step versus Two-Step Termolecular Hydrolyis of Formyl Halides

QM/MM modelling of the termolecular hydrolysis of the formyl halides occurring within a water droplet has shown that the preferred reaction mechanism remains the same as for the gas phase process. Thus for formyl fluoride the two-step mechanism is energetically favoured and for formyl chloride the one-step mechanism is favoured.

The AM1/TIP3P lowest energy barrier for the one-step process for formyl chloride is 106 kJ mol^{-1} compared to 129 kJ mol^{-1} for the rate-determining first step of the two-step mechanism. The AM1/TIP3P energy barrier for the rate-determining first step of the preferred two-step mechanism for formyl fluoride 120 or 148 kJ mol^{-1} compared to the 214 kJ mol^{-1} barrier for the one-step process.

The energy barriers for the extra step required for dissociation of the C-F bond in the X=F species are very small. This step is only necessary due to the stabilisation imparted to the initially formed product structures, which results in them becoming minimum energy species on the potential energy surface.

6.3.3 Investigation of the Nature of the Eliminated HX Species, and the Effect of Hydrogen Bonding on C-F Bond Dissociation

This section is concerned with the two major uncertainties observed in the QM/MM modelling of formyl halide hydrolysis occurring within a water droplet. The first point under investigation arose from the difficulties noticed in carbon-fluorine bond dissociation. In the gas phase the elimination of HF, and consequently C-F bond cleavage, is a one-step process whereas the AM1/TIP3P results predict a two-step process in which proton transfer occurs before the C-F bond dissociation.

It has been noted that the AM1 description results in a much stronger C-F bond than the *ab initio* methods used in previous chapters. However, as mentioned earlier, AM1 calculations performed *in vacuo* also predict a one-step HF elimination process. This indicates that although the method used to describe the QM atoms may exacerbate the problem of C-F bond cleavage it is not the sole cause. In section 6.3.1.2 it was therefore hypothesised that the weak solute-solvent hydrogen bond interactions observed in the AM1/TIP3P transition structures, such as [TS 6-6], may not provide enough stabilisation of the charge separation involved in C-F bond dissociation. Another possible source of error is the fact that the values of the non-bonded parameters for the QM atoms in the QM/MM energy do not change during the course of the reaction. Although the electrostatic charges should account for the major effect, treating a

covalently bonded halogen in the same way as a halide ion may affect the efficiency of the hydrogen bonding around this atom.

The solute-solvent hydrogen bond interactions in question occur across the QM/MM boundary. Although the QM atoms may be polarised by the MM atoms, the MM atoms are not polarised by the QM atoms in the QM/MM method used in this thesis. Transferring a number of MM molecules to the QM region would therefore enable polarisation of these solvent molecules by the solute. This may result in stronger interactions between the HF species and these solvent molecules, which could allow C-F bond dissociation to proceed as a one-step process.

The second major question arising from the AM1/TIP3P results reported in this chapter, is the nature of the HX species eliminated during the hydrolysis process. The results presented in earlier sections suggest that the HX was produced as a covalent molecule. However, the limited size of the QM region used for these calculations meant that it was not possible to determine whether this was an accurate representation of the HX species. The possibility existed that if the QM region was enlarged to include some solvent water molecules, then the elimination of HX could produce H^+ and X^- ions hydrogen bonded to solvent molecules, rather than the covalent HX species.

It has been possible to use the same method to study both the points outlined above. In both cases it was thought that increasing the size of the QM part of the system could provide further insight into the HX elimination process. The enlargement of the QM region was achieved using the procedure described below. As the main interest lay with the nature of the products of the reaction, the study was restricted to the AM1/TIP3P

transition states involving C-X bond cleavage and HX elimination. Therefore only the [TS 6-6] to [TS 6-11], and [TS 6-15] to [TS 6-19] transition states were examined.

The relevant transition structures were inspected using QUANTA.[150] The TIP3P water molecules that formed hydrogen bonds with QM atoms likely to undergo the largest charge redistribution during the reaction were chosen for transfer to the QM region. *E.g.* TIP3P water molecules hydrogen bonded to the halogen substituent were transferred to the QM region. A conscious decision was therefore made to expand the QM part of the system in a limited way, instead of including a full first solvation shell. It was hoped that by transferring a restricted number of solvent molecules to the QM region, the balance could be achieved between computational cost and the benefit of describing more atoms quantum mechanically.

Saddle point searches were started using the previously refined [TS 6-X] structures, with the extra water molecules defined as QM atoms, as initial guess structures. Once transition states were located using CHARMM and GRACE, IRC calculations were performed, and the reactant- and product-like species optimised to minimum energy structures. In several cases it proved difficult to locate transition structures with a single negative eigenvalue in the Hessian using the convergence criteria detailed in section 6.2.4. The convergence criteria were therefore tightened so that the MM environment was continually optimised to a minimum rms gradient of 0.0005 kcal mol^{-1} $Å^{-1}$. The QM core was optimised to a first order saddle point until no element of the gradient vector of the entire system was greater than 0.01 kcal mol^{-1} $Å^{-1}$.

6.3.3.1 C-F Bond Dissociation

AM1/TIP3P transition structures have been located that were derived from both the bimolecular and termolecular elimination transition structures, namely [TS 6-6], [TS 6-8], [TS 6-9], [TS 6-15] and [TS 6-17]. The new species have been named according to the transition structures from which they were derived, and the number of additional water molecules in the QM core. For example the transition structure based on the [TS 6-6] species is named [TS 6-6 + $4H_2O$].

The geometries of the seven reacting atoms of the [TS 6-6 + $4H_2O$], [TS 6-8 + $3H_2O$], and [TS 6-9 + $3H_2O$] transition structures are not very different to those of the [TS 6-6], [TS 6-8], and [TS 6-9] species. Hence pictures of them have been omitted from this section. The structures of the reactant species were consistent with those shown in sections 6.3.1.2 and 6.3.1.3. The structures of the product species [P 6-6 + $4H_2O$] and [P 6-8 + $3H_2O$] also resembled those pictured in earlier sections. The C-F bond is elongated but remains largely intact, and the need for a further dissociation step is not affected by the expansion of the QM core in these cases.

The product species [P 6-9 + $3H_2O$], however, consists of the separated HF and formic acid molecules surrounded by solvent. In this case treating some solvent molecules quantum mechanically provided solute-solvent interactions that resulted in the elimination of HX occurring as a concerted reaction. The [TS 6-9 + $3H_2O$] and [P 6-9 + $3H_2O$] species are pictured in Figure 6.27.

[TS 6-9 + $3H_2O$] [P 6-9 + $3H_2O$]

Figure 6.27

It is not clear why this particular process would be more affected by solute-solvent interactions than those *via* [TS 6-6 + $4H_2O$] and [TS 6-8 + $3H_2O$]. The only significant difference between the processes is the conformer of the formic acid produced. In the [TS 6-9 + $3H_2O$] process the formic acid is produced in the higher energy conformer where HOCO = 180°. However, this is the same conformer that is produced during the [TS 6-9] process. The difference in behaviour may be caused because the solvent arrangement around [TS 6-9 + $3H_2O$] forms stronger hydrogen bonds with the reacting atoms than in the [TS 6-6 + $4H_2O$] and [TS 6-8 + $3H_2O$] species.

The total and relative energies of the species with the expanded QM regions are reported in Table 6.7.

Table 6.7 – Total and Relative Energies of the AM1/TIP3P Reaction Species for the Elimination of HF Based on Bimolecular Hydrolysis Species with Expanded QM Regions

	AM1/TIP3P	
Species	Total (kcal/mol)	Relative (kJ/mol)
[D 6-6 + $4H_2O$]	-6583.3	0
[TS 6-6 + $4H_2O$]	-6526.6	237
[P 6-6 + $4H_2O$]	-6574.6	36
[R 6-8 + $3H_2O$]	-6518.6	0
[TS 6-8 + $3H_2O$]	-6466.6	218
[P 6-8 + $3H_2O$]	-6525.5	-29
[R 6-9 + $3H_2O$]	-6516.5	0
[TS 6-9 + $3H_2O$]	-6456.1	253
[P 6-9 + $3H_2O$]	-6533.0	-69

The decomposition process of $CFH(OH)_2$ through [TS 6-6 + $4H_2O$] is the only one of the three for which there is a significant lowering of the energy barrier. The barrier decreases by 31 kJ mol^{-1} when the four solvent molecules are treated as QM atoms. This does not occur for the direct elimination reactions through [TS 6-8 + $3H_2O$] and [TS 6-9 + $3H_2O$], where the energy barriers are only slightly reduced by the treatment of solvent molecules as QM species.

The additional QM atoms also affect the reaction energies. The decomposition of $CFH(OH)_2$ becomes less endothermic by 31 kJ mol^{-1}. The transition state and product species are therefore stabilised to the same extent when some solvent molecules are treated quantum mechanically. However, the interactions responsible for this stabilisation are clearly not strong enough for C-F bond dissociation to occur. The

reaction energy for the direct elimination process through [TS 6-8 + $3H_2O$] is essentially unaffected by the additional QM atoms. Treating solvent molecules quantum mechanically therefore seems to have absolutely no effect on this reaction. In contrast, although the energy barrier for the reaction *via* [TS 6-9 + $3H_2O$] is only marginally lower than that *via* [TS 6-9], the complete dissociation of the C-F bond in the [P 6-9 + $3H_2O$] species means that the reaction becomes much more exothermic.

The transition structures based on the [TS 6-15] and [TS 6-17] species, with expanded QM regions, are named [TS 6-15 + $5H_2O$] and [TS 6-17 + $4H_2O$]. These relate to the bimolecular decomposition of $CFH(OH)_2$ and termolecular direct elimination process respectively. The reaction path *via* [TS 6-17 + $4H_2O$] exhibits the same features as the reaction *via* [TS 6-17]. The relative energies of the reaction species reported in Table 6.8 led to the expectation that the product molecules were separate in [P 6-17 + $4H_2O$]. Inspection of this species proved that this was not the case, and the carbon and fluorine atoms remained partially bonded.

Table 6.8 – Total and Relative Energies of the AM1/TIP3P Reaction Species for the Elimination of HF Based on Termolecular Hydrolysis Species with Expanded QM Regions

	AM1/TIP3P	
Species	Total (kcal/mol)	Relative (kJ/mol)
[D 6-15 + $5H_2O$]	-6668.9	0
[TS 6-15 + $5H_2O$]	-6661.2	32
[P 6-15 + $5H_2O$]	-6692.6	-99
[R 6-17 + $4H_2O$]	-6645.4	0
[TS 6-17 + $4H_2O$]	-6593.6	217
[P 6-17 + $4H_2O$]	-6663.7	-77

The location of an equivalent transition structure based on [TS 6-15] for the decomposition of $CFH(OH)_2$ proved problematic. The reacting atoms of the [TS 6-15 + $5H_2O$] species finally located, have similar geometries to those in [TS 6-15]. The product species [P 6-15 + $5H_2O$] also has a structure consistent with previous results, with the C-F bond still partially intact. The difference lay in the structure of the reactant species [D 6-15 + $5H_2O$]. The anticipated structure would have the (+60,+60) conformer of the $CFH(OH)_2$ diol hydrogen bonded to the originally defined QM water molecule and solvent molecules. The [D 6-15 + $5H_2O$] species pictured in Figure 6.28 was located from the optimisation of the reactant-like structure from an IRC calculation.

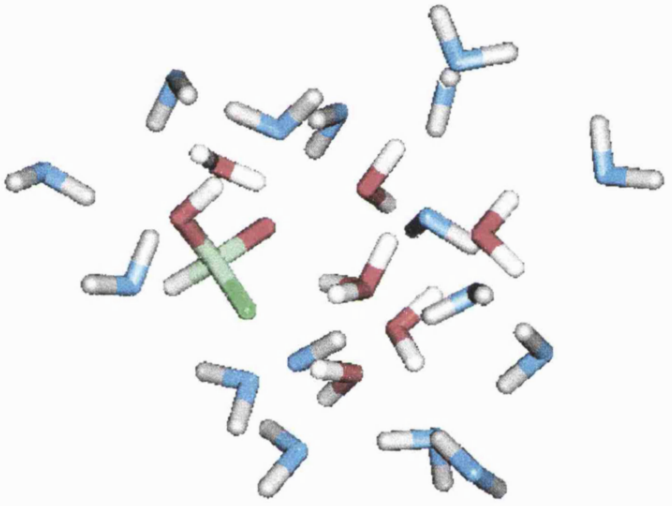

[D 6-15 + $5H_2O$]

Figure 6.28

It would appear that the transfer of solvent molecules to the QM region results in the stabilisation of an intermediate species, where one of the protons of the diol has transferred to a water molecule. A transition state for this proton transfer should therefore exist on the potential energy surface, which connects the $CFH(OH)_2$ intermediate to the [D 6-15 + $5H_2O$] species. However, since this section was mainly concerned with the structures of the product species it was not considered worthwhile to try to locate this extra transition state.

The expansion of the QM region to include solvent water molecules only results in the concerted elimination of HF in a single case, the path through [TS 6-9 + $3H_2O$]. This result suggests that for this species the solute-solvent interactions are strong enough for C-F bond dissociation to occur in a single step. However, the solvent structures around the solute are snapshots of the instantaneous positions of the solvent molecules. It may be that different solvent structures could exist, which would also allow elimination of HF to proceed through a single transition structure for the other reaction paths. The conclusion of this investigation is that the elimination of HF may proceed *via* a concerted or stepwise process, depending on the solvent arrangement around the solute atoms. In addition the structure of the [D15 + $5H_2O$] species indicates that the introduction of more water molecules into the QM region may promote ionic mechanisms that have not been considered here.

6.3.3.2 The Nature of the Eliminated HX Species

This section concerns the nature of the eliminated HX species. AM1/TIP3P transition structures have been located that were derived from both bimolecular and termolecular elimination transition structures. This section mainly concerns the elimination of HCl, as it was only for the reaction *via* [TS 6-9 + $3H_2O$] that HF was produced as a separate species. Inspection of the [P 6-9 + $3H_2O$] species showed that the HF eliminated during the process was a covalent molecule.

Transition states were located for the elimination of HCl with expanded QM regions. These were based on the [TS 6-7], [TS 6-10], [TS 6-11], [TS 6-16], [TS 6-18], and [TS 6-19] transition structures. IRC calculations were performed on the 'new' transition structures and the reactant and product species determined. Inspection of the

product structures showed that in each case HCl was eliminated as a covalent molecule. The [P 6-10 + $5H_2O$] structure pictured in Figure 6.29 is shown as an example of the product species.

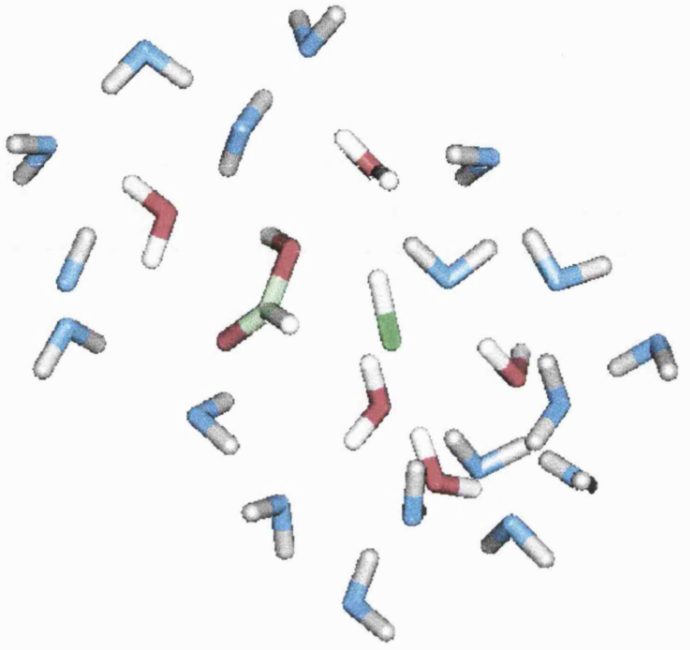

[P 6-10 + $5H_2O$]

Figure 6.29

The structures and partial charges of the relevant atoms indicate that HX is produced as a covalent molecule. Thus the expansion of the QM part of the system in order to promote the possibility of elimination of HX as ionic H^+ and X^- species does not appear to make a difference to the nature of the products.

If the HX is produced as a covalent molecule then dissociation into H^+ and X^- ions would follow. The ionisation of the product species is beyond the scope of this investigation, however the ionisation of HF and HCl in water and on the surface of ice is well documented.[151-157]

6.4 Conclusions

In this chapter the hydrolysis of the formyl halides has been modelled using a hybrid QM/MM technique involving GRACE and CHARMM. This method allows the location of refined transition structures of species in solution, and explicit representations of solvent molecules. Reaction paths have been determined for the one- and two-step mechanisms and both bimolecular and termolecular processes occurring within a water droplet.

The AM1/TIP3P transition structures, and the minimum energy species they connect, enable examination of specific solute-solvent interactions. However, it must be remembered that the species depicted in this chapter are merely snapshots of stationary points. They are not unique and may be considered as members of a large group of similar stationary points.

The energetically favoured reaction paths for the hydrolysis of the formyl halides in a water droplet are the same as in the gas phase for both the bimolecular and termolecular processes. The one-step mechanism is preferred for bimolecular hydrolysis of formyl fluoride and chloride with energy barriers of 225 and 126 kJ mol^{-1} respectively.

The one-step mechanism is also preferred for the termolecular hydrolysis of formyl chloride with an associated energy barrier of 106 kJ mol^{-1}. The two-step mechanism is favoured for the termolecular hydrolysis of formyl fluoride, and has a barrier height of 120 or 148 kJ mol^{-1} for the rate-determining first step of the process. The termolecular processes are clearly still the more energetically favoured mechanisms for the hydrolysis reactions of formyl halides within a water droplet.

The energetically favoured mechanisms for the hydrolysis reactions may not change in the presence of solvent, but using the AM1 Hamiltonian to describe the solute atoms does cause alterations to the processes. AM1 predicts the decomposition of the $CFH(OH)_2$ diol to be the rate-determining step of the bimolecular two-step mechanism both *in vacuo* and *in aqua*. However, the MP2(fu)/6-31G* gas phase results predict the diol formation as the rate-determining step.

Inspection of the energy barriers for the C-F bond cleavage processes shows that they are in the order of 100 kJ mol^{-1} higher when the AM1 Hamiltonian is used instead of the *ab initio* description of the solute. The high energy cost associated with C-F bond cleavage when the AM1 Hamiltonian is used may contribute to the existence of the partially dissociated product-like structures reported in this chapter (*e.g.* [P 6-5]).

The gas phase results reported in earlier chapters indicated that the conformation of the $CXH(OH)_2$ intermediates formed during the two-step mechanism was very important to how the reaction could proceed. It would appear from the AM1/TIP3P structures that in solution the conformer formed is affected by the solvent arrangement surrounding the reacting atoms. The species located using GRACE and CHARMM have non-unique solvent structures, a different solvent arrangement could result in the production of, or decomposition from, a different conformer of the intermediate as observed for [TS 6-5] and [TS 6-6]. The results suggest that the conformation of the $CXH(OH)_2$ intermediate becomes less significant when the hydrolysis occurs within a water droplet.

The AM1/TIP3P structures obtained using GRACE and CHARMM appear to give reasonable descriptions of the reaction species in solution. However, it would have been preferable to use an *ab initio* description of the solute, and to include polarization

of the solvent water molecules. This is possible with GRACE and CHARMM by using a three-zone optimiser and an interface to the GAMESS-UK[158] program. The computational expense involved in using an *ab initio* description of the solute, plus accounting for solvent polarization, and the fact that the interface between GRACE and GAMESS-UK is not as refined as that between GRACE and CHARMM precluded its use in this investigation. This was due to the large number of reaction species it was necessary to locate in order to compare the competing reaction paths.

The energies calculated for the reaction species located in this chapter are potential energies for the particular solute-solvent arrangements obtained. These energies have supplied valuable information regarding solvation effects, but in order to gain a more quantitative view of solvation energies it would be desirable to calculate free energies for the solvated species. The free energy of solvation is a property averaged over all possible solvent configurations. To calculate this property solvated species must therefore be examined, not as static systems as in this chapter, but as dynamic systems in which the solvent molecules are free to rearrange themselves around the solute atoms. The calculation of free energies of solvation for the hydrolysis of the formyl halides within a water droplet, and the methods used to achieve this, are the subject of the following chapter.

7. MOLECULAR DYNAMICS SIMULATIONS OF FORMYL HALIDE HYDROLYSIS

7.1 Introduction

In the previous chapter the hydrolysis of the formyl halides occurring within a water droplet was investigated. AM1/TIP3P transition state, reactant and product species were located and the potential energy barriers and reaction energies evaluated. Although potential energies give an indication of how the reaction proceeds in solution it would be advisable to obtain free energies of the species along the reaction co-ordinate to gain a more quantitative view of solvent effects on the reaction. The aim in this chapter has therefore been to calculate solvation free energies for these reaction species.

Experimentally determined properties of a system generally depend upon the positions and momenta of the N particles that make up the system. For a system containing N atoms, 6N values are needed to define the state of the system (3 co-ordinates per atom and 3 components of momentum). Thus each combination of 3N positions and 3N momenta defines a point in 6N-dimensional phase space. The instantaneous value of a property A can be written as $A(\mathbf{p}^N(t),\mathbf{r}^N(t))$, where $\mathbf{p}^N(t)$ and $\mathbf{r}^N(t)$ represent the N momenta and positions respectively at time t. This property A will fluctuate over time as a result of interactions between the particles. The experimentally determined value of property A is therefore a time average over the time of the measurement. As the measurement time increases to infinity the value obtained for property A approaches the 'true' average value of the property. This can be represented by the integral in Equation 7.1:

$$A_{ave} = \lim_{\tau \to \infty} \frac{1}{\tau} \int_{t=0}^{\tau} A\left(\mathbf{p}^N(t), \mathbf{r}^N(t)\right) dt \qquad \text{(Equation 7.1)}$$

In order to calculate the average values of the properties of a system it is therefore necessary to simulate the dynamical behaviour of the system (*i.e.* to determine values of $A(\mathbf{p}^N(t),\mathbf{r}^N(t))$), based on the intra- and intermolecular interactions present in the model. This can be achieved by solving Newton's equations of motion. For any arrangement of atoms in the system, the force acting on each atom due to interactions with other atoms can be calculated by differentiating the energy function. The acceleration of each atom can then be determined from the force by solving Newton's second law (F = ma). Integration of the equations of motion yields a trajectory that describes how the positions, velocities, and accelerations of the particles change with time. The average values of properties can then be calculated. However a problem arises because for large numbers of molecules it can be difficult enough to determine an initial configuration without having to then integrate the equations of motion. This can be overcome using statistical mechanics in which large numbers of replications of the system are considered simultaneously and replace a system evolving in time. The time average of the required property is determined by integrating over all possible configurations of the system. The Monte Carlo and molecular dynamics techniques that can be used to calculate time average properties are described below.

7.1.1 Monte Carlo

Monte Carlo simulations generate configurations of a system by making random changes to the positions of the atoms or molecules present, as well as to their orientations and conformations where appropriate. Each configuration depends only on its predecessor and not on any of the other configurations of phase space previously

visited. A set of criteria is used to decide whether or not to accept a new configuration. The process involves calculating the energy of the configuration directly from the potential energy function. If the energy of the new configuration is lower than that of the previous configuration then the new one is accepted and becomes the next state. If the energy of the new configuration is higher than that of its predecessor then the Boltzmann factor of the energy difference is calculated:

$$\text{Boltzmann factor} = \exp\left[-\left(V_{new}(\mathbf{r}^N) - V_{old}(\mathbf{r}^N)\right)/k_B T\right] \qquad \text{(Equation 7.2)}$$

where V_{new} and V_{old} are the potential energies of the new and old configurations respectively, k_B is the Boltzmann constant, and T the temperature. The Boltzmann factor is then compared with a random number generated between 0 and 1. If the Boltzmann factor is higher than this random number then the step is accepted. If it is lower then the new configuration is rejected and the original configuration is retained for the next iteration. This procedure means that although moves to states of higher energy are permitted, the smaller the increase in energy going from one configuration to the next, the greater the probability that the move will be accepted. The values of the desired properties are calculated for each accepted configuration from the positions of the atoms. At the end of the calculation the mean average of these properties is obtained by averaging over the number of values calculated, M:

$$\langle A \rangle = \frac{1}{M}\sum_{i=1}^{M} A(\mathbf{r}^N) \qquad \text{(Equation 7.3)}$$

where $\langle A \rangle$ is the ensemble average of property A (which is equal to the time average of property A) and $\mathbf{r}^N$ represents the positions of the N particles.

Monte Carlo methods generally sample from the canonical ensemble, *i.e.* constant N (number of particles), V (volume), and T (temperature). Thus the total energy of the system is permitted to vary. As stated above there is also no time dependence of the

properties of the system, and the total energy is determined directly from the potential energy function.

7.1.2 Molecular Dynamics

The first major difference between molecular dynamics and Monte Carlo methods is that molecular dynamics provides information about the time dependence of the properties of a system. Therefore the state of the system at any future time can be predicted from its current state. As it was originally hoped to examine how the solvent structures changed with time around the solute atoms molecular dynamics was chosen as the method for the investigation undertaken in this chapter.

Integrating Newton's laws of motion generates successive configurations of the system. The resulting trajectory is obtained by solving Newton's second law:

$$\frac{d^2x_i}{dt^2} = \frac{Fx_i}{m_i} \qquad \text{(Equation 7.4)}$$

which in this case describes the motion of a particle of mass m_i along one co-ordinate (x_i). Fx_i is the force on the particle in that direction. In conditions where intermolecular interactions are modelled using continuous potentials (*e.g.* a Lennard-Jones potential) the force on each particle changes whenever that particle changes its position, or whenever any of the particles with which it interacts change position. The motions of all the particles are therefore coupled together and the result is a many-body problem that cannot be solved analytically. The calculation is therefore broken down into a series of very short time steps (typically between 10^{-15} to 10^{-14} s). At each time step the total force on each particle is calculated as the vector sum of its interactions with other particles. The accelerations of the particles are determined from the force.

These are then combined with the positions and velocities to generate new positions and velocities a short time ahead. The force acting on each atom is assumed to be constant during the time step. The particles are then moved to the new positions, and the forces on the particles recomputed etc. Thus a molecular dynamics trajectory is built up and describes how the dynamic variables change with time.

The equations of motion are integrated using finite difference methods to generate the trajectories for continuous potential models. The algorithms used to do this assume that the positions and dynamical properties can be approximated as Taylor series expansions, *e.g.*:

$$\mathbf{r}(t+\delta t) = \mathbf{r}(t) + \delta t\mathbf{v}(t) + \tfrac{1}{2}\delta t^2\mathbf{a}(t) + \tfrac{1}{6}\delta t^3\mathbf{b}(t) + \tfrac{1}{24}\delta t^4\mathbf{c}(t) + \ldots \qquad \text{(Equation 7.4)}$$

$$\mathbf{v}(t+\delta t) = \mathbf{v}(t) + \delta t\mathbf{a}(t) + \tfrac{1}{2}\delta t^2\mathbf{b}(t) + \tfrac{1}{6}\delta t^3\mathbf{c}(t) + \ldots \qquad \text{(Equation 7.5)}$$

$$\mathbf{a}(t+\delta t) = \mathbf{a}(t) + \delta t\mathbf{b}(t) + \tfrac{1}{2}\delta t^2\mathbf{c}(t) + \ldots \qquad \text{(Equation 7.6)}$$

where **r** is the position, **v** is the velocity (the first derivative of the positions with respect to time), **a** is the acceleration (the second derivative), **b** and **c** are the third and fourth derivatives respectively. t represents a specific time point, and δt is the time step.

A popular method used to integrate the equations of motion is the Verlet[159] algorithm. This algorithm uses the positions and accelerations at time t, and the positions from the previous step $\mathbf{r}(t-\delta t)$ to calculate new positions at time $(t+\delta t)$, *i.e.* $\mathbf{r}(t+\delta t)$:

$$\mathbf{r}(t+\delta t) = 2\mathbf{r}(t) - \mathbf{r}(t-\delta t) + \delta t^2\mathbf{a}(t) \qquad \text{(Equation 7.7)}$$

The velocities do not explicitly appear in the Verlet integration algorithm, but can be calculated in a variety of ways, for example dividing the difference in positions at times $(t+\delta t)$ and $(t-\delta t)$ by $2\delta t$:

$$\mathbf{v}(t) = \left[\mathbf{r}(t+\delta t) - \mathbf{r}(t-\delta t)\right]/2\delta t \qquad \text{(Equation 7.8)}$$

The storage needs of the Verlet algorithm are modest as it only requires the two sets of positions $\mathbf{r}(t)$ and $\mathbf{r}(t-\delta t)$ and the accelerations $\mathbf{a}(t)$, however it does have its limitations. Precision may be lost because the positions $\mathbf{r}(t+\delta t)$ are obtained by adding a small term ($\delta t^2\mathbf{a}(t)$) to the difference of two much larger terms (Equation 7.7). Additionally, the lack of an explicit velocity term means that the velocities are not available until the positions have been calculated at the next step. It is also not a self-starting algorithm as the new positions are obtained from the current positions and the positions from the previous time step. Therefore at t=0 other means are needed to obtain positions at $t-\delta t$, *e.g.* by truncating Equation 7.4 after the first term. It then becomes:

$$\mathbf{r}(-\delta t) = \mathbf{r}(0) - \delta t\mathbf{v}(0) \qquad \text{(Equation 7.9)}$$

Variations of the Verlet algorithm are also used. The calculations reported in this chapter were performed using the leap-frog[160] algorithm which uses the following relationships:

$$\mathbf{r}(t+\delta t) = \mathbf{r}(t) + \delta t\mathbf{v}(t+\tfrac{1}{2}\delta t) \qquad \text{(Equation 7.10)}$$

$$\mathbf{v}(t+\tfrac{1}{2}\delta t) = \mathbf{v}(t-\tfrac{1}{2}\delta t) + \delta t\mathbf{a}(t) \qquad \text{(Equation 7.11)}$$

The velocities $\mathbf{v}(t+½\delta t)$ are calculated first from the velocities at time $t-½\delta t$ and the accelerations at time t. The positions $\mathbf{r}(t+\delta t)$ are then deduced from these velocities and the positions $\mathbf{r}(t)$ using Equation 7.10. The velocities at time t are calculated from:

$$\mathbf{v}(t) = \tfrac{1}{2}\left[\mathbf{v}(t+\tfrac{1}{2}\delta t) + \mathbf{v}(t-\tfrac{1}{2}\delta t)\right] \qquad \text{(Equation 7.12)}$$

The advantages of the leap-frog algorithm are that it explicitly includes velocities, and does not require the calculation of the differences of large numbers. However, as the positions and the velocities are not synchronised the kinetic energy contribution to the total energy cannot be computed at the same time as the potential energy.

Once the molecular dynamics trajectories have been generated thermodynamic averages, ⟨A⟩, are obtained as time averages using Equation 7.13:

$$\langle A \rangle = \frac{1}{M}\sum_{i=1}^{M} A\left(\mathbf{p}^N, \mathbf{r}^N\right) \qquad \text{(Equation 7.13)}$$

where M is the number of time steps. $\mathbf{p}^N$ and $\mathbf{r}^N$ are as defined previously.

Molecular dynamics samples from a different ensemble to Monte Carlo methods. Molecular dynamics calculations traditionally sample from the microcanonical ensemble, *i.e.* under conditions of constant number of particles (N), volume (V), and energy (E). Another difference between the two methods is that molecular dynamics has a kinetic energy contribution to the total energy of the system whereas in Monte Carlo simulations the total energy is derived purely from the potential energy function.

As stated earlier the molecular dynamics method of sampling phase space was chosen to compute the solvation free energies for reactions species involved in formyl halide hydrolysis. The protocol used to do this is described below.

7.2 Methods

Optimised AM1/TIP3P structures from Chapter 6 were chosen as initial geometries for molecular dynamics simulations. The species chosen were those associated with the transition states numbered [TS 6-1] to [TS 6-19] and include the reactant and product structures for these processes as well as the transition structures. The transition states [TS 6-5] and [TS 6-5(a)] and their associated minimum energy species were not taken through the dynamics simulations. This was because the solute geometries for these

species were very similar to those for [TS 6-6] and [TS 6-6(a)] and would therefore result in comparable values for the solvation energies.

7.2.1 Solution Phase Molecular Dynamics Simulations

The same procedure was used for each of the structures and involved setting up the system as follows. Mulliken charges[161] determined from gas phase single point energy calculations at the semi-empirical AM1 level of theory were assigned to the solute atoms for each of the solvated structures. The default CHARMM24[143] van der Waals parameters were used for the solute atoms. The solvent was represented by the standard TIP3P[147] parameters for the 15 Å sphere of solvent water molecules.

The molecular dynamics calculations were performed with the solute atoms fixed throughout the simulations. The systems were prepared for the dynamics calculations by minimising the solvent around the solute to a r.m.s. gradient of less than 0.0005 kcal mol^{-1} $Å^{-1}$. The whole system was propagated by full molecular dynamics using the leap-frog algorithm. A deformable boundary was used to prevent water molecules evaporating. CHARMM achieves this by calculating an additional energy term in which a constraining sphere is constructed around the entire water droplet, effectively placing the droplet in a cage. The potential used is scaled so that atom positions furthest from the centre of the sphere have the greatest restraining force applied.

The SHAKE[162] algorithm was applied to bonds containing hydrogen as the high frequency motions of these bonds were of less interest than the lower frequency modes corresponding to major conformational changes. This meant that a larger time step of 0.001 ps could be used. The system was heated to 300 K over a period of 18 ps

followed by 2 ps equilibration. The system was then equilibrated for a further 20 ps before a production period of 60 ps. During the course of the production dynamics a co-ordinate set was saved every 0.2 ps to give a total of 300 frames for analysis. The stability of the dynamics runs during the production period was tested by calculating the ratio of the r.m.s. deviation of the total energy to the average total energy of the system. If this ratio was <0.001 the dynamics run was accepted.

7.2.2 Calculation of Solvation Free Energies

The classical molecular dynamics trajectories produced using the protocol described in the previous section do not directly give the free energies of the reaction species in solution. It is possible to determine free energies using molecular dynamics or Monte Carlo averages over the phase space of the system,[163,164] however simulations of this type require a large number of time consuming calculations to be performed. These options were therefore not viable for the current study due to the large number of reaction species being examined.

A practical alternative to these methods is an approach based on the Born theory of solvation.[165] This uses a macroscopic solvent model in which the electrostatic contribution to the solvation free energy of a spherical ion can be written as:

$$\Delta G_{elec} = \frac{-q^2}{2a}\left(1-\frac{1}{\varepsilon}\right) \qquad \text{(Equation 7.13)}$$

q is the charge on the ion, a is its radius, and ε is the dielectric constant of the solvent. This expression was based on a linear response approximation of the solvent to changes in the solute charge distribution. The theory has since been extended to non-spherical

solutes,[166-168] and also to microscopic water models.[169-171] The result is that the free energy of solvation of an ionic or polar solute (ΔG_{solv}) can be approximated as:

$$\Delta G_{solv} \approx \tfrac{1}{2}\langle E_{i-s} \rangle \qquad \text{(Equation 7.14)}$$

where $\langle\ \rangle$ denotes a mean evaluated value, and E_{i-s} is the solute-solvent electrostatic interaction energy.[172-175] This relationship provides an effective method of obtaining free energies of solvation in a relatively computationally inexpensive manner.

The electrostatic interaction energies between the solute and solvent were computed using the standard CHARMM QM/MM parameters. Single point energy calculations using the AM1 Hamiltonian and TIP3P molecular mechanics description of the solvent were performed for each of the 300 trajectory frames obtained from the molecular dynamics simulations. The mean average of these values was then evaluated. This produced a value for the total electrostatic energy of the solute in solution. The electrostatic interaction energy between the solute and solvent was then determined by subtracting the semi-empirical gas phase solute energy from the total electrostatic energy of the solute in solution. This is summarised in Equation 7.16.

$$E_{QM/MM}^{Elec} = \left\langle \Psi_s \middle| H_{QM} + H_{QM/MM} \middle| \Psi_s \right\rangle - \left\langle \Psi^0 \middle| H_{QM} \middle| \Psi^0 \right\rangle \qquad \text{(Equation 7.16)}$$

where H_{QM} and $H_{QM/MM}$ are the AM1 Hamiltonian and QM/MM Hamiltonian respectively (see section 6.2.2 for further details). Ψ_s is the wavefunction of the system in solution and Ψ^0 is the gas phase wavefunction. It was thus possible to calculate solvation free energies from classical molecular dynamics trajectories. The free energy in solution of each reaction, transition state, and product structure studied was then estimated by adding the solvation free energy to the AM1 gas phase energy. The barrier heights and reaction energies for the free energies in solution were then calculated.

7.2.3 Calculation of Solvation Free Energies Using Continuum Methods

In addition to investigating the solvation effects on formyl halide hydrolysis using explicit representations of the solvent the results were compared to those obtained using continuum models. The continuum models used were the COSMO[176] implementation in Gaussian 98[28] and the SM5.4A[25] method in AMSOL.[26] Brief descriptions of these solvent models can be found in section 1.5.1.

Single point energy calculations were performed on the gas phase reactant, transition state, and product structures located at the MP2(fu)/6-31G* level of theory (see Chapter 4) using the COSMO continuum model. The SM5.4A solvation model was used to perform single point energy calculations on the solute atoms of the AM1/TIP3P optimised structures named in section 7.2. These sets of calculations allowed comparisons to be made between the solvation free energies obtained using the explicit water molecules and the continuum solvent representation. Additionally they allowed comparison of the *ab initio* solvation free energies with the values obtained using the semi-empirical description of the quantum atoms.

7.2.4 Test Calculations of Solvation Free Energies

Calculations of solvation free energies were performed on species either similar to those involved in formyl halide hydrolysis, or on the individual reactant and product molecules for the process. These were performed as test cases for the procedure described in the preceding sections as it was thought prudent to check that the specific molecular dynamics protocol used in this thesis produced sensible results for species where comparable data was available in the literature.

The initial embedding of the solutes into the water sphere and AM1/TIP3P optimisation was achieved using the procedure detailed in Chapter 6. The molecular dynamics calculations were carried out using the protocol described above. The values obtained from this method were then compared with those from the AM1/SM5.4A continuum model and with experimental data where possible. The results of these calculations are reported in Table 7.1.

As the molecular dynamics simulation has a system with a radius of 15 Å only water molecules within this radius contribute to the solvation energy. Continuum models do not employ a cut off and so a Born or Onsager correction was included so that the solvation free energies from the test dynamics simulations could be directly compared with the continuum results. The Born correction is used for charged solutes and has the form:

$$\Delta G_{bulk}(\text{ionic solute}) = -166\left(1 - \tfrac{1}{\varepsilon}\right)q^2/r_{cut} \qquad \text{(Equation 7.17)}$$

For neutral solutes Onsager's formula is used:

$$\Delta G_{bulk}(\text{neutral solute}) = -166\left[(2\varepsilon - 2)/(2\varepsilon + 1)\right]\mu^2/r_{cut}^3 \qquad \text{(Equation 7.18)}$$

ΔG_{bulk} is the contribution to the solvation free energy originating from the solvent region outside the 15 Å cut off radius, r_{cut} is the cut off radius (Å), q and μ are the charge and dipole (Debye) of the ionic and neutral solutes respectively, and ε is the dielectric constant of the solvent (ε=80 for water).

Table 7.1 – Solvation Free Energies Calculated for Test Solute Species

Species	ΔG_{solv} (kcal/mol)			
	Molecular Dynamics AM1/TIP3P	Molecular Dynamics AM1/TIP3P + Born Correction	Continuum AM1/SM5.4	Experimental
F^-	-110.0	-120.9	-106.8	-107±6[a], -107[b]
Cl^-	-86.1	-97.0	-77.2	-78±7[a], -77[b]
H_3O^+	-78.0	-88.9	-113.0	-105±5[a], -104[b]
H_2O	-2.7	-2.9	-9.4	-6.4[a], -4.4[b]
CH_2O	-3.1	-3.4	-3.2	
CFHO	-4.2	-4.5	-4.5	
CClHO	-2.4	-2.6	-3.8	
HF	-2.6	-2.8	0.6	-5.6[b]
HCl	-1.5	-1.6	-0.9	1.4[b]
HCO_2H	-5.0	-5.6	-6.3	-5.5

[a] Reference [177].
[b] References [25,178,179].

The values in Table 7.1 show that for the charged solutes the agreement between the solvation free energies derived from dynamics simulations and the continuum and experimental data is actually better without the Born correction. H_3O^+ is the exception to this trend with the AM1/TIP3P method underestimating the free energy of solvation by a minimum of 11.1 kcal mol^{-1} even when the contribution of the bulk solvent is included.

The solvation free energy for H_3O^+ calculated using the AM1/SM5.4A method also deviates considerably from the experimental values, but in this case the free energy is overestimated. This is a general problem with continuum models in that they produce low accuracy values of ΔG_{solv} for ions containing sp^3-hybidised oxygen atoms.[180] The

solvation free energies for the neutral solutes are in relatively good agreement with the continuum results. In general, the agreement with the available experimental data for the neutral solutes is within ±3 kcal mol^{-1}.

These results, in which the same solute geometry was used for both solvation models, show that the method used to derive free energies of solvation from molecular dynamics trajectories does provide a practical alternative to other, more computationally demanding methods.

7.3 Results

The free energies of solvation (ΔG_{solv}) calculated for the CXHO + $1H_2O$ reaction species, in which seven atoms were included in the quantum region, are reported in Tables 7.2 and 7.3. The free energies of solvation calculated for the CXHO + $2H_2O$ reaction species, where ten atoms were included in the QM region, are reported in Tables 7.4 and 7.5. The results include evaluations of the free energies of solvation using the molecular dynamics protocol and the AM1/SM5.4A continuum method discussed above.

The free energies of solvation were used to calculate free energies in solution (ΔG_{soln}) of the reaction species by adding ΔG_{solv} to the AM1 gas phase energy computed for the bare solute atoms. The absolute and relative values obtained for the free energies in solution are reported in Tables 7.6 to 7.13.

7.3.1 Free Energies of Solvation for the CXHO + $1H_2O$ Reaction Species

The free energies of solvation reported in Tables 7.2 and 7.3 represent the energies of the reaction species involved in the one- and two-step hydrolysis mechanisms. The free energies of solvation for the two-step mechanism species show clearly that solvation stabilises the transition states to a greater extent than the minimum energy species along the reaction path.

Table 7.2 – Free Energies of Solvation for the CXHO + $1H_2O$ Two-Step Mechanism Reaction Species

	ΔG_{solv} (kJ mol^{-1})			ΔG_{solv} (kJ mol^{-1})	
Species X=F	MD AM1/TIP3P	Continuum AM1/SM5.4A	Species X=Cl	MD AM1/TIP3P	Continuum AM1/SM5.4A
[R 6-1]	-23	-33	[R 6-3]	-21	-29
[TS 6-1]	-43	-63	[TS 6-3]	-41	-70
[D 6-1]	-17	-38	[D 6-3]	-16	-42
[R 6-2]	-26	-26	[R 6-4]	-26	-39
[TS 6-2]	-48	-68	[TS 6-4]	-44	-75
[D 6-2]	-21	-37	[D 6-4]	-18	-40
[D 6-6]	-19	-37	[D 6-7]	-14	-37
[TS 6-6]	-48	-60	[TS 6-7]	-110	-112
[P 6-6]	-60	-55	[P 6-7]	-20	-27
[TS 6-6(a)]	-41	-35			
[P 6-6(a)]	-28	-23			

The free energies of solvation obtained from the molecular dynamics calculations are consistently lower than those from the continuum solvation calculations. This may be a further example of the problems continuum models have producing accurate free energies of solvation for systems containing sp^3-hybridised oxygen atoms. The differences in the free energies of solvation between the MD and continuum results

increases with the number of sp^3-hybridised oxygen atoms present. Thus for the reactant species, which contain one sp^3-hybridised oxygen the difference is less than for the diol species which have two sp^3 oxygen atoms.

The effect of solvation is to lower the energies of all the reaction species, with only minor substituent effects observable for the first step of the two-step mechanism. In agreement with the potential energies reported in chapter 6, the nature of the halogen substituent becomes important for the second step of the process. When the substituent is fluorine the transition state for diol decomposition is stabilised to approximately the same extent as those for diol formation. However, if the halogen present is chlorine then the free energy of solvation for the [TS 6-7] transition state is almost double that for the equivalent fluorine species [TS 6-6].

The greater stability imparted to the [TS 6-7] transition state is again likely to be caused by the fact that the carbon-chlorine bond is essentially broken in this species, thus the chlorine has a large partial charge and consequently forms multiple strong hydrogen bonds with solvent molecules. In the decomposition of the fluorine substituted diol proton transfer occurs before carbon-fluorine bond cleavage. Thus the fluorine atom remains covalently bonded to the carbon in [TS 6-6] and does not experience the charge build up that occurs in the [TS 6-7] species, and only forms weak hydrogen bonds with the solvent. The solvent stabilisation is therefore reduced compared to the analogous chlorine process.

Table 7.3 – Free Energies of Solvation for the CXHO + 1H_2O One-Step Mechanism Reaction Species

	ΔG_{solv} (kJ mol^{-1})			ΔG_{solv} (kJ mol^{-1})	
Species X=F	MD AM1/TIP3P	Continuum AM1/SM5.4A	Species X=Cl	MD AM1/TIP3P	Continuum AM1/SM5.4A
[R 6-8]	-29	-46	[R 6-10]	-15	-25
[TS 6-8]	-61	-74	[TS 6-10]	-93	-110
[P 6-8]	-64	-56	[P 6-10]	-25	-25
[TS 6-8(a)]	-50	-44			
[P 6-8(a)]	-33	-23			
[R 6-9]	-33	-46	[R 6-11]	-17	-23
[TS 6-9]	-77	-95	[TS 6-11]	-119	-140
[P 6-9]	-72	-80	[P 6-11]	-36	-48
[TS 6-9(a)]	-54	-60			
[P 6-9(a)]	-39	-44			

The free energies of solvation calculated for the one-step bimolecular reaction show the same differences between the MD and continuum results as the two-step mechanism reaction species. The variations due to the nature of the halogen substituent are also evident.

The free energies of solvation for the two reaction paths of the one-step mechanism exhibit significant differences for the transition state and product species. The transition states and product species for the reaction paths that yield formic acid in its lowest energy conformer (*via* [TS 6-8] and [TS 6-10]) are less stabilised by solvation than those species arising from the alternative reaction paths. These differences in stabilisation are less pronounced for the MD results than the continuum values when the halogen substituent is fluorine. When X=Cl, although the degree of stabilisation of the reaction species is different for the MD and continuum calculations, the extra stability

of the species *via* [TS 6-11] over [TS 6-10] remains essentially unchanged for both methods.

The free energies of solvation for the equivalent fluorine and chlorine containing transition states show the expected preference for solvent stabilisation of the chlorinated species. This additional stabilisation of [TS 6-10] and [TS 6-11] over [TS 6-8] and [TS 6-9] is again caused by the greater partial charge on the chlorine than fluorine atom in these transition states. This results in stronger and more numerous hydrogen bond interactions between the chlorine and the solvent water molecules than between the solvent and fluorine.

7.3.2 Free Energies of Solvation for the CXHO + $2H_2O$ Reaction Species

The free energies of solvation that are reported in Tables 7.4 and 7.5 represent the energies for the reaction species involved in the one- and two-step termolecular hydrolysis mechanisms. In common with the bimolecular reaction species the transition structures are stabilised to a greater extent than the minimum energy species along the reaction paths. The continuum method again produces more negative free energies of solvation than the MD technique.

Table 7.4 – Free Energies of Solvation for the CXHO + $2H_2O$ Two-Step Mechanism Reaction Species

	ΔG_{solv} (kJ mol^{-1})			ΔG_{solv} (kJ mol^{-1})	
Species X=F	MD AM1/TIP3P	Continuum AM1/SM5.4A	Species X=Cl	MD AM1/TIP3P	Continuum AM1/SM5.4A
[R 6-12]	-28	-32			
[TS 6-12]	-79	-91			
[D 6-12]	-21	-38			
[R 6-13]	-31	-55	[R 6-14]	-18	-26
[TS 6-13]	-90	-108	[TS 6-14]	-94	-122
[D 6-13]	-26	-49	[D 6-14]	-21	-49
[D 6-15]	-29	-43	[D 6-16]	-32	-46
[TS 6-15]	-93	-116	[TS 6-16]	-86	-96
[P 6-15]	-49	-48	[P 6-16]	-18	-48
[TS 6-15(a)]	-34	-35			
[P 6-15(a)]	-25	-27			

If just the minimum energy species are considered, the solvation free energies of the reaction species for the two-step mechanism where X=F have similar values to the analogous bimolecular reaction species. However, the free energies of solvation of the termolecular transition states are markedly larger than those computed for the bimolecular transition states. The difference ranges from 37 – 45 kJ mol^{-1} for the MD results and 28 – 56 kJ mol^{-1} for the continuum results. These results suggest that the quantum atoms of the termolecular transition states form more favourable intermolecular hydrogen bond interactions with the solvent water molecules than the quantum atoms of the analogous bimolecular transition states.

The likely cause of the difference in behaviour between the bimolecular and termolecular species is the nature of the additional QM water molecule in the

termolecular transition structures. This water molecule acts as a bifunctional catalyst both donating and accepting a proton during the reaction. In the transition states, however, one proton transfer is generally further advanced than the other, leading to the QM water molecule resembling a hydroxonium ion in these structures. The separation of charge in the termolecular transition states may therefore promote stronger interactions with the solvent that could stabilise these structures. The reactant, intermediate, and product species do not have this charge separation and consequently the solvation free energies for them are very similar to those for the bimolecular systems.

The solvation free energies for the chlorinated reaction species for the two-step mechanism show different trends to those of the analogous fluorinated species. The free energies of solvation for the first step of the mechanism (*via* [TS 6-14]) are very similar to those for the equivalent fluorinated process through [TS 6-13], and the values calculated for the intermediate and product species are also consistent with previous results. However, the free energy of solvation of [TS 6-16] is lower than would be anticipated from the values obtained for the fluorine species, [TS 6-15]. The MD and continuum results both predict a less negative free energy of solvation for [TS 6-16] than [TS 6-15], which is in contrast to the bimolecular results. As the difference between the bimolecular and termolecular transition states for decomposition of the diol intermediate lies in the presence of an additional QM water molecule, it seems apparent that the nature of this molecule in the transition state significantly affects the relative solvation energies.

In [TS 6-15] the proton transfers to and from the QM water molecule are concerted, although asynchronous, resulting in the formation of a H_3O^+ like species in the

transition state that promotes hydrogen bonding interactions with the solvent. However, in [TS 6-16] the C-Cl bond is essentially broken before any proton transfers to or from the QM water molecule occur, and consequently the charge build up is centred on the chlorine atom rather than the additional water molecule. It is thus the chlorine atom that dominates the solute-solvent interactions in this species. It appears from these results that this produces less favourable solute-solvent interactions than those that occur for [TS 6-15].

Table 7.5 – Free Energies of Solvation for the CXHO + $2H_2O$ One-Step Mechanism Reaction Species

	ΔG_{solv} (kJ mol^{-1})			ΔG_{solv} (kJ mol^{-1})	
Species X=F	MD AM1/TIP3P	Continuum AM1/SM5.4A	Species X=Cl	MD AM1/TIP3P	Continuum AM1/SM5.4A
[R 6-17]	-21	-21	[R 6-18]	-18	-22
[TS 6-17]	-58	-53	[TS 6-18]	-77	-75
[P 6-17]	-53	-50	[P 6-18]	-27	-18
[TS 6-17(a)]	-52	-44			
[P 6-17(a)]	-33	-35			
			[R 6-19]	-22	-35
			[TS 6-19]	-73	-93
			[P 6-19]	-22	-28

The free energies of solvation for the minimum energy reaction species of the one-step termolecular process are again similar to the reaction species for the equivalent bimolecular process. The transition states [TS 6-17] to [TS 6-19] actually have lower solvation free energies than those of [TS 6-8] to [TS 6-11], the analogous bimolecular species, by as much as 19 kJ mol^{-1} (MD) and 42 kJ mol^{-1} (continuum) when X=F, and 46 kJ mol^{-1} (MD) and 65 kJ mol^{-1} (continuum) when X=Cl.

The bimolecular and termolecular transition states have similar quantum atom geometries, with the additional QM water molecule stabilising the reaction through hydrogen bonding rather than acting as a bifunctional catalyst. It may be that the QM water forms interactions with the remaining QM atoms of the solute that would otherwise have formed interactions with the solvent. The consequence of this being that this essentially solute-solvent interaction is included in the quantum mechanical part of the system, instead of being accounted for by the electrostatic interaction between solute and solvent across the QM/MM boundary. The solvation free energies for the one-step processes do however follow the trend of the bimolecular species in that when X=Cl the values are greater than for X=F. This provides further evidence that the more asynchronous processes for X=Cl result in stronger solute-solvent interactions than the X=F process.

7.3.3 Free Energies in Solution for the CXHO + nH_2O Reaction Species

The free energies in solution of the reaction species for the various possible reaction pathways for formyl halide hydrolysis are reported in Tables 7.6 to 7.16. The values in Tables 7.6 to 7.13 have been calculated using the procedure outlined in section 7.2. Tables 7.14 to 7.16 give free energies in solution calculated using the COSMO[177] implementation in Gaussian 98.[28] These free energies were computed as single point energies on the MP2(fu)/6-31G* geometries of the species described in Chapters 3 and 4 of this thesis. These values have been included in order that some comparison may be made between the free energies obtained from the MP2(fu)/6-31G*/COSMO, AM1/SM5.4A, and AM1/TIP3P(MD) methods. The energies obtained from these various techniques have also been plotted in Figures 7.1 to 7.8.

7.3.3.1 Free Energies in Solution for the CFHO + $1H_2O$ Reaction

The free energies in solution for the CFHO + $1H_2O$ (solute) reaction species exhibit the same trends in the energies for the one- and two-step mechanisms as those observed for the AM1/TIP3P potential energies reported in Chapter 6 (see Figures 7.1 and 7.2). The consequence of using free energies to describe the energetics of the reaction in solution is that the energy barriers for both mechanisms are significantly lowered. A further result of averaging the energies over large numbers of solvent configurations is that the relative energies of the $CFH(OH)_2$ species for the two-step process are much closer than when evaluated for a single configuration as in Chapter 6. The relative energies of the product species are markedly altered when free energies are considered, although the results are also method and mechanism dependent.

Table 7.6 – Free Energies in Solution for the CFHO + $1H_2O$ Two-Step Mechanism Reaction Species

		ΔG_{soln} (kcal/mol)		$\Delta(\Delta G_{soln})$ (kJ mol^{-1})	
Species X=F	AM1 (qm) (kcal/mol)	MD AM1/TIP3P	Continuum AM1/SM5.4A	MD AM1/TIP3P	Continuum AM1/SM5.4A
[R 6-1]	-155.8	-161.4	-163.6	0	0
[TS 6-1]	-115.3	-125.5	-130.4	150	139
[D 6-1]	-174.1	-178.1	-183.1	-70	-82
[R 6-2]	-155.1	-161.4	-161.2	0	0
[TS 6-2]	-112.5	-123.9	-128.7	157	137
[D 6-2]	-172.8	-177.8	-181.6	-69	-85
[D 6-6]	-174.0	-178.5	-182.7	0	0
[TS 6-6]	-109.8	-121.2	-124.1	240	245
[P 6-6]	-155.0	-169.4	-168.2	38	60
[TS 6-6(a)]	-157.8	-167.6	-166.0	46	70
[P 6-6(a)]	-173.0	-179.6	-178.5	-5	18

The free energies in solution for the two-step mechanism calculated using the MD technique lower the energies of [P 6-6], [TS 6-6(a)], and [P 6-6(a)] relative to the solvated diol species [D 6-6] by 29, 29, and 22 kJ mol^{-1} respectively. In contrast the relative free energies for these species calculated using the AM1/SM5.4A continuum method show much less deviation from the AM1/TIP3P potential energies.

Table 7.7 – Free Energies in Solution for the CFHO + $1H_2O$ One-Step Mechanism Reaction Species

		ΔG_{soln} (kcal/mol)		$\Delta(\Delta G_{soln})$ (kJ mol^{-1})	
Species X=F	AM1 (qm) (kcal/mol)	MD AM1/TIP3P	Continuum AM1/SM5.4A	MD AM1/TIP3P	Continuum AM1/SM5.4A
[R 6-8]	-154.5	-161.5	-165.5	0	0
[TS 6-8]	-97.5	-112.1	-115.1	207	211
[P 6-8]	-152.1	-167.3	-165.4	-24	1
[TS 6-8(a)]	-153.7	-165.6	-164.1	-17	6
[P 6-8(a)]	-172.3	-180.1	-177.8	-78	-51
[R 6-9]	-153.5	-161.4	-164.5	0	0
[TS 6-9]	-89.3	-107.6	-111.9	225	220
[P 6-9]	-147.1	-164.2	-166.2	-12	-8
[TS 6-9(a)]	-150.1	-163.1	-164.3	-7	1
[P 6-9(a)]	-167.3	-176.6	-177.8	-64	-56

It is evident from the free energies reported in Table 7.6 and plotted in Figure 7.1 that for both the MD and continuum methods [TS 6-6] is the highest energy species along the reaction profile. Therefore in common with the AM1/TIP3P potential energies the rate-determining step of the mechanism is the decomposition of the $CFH(OH)_2$ intermediate. This is in contrast to the free energy profile at the MP2(fu)/6-31G*/COSMO level of theory where the first step is the rate-determining step for the process.

The pattern is slightly different when the one-step mechanism is considered. The product species [P 6-8(a)] and [P 6-9(a)] have slightly higher relative free energies than potential energies for both methods of calculation, although the variation is more marked for the continuum results.

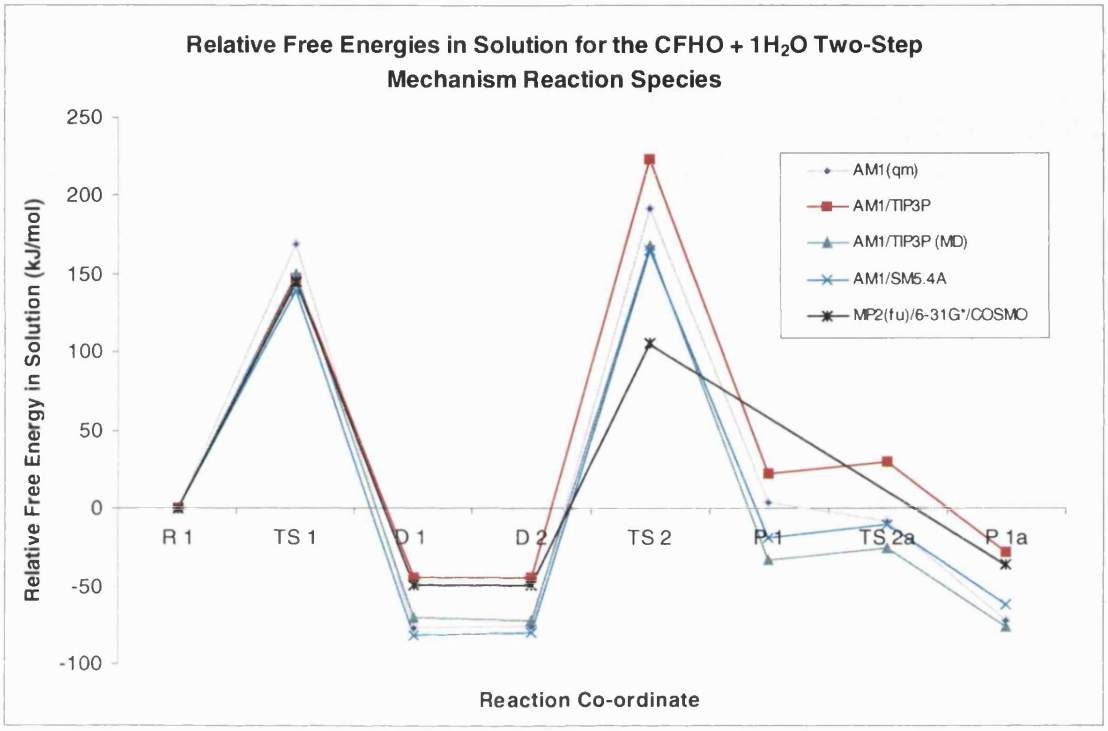

Figure 7.1 Lowest Energy Profile for the Two-Step Bimolecular Hydrolysis of Formyl Fluoride

The two steps of the mechanism are shown linked by two separate diol species in Figure 7.1. Although the conformer of the diol produced from the first step of the mechanism is the same conformer that decomposes to products, the two species have slightly different energies for the AM1 (qm), AM1/TIP3P MD and AM/SM5.4A methods. This difference is due to the effect of variations in the solvent structures on the quantum atom geometries in the [D 6-1] and [D 6-6] species. The AM1/TIP3P relative energies for these diol species have been given equal values in Figure 7.1 (and subsequent figures showing energy profiles for the two-step mechanism) to enable comparisons to be made between the various methods.

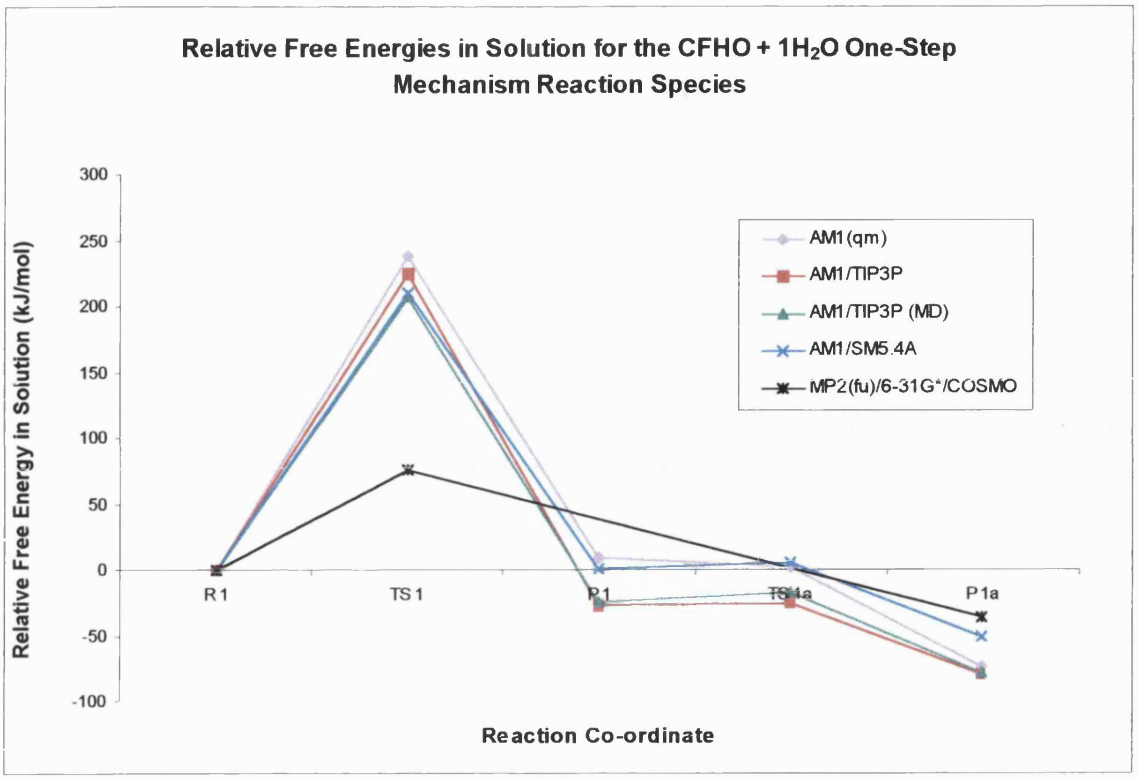

Figure 7.2 Lowest Energy Profile for the One-Step Bimolecular Hydrolysis of Formyl Fluoride

The relative free energies of the [P 6-9] and [TS 6-9(a)] species follow the trend described above for the product species of the two-step mechanism, being lower in energy than suggested by the potential energies. The relative free energies in solution for [P 6-8] and [TS 6-8(a)] do not follow this trend. The difference in energy between these species increases from 1 to 7 or 5 kJ mol^{-1} respectively for the MD and continuum results compared to the potential energies. These species are also less stable with respect to the reactants than if just the potential energies are considered, however the effect is again more significant when the continuum method is used to evaluate the free energy.

The one-step reaction path *via* [TS 6-8] to produce formic acid in its lower energy conformer has a lower energy barrier than the rate-determining step of the two-step

mechanism. The path *via* [TS 6-8] is therefore predicted as the lowest energy reaction route for the bimolecular hydrolysis of formyl fluoride within a water droplet. The preferred reaction path when free energies are considered is therefore consistent with the potential energy results.

7.3.3.2 Free Energies in Solution for the CFHO + $2H_2O$ Reaction Species

The free energies in solution for the CFHO + $2H_2O$ (solute) reaction species exhibit similar trends for the relative energies as the CFHO + $1H_2O$ reaction species and are reported in Tables 7.8 and 7.9. The energy barriers decrease compared to the potential energies although by lesser amounts than for the smaller solute. The effect of the solvent appears to be reduced when the larger solute is used. A possible explanation for this is that the additional water molecule acting as a bifunctional catalyst in the solute is in effect a solvent molecule that has been included in the QM region of the system. The stabilisation imparted to the system by this molecule is thus included in the evaluation of the QM energy rather than being treated as a solvent effect when the reaction takes place within a water droplet. The stabilisation of the transition states differs with the reaction step and is also method dependent.

Table 7.8 – Free Energies in Solution for the CFHO + $2H_2O$ Two-Step Mechanism Reaction Species

		ΔG_{soln} (kcal/mol)		$\Delta(\Delta G_{soln})$ (kJ mol^{-1})	
Species X=F	AM1 (g) (kcal/mol)	MD AM1/TIP3P	Continuum AM1/SM5.4A	MD AM1/TIP3P	Continuum AM1/SM5.4A
[R 6-12]	-222.1	-228.9	-229.6	0	0
[TS 6-12]	-186.0	-204.8	-207.7	101	92
[D 6-12]	-239.0	-243.9	-247.9	-62	-76
[R 6-13]	-218.6	-225.9	-231.7	0	0
[TS 6-13]	-180.0	-201.6	-205.8	102	108
[D 6-13]	-235.9	-242.1	-247.5	-68	-67
[D 6-15]	-234.4	-241.3	-244.6	0	0
[TS 6-15]	-180.8	-203.0	-208.4	161	152
[P 6-15]	-223.5	-235.2	-234.8	26	42
[TS 6-15(a)]	-224.0	-232.2	-232.2	38	52
[P 6-15(a)]	-238.9	-245.0	-245.2	-15	-3

Table 7.9 – Free Energies in Solution for the CFHO + $2H_2O$ One-Step Mechanism Reaction Species

		ΔG_{soln} (kcal/mol)		$\Delta(\Delta G_{soln})$ (kJ mol^{-1})	
Species X=F	AM1 (g) (kcal/mol)	MD AM1/TIP3P	Continuum AM1/SM5.4A	MD AM1/TIP3P	Continuum AM1/SM5.4A
[R 6-17]	-223.9	-228.8	-228.8	0	0
[TS 6-17]	-168.5	-182.3	-181.0	194	200
[P 6-17]	-223.1	-235.7	-234.9	-29	-26
[TS 6-17(a)]	-221.5	-232.3	-232.0	-15	-13
[P 6-17(a)]	-236.0	-244.0	-244.3	-64	-65

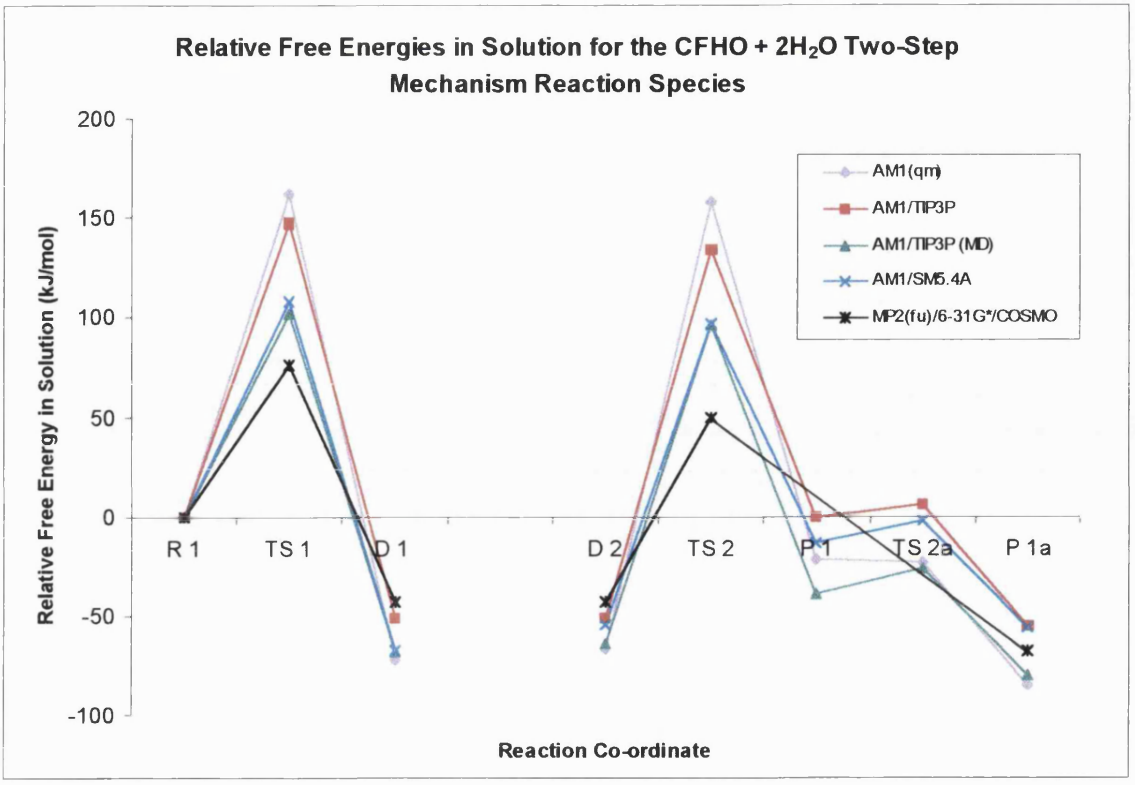

Figure 7.3 Energy Profiles for the Two-Step Termolecular Hydrolysis of Formyl Fluoride

The relative free energies in solution for the species involved in the formation of the diol intermediate determined using the MD method show that when many solvent configurations are considered the two possible reaction paths have very similar energetics and are thus equally likely to occur. Figure 7.3 contains the data for intermediate formation *via* [TS 6-13] as this is the route that yields the (+60,+60) conformer of $CFH(OH)_2$. It is this same conformer, albeit with a different solvent configuration, that decomposes through [TS 6-15] to products. In recognition that reorganisation of the QM water and solvent molecules is necessary for the reaction to proceed the two steps of the mechanism are shown as disconnected in Figure 7.3.

The energetics of the diol decomposition exhibit the same type of differences between the MD and continuum derived results as described in the previous section for the

bimolecular processes. The MD results suggest that the product species are stabilised to a greater extent by the solvent than if the free energies are determined using the AM1/SM5.4A method.

Inspection of the free energies reported in Table 7.8 and plotted in Figure 7.3 shows that it is the transition structure for diol formation that is the highest energy species along the energy profile. The first step is therefore rate-determining for the two-step mechanism. This is consistent with both the AM1/TIP3P potential energies and the MP2(fu)/6-31G*/COSMO free energies, but is the reverse of the situation for the two-step bimolecular hydrolysis.

The energetics of the one-step mechanism are very similar for the MD and continuum based results. The results for the bimolecular one-step mechanism suggested that for the energy barrier this would be the case, but in contrast to those earlier results there is little difference between the relative free energies of the product species between the two methods. The MD and continuum results both indicate that the product species [P 6-17] and the C-F bond breakage transition state [TS 6-17(a)] are stabilised to a greater extent than suggested by the AM1/TIP3P potential energies. However, both techniques also result in less stable final products [P 6-17(a)] compared to the potential energies (see Figure 7.4).

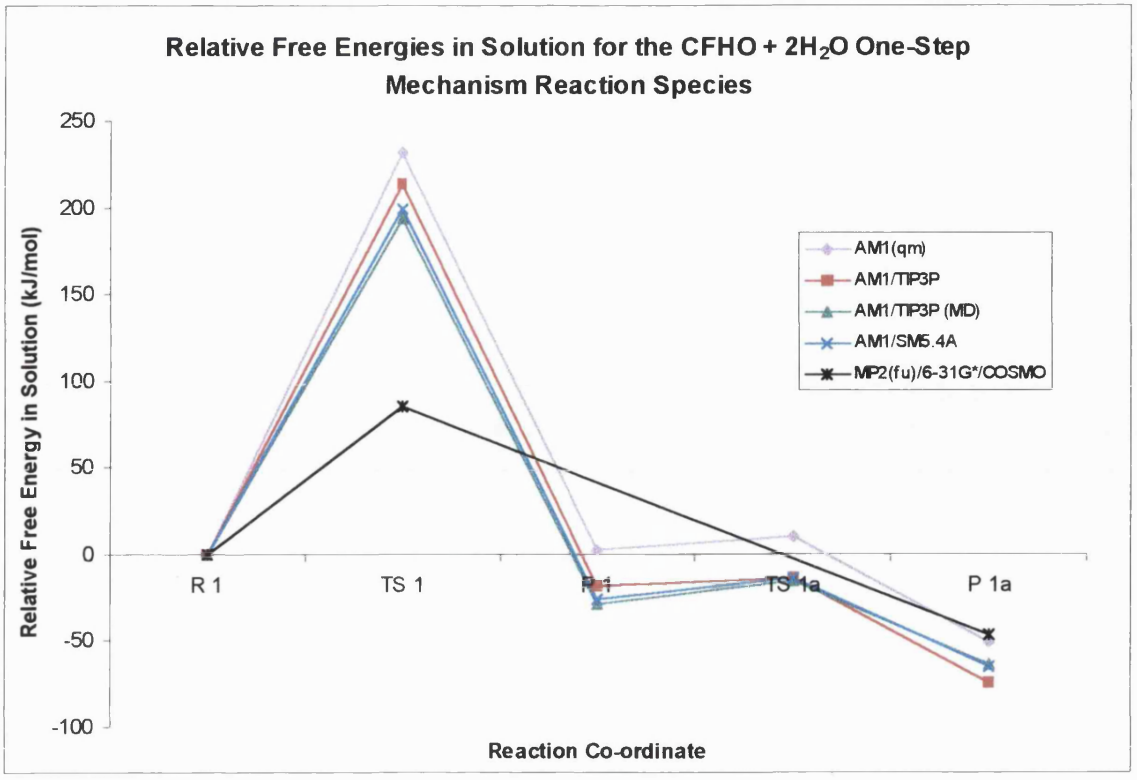

Figure 7.4 Lowest Energy Profiles for the One-Step Termolecular Hydrolysis of Formyl Fluoride

The cause of the similarity between the two sets of energies may again be the result of the presence of an additional water molecule in the QM region of the system. In the one-step termolecular reaction process this water molecule does not act as a bifunctional catalyst, but rather stabilises all the reaction species through hydrogen bonding. The nature of the interactions between this water molecule and the remaining solute atoms are essentially solute-solvent interactions and mean that for the AM1/SM5.4A method some explicit solute-solvent interactions have been included. The difference between the MD and continuum energies is therefore reduced as one of the most significant solute-solvent interactions for this system is already accounted for in the QM description of the solute.

The free energies in solution for the various termolecular processes indicate that the two-step mechanism is the energetically preferred reaction path. However a distinction cannot be made between the two diol forming processes. The examination of free energies for the termolecular hydrolysis of formyl fluoride within a water droplet therefore does not affect which reaction path is favoured, even though significant changes are observed in the relative energies of the reaction species compared to the potential energies reported in chapter 6.

7.3.3.3 Free Energies in Solution for the CClHO + 1H_2O Reaction Species

The free energies in solution for the CClHO + 1H_2O reaction species reported in Tables 7.10 and 7.11 show that for both the one- and two-step mechanisms the energy barriers decrease compared to the AM1/TIP3P potential energy barriers obtained in Chapter 6 (see Figures 7.5 and 7.6).

The energy profiles in Figure 7.5, where AM1 is used to describe the QM part of the system, have been purposely plotted with the two steps of the process disconnected. This is because the conformer of $CClH(OH)_2$ formed *via* [TS 6-3] is not the same conformer that decomposes to products *via* [TS 6-7]. Technically the two steps of the mechanism are therefore not joined, as an interconversion from the (+60,-60) to the (+60,+60) diol conformer would be required before decomposition could occur. This situation does not arise for the MP2(fu)/6-31G*/COSMO profile as the $CClH(OH)_2$ conformer produced in the first step is also the species that decomposes to products in the second step.

The free energies for the two-step mechanism indicate that the first step remains the rate-determining step of the process. The free energy barriers for the two-step mechanism exhibit the same differences between the MD and continuum estimated values as observed for the CFHO + $1H_2O$ two-step process. The continuum technique predicts lower energy barriers for the diol formation, and a higher energy barrier for diol decomposition than the MD method. A further similarity with the analogous fluorine results is that the AM1/SM5.4A method predicts more negative relative free energies for the diol species than the MD technique.

The energy barrier for the second step of the two-step process is lowered to a greater extent than the same step for the fluorinated species. When X=Cl the free energy barrier is decreased by 62 or 40 kJ mol^{-1} respectively for the MD or continuum results compared to the potential energies reported in Chapter 6. The increased effect of solvation on the relative energy of the [TS 6-7] species over the [TS 6-6] species will again be due to different charge distributions of the solute atoms in the two transition states. Greater charge separation occurs for [TS 6-7] than [TS 6-6], the chlorine atom therefore forms better interactions with the solvent than fluorine, and consequently solvation stabilises [TS 6-7] more than [TS 6-6].

Table 7.10 – Free Energies in Solution for the CClHO + 1H_2O Two-Step Mechanism Reaction Species

		ΔG_{soln} (kcal/mol)		$\Delta(\Delta G_{soln})$ (kJ mol^{-1})	
Species X=Cl	AM1 (qm) (kcal/mol)	MD AM1/TIP3P	Continuum AM1/SM5.4A	MD AM1/TIP3P	Continuum AM1/SM5.4A
[R 6-3]	-104.1	-109.0	-111.1	0	0
[TS 6-3]	-60.5	-70.2	-77.3	162	142
[D 6-3]	-117.1	-121.0	-127.1	-50	-67
[R 6-4]	-102.8	-109.1	-112.1	0	0
[TS 6-4]	-58.0	-68.5	-75.9	169	152
[D 6-4]	-115.6	-119.9	-125.2	-46	-55
[D 6-7]	-117.1	-120.5	-126.0	0	0
[TS 6-7]	-76.3	-102.7	-103.0	74	96
[P 6-7]	-123.7	-128.4	-130.1	-33	-17

Table 7.11 – Free Energies in Solution for the CClHO + 1H_2O One-Step Mechanism Reaction Species

		ΔG_{soln} (kcal/mol)		$\Delta(\Delta G_{soln})$ (kJ mol^{-1})	
Species X=Cl	AM1 (qm) (kcal/mol)	MD AM1/TIP3P	Continuum AM1/SM5.4A	MD AM1/TIP3P	Continuum AM1/SM5.4A
[R 6-10]	-105.6	-109.3	-111.6	0	0
[TS 6-10]	-69.3	-91.6	-95.5	74	68
[P 6-10]	-121.6	-127.6	-127.6	-77	-67
[R 6-11]	-104.8	-108.9	-110.4	0	0
[TS 6-11]	-60.8	-89.2	-94.1	83	68
[P 6-11]	-114.6	-123.1	-126.0	-59	-65

A further apparent example of the variation in free energies observed for the two methods of evaluation is that the product species [P 6-7] seems to have a lower relative

free energy when the MD method is used. However, the energy is calculated relative to the [D 6-7] species rather than the reactants [R 6-3] or [R 6-4]. The AM1/SM5.4A method predicts greater stabilisation of the intermediate diol species than the MD technique, and therefore the difference between [D 6-7] and [P 6-7] is reduced. If the energies are calculated relative to the reactants then the variation between the two methods becomes much less marked (see Figure 7.5).

The relative free energies in solution of the two diol species [D 6-3] and [D 6-4] are much closer in value than the AM1/TIP3P potential energies. Averaging over many possible solvent configurations therefore appears to be vital to gain reliable energetics in order to compare competing reaction paths if explicit solvent molecules are being used to simulate the solvated reaction system.

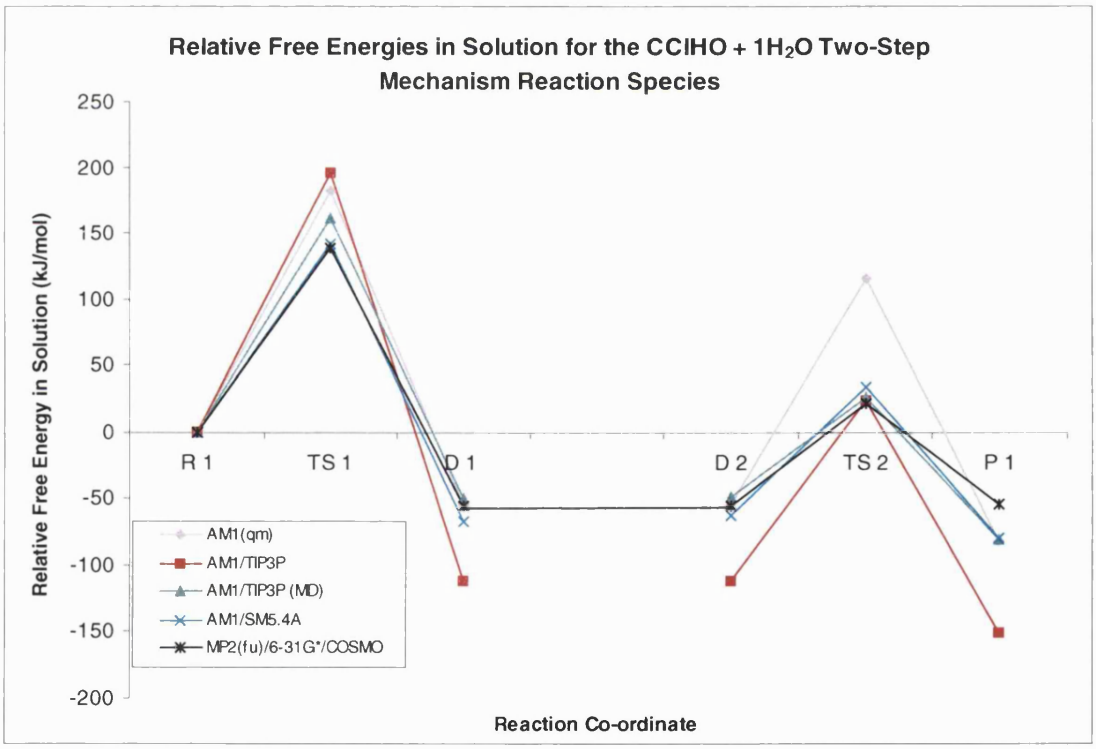

Figure 7.5 Lowest Energy Profiles for the Two-Step Bimolecular Hydrolysis of Formyl Chloride

The energetics of the one-step mechanism are also markedly altered when free energies in solution are examined instead of potential energies. The energy barriers are reduced by 52 (MD) or 58 (AM1/SM5.4A) kJ mol^{-1} for the path *via* [TS 6-10] or by 71 (MD) or 86 (AM1/SM5.4A) kJ mol^{-1} for the route *via* [TS 6-11]. In contrast, the products are slightly less stable relative to the reactants, for both reaction paths, if free energies are considered instead of potential energies (see Figure 7.6).

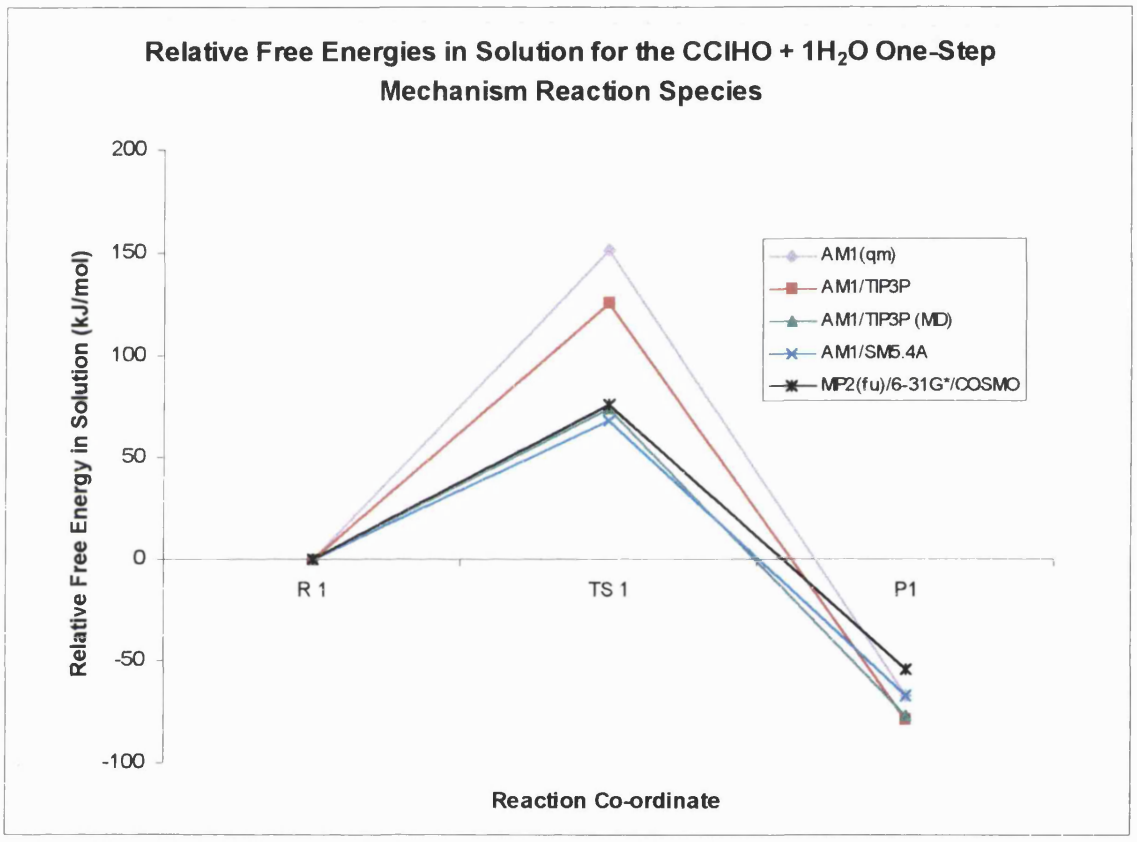

Figure 7.6 Lowest Energy Profiles for the One-Step Bimolecular Hydrolysis of Formyl Chloride

The MD results predict that the reaction path *via* [TS 6-10] will be the preferred route, as it has a lower energy barrier and more stable product species. The continuum results, however, show no such preference with both paths having the same energy barrier and almost identical relative energies of the products.

The free energy barriers in solution for both suggested mechanisms of the CClHO + $1H_2O$ reaction clearly show that the one-step process will be the preferred reaction route. In fact the MD and continuum results both accentuate the differences between the energy barriers for the one- and two-step processes, making the preference for the one-step mechanism even more pronounced than the potential energies suggested.

7.3.3.4 Free Energies in Solution for the CClHO + $2H_2O$ Reaction Species

The free energies in solution of the CClHO + $2H_2O$ reaction species reported in Tables 7.12 and 7.13 again decrease compared to the potential energies reported in Chapter 6. In the case of the two-step mechanism, the potential energies indicated that the second step had the larger energy barrier (see Figure 7.7). This pattern is retained if the continuum results are examined, with a greater reduction in the first step energy barrier than the second step of the mechanism. The situation is reversed for the MD results, where the first step has the larger energy barrier. This may be a further example of the overestimation of the solvent stabilisation of the diol species [D 6-14] and [D 6-16] by the continuum method.

Inspection of Table 7.12 and Figure 7.7 shows that for either of the AM1 based methods for determining free energies and the AM1/TIP3P potential energies [TS 6-14] remains the highest energy species along the energy profile. In all cases it is therefore the first step of the mechanism which is rate-determining. However, whichever set of results are used the energy barrier for the rate-determining step is considerably lower than for the CClHO + $1H_2O$ two-step mechanism.

Table 7.12 – Free Energies in Solution for the CClHO + $2H_2O$ Two-Step Mechanism Reaction Species

		ΔG_{soln} (kcal/mol)		$\Delta(\Delta G_{soln})$ (kJ mol^{-1})	
Species X=Cl	AM1 (qm) (kcal/mol)	MD AM1/TIP3P	Continuum AM1/SM5.4A	MD AM1/TIP3P	Continuum AM1/SM5.4A
[R 6-14]	-172.9	-177.1	-179.0	0	0
[TS 6-14]	-128.9	-151.4	-157.8	108	89
[D 6-14]	-181.2	-186.3	-192.9	-38	-58
[D 6-16]	-180.9	-185.2	-191.7	0	0
[TS 6-16]	-144.5	-165.1	-167.3	84	102
[P 6-16]	-184.4	-192.1	-195.9	-29	-18

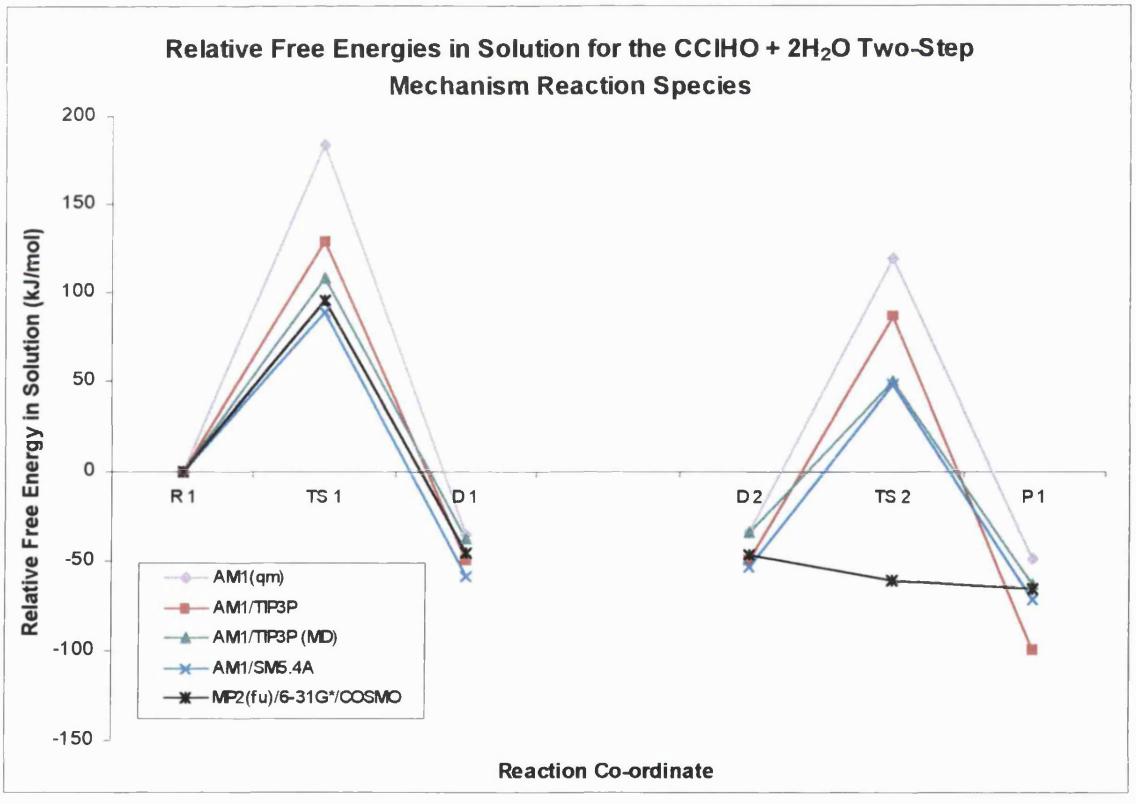

Figure 7.7 Energy Profiles for the Two-Step Termolecular Hydrolysis of Formyl Chloride

The two steps of the reaction mechanism are shown with a disconnection in the energy profiles plotted in Figure 7.7. This is because, although the (+60,+60) conformer of $CClH(OH)_2$ is the species produced by step one of the process, a reorientation of the QM water molecule hydrogen bonded to it, and of the solvent (for the species with explicit solvent molecules), must occur before this conformer can decompose to products *via* [TS 6-16].

The energetics of the one-step mechanism are also significantly altered when the free energies in solution are examined instead of the potential energies. The two sets of product species [P 6-18] and [P 6-19] are much closer in energy for both methods of determining the free energies compared to the potential energy results.

Table 7.13 – Free Energies in Solution for the CClHO + $2H_2O$ One-Step Mechanism Reaction Species

		ΔG_{soln} (kcal/mol)		$\Delta(\Delta G_{soln})$ (kJ mol^{-1})	
Species X=Cl	AM1 (qm) (kcal/mol)	MD AM1/TIP3P	Continuum AM1/SM5.4A	MD AM1/TIP3P	Continuum AM1/SM5.4A
[R 6-18]	-171.2	-175.5	-176.4	0	0
[TS 6-18]	-141.0	-159.4	-158.8	67	74
[P 6-18]	-186.2	-192.7	-190.3	-72	-58
[R 6-19]	-172.1	-177.3	-180.3	0	0
[TS 6-19]	-132.3	-149.8	-154.4	115	108
[P 6-19]	-188.6	-193.8	-195.2	-69	-63

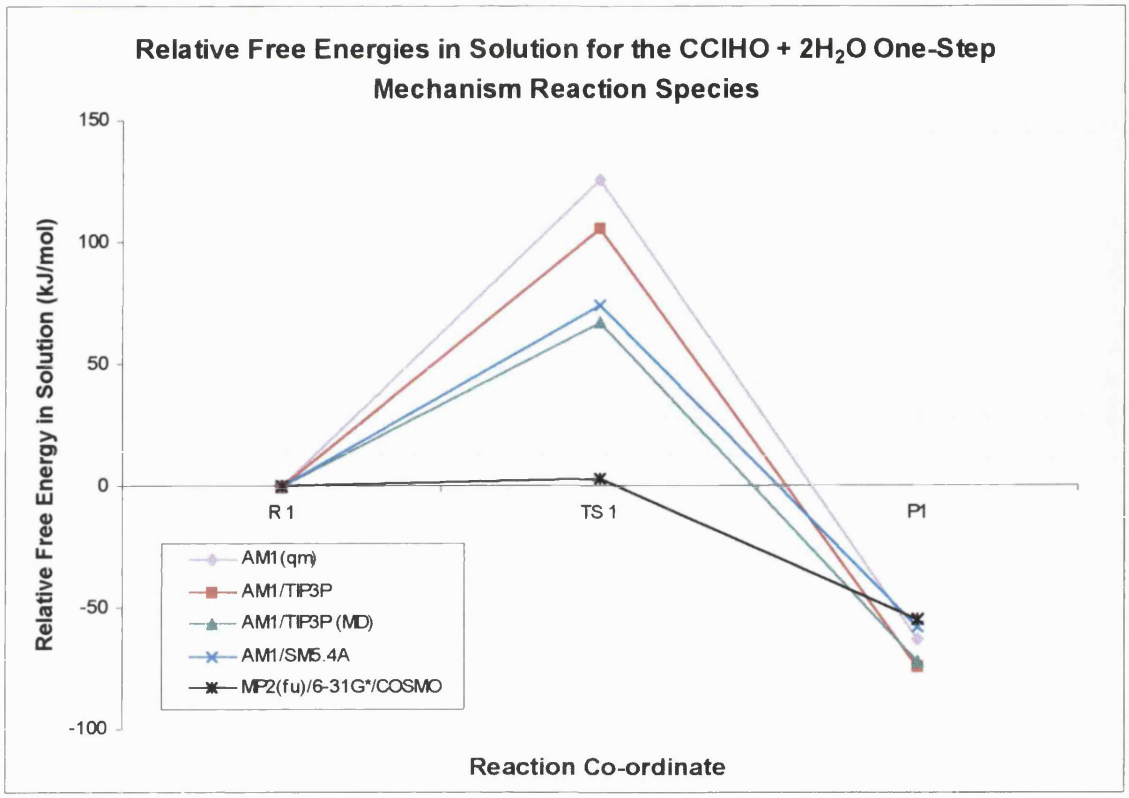

Figure 7.8 Lowest Energy Profiles for the One-Step Termolecular Hydrolysis of Formyl Chloride

The decrease in the energy barrier is greater for the reaction path *via* [TS 6-18], which more closely resembles the fluorinated transition state [TS 6-17]. As described in Chapter 6 the route through [TS 6-19] was expected to result in the formation of a diol species, but instead led to the direct elimination of HCl. The energy barrier for this reaction path is therefore closer to the route *via* [TS 6-14] as the QM regions of the reactants and transition states of the two paths are structurally similar.

The structure of [TS 6-18] is similar to [TS 6-10] and [TS 6-11], with the second water molecule stabilising the transition state *via* hydrogen bonding rather than actively participating in the reaction. The relative energies of the reaction species for the [TS 6-18] path are therefore close to those for the direct elimination routes in which only a single water molecule is treated quantum mechanically.

The reaction path through [TS 6-18] for direct elimination of HCl, with two water molecules designated as part of the solute, is the lowest energy route of those investigated. This is in agreement with the results obtained using the potential energies, and so for the hydrolysis of formyl chloride the examination of free energies does not affect the energetically preferred reaction route, although the energy barriers for each possible reaction path are significantly lowered.

7.3.4 Free Energies of Solvation and Free Energies in Solution for the Formyl Halide Hydrolysis Reaction Species Calculated at the MP2(fu)/6-31G* Level of Theory

Free energies of solvation and free energies in solution have been calculated as single point energies for the gas phase structures of the *ab initio* reaction species described in Chapters 3 and 4. This was achieved using the implementation of COSMO[177] in Gaussian 98.[28] The purpose of these calculations was to provide a way of comparing the free energies reported in this chapter, in which the solute is described using the AM1 Hamiltonian, with the *ab initio* results. The MP2(fu)/6-31G*/COSMO free energies are reported in Tables 7.14 to 7.16.

The free energies of solvation of the reactant species for the bimolecular hydrolysis appear to be more negative for the MP2(fu)/6-31G*/COSMO description of the solvated system than for both the alternative AM1 methods. However the free energies of solvation for the MP2(fu)/6-31G*/COSMO reactants were calculated by summation of the solvation free energies for the separate CXHO and H_2O molecules, whereas the values reported for the AM1/TIP3P MD and AM1/SM5.4A methods were based on hydrogen bonded reactant complexes. The values derived from the different methods

are therefore not directly comparable, but do give a reasonable idea of the variation between the *ab initio* and semi-empirical evaluations of the free energies.

Table 7.14 – Free Energies of Solvation and Free Energies in Solution for the CXHO + 1H_2O Reaction Species

	MP2(fu)/6-31G*/COSMO		
Species	ΔG_{solv} (kcal/mol)	ΔG_{soln} (Hartrees)	$\Delta(\Delta G_{soln})$ (kJ mol^{-1})
CFHO + 1H_2O	-10.2	-289.44179	0
[TS 4-9]	-12.0	-289.38671	145
F-(+60,+60)	-12.8	-289.46027	-49
[TS 4-10]	-12.9	-289.40131	106
HF + HCO_2H	-14.2	-289.45564	-36
CClHO + 1H_2O	-9.2	-649.44479	0
[TS 3-2]	-13.3	-649.39203	139
Cl-(+60,+60)	-14.1	-649.46575	-55
[TS 3-4]	-21.3	-649.43661	21
HCl + HCO_2H	-8.6	-649.46524	-54
CFHO + 1H_2O	-10.2	-289.44179	0
[TS 4-11]	-24.3	-289.41268	76
HF + HCO_2H	-14.2	-289.45564	-36
CClHO + 1H_2O	-9.2	-649.44479	0
[TS 3-7]	-13.8	-649.41580	76
HCl + HCO_2H	-8.6	-649.46524	-54

The free energies of solvation for the reaction species of the two-step mechanism for the bimolecular hydrolysis of formyl fluoride show that for the reactants and intermediate diol species the MP2(fu)/6-31G*/COSMO values are larger than the AM1/TIP3P MD and AM1/SM5.4A values. The pattern of the diols being slightly less well solvated than the reactants is reversed for the *ab initio* results. The difference between the free

energies of solvation of the first step of the mechanism of the reactants, transition states, and diol species are also decreased if the MP2(fu)/6-31G*/COSMO results are examined. The values for [TS 4-9] and [TS 3-2] are similar to those for the equivalent transition states calculated at the AM1/TIP3P MD level, but smaller than the AM1/SM5.4A results.

The free energies of solvation for the second step of the mechanism show the expected variation between the decomposition of $CFH(OH)_2$ and $CClH(OH)_2$, with a much larger solvent stabilisation of [TS 3-4] over [TS 4-10]. In contrast to the second step of the two-step mechanism at the *ab initio* level, and both the AM1 methods for the one-step process, this trend is reversed for the [TS 4-11] and [TS 3-7] species.

The free energies in solution evaluated at the MP2(fu)/6-31G*/COSMO level of theory show that the energetics for the first step of the two-step mechanism are very similar for the CFHO and CClHO cases. The energy barriers are also consistent with those obtained using both the AM1 methods. However the formation of the diol species is less exoergonic for the *ab initio* results than the semi-empirical results indicate.

The energetics of the second step of the mechanism differ for the halogen substituents and between the *ab initio* and semi-empirical methods. In the case of the MP2(fu)/6-31G* results the first step is the rate-determining step of the process for either halogen substituent, however the energy barrier for the second step is much lower when X=Cl rather than F. The AM1 results of either method show the same trend when X=Cl, with the first step being the rate-determining step, although the difference in the energy barriers between the two steps is reduced. However, if X=F the AM1 results

indicate that the second step of the mechanism is the rate-determining step as the transition state for this process is the highest energy species along the energy profile.

The free energies in solution of the one-step mechanism exhibit the same variations between the *ab initio* and semi-empirical methods as for the second step of the two-step mechanism. When X=Cl the free energy barriers are very similar for the three methods (see Figure 7.6), and are also equivalent to the MP2(fu)/6-31G*/COSMO free energy barrier when X=F. This was not anticipated for the MP2(fu)/6-31G*/COSMO results as it was expected that the barrier for the one-step process would be lower for the X=Cl case. The AM1 free energy barriers for the bimolecular one-step elimination of HF are again much larger than the *ab initio* value (see Figure 7.2).

The free energies in solution calculated at the MP2(fu)/6-31G*/COSMO level of theory for the bimolecular hydrolysis processes indicate that the one-step mechanism is the lower energy process for both halogen substituents. This is consistent with the MP2(fu)/6-31G* gas phase, and the AM1/TIP3P MD and AM1/SM5.4A results.

Table 7.15 – Free Energies of Solvation and Free Energies in Solution for the CXHO + $2H_2O$ Two-Step Mechanism Reaction Species

	MP2(fu)/6-31G*/COSMO		
Species	ΔG_{solv} (kcal/mol)	ΔG_{soln} (Hartrees)	$\Delta(\Delta G_{soln})$ (kJ mol^{-1})
CFHO + $2H_2O$	-17.0	-365.65145	0
[RC 4-3]	-4.8	-365.66209	-28
[TS 4-3]	-11.9	-365.63302	48
[DC 4-3]	-12.6	-365.67864	-71
F-(+60,+60) + H_2O	-19.6	-365.66993	-49
[DC 4-5]	-12.0	-365.67833	-71
[TS 4-5]	-13.0	-365.64315	22
[PC 4-5]	-9.2	-365.68798	-96
HF + HCO_2H + H_2O	-21.0	-365.66530	-36
CClHO + $2H_2O$	-16.0	-725.65445	0
[RC 4-4]	-5.6	-725.66672	-32
[TS 4-4]	-14.3	-725.64226	64
[DC 4-4]	-13.9	-725.68430	-78
Cl-(+60,+60) + H_2O	-20.8	-725.67541	-55
[DC 4-6]	-13.7	-725.68440	-79
[TS 4-6]	-28.1	-725.68990	-93
[PC 4-6]	-7.2	-725.69166	-98
HCl + HCO_2H + H_2O	-15.4	-725.67490	-54

The free energies of solvation for the solvated MP2(fu)/6-31G* CXHO + $2H_2O$ reaction species exhibit different trends to those calculated for the AM1/TIP3P reaction species. The *ab initio* results for the two-step mechanism show that there is a clear stabilisation of the transition states over the reactant complexes as a result of solvation. However, the free energies of solvation for the fluorinated diol species and the subsequent HF elimination transition state [TS 4-5] are very similar and consequently preferential stabilisation of the transition state does not occur for the second step of the mechanism.

The opposite is true for the analogous chlorine mechanism where the free energy of solvation for [TS 4-6] is 14.4 kcal/mol more negative than for [DC 4-6]. The free energies of solvation for the product complexes are also slightly larger than for the reactant complexes.

The trend for the MD AM1/TIP3P and AM1/SM5.4A free energies is the same for both fluorine and chlorine species. The free energies of solvation calculated using these techniques show that the stabilisation of the transition states is much larger than that for the minimum energy species along the reaction paths.

The free energies of solvation for the one-step CXHO + $2H_2O$ mechanism show the same similarity between the values for the reactant and product complexes. The stabilisation imparted by the solvent is much greater for the transition states. The solvation free energy is larger for [TS 4-8] than [TS 4-7] and this difference is again likely to be due to the difference in the structures of these transition states.

Table 7.16 – Free Energies of Solvation and Free Energies in Solution for the $CXHO + 2H_2O$ One-Step Mechanism Reaction Species

	MP2(fu)/6-31G*/COSMO		
Species	ΔG_{solv} (kcal/mol)	ΔG_{soln} (Hartrees)	$\Delta(\Delta G_{soln})$ (kJ mol^{-1})
$CFHO + 2H_2O$	-17.0	-365.65145	0
[RC 4-7]	-4.8	-365.66209	-28
[TS 4-7]	-18.2	-365.62964	57
[PC 4-7]	-6.4	-365.68006	-75
$HF + HCO_2H + H_2O$	-21.0	-365.66530	-36
$CClHO + 2H_2O$	-16.0	-725.65445	0
[RC 4-8]	-4.3	-725.66821	-36
[TS 4-8]	-25.5	-725.66689	-33
[PC 4-8]	-4.3	-725.68900	-91
$HCl + HCO_2H + H_2O$	-15.4	-725.67490	-54

The *ab initio* free energy barriers for the termolecular hydrolysis reaction in water are lower than those calculated using the AM1 Hamiltonian and explicit or continuum representations of the solvent (see Figures 7.3, 7.4, 7.7 and 7.8). The difference in barriers between the first and second step of the two-step mechanism for fluorinated species is, as expected, much less significant for the *ab initio* results. In the case where X=Cl for the two-step mechanism, the energy barrier is ~40 kJ mol^{-1} lower when calculated at the MP2(fu)/6-31G*/COSMO level compared to the AM1/TIP3P, MD and AM1/SM5.4A results. Although this difference is marked the more significant variation occurs for the second step of the mechanism. When the AM1 Hamiltonian is used to describe the reacting atoms this step has a barrier of 84/102 kJ mol^{-1} depending upon the method used to evaluate the free energy. In contrast *ab initio* results have the transition state for diol decomposition as a lower energy species than the diol for the reaction occurring in solution. This may just be because the MP2(fu)/6-31G*/COSMO free

energies were calculated as single points, and consequently the solute did not have the opportunity to reorganise in the presence of solvent. However, even when taking this into account it would appear that the decomposition of the $CClH(OH)_2$ species catalysed by a solvent water molecule is an extremely facile process when an *ab initio* description of the solute is used.

The *ab initio* free energy barriers for the termolecular one-step mechanism show a similar pattern. When X=F solvent stabilisation does reduce the energy barrier, however it is again the X=Cl case that is the more significant. In solution the stabilisation imparted by the solvent results in this having an extremely low energy barrier when the MP2(fu)/6-31G*/COSMO method of evaluating the free energy is used.

The MP2(fu)/6-31G*/COSMO free energy barriers in solution predict that the lowest energy reaction path for the termolecular hydrolysis of formyl chloride is *via* the one-step mechanism. When the halogen substituent is fluorine the two-step mechanism is preferred. These energetically preferred reaction paths are consistent with both the MP2(fu)/6-31G* gas phase and the AM1/TIP3P MD and AM1/SM5.4A results.

As a final note it is evident that for each case examined the difference between the values of the free energies calculated at the MP2(fu)/6-31G*/COSMO level and those at the MD AM1/TIP3P or AM1/SM5.4A level is significant. The differences are likely to be caused as much by the different descriptions of the solute atoms as by the differing methods used to account for the solvent.

7.4 Conclusions

In this chapter free energies of solvation and free energies in solution have been reported that were calculated using three separate methods. The energetically preferred reaction paths for the hydrolysis of the formyl halides within a water droplet are the same for each technique. The AM1/TIP3P MD, AM1/SM5.4A, and MP2(fu)/6-31G*/COSMO methods all predict that for bimolecular hydrolysis of formyl fluoride and chloride the one-step mechanism is preferred. Each method also predicts that for the termolecular hydrolysis of formyl fluoride the two-step mechanism is the lower energy path, but that for formyl chloride the one-step mechanism is favoured.

Although the energetically preferred reaction paths are the same for each method significant variations do occur in the free energies of solvation and in solution calculated using the three methods. The AM1/TIP3P MD method has been shown to produce free energies of solvation similar to those for the AM1/SM5.4A continuum method. The advantage of the MD technique is that as well as being a relatively computationally inexpensive way of calculating free energies, it also produces a trajectory that can be examined to show individual solute-solvent interactions.

The major differences between the free energies calculated using the MP2(fu)/6-31G*/COSMO method and the AM1/TIP3P MD and AM1/SM5.4A techniques lay with the values obtained for the energy barriers related to HX elimination. These differences are also evident in the *ab initio* versus semi-empirical gas phase results, and so it appears that the description of the solute remains a significant factor in the energetics of this hydrolysis reaction occurring in solution. A future possibility to improve the description of the whole system would be to use an *ab initio* method, preferably at the MP2 level, to describe the solute atoms, and an explicit

representation of the solvent molecules such as TIP3P. A molecular dynamics protocol such as that used in this chapter could then be utilised to calculate MP2/TIP3P free energies of solvation and free energies in solution. The method would remain relatively cheap compared to other techniques for calculating free energies for such solvated systems as only single point energies would be calculated at the MP2 level of theory. The difficulty remains creating a suitable interface between an *ab initio* program and a program such as CHARMM.

References

1. Foresman, J.B.; Frisch, A. 'Exploring Chemistry with Electronic Structure Methods' 2nd Edition, **1996**, Gaussian, Inc., Pittburgh.

2. Grant, G.H.; Richards, W.G. 'Computational Chemistry' **1995**, Oxford University Press.

3. Hehre, W. J.; Radom, L.; Schleyer, P.v.R.; Pople, J.A. 'Ab Initio Molecular Orbital Theory' **1986**, Wiley and Sons, Inc.

4. Lowe, J.P. 'Quantum Chemistry – Student Edition' **1978**, Academic Press, Inc.

5. Leach, A.R. 'Molecular Modelling – Principles and Applications' **1996**, Longman.

6. Roothaan, C.C.J. 'New Developments in Molecular Orbital Theory' *Rev. Mod. Phys.*, **1951**, *23*, 69-89.

7. Hall, G.G. 'The Molecular Orbital Theory of Chemical Valency VIII. A Method for Calculating Ionisation Potentials' *Proc. Royal Soc. (London)*, **1951**, *A205*, 541-552.

8. Møller, C.; Plesset, M.S. 'Note on an Approximate Treatment for Many-Electron Systems' *Phys. Rev.*, **1934**, *46*, 618-622.

9. Pople, J.A.; Segal, G.A. 'Approximate Self-Consistent Molecular Orbital Theory. II. Calculations with Complete Neglect of Differential Overlap' *J. Chem. Phys.*, **1965**, *43*, 5136-5149.

10. Pople, J.A.; Beveridge, D.L.; Dobosh, P.A. 'Approximate Self-Consistent Molecular Orbital Theory. V. Intermediate Neglect of Differential Overlap' *J. Chem. Phys.*, **1967**, *47*, 2026-2033.

11. Pople, J.A.; Santry, D.P.; Segal, G.A. 'Approximate Self-Consistent Molecular Orbital Theory. I. Invariant Procedures' *J. Chem. Phys.*, **1965**, *43*, 129-135.

12. Bingham, R.C.; Dewar, M.J.S.; Lo, D.H. 'Ground States of Molecules. XXV. MINDO/3. An Improved Version of the MINDO Semi-Empirical SCF-MO Method' *J. Am. Chem. Soc.*, **1975**, *97(6)*, 1285-1293.

13. Dewar, M.J.S.; Thiel, W. 'Ground States of Molecules. 38. The MNDO Method. Approximations and Parameters' *J. Am. Chem. Soc.*, **1977**, *99*, 4899-4907.

14. Dewar, M.J.S.; Zoebisch, E.G.; Healy, E.F.; Stewart, J.J.P. 'AM1: A New General Purpose Quantum Mechanical Molecular Model' *J. Am. Chem. Soc.*, **1985**, *107(13)*, 3902-3909.

15. Pople, J.A.; Krischnan, R.; Schlegel, H.B.; DeFrees, D.; Binkley, J.S.; Frisch, M.J.; Whiteside, R.F.; Hout, R.F.; Hehre, W.J. 'Molecular Orbital Studies of Vibrational Frequencies' *Int. J. Quant. Chem., Symp.*, **1981**, *S15*, 269-278.

16. Pople, J.A.; Scott, A.P.; Wong, M.W.; Radom, L. 'Scaling Factors for Obtaining Fundamental Vibrational Frequencies and Zero-Point Energies from HF/6-31G* and MP2/6-31G* Harmonic Frequencies' *Israel J. Chem.*, **1993**, *33*, 345.

17. Scott, A.P.; Radom, L. 'Harmonic Vibrational Frequencies: An Evaluation of Hartree-Fock, Møller-Plesset, Quadratic Configuration Interaction, Density Functional Theory, and Semi-Empirical Scale Factors' *J. Phys. Chem.*, **1996**, *100*, 16502-16513.

18. Fukui, K. 'The Path of Chemical Reactions – The IRC Approach' *Acc. Chem. Res.*, **1981**, *14(12)*, 363-368.

19. Atkins, P.W. 'Physical Chemistry' 4th Edition. **1992**, Oxford University Press.

20. Onsager, L. 'Electric Moments of Molecules in Liquids' *J. Am. Chem. Soc.*, **1938**, *58*, 1486-1493.

21. Miertus, S.; Scrocco, E. 'Electrostatic Interaction of a Solute with a Continuum. A Direct Utilization of *ab initio* Molecular Potentials for the Prevision of Solvent Effects' *Chem. Phys.*, **1981**, *55*, 117-129.

22. Miertus, S.; Tomasi, J. 'Approximate Evaluations of the Electrostatic Free Energy and Internal Energy Changes in Solution Processes' *Chem. Phys.*, **1982**, *65*, 239.

23. Klamt, A.; Schüürmann, G. 'COSMO: A New Approach to Dielectric Screening in Solvents with Explicit Expressions for the Screening Energy and its Gradient' *J. Chem. Soc. Perkin Trans.2*, **1993**, 799-805.

24. GAUSSIAN 98, Revision A.6, M.J. Frisch, G.W. Trucks, H.B. Schlegel, G.E. Scuseria, M.A. Robb, J.R. Cheeseman, V.G. Zakrzeewski, J.J.A. Montgomery, R.E. Stratmann, J.C. Burant, S. Dapprich, J.M. Millam, A.D. Daniels, K.N. Kudin, M.C. Strain, O. Farkas, J. Tomasi, V. Barone, M. Cossi, R. Cammi, B. Mennucci, C. Pomelli, C. Adamo, S. Clifford, J. Ochterski, G.A. Petersson, P.Y. Ayala, Q. Cui, K. Morokuma, D.K. Malick, A.D. Rabuck, K. Raghavachari, J.B. Foresman, J. Cioslowski, J.V. Ortiz, A.G. Baboul, B.B. Stefanov, G. Lui, A. Liashenko, P. Piskorz, I. Komaromi, R. Gomperts, R.L. Martim, D.J. Fox, T. Keith, M.A. Al-Laham, C.Y. Peng, A. Nanayakkara, C. Gonzalez, M. Challacombe, P.M.W. Gill, B. Johnson, W. Chen, M.W. Wong, J.L. Andres, M. Head-Gordon, E.S. Replogle, J.A. Pople, Gaussian, Inc., Pittsburgh, PA, 1998.

25. Chambers, C.C.; Cramer, C.J.; Truhlar, D.G. 'A Model for Aqueous Solvation Based on Class IV Atomic Charges and First-Solvation-Shell Effects' *J. Phys. Chem.*, **1996**, *100*, 16385-16398.

26. AMSOL-version 6.1 G.D. Hawkins, D.J. Giesen, G.C. Lynch, C.C. Chambers, I. Rossi, J.W. Storer, D. Rinaldi, D.A. Liotard, C.J. Cramer, and D.G. Truhlar, University of Minnesota, Minneapolis, 1997, based in part on AMPAC-version 2.1 by D.A. Liotard, E.F. Healy, J.M. Ruiz, and M.J.S. Dewar, and on the EF routines by Frank Jensen.

27. Storer, J.W.; Giesen, D.J.; Cramer, C.J.; Truhlar, D.G. 'Class IV Charge Models: A New Semiempirical Approach in Quantum Chemistry' *J. Comp.-Aided Mol. Des*, **1995**, *9*, 87-110.

28. Fletcher, R.; Reeves, C.M. 'Function Minimisation by Conjugate Gradients' *The Computer Journal*, **1964**, *7*, 149-154.

29. Brooks, B.R.; Bruccoleri, R.E.; Olafson, B.D.; States, D.J.; Swaminathan, S.; Karplus, M. 'CHARMM: A Program for Macromolecular Energy, Minimisation, and Dynamics Calculations' *J. Comp. Chem.*, **1983**, *4(2)*, 187-217.

30. Cerjan, C.J.; Miller, W.H. 'On Finding Transition States' *J. Chem. Phys.*, **1981**, *75(6)*, 2800-2806.

31. Banerjee, A.; Adams, N.; Simons, J.; Shepard, R. 'Search for Stationary Points on Surfaces' *J. Phys. Chem.*, **1985**, *89*, 52.

32. Baker, J. 'An Algorithm for the Location of Transition States' *J. Comp. Chem.*, **1986**, *7(4)*, 385-395.

33. Fischer, S.; Karplus, M. 'Conjugate Peak Refinement: An Algorithm for Finding Reaction Paths and Accurate Transition States in Systems with Many Degrees of Freedom' *Chem. Phys. Lett.*, **1992**, *194(3)*, 252-261.

34. Wayne, R.P. *Chemistry of Atmospheres*. 2nd Edition. 1991. Oxford University Press.

35. Wayne, R.P. 'Atmospheric Chemistry' *Sci. Prog. (Oxford)*, **1990**, *74(296) Part 4*, 379-409.

36. Graedel, T.E.; Crutzen, P.J. 'The Changing Atmosphere' *Sci. Am.*, **1989**, *261*, 58-&SEP.

37. Farman, J.C.; Gardiner, B.G.; Shanklin, J.D. 'Large Losses of Total Ozone in Antarctica Reveal Seasonal ClO_X/NO_X Interaction' *Nature*, **1985**, *315*, 207-210.

38. Molina, M.J.; Rowland, F.S. 'Stratospheric Sink for Chlorofluoromethanes: Chlorine Atom Catalysed Destruction of Ozone' *Nature*, **1974**, *249*, 810-812.

39. Sidebottom, H.; Franklin, J. 'The Atmospheric Fate and Impact of Hydrochlorofluorocarbons and Chlorinated Solvents' *Pure and Appl. Chem.*, **1996**, *68(9)*, 1757-1769.

40. Francisco, J.S.; Williams, I.H. 'Atmospheric Chemistry of Organic Halides', The Chemistry of Functional Groups, Supplement D2: The Chemistry of Halides, Pseudohalides and Azides. Eds. S. Patai and Z. Rappoport, Wiley: Chichester, UK, 1995, chapter 26, 1559-1583.

41. Scientific Assessment of Stratospheric Ozone: 1989, Vol. 2, Appendix: AFEAS Report, *World Meteorological Organisation Global Ozone Research and Monitoring Project Report No. 20.*

42. Scientific Assessment of Ozone Depletion: 1991, *World Meteorological Organisation Global Ozone Research and Monitoring Project Report No. 25.*

43. Nielsen, O.J. 'Rate Constants for the Gas-Phase Reactions of OH Radicals with CH_3CHF_2 and $CHCl_2CF_3$ over the Temperature Range 295-388 K' *Chem. Phys. Lett.*, **1991**, *187(3)*, 286-290.

44. Talukdar, R.; Mellouri, A.; Gierczak, T.; Burkholder, J.B.; McKeen, S.A.; Ravishankara, A.R. 'Atmospheric fate of CF_2H_2, CH_3CF_3, and CH_3CFCl_2: Rate Coefficients for Reactions with OH and UV Absorption Cross Sections of CH_3CFCl_2.' *J. Phys. Chem.*, **1991**, *95*, 5815-5821.

45. Wallington, T.J.; Hurley, M.D. 'A Kinetic Study of the Reaction of Chlorine Atoms with CF_3CHCl_2, CF_3CH_2F, $CFCl_2CH_3$, CHF_2CH_3, CH_3D, CH_2D_2, CHD_3, CD_4, and CD_3Cl at 295±2 K' *Chem. Phys. Lett.*, **1992**, *189(4,5)*, 437-442.

46. Zhang, Z.; Huie, R.E.; Kurylo, M.J. 'Rate Constants for the Reactions of OH with CH_3CFCl_2 (HCFC-141b), CH_3CF_2Cl (HCFC-142b), and CH_2FCF_3 (HFC-134a)' *J. Phys. Chem.*, **1992**, *96*, 1533-1535.

47. Nimitz, J.S.; Skaggs, S.R. 'Estimating Tropospheric Lifetimes and Ozone-Depletion potentials of One- and Two-Carbon Hydrofluorocarbons and Hydrochlorofluorocarbons' *Environ. Sci. Technol.*, **1992**, *26*, 739-744.

48. Tuazon, E.C.; Atkinson, R. 'Tropospheric Reaction Products and Mechanisms of the Hydrochlorofluorocarbons 141b, 142b, and 225cb' *Environ. Sci. Technol.*, **1994**, *28*, 2306-2313.

49. Fang, T.D.; Taylor, P.H.; Dellinger, B. 'Absolute Rate Measurements of the Reaction of OH Radicals with HCFC-21 ($CHFCl_2$) and HCFC-22 (CHF_2Cl) over an Extended Temperature Range' *J. Phys. Chem.*, **1996**, *100*, 4048-4054.

50. Scientific Assessment of Ozone Depletion: 1994, *World Meteorological Organisation Global Ozone Research and Monitoring Project Report No. 37.*

51. a) Bednarek, G.; Brown, A.C.; Canosa-Mas, C.E.; Dessent, C.; Kinnison, D.J.; Parr, A.D.; Wayne, R.P. 'Investigations of Reaction Pathways of Halogenated Hydrocarbons in the Troposphere' *STEP-HALOSCIDE/AFEAS Workshop*, Dublin, May **1991**, 1-8.
b) Balestra-Garcia, C.; Poulet, G.; Le Bras, G.; MacLeod, H. 'Kinetic Study of the Reaction of OH + CH_3CFCl_2 (HCFC 141b) and OH + CH_3CCl_3' *STEP-HALOSCIDE/AFEAS Workshop*, Dublin, May **1991**, 9-16.

52. Liu, R.; Huie, R.E.; Kurylo, M.J. 'Rate Constants for the Reactions of the OH Radical with some Hydrochlorofluorocarbons over the Temperature Range 270-400 K' *J. Phys. Chem.*, **1990**, *94*, 3247-3249.

53. Cobos, C.J.; Hippler, H.; Luther, K.; Ravishankara, A.R.; Troe, J. 'High Pressure Falloff Curves and Specific Rate Constants for the Reaction $CH_3+O_2 \rightarrow CH_3O_2 \rightarrow CH_3O+O$' *J. Phys. Chem.*, **1985**, *89*, 4332-4338.

54. Ryan, K.R.; Plumb, I.C. 'Kinetics of the Reaction of CF_3 with O(P-3) and O_2 at 295 K' *J. Phys. Chem.*, **1982**, *86*, 4678-4683.

55. Russell, J.J.; Seetula, J.A.; Gutman, D. Danis, F.; Caralp, F.; Lightfoot, P.D.; Lesclaux, R.; Melius, C.F.; Senkan, S.M. 'Kinetics and Thermochemistry of the Equilibrium $CCl_3+O_2 \rightarrow CCl_3O_2$' *J. Phys. Chem.*, **1990**, *94*, 3277-3283.

56. Danis, F.; Caralp, F.; Rayez, M.T.; Lesclaux, R. 'Kinetic Study of the Reaction $CCl_3+O_2+M \rightarrow CCl_3O_2+M$ from 1 to 760 Torr and from 233 K to 333 K' ' *J. Phys. Chem.*, **1991**, *95*, 7300-7307.

57. Fenter, F.F; Lightfoot, P.D.; Caralp, F.; Lesclaux, R.; Niiranen, J.T.; Gutman, D. 'Kinetics of the $CHCl_2$ and CH_2Cl Association Reactions with Molecular Oxygen between 298 K and 448 K and from 1 to 760 Torr of Total Pressure' *J. Phys. Chem.*, **1993**, *97*, 4695-4703.

58. Fenter, F.F.; Lightfoot, P.D.; Niiranen, J.T.; Gutman, D. 'Kinetics of the CCl_3 Association Reaction with Molecular Oxygen at 298 K and 333 K and from 1 to 760 Torr of Total Pressure' *J. Phys. Chem.*, **1993**, *97*, 5313-5320.

59. Møgelberg, T.E.; Nielsen, O.J.; Sehested, J.; Wallington, T.J. 'Atmospheric Chemistry of HCFC-133a: The UV Absorption Spectra of CF_3CClH and CF_3CClHO_2 Radicals, Reactions of CF_3CClHO_2 with NO and NO_2, and Fate of CF_3CClHO' *J. Phys. Chem.*, **1995**, *99*, 13437-13444.

60. Bhatnagar, A.; Carr, R.W. 'HCFC-31: The $CHClFO_2 + NO \rightarrow CHClFO + NO_2$ Reaction and Cl Atom Elimination from CHClFO' *Chem. Phys. Lett.*, **1996**, *258*, 651-656.

61. Hayman, G.D.; Battin-Leclerc, F. 'Kinetics of the Reactions of the HO_2 Radical with Peroxyl radicals Derived from Hydrochlorofluorocarbons and Hydrofluorocarbons' *J. Chem. Soc. Faraday Trans.*, **1995**, *91(9)*, 1313-1323.

62. Dognon, A.M.; Caralp, F.; Lesclaux, R. 'Reactions of Chlorofluoromethyl Peroxy Radicals with NO: A Kinetic Study in the Temperature Range 230-430 K' *J. Chem. Phys.*, **1985**, *82*, 349-352.

63. Caralp, F.; Lesclaux, R.; Rayez, M.T.; Rayez, J.C.; Forst, W. 'Kinetics of the Combination Reactions of Chlorofluoromethyl-peroxy Radicals with NO_2 in the Temperature Range 233-376 K' *J. Chem. Soc. Faraday Trans. II*, **1988**, *84*, 569-585.

64. a) Hayman, G.D.; Jenkin, M.E.; Murrells, T.P.; Shalliker, S.J. 'Kinetic and Mechanistic Studies Associated with the Atmospheric Degradation of HCFC-123' *STEP-HALOSCIDE/AFEAS Workshop*, Dublin, May **1991**, 79-87.
b) Hanson, D.R.; Howard, C.J. 'Studies of the CFC Replacement Compound Oxidation Mechanisms: Chemical Ionization Mass Spectrometry of CF_3 Oxidation Products' *STEP-HALOSCIDE/AFEAS Workshop*, Dublin, May **1991**, 64-66.
c) Zellner, R.; Hoffmann, A.; Bingemann, D.; Mörs, V.; Kohlmann, J.P. 'Time-Resolved Product Studies in the Oxidation of HCFC-22 and HFC-134a under Simulated Tropospheric Conditions' *STEP-HALOSCIDE/AFEAS Workshop*, Dublin, May **1991**, 94-103.

65. Francisco, J.S.; Maricq, M.M. 'Making Sure that Hydrofluorocarbons are Ozone Friendly' *Acc. Chem. Res.*, **1996**, *29*, 391-397.

66. Wu, F.; Carr, R.W. 'Kinetic Study of the Reaction of the $CFCl_2CH_2O$ radical with O_2' *J. Phys. Chem.*, **1996**, *100*, 9352-9359.

67. Li, Z.; Francisco, J.S. 'Dissociation Dynamics of Perhaloalkoxy Radicals' *J. Am. Chem. Soc.*, **1989**, *111*, 5660-5667.

68. Mörs, V.; Hoffmann, A.; Malms, W.; Zellner, R. 'Time Resolved Studies of Intermediate Products in the Oxidation of HCFC 141b ($CFCl_2CH_3$) and HCFC 142b (CF_2ClCH_3)' *Ber. Bunsenges. Phys. Chem.*, **1996**, *100*, 540-552.

69. Rattigan, O.V.; Rowley, D.M.; Wild, O.; Jones, R.L. 'Mechanism of Atmospheric Oxidation of 1,1,1,2-Tetrafluoroethane (HFC 134a)' *J. Chem. Soc. Faraday Trans.*, **1994**, *90(13)*, 1819-1829.

70. Wu, F.; Carr, R.W. 'Time-Resolved Observation of the Formation of CF_2O and CFClO in the $CF_2Cl + O_2$ and $CFCl_2 + O_2$ Reactions. The Unimolecular Elimination of Cl Atoms from CF_2ClO and $CFCl_2O$ Radicals' *J. Phys. Chem.*, **1992**, *96*, 1743-1748.

71. Libuda, H.G.; Zabel, F.; Becker, K.H. 'UV Spectra of some Organic Chlorine and Bromine Compounds of Atmospheric Interest' *STEP-HALOSCIDE/AFEAS Workshop*, Dublin, May **1991**, 110-115.

72. Libuda, H.G.; Zabel, F.; Fink, E.H.; Becker, K.H. 'Formyl Chloride: UV Absorption Cross Sections and Rate Constants for the Reactions with Cl and OH' *J. Phys. Chem.*, **1990**, *94*, 5860-5865.

73. Giddings Jr, L.E.; Innes, K.K. *J. Mol. Spectrosc.*, **1961**, *6*, 528.

74. Rogers, J.D. 'Ultraviolet-Absorption Cross-Sections and Atmospheric Photodissociation Rate Constants of Formaldehyde' *J. Phys. Chem.*, **1990**, *94*, 4011-4015.

75. Reed, C.L.; Kono, M.; Langford, S.R.; Dixon, R.N.; Ashfold, M.N.R. 'Ultraviolet Photodissociation Dynamics of Formyl Fluoride' *J. Chem. Soc. Faraday Trans.*, **1997**, *93(16)*, 2721-2729.

76. Reed, C.L.; Kono, M.; Langford, S.R.; Hancock, T.W.R.; Dixon, R.N.; Ashfold, M.N.R. 'Near Ultraviolet Photolysis of HFCO: The H + FCO Channel' *J. Chem. Phys.*, **1997**, *106(14)*, 6198-6201.

77. Maul, C.; Dietrich, C.; Haas, T.; Gericke, K.-H.; Tachikawa, H.; Langford, S.R.; Kono, M.; Reed, C.L.; Dixon, R.N.; Ashfold, M.N.R. 'Ultraviolet Photolysis of Formyl Fluoride: The F + HCO product Channel' *Phys. Chem. Chem. Phys.*, **1999**, *1*, 767-772.

78. Tachikawa, H. 'Photodissociation Dynamics of Formyl Fluoride via the Triplet State Surface: A Direct *ab initio* Dynamics Study' *Phys. Chem. Chem. Phys.*, **1999**, *1*, 2675-2679.

79. Francisco, J.S.; Williams, I.H. 'Reaction Pathways for Gas-Phase Hydrolysis of Formyl Compounds HXCO (X=H,F, and Cl)' *J. Am. Chem. Soc.*, **1993**, *115*, 3746-3751.

80. Williams, I.H.; Spangler, D.; Femec, D.A.; Maggiora, G.M.; Schowen, R.L. 'Theoretical Models for Solvation and Catalysis in Carbonyl Addition' *J. Am. Chem. Soc.*, **1983**, *105*, 31-40.

81. Gaussian 92, Revision C.4, M.J. Frisch, G.W. Trucks, M. Head-Gordon, P.M.W. Gill, M.W. Wong, J.B. Foresman, B.G. Johnson, H.B. Schlegel, M.A. Robb, E.S. Replogle, R. Gomperts, J.L. Andres, K. Raghavachari, J.S. Binkley, C. Gonzalez, R.L. Martin, D.J. Fox, D.J. Defrees, J. Baker, J.J.P. Stewart and J.A. Pople, Gaussian, Inc., Pittsburgh PA, 1992.

82. Kirby, A.J. The Anomeric Effect and Related Stereoelectronic Effects at Oxygen. Springer-Verlag, Berlin, **1983**, *chapter A*, p4.

83. Lemieux, R.U. 'Effects of Unshared Pairs of Electrons and their Solvation on Conformational Equilibria' *Pure Appl. Chem.* **1971**, *25*, 527.

84. Bailey, W.F.; Eliel, E.L. 'Conformational Analysis. XXIX. 2-Substituted and 2,2-Disubstituted 1,3-Dioxanes. The Generalised and Reverse Anomeric Effects' *J. Am. Chem. Soc.* **1974**, *96*, 1798.

85. Dill, J.D.; Schleyer, P.v.R.; Pople, J.A. 'Molecular Orbital Theory of the Electronic Structure of Molecules. XXVII. Energies and Conformations of XCH_2Y Systems Involving Li, Be, and B' *J. Am. Chem. Soc.* **1976**, *98*, 1663-1668.

86. Reed, A.E.; Schleyer, P.v.R. 'The Anomeric Effect with Central Atoms Other Than Carbon. 1. Strong Interactions between Nonbonded Substituents in Polyfluorinated First- and Second-Row Hydrides' *J. Am. Chem. Soc.* **1987**, *109*, 7362-7373.

87. Krol, M.C.; Huige, C.J.M.; Altona, C. 'The Anomeric Effect: *Ab-Initio* Studies on Molecules of the Type $X\text{-}CH_2\text{-}O\text{-}CH_3$' *J. Comput. Chem.* **1990**, *11(7)*, 765-790.

88. Erdem, S.S.; Varnali, T; Aviyente, V. '*Ab Initio* Study on the Conformational Behaviour of Ethane-1,1-diol and Ethane-1,1,2-triol in Solution' *J. Phys. Org. Chem.*, **1997**, *10*, 196-206.

89. Carballeira, L.; Pérez-Juste, I. 'Ab Initio Study of the Axial/Equatorial Equilibrium in N- and O-Containing Rings in Gas Phase and Aqueous Solution: 1-Oxa-3-aza-, 1-Oxa-3,5-diaza-, 1,3-Dioxa-5-azacyclohexanes and N-Methyl Derivatives' *J. Org. Chem.* **1997**, *62*, 6144-6151.

90. Jeffrey, G.A.; Pople, J.A.; Radom, L. 'The Application of *Ab Initio* Molecular Orbital Theory to the Anomeric Effect. A Comparison of Theoretical Predictions and Experimental Data on Conformations and Bond Lengths in some Pyanoses and Methyl Pyranosides' *Carbohyd. Res.* **1972**, *25*, 117-131.

91. Jeffrey, G.A.; Pople, J.A.; Binkley, J.S.; Vishveshwara, S. 'Application of *Ab Initio* Molecular Orbital Calculations to the Structural Moieties of Carbohydrates. 3' *J. Am. Chem. Soc.* **1978**, *100(2)*, 373-379.

92. Woods, R.J.; Szarek, W.A.; Smith Jr, V.H. 'A Comparison of Semiempirical and *Ab Initio* Methods for the Study of Structural Features of Relevance in Carbohydrate Chemistry' *J. Chem. Soc., Chem. Commun.* **1991**, 334-337.

93. Salzner, U.; Schleyer, P.v.R. 'Generalised Anomeric Effects and Hyperconjugaion in $CH_2(OH)_2$, $CH_2(SH)_2$, $CH_2(SeH)_2$, and $CH_2(TeH)_2$' *J. Am. Chem. Soc.* **1993**, *115*, 10231-10236.

94. Chang, Y.-P.; Su, T.-M. 'Global Conformational Analysis and the Anomeric Interactions of Methanediol, Methanediamine, and Aminomethanol' *J. Mol. Struct. (Theochem)* **1996**, *365*, 183-200.

95. Romers, C.; Altona, C.; Buys, H.R.; Havinga, E. 'Heterocyclic Compounds' *Top. Stereochem* **1969**, *4*, 39.

96. Wolfe, S.; Whangbo, M.-H.; Mitchell, D.J. 'On the Magnitudes and Origins of the "Anomeric Effects", "Exoanomeric Effects", "Reverse Anomeric Effects", and C-X and C-Y Bond Lengths in XCH_2YH Molecules' *Carbohyd. Res.* **1979**, *69*, 1-26.

97. Jeffrey, G.A.; Yates, J.H. 'Application of *Ab Initio* Molecular Orbital Calculations to the Structural Moieties of Carbohydrates. 4' *J. Am. Chem. Soc.* **1979**, *101(4)*, 820-825.

98. Schneider, W.F.; Nance, B.I.; Wallington, T.J. 'Bond Strength Trends in Halogenated Methanols: Evidence for Negative Hyperconjugation?' *J. Am. Chem. Soc.* **1995**, *117(1)*, 478-485.

99. Schleyer, P.v.R.; Jemmis, E.D.; Spitznagel, G.W. 'Do Anomeric Effects Involving the Second-Row Substituents Cl, SH, and PH_2 Exist? Stabilisation Energies and Structural Preferences' *J. Am. Chem. Soc.* **1985**, *107*, 6393-6394.

100. Anet, F.A.L.; Yavari, I. 'Generalised Anomeric Effect and Barrier to Internal Rotation about the Oxygen-Methylene Bond in Chloromethyl Methyl Ether' *J. Am. Chem. Soc.* **1977**, *99*, 6752-6753.

101. Edward, J.T. *Chem. Ind.* **1955**, *36*, 563.

102. Wolfe, S.; Rauk, A.; Tel, L.M.; Csizmadia, I.G. 'A Theoretical Study of the Edward-Lemieux Effect (The Anomeric Effect). The Stereochemical Requirements of Adjacent Electron Pairs and Polar Bonds' *J. Chem. Soc. (B)*, **1971**, 1971.

103. Schleyer, P.v.R.; Kos, A.J. 'The Importance of Negative (Anionic) Hyperconjugation' *Tetrahedron* **1983**, *39(7)*, 1141-1150.

104. Kirby, A.J. The Anomeric Effect and Related Stereoelectronic Effects at Oxygen. Springer-Verlag, Berlin, **1983**, *chapter B*, p62.

105. Wolfe, S.; Whangbo, M.-H.; Mitchell, D.J.; *Carbohydrate Research*, **1979**, *69*, 1.

106. a) Williams, I.H.; Spangler, D.; Femec, D.A.; Maggiora, G.M.; Schowen, R.L. 'Theoretical Models for Transition-State Structure and Catalysis in Carbonyl Addition' *J. Am. Chem. Soc.*, **1980**, *102*, 6619-6621.
b)Williams, I.H.; Maggiora, G.M.; Schowen, R.L. 'Theoretical Models for Mechanism and Catalysis in Carbonyl Addition' *J. Am. Chem. Soc.*, **1980**, *102*, 7831-7839.

107. Williams, I.H.; Spangler, D.; Femec, D.A.; Maggiora, G.M.; Schowen, R.L. 'Theoretical Models for Solvation and Catalysis in Carbonyl Addition' *J. Am. Chem. Soc.*, **1983**, *105*, 31-40.

108. Williams, I.H. 'Theoretical Modelling of Specific Solvation Effects upon Carbonyl Addition' *J. Am. Chem. Soc.*, **1987**, *109*, 6299-6307.

109. Wolfe, S.; Kim, C.-K.; Yang, K.; Weinberg, N.; Shi, Z. 'Hydration of the Carbonyl Group. A Theoretical Study of the Cooperative Mechanism' *J. Am. Chem. Soc.*, **1995**, *117*, 4240-4260.

110. Wolfe, S.; Shi, Z.; Yang, K.; Ro, S.; Weinberg, N.; Kim, C.-K. 'Hydration of the Carbonyl Group. Further Evidence for a Cooperative Mechanism from Experimental and Theoretical Studies of the Hydrations of Formaldehyde, Acetaldehyde, Acetone, and Cyclohexanone' *Can. J. Chem.*, **1998**, *76*, 114-124.

111. Gaussian 94, Revision B.3, M.J. Frisch, G.W. Trucks, H.B. Schlegel, P.M.W. Gill, B.G. Johnson, M.A. Robb, J.R. Cheeseman, T. Keith, G.A. Peterson, J.A. Montgomery, K. Raghavachari, M.A. Al-Laham, V.G. Zakrzewski, J.V. Ortiz, J.B. Foresman, C.Y. Peng, P.Y. Ayala, W. Chen, M.W. Wong, J.L. Andres, E.S. Replogle, R. Gomperts, R.L. Martin, D.J. Fox, J.S. Binkley, D.J. Defrees, J. Baker, J.P. Stewart, M. Head-Gordon, C. Gonzalez, and J.A. Pople, , Gaussian, Inc., Pittsburgh PA, 1995.

112. Pauling, L. 'Atomic Radii and Interatomic Distances in Metals' *J. Am. Chem. Soc.*, **1947**, *69*, 542-553.

113. Wilkie, J.; Williams, I.H. 'Geometrical Preferences for General Acid-Catalysed Hydride Transfer - Comparative Theoretical Study of Transition Structures for Reduction of Formaldehyde.' *J. Chem. Soc. Perkin Trans. 2*, **1995**, *7*, 1559-1567.

114. Houghton, J.T. *The Physics of Atmospheres.* 1977. Cambridge University Press.

115. Lutgens, F.K.; Tarbuck, E.J. *The Atmosphere. An Introduction to Meteorology.* 2nd Edition. 1982. Prentice-Hall, Inc.

116. Maskill, H. *The Physical Basis of Organic Chemistry.* 1985. Oxford University Press.

117. Nash, L.K. *Elements of Statistical Thermodynamics.* 2nd Edition. 1974. Addison-Wesley Publishing Company, Inc.

118. Bowley, R.; Sánchez, M. *Introductory Statistical Mechanics.* 1996. Oxford University Press.

119. Scott, A.P.; Radom, L. 'Harmonic Vibrational Frequencies: An Evaluation of Hartree-Fock, Møller-Plesset, Quadratic Configuration Interaction, Density Functional Theory, and Semi-Empirical Scale Factors.' *J. Phys. Chem.*, **1996**, *100*, 16502-16513.

120. Wolfe, S.; Kim, C.-K.; Yang, K.; Weinberg, N.; Shi, Z. 'Hydration of the Carbonyl Group. A Theoretical Study of the Cooperative Mechanism' *J. Am. Chem. Soc.*, **1995**, *117*, 4240-4260.

121. Wolfe, S.; Shi, Z.; Yang, K.; Ro, S.; Weinberg, N.; Kim, C.-K. 'Hydration of the Carbonyl Group. Further Evidence for a Cooperative Mechanism from Experimental and Theoretical Studies of the Hydrations of Formaldehyde, Acetaldehyde, Acetone, and Cyclohexanone' *Can. J. Chem.*, **1998**, *76*, 114-124.

122. Ravishankara, A.R. 'Heterogeneous and Multiphase Chemistry in the Troposphere' *Science*, **1997**, *276*, 1058-1064.

123. Schweitzer, F.; Mirabel, P.; George, C. 'Multiphase Chemistry of N_2O_5, $ClNO_2$, and $BrNO_2$' *J. Chem. Phys. A.*, **1998**, *102*, 3942-3952.

124. Quinlan, M.A.; Reihs, C.M.; Golden, D.M.; Tolbert, M.A. 'Heterogeneous Reactions on Model Polar Stratospheric Cloud Surfaces: Reaction of N_2O_5 on Ice and Nitric Acid Trihydrate' *J. Phys. Chem.*, **1990**, *94*, 3255-3260.

125. Hanson, D.R.; Ravishankara, A.R. 'Investigation of the Reactive and Nonreactive Processes Involving $ClONO_2$ and HCl on Water and Nitric Acid Doped Ice' *J. Phys. Chem.*, **1992**, *96*, 2682-2691.

126. Chu, L.T.; Leu, M.-T.; Keyser, L.F. 'Uptake of HCl in Water Ice and Nitric Acid Ice Films' *J. Phys. Chem.*, **1993**, *97*, 7779-7785.

127. Horn, A.B.; Koch, T.; Chesters, M.A.; McCoustra, M.R.S.; Sodeau, J.R. 'A Low-Temperature Infrared Study of the Reactions of the Stratospheric NO_Y Reservoir Species Dinitrogen Pentoxide with Water Ice, 80-160 K' *J. Phys. Chem.*, **1994**, *98*, 946-951.

128. Banham, S.F.; Horn, A.B.; Koch, T.G.; Sodeau, J.R. 'Ionisation and Solvation of Stratospherically Relevant Molecules on Ice Films' *Faraday Discuss.*, **1995**, *100*, 321-332.

129. Akhmatskaya, E.V.; Apps, C.J.; Hillier, I.H.; Masters, A.J.; Plamer, I.J.; Watt, N.E.; Vincent, M.A.; Whitehead, J.C. 'Hydrolysis of SO_3 and $ClONO_2$ in Water Clusters' *J. Chem. Soc. Faraday Trans.*, **1997**, *93(16)*, 2775-2779.

130. Ahmed, M.; Apps, C.J.; Buesnel, R.; Hughes, C.; Hillier, I.H.; Watt, N.E.; Whitehead, J.C. 'Adsorption of N_XO_Y-Based Molecules on Large Water Clusters: An Experimental and Theoretical Study' *J. Phys. Chem. A*, **1997**, *101*, 1254-1259.

131. Oppliger, R.; Allanic, A.; Rossi, M.J. 'Real-Time Kinetics of the Uptake of $ClONO_2$ on Ice and in the Presence of HCl in the Temperature range 160 K $\leq$ T $\leq$ 200 K' *J. Phys. Chem. A*, **1997**, *101*, 1903-1911.

132. Zondlo, M.A.; Barone, S.B.; Tolbert, M.A. 'Condensed-Phase Products in Heterogeneous Reactions: N_2O_5, $ClONO_5$, and HNO_3 Reacting on Ice Films at 185 K' *J. Phys. Chem. A*, **1998**, *102*, 5735-5748.

133. Van Doren, J.M.; Watson, L.R.; Davidovits, P.; Worsnop, D.R.; Zahniser, M.S.; Kolb, C.E. 'Uptake of N_2O_5 and HNO_3 by Aqueous Sulfuric Acid Droplets' *J. Phys. Chem.*, **1991**, *95*, 1684-1689.

134. Rodriguez, J.M.; Ko, M.K.W.; Sze, N.D. 'Role of Heterogeneous Conversion of N_2O_5 on Sulphate Aerosols in Global Ozone Losses' *Nature*, **1991**, *352*, 134-137.

135. Zhang, R.; Wooldridge, P.J.; Molina, M.J. 'Vapor Pressure Measurements for the $H_2SO_4/HNO_3/H_2O$ and $H_2SO_4/HCl/H_2O$ Systems: Incorporation of Stratospheric Acids into Background Sulfate Aerosols' *J. Phys. Chem.*, **1993**, *97*, 8541-8548.

136. Hanson, D.R.; Ravishankara, A.R. 'Uptake of HCl and HOCl onto Sulfuric Acid: Solubilities, Diffusivities, and Reaction' *J. Phys. Chem.*, **1993**, *97*, 12309-12319.

137. Zhang, R.; Jayne, J.T.; Molina, M.J. 'Heterogeneous Interactions of $ClONO_2$ and HCl with Sulfuric Acid Tetrahydrate: Implications for the Stratosphere' *J. Phys. Chem.*, **1994**, *98*, 867-874.

138. Zhang, R.; Leu, M.-T.; Keyser, L.F. 'Heterogeneous Reactions of $ClONO_2$, HCl, and HOCl on Sulfuric Acid Surfaces' *J. Phys. Chem.*, **1994**, *98*, 13563-13574.

139. Elrod, M.J.; Koch, R.E.; Kim, J.E.; Molina, M.J. 'HCl Vapour Pressures and Reaction Probabilities for $ClONO_2$ + HCl on Liquid H_2SO_4-HNO_3-HCl-H_2O Solutions' *Faraday Discuss.*, **1995**, *100*, 269-278.

140. Hanson, D.R.; Lovejoy, E.R. 'Hetergeneous Reactions in Liquid Sulfuric Acid: HOCl + HCl as a Model System' *J. Phys. Chem.*, **1996**, *100*, 6397-6405.

141. Hu, J.H.; Abbatt, J.P.D. 'Reaction Probabilities for N_2O_5 Hydrolysis on Sulfuric Acid and Ammonium Sulfate Aerosols at Room Temperature' *J. Phys. Chem. A*, **1997**, *101*, 871-878.

142. Turner, A.J. 'Combined Classical/Quantum Modelling of Chemical Reactions in Enzymes and Solution' *Ph.D. thesis*, University of Bath, 1997.

143. CHARMM24b2, M. Karplus, Harvard University, 1996.

144. R. Sayle., *RasMol v2.5: A Molecular Visualisation program,* Biomolecular Structure, Glaxo Research and Development, Greenford, Middlesex, UK.

145. Xmol version 1.3.1., Minnesota Supercomputer Center Inc.

146. Turner, A.J.; Moliner, V.; Williams, I.H. 'Transition-State Structural Refinement with GRACE and CHARMM: Flexible QM/MM Modelling for Lactate Dehydrogenase' *Phys. Chem. Chem. Phys.*, **1999**, *1*, 1323-1331.

147. Jorgensen, W.L.; Chandrasekhar, J.; Madura, J.D.; Impey, R.W.; Klein, M.L. 'Comparison of Simple Potential Functions for Simulating Liquid Water' *J. Chem. Phys.*, **1983**, *79*, 926-935.

148. Rzepa, H.S.; Man Y.Y. 'An AM1 and PM3 Molecular-Orbital and Self-Consistent Reaction-Field Study of the Aqueous Solvation of Glycine, Alanine and Proline in their Neutral and Zwitterionic Forms' *J. Chem. Soc. Perkin Trans. 2*, **1991**, *4*, 531.

149. Ruggiero, G.D., *Ph.D. thesis*, University of Bath, 1999.

150. QUANTA™, Molecular Simulations Incorporated.

151. Buesnel, R.; Hillier, I.H.; Masters, A.J. 'Molecular Dynamics Simulation of the Ionization of Hydrogen Chloride in Water Clusters using a Quantum Mechanical Potential' *Chem. Phys. Lett.*, **1995**, *247*, 391-394.

152. Robertson, S.H.; Clary, D.C. 'Solvation of Hydrogen Halides on the Surface of Ice' *Faraday Discuss.*, **1995**, *100*, 309-320.

153. Ando, K.; Hynes, J.T. 'HF Acid Ionization in Water: The First Step' *Faraday Discuss.*, **1995**, *102*, 435-441.

154. Wang, L.; Clary, D.C. 'Time-Dependent Wave-Packet Studies on the Sticking of HCl to an Ice Surface' *J. Chem. Phys.*, **1996**, *104(14)*, 5663-5673.

155. Gertner, B.J.; Hynes, J.T. 'Molecular Dynamics Simulation of Hydrochloric Acid Ionization at the Surface of Stratospheric Ice' *Science*, **1996**, *271*, 1563-1566.

156. Ando, K.; Hynes, J.T. 'Molecular Mechanism of HCl Acid Ionization in Water: *Ab Initio* Potential Energy Surfaces and Monte Carlo Simulations' OH' *J. Phys. Chem. B*, **1997**, *101*, 10464-10478.

157. Gertner, B.J.; Hynes, J.T. 'Model Molecular Dynamics Simulation of Hydrochloric Acid Ionization at the Surface of Stratospheric Ice' *Faraday Discuss.*, **1998**, *108*, 1-22.

158. GAMESS-UK. (1995-7). Daresbury Laboratories. Guest, M. F., Van Lenthe, J.H., Schoffel, K., Sherwood, P. and Harrison, R.J. Contributors: Amos, R.D., Buenker, R.J., Dupuis, M., Handy, N.C., Hillier, I.H., Knowles, P.J., Bonacic-Koutecky, V., Von Niessen, W., Saunders, V.R. and Stone, A.J. The package is derived from the original GAMESS code due to Dupuis, M., Spangler, D. and Wendoloski, J.

159. Verlet, L. 'Computer 'Experiments' on Classical Fluids. I. Thermodynamical Properties of Lennard-Jones Molecules.' *Phys. Rev.*, **1967**, *159*, 98-103.

160. Hockney, R.W. 'The Potential Calculation and Some Applications.' *Methods in Comput. Phys.*, **1970**, *9*, 136-211.

161. Mulliken, R.S. 'Electronic Population Analysis on LCAO-MO Molecular Wave Functions I' *J. Chem. Phys.*, **1955**, *23*, 1833-1840.

162. Ryckaert, J.P.; Cicotti, G; Berensden, H.J.C. 'Numerical Integration of the Cartesian Equations of Motion of a System with Constraints: Molecular Dynamics on *n*-Alkanes.' *J. Comp. Phys.*, **1977**, *23*,327-341.

163. a) Gao, J. 'Absolute Free Energy of Solvation from Monte Carlo Simulations Using Combined Quantum and Molecular Mechanical Potentials' *J. Phys. Chem.*, **1992**, *96*, 537-540.
b) Kollman, P. 'Free Energy Calculations: Applications to Chemical and Biochemical Phenomena' *Chem. Rev.*, **1993**, *93*, 2395-2417.

164. Reddy, M.R.; Erion, M.D. 'Calculation of Relative Solvation Free Energy Differences by Thermodynamic Perturbation Method: Dependence of Free Energy Results on Simulation Length' *J. Comp. Chem.*, **1999**, *20(10)*, 1018-1027.

165. Born, M,'Volumen und Hydratationswärme der Ionen' *Z. Phys.*, **1920**, *1*, 45-48.

166. Honig, B.; Sharp, K.; Yang, A.-S. 'Macroscopic Models of Aqueous Solutions: Biological and Chemical Applications' *J. Phys. Chem.*, **1993**, *97*, 1101-1109.

167. Warwicker, J.; Watson, H.C. 'Calculation of the Electric Potential in the Active Site Cleft due to α-Helix Dipoles' *J. Mol. Biol.*, **1982**, *157*, 671-679.

168. Gilson, M.K.; Sharp, K.A.; Honig, B.H. 'Calculating the Electrostatic Potential of Molecules in Solution – Method and Error Assessment' *J. Comp. Chem.*, **1988**, *9*, 327-335.

169. Jean-Charles, A.; Nicholls, A.; Sharp, K.; Honig, B.; Tempczyk, A.; Hendrickson, T.F.; Still, W.C. 'Electrostatic Contributions to Solvation Energies: Comparison of Free Energy Perturbation and Continuum Calculations' *J. Am. Chem. Soc.*, **1991**, *113*, 1454-1455.

170. Dejaegere, A.; Karplus, M. 'Analysis of Coupling Schemes in Free Energy Simulations: A Unified Description of Nonbonded Contributions to Solvation Free Energies' *J. Phys. Chem.*, **1996**, *100*, 11148-11164.

171. Yu, H.-A.; Karplus, M. 'A Thermodynamic Analysis of Solvation' *J. Chem. Phys.*, **1988**, *89*, 2366-2379.

172. Roux, B.; Yu, H.-A.; Karplus, M. 'Molecular Basis for the Born Model of Ion Solvation' *J. Phys. Chem.*, **1990**, *94*, 4683-4688.

173. Jayaram, B.; Fine, R.; Sharp, K.; Honig, B. 'Free Energy Calculations of Ion Hydration: An Analysis of the Born Model in Terms of Microscopic Simulations' *J. Phys. Chem.*, **1989**, *93*, 4320-4327.

174. Åqvist, J.; Medina, C.; Samuelsson, J.-E. 'A New Method for Predicting Binding Affinity in Computer-Aided Drug Design' *Protein Eng.*, **1994**, *7(3)*, 385-391.

175. Rashin, A.A.; Honig, B. 'Reevaluation of the Born Model of Ion Hydration' *J. Phys. Chem.*, **1985**, *89*, 5588-593.

176. Barone, V.; Cossi, M.; Tomasi, J. 'Geometry Optimisation of Molecular Structures in Solution by the Polarizable Continuum Model' *J. Comp. Chem.*, **1998**, *19*, 404-417.

177. Pearson, R.G. 'Ionization Potentials and Electron Affinities in Aqueous Solution' *J. Am. Chem. Soc.*, **1986**, *108*, 6109-6114.

178. Wagman, D.D. *J. Phys.Chem. Ref. Data*, **1992**, *11*, Suppl.2.

179. Cabani, S.; Gianni, P.; Mollica, V.; Lepori, L. 'Group Contributions to the Thermodynamic Properties of Non-Ionic Organic Solutes in Dilute Aqueous Solution' *J. Solution Chem.*, **1981**, *10*, 563-595.

180. Florián, J.; Warshel, A. 'Langevin Dipoles Model for ab Initio Calculations of Chemical Processes in Solution: Parametrization and Application to Hydration Free Energies of Neutral and Ionic Solutes and Conformational Analysis in Aqueous Solution' *J. Phys. Chem. B*, **1997**, *101*, 5583-5595.